HEAT TRANSFER TO GRAPHENE NANOPLATELETS AND METALOXIDES-STUDIES IN THERMOPHYSICAL PROPERTIES AND PARTICLE CHARACTERIZATION

SOLANGI KHALID HUSSAIN

FACULTY OF ENGINEERING
UNIVERSITY OF MALAYA
KUALA LUMPUR

2016

HEAT TRANSFER TO GRAPHENE NANOPLATELETS AND METALOXIDES-STUDIES IN THERMOPHYSICAL PROPERTIES AND PARTICLE CHARACTERIZATION

SOLANGI KHALID HUSSAIN

THESIS SUBMITTED IN FULFILMENT OF THE REQUIREMENTS FOR THE DEGREE OF DOCTOR OF PHILOSOPHY

FACULTY OF ENGINEERING
UNIVERSITY OF MALAYA
KUALA LUMPUR

2016

UNIVERSITY OF MALAYA

ORIGINAL LITERARY WORK DECLARATION

Name of Candidate: SOLANGI KHALID HUSSAIN

Registration/Matric No: KHA 120065

Name of Degree: **DOCTOR OF PHILOSOPHY**

Title of Project Paper/Research Report/Dissertation/Thesis ("this Work"):

Heat transfer to graphene nanoplatelets and metaloxides-studies in thermophysical properties and particle characterization

Field of Study: **HEAT TRANSFER**

I do solemnly and sincerely declare that:

(1) I am the sole author/writer of this Work;
(2) This Work is original;
(3) Any use of any work in which copyright exists was done by way of fair dealing and for permitted purposes and any excerpt or extract from, or reference to or reproduction of any copyright work has been disclosed expressly and sufficiently and the title of the Work and its authorship have been acknowledged in this Work;
(4) I do not have any actual knowledge nor do I ought reasonably to know that the making of this work constitutes an infringement of any copyright work;
(5) I hereby assign all and every rights in the copyright to this Work to the University of Malaya ("UM"), who henceforth shall be owner of the copyright in this Work and that any reproduction or use in any form or by any means whatsoever is prohibited without the written consent of UM having been first had and obtained;
(6) I am fully aware that if in the course of making this Work I have infringed any copyright whether intentionally or otherwise, I may be subject to legal action or any other action as may be determined by UM.

Candidate's Signature Date:

Subscribed and solemnly declared before,

Witness's Signature Date:

Name:

Designation:

ABSTRACT

Nanofluids investigated in the present study are suspensions of highly conductive particles in base fluids that exhibit enhanced suspension thermal properties at modest nanoparticle concentrations. Specific nanofluids have unique heat transfer properties and are utilized in high heat flux systems (e.g., electronic cooling systems, heat exchanger liquids, solar collectors, and nuclear reactors). This study has focused on heat transfer and friction loss characteristics of propylene glycol-Treated Graphene Nanoplatelets (PGGNP-water), trimethylolpropane tris [poly(propylene glycol), amine terminated] ether-Treated Graphene Nanoplatelets (TMP-treated GNP-water), Al_2O_3 and SiO_2 water based nanofluids. In this investigation the convective heat transfer in circular tubes of different diameters and materials were considered at constant wall heat fluxes of 23870 W/m^2 and 18565 W/m^2. The experiments were conducted at the Reynolds number range of 3,900–11,700. A novel functionalization approach for preparing highly dispersed PGGNP-Water and TMP-treated GNP-water were developed. Characterization instruments showed a good degree of GNP functionalization with PG and TMP functionality. Stability study showed more than 88% of both PGGNP-water and TMP-treated GNP-water dispersed even after 1 month. In the materials effect study of the test sections the copper material showed highest heat transfer performance while in size effect study the lowest diameter of the test section showed the maximum increment in heat transfer performance. In this research all the prepared nanofluids have provided significant enhancement in heat transfer characteristics. The measured thermal conductivity, viscosity, specific heat capacity and density of all the samples showed reasonable required performance for a good heat exchanging liquid. Heat transfer and friction loss experiments were conducted in closed conduit (pipe) flow with distilled water for validation of experimental data. The impact

of the dispersed nanoparticles concentration on thermal properties, convective heat transfer coefficient, Nusselt number, Friction factor, performance index, pumping power and efficiency of loop were systematically investigated. The enhancement in thermal conductivity of PGGNP-water was observed in between 20% and 32% (0.025-0.1wt%, 20-50^{o}C), compared to base fluid. Among all the tested nanofluids the PGGNP-water at 0.1wt% showed the maximum, 119% enhancement in heat transfer coefficient compared to that of the base fluid whereas the TMP-treated GNP-water showed enhancement in heat transfer coefficient up to 107%. Beside GNPs, Al_2O_3 and SiO_2 nanofluids also showed good enhancement in heat transfer coefficient up to 29% and 31.6% respectively at 0.1 wt% concentrations. The maximum increment in Nusselt number was observed up to 82% in PGGNP-water at the heat flux of 23870 W/m^2. The performance index and pumping power showed a positive effect over all types of tested nanofluids. The results indicated that both the Nusselt number and the friction factor of the nanofluids increase with the increasing of particle volume concentration and Reynolds number. However, by increasing little amount of concentration has shown much effect on heat transfer enhancement. The ultimate goal is to disseminate the understanding of the mechanisms of the colloidal behavior of the nanoparticles as well as to broaden the experimental database of these new heat transfer media. It appears that functionalized GNPs, Al_2O_3 and SiO_2 nanofluids could be recommended as a heat exchanging fluid which could be a potential alternative to the presently used conventional working fluids.

ABSTRAK

Bendalir-Nano adalah penggantungan partikel-nano di dalam cecair yang memberikan peningkatan kepada sifat-sifat cacair pada kepekatan partikel-nano sederhana. Bendalir-nano mempunyai ciri-ciri pemindahan haba yang unik dan digunapakai di dalam sistem fluks haba yang tinggi (contohnya, system penyejukan elektronik, cecair pemindahan haba, pengumpul suria, dan reaktor nuklear). Penyelidikan ini menyiasat ciri-ciri pemindahan haba bendalir-nano Propylene glycol-dirawat Graphene Nano-platlet berasaskan air (PGGNP-Air), trimethylolpropane tris [poli (propilena glikol), amine ditamatkan] eter-dirawat Graphene Nanoplatlet (TMP dirawat GNP), Al_2O_3 dan SiO_2. Dalam penyelidikan ini bendalir-nano yang dipilih telah digunakan di dalam pemindahan haba olakan gelora saluran tertutup menerusi tiub bulat dengan diameter dan bahan-bahan yang berbeza dan terdedah kepada fluks haba dinding malar 23870 W/m^2 dan 18565 W/m^2. Ekperimen telah dijalankan untuk nombor Reynolds berjulat 3,900-11,700. Pendekatan Pengfungsian baru untuk menyediakan TMP-dirawat GNP dan PGGNP-air yang berlarutan tinggi telah dibangunkan. Instrumen pencirian menunjukkan tahap pengfungsian GNP yang baik dengan TMP dan PG. Juga, lebih daripada 88% daripada kedua-dua air-PGGNP dan TMP-dirawat GNP kekal stabil selepas satu bulan. Dalam penyelidikan ini semua bendalir-nano yang disediakan menunjukkan peningkatan yang ketara dalam ciri-ciri pemindahan haba. Kekonduksian terma, kelikatan, muatan haba tentu dan ketumpatan semua sampel menunjukkan prestasi yang munasabah bagi penggunaan dalam alatan tukaran haba. Sifat-sifat pengangkutan haba bendalir-nano, termasuk kekonduksian terma, kelikatan, kapasiti haba dan ketumpatan telah diukur. Eksperimen awal telah dilakukan dengan menggunakan air tulen untuk pengesahan data eksperimen dan ketepatan. Kesan kepekatan partikel-nano terlarut pada sifat haba, pekali pemindahan haba olakan,

nombor Nusselt, faktor geseran, indeks prestasi, kuasa mengepam dan kecekapan gelung telah disiasat. Peningkatan dalam kekonduksian terma bagi PGGNP telah diperolehi di antara 20% dan 32% berbanding dengan cecair asas. Di antara semua bendalir-nano PGGNP-Water menunjukan pekali pemindahan haba maksimum 119% lebih tinggi berbanding dengan cecair asas pada 0.1wt%. Indeks prestasi dan kuasa mengepam menunjukkan kesan yang positif. Keputusan menunjukkan bahawa kedua-dua nombor Nusselt dan faktor geseran bendalir-nano meningkat dengan peningkatan kepekatan isipadu partikel dan nombor Reynolds. Walau bagaimanapun, peningkatan sedikit kepekatan dalam julat kepekatan yang rendah di dalam kajian ini telah menunjukkan kesan ketara ke atas peningkatan pemindahan haba. Matlamat utama adalah untuk menyumbang kepada pemahaman mekanisma tingkah laku koloid berasakan partikel-nano, dan juga untuk meluaskan pangkalan data eksperimen bagi media pemindahan haba yang baru ini. Diperlihatkan bahawa bendalir nano berasaskan GNPs difungsikan, Al_2O_3 dan SiO_2 boleh beroperasi sebagai cecair gunaan dalam aplikasi pemindahan haba dan menyediakan alternatif yang baik untuk cecair gunaan konvensional di dalam sistem haba cecair.

ACKNOWLEDGEMENTS

In the name of ALLAH, the most Gracious, the most Compassionate. First and foremost, I wish to express my sincere gratitude to my supervisors, Dr. Kazi Md. Salim Newaz and Dr. Ahmad Badarudin Mohamad Badry, for all their invaluable advice and guidance of this research project and thesis. Working with them have been a fruitful learning and research experience.

I would also like to thank Dr. M.N.M. Zubir, K.H Teng, Samira Gharehkhani and Hamed arzani for their help on experimental design, and valuable suggestions. I would like to thank to my colleague Mr. Ahmad Amiri for his help on preparation of nanofluids and fruitful suggestions, which we experienced in all steps of my study. A final word of thanks goes to all my labmates over the past 3 years. The writing of this thesis had been the most challenging undertaking of my life to date. I could not have completed this work without the support and help of many people. I would also like to convey thanks to the University of Malaya and High Impact Research (MOHE-HIR) grant UM.C/625/1/HIR/MOHE/ENG/46-(D000046-16001), for providing the financial support and laboratory facilities.

Last but not the least; heartfelt thanks are extended to my lovely parents and my love Jana for their support and encouragement. This would be incomplete without sincere thanks to my Brother Aijaz who always encouraged me to achieve the best, and to my Father for their support and faith in me during the hardship.

TABLE OF CONTENTS

Abstract ii

Abstrak iv

Acknowledgements vi

Table of Contents vii

List of Figures xii

List of Tables xx

List of Symbols and Abbreviations xxii

List of Appendices xxvi

CHAPTER 1: INTRODUCTION 1

1.1 Background 1

1.2 Development of nanofluids 3

1.3 Potential features of nanofluids 5

1.4 Applications of nanofluids 6

1.5 Objectives of the present research 10

1.6 Layout of thesis 10

CHAPTER 2: LITERATURE REVIEW 12

2.1 Background 12

2.2 Preparation of nanofluids 12

2.2.1 Two-step method 12

2.2.2 One-step method 14

2.3 Stability of nanofluids 16

2.4 Effects of pH on stability of nanofluids 31

2.5 Thermal and rheological properties of nanofluids 37
2.6 Heat transfer performance 57
2.7 Friction loss of nanofluids 65
2.8 Summary 72

CHAPTER 3: CHARACTERIZATION METHOD, INSTRUMENT AND EXPERIMENTAL SET-UP 74

3.1 Analysis methods 74
3.1.1 Field emission scanning electron microscopy 74
3.1.2 Transmission electron microscopy 75
3.1.3 Fourier transform infrared spectroscopy 76
3.1.4 Raman 76
3.1.5 Differential scanning calorimetry 77
3.1.6 Rheometer 77
3.1.7 UV-vis photo spectrometer 78
3.1.8 Electrical conductivity 78
3.1.9 KD2-Pro 79
3.2 Description of the experiment 81
3.2.1 Experimental system 81
3.2.2 Design and Construction 86
3.2.2.1 Test sections 86
3.2.2.2 Reservoir Tank 87
3.2.2.3 Gear Pump 88
3.2.2.4 Inverter 89
3.2.2.5 Electromagnetic Flow Meter 90
3.2.2.6 Differential Pressure Transducers 92

3.2.2.7 Cooling unit 93
3.2.2.8 Digital multimeter and clamp meter 95
3.2.2.9 Power Supply 96
3.2.2.10 Heater 97
3.2.2.11 Thermocouple 98
3.2.2.12 Data logging system 100
3.2.2.13 Test section 102

CHAPTER 4: NANOFLUIDS PREPARATION, EXPERIMENTS AND ANALYLSYS……..... 106

4.1 Introduction 106
4.2 Nanofluids preparation 106
4.2.1 Chemical-assisted functionalization and preparation of PGGNP-water based nanofluids 106
4.2.2 Chemical-assisted functionalization and preparation of TMP-treated nanofluids 108
4.2.3 Preparation of Al_2O_3 and SiO_2 nanofluids 109
4.3 Functionalization Analysis 111
4.3.1 Characterization of PGGNP-water 111
4.3.2 TMP-treated GNP 114
4.4 Characterization of Al_2O_3 and SiO_2 117
4.4.1 Al_2O_3 117
4.4.2 SiO_2 119
4.5 Stability 120
4.5.1 PGGNP-water 120
4.5.2 TMP-treated GNP 121

4.5.3 Al_2O_3 123

4.5.4 SiO_2 124

4.6 Thermo-physical properties 127

4.6.1 Viscosity 127

4.6.2 Thermal conductivity 132

CHAPTER 5: DATA REDUCTION, CALIBRATION, EXPERIMENTAL OBSERVATION AND ANALYSIS 138

5.1 Introduction 138

5.2 Data reduction 138

5.2.1 Heat transfer coefficient 138

5.3 Experimental procedure 141

5.4 Validation test for distilled water 144

5.5 Uncertainty analysis of the test results 148

5.6 Data reproducibility 148

CHAPTER 6: STUDY OF HEAT TRANSFER AND FRICTION FACTOR OF NANOFLUIDS IN CLOSED CONDUIT 151

6.1 Convective heat transfer to functionalized GNPs and Metal oxide nanofluids 151

6.2 PGGNP-Water, TMP-treated GNP, Al_2O_3 and SiO_2 nanofluids 152

6.2.1 Effect of heat flux on heat transfer coefficient and Nusselt number 152

6.2.2 Effect of size (diameter) 164

6.2.3 Effect of Materials 172

6.2.4 Pressure drop 179

6.2.5 Performance index of the tested nanofluids 184

6.2.6 Pumping power 189

6.2.7 Efficiency of loop 194
6.3 Numerical investigation of heat transfer to PGGNP-water nanofluids 198
6.3.1 Methodology 199
6.3.1.1 Boundary conditions 199
6.3.1.2 Numerical method 200
6.3.1.3 Mesh dependency 202
6.3.1.4 Simulation cases 203
6.3.2 Results and discussion 204
6.3.2.1 Validation of the numerical method for the case of distilled water 204
6.3.2.2 Thermal analysis of PGGNP-water 205
6.3.2.3 Pressure drop 209
6.4 CONCLUSION 210

CHAPTER 7: GENERAL CONCLUSIONS 214
RECOMMENDATIONS FOR FUTURE WORK 217
REFERENCES 220
LIST OF PUBLICATIONS 249
APPENDIX 253

LIST OF FIGURES

Figure 1.1. Common base fluids, nanoparticles, and surfactants for synthesizing nanofluids. 3

Figure 2.1. Two-step preparation process of nanofluids (S. Mukherjee & S. Paria, 2013), reproduced with permission from principal author and publishers IOSR JMCE 14

Figure 2.2. Stable (left) and unstable (right) nanofluids 18

Figure 2.3. Schematic diagram of the modified magnetron sputtering system that produced nanofluids (Hwang, Yujin et al., 2008), reproduced with permission from elsevier (license number 3499320311083) 22

Figure 2.4. Zeta potential curves for 1 wt% suspension of Al_2O_3 in WEG and WPG at 20 °C (Witharana, Sanjeeva et al., 2013), reproduced with permission from elsevier (license number 3499320407975) 23

Figure 2.5. Thermal decomposition profiles of [HMIM]BF_4 and GE-dispersed ionanofluids at mass fractions of 0.03% and 0.06%, respectively (Liu, J. et al., 2014), reproduced with permission from elsevier (license number 3499320145610) 25

Figure 2.6. Zeta potential and average particle size of nanoparticles vs different pH values of ZrO_2 (Carine.T. Wamkam et al., 2011), Reproduced with permission from Susann Brailey, Manager, Rights and Permissions AIP Publishing LLC 33

Figure 2.7. Effect of pH on the convective heat transfer (Yulong Ding, 2006) 36

Figure 2.8. (a) Thermal conductivity enhancement of TiO2eEG nanofluid with pH of 9.5 and SDBS mass fraction of 1%, (b) Fig. 2.10. ke/k0 As a function of volume concentration, for various nanofluids. Role of pH. Right side: Al_2O_3 60 nm NP in water; left side CuO 25 nm NPs in water, (c) The efficiency of the cylindrical solar collector with CuO nanofluid at three different pH values (Goudarzi et al., 2015; Iranidokht et al., 2013; Lomascolo et al., 2015) 44

Figure 2.9. Experimental setup for the study of the flow and heat transfer characteristics of the CuO-base oil nanofluid flow inside the round tube and flattened tubes under constant heat flux (Razi et al., 2011) 60

Figure 2.10. Experimental setup for the study of the flow and heat transfer characteristics of the TiO2/water nanofluid flow inside horizontal double-tube heat exchanger under turbulent flow (Duangthongsuk and Wongwises) 67

Figure 3.1. Schematic setup of KD2 thermal properties analyzer 80

Figure 3.2. Comparison between distilled water and previous data 81

Figure 3.3. Schematic view of test section 84

Figure 3.4. The schematic diagram of the experimental setup for the measurement of the convective heat transfer coefficient. 84

Figure 3.5. Schematic of temperature variation through heated wall 84

Figure 3.6. Shows the different test sections diameters of stainless steel (2mm, 4mm and 15mm) 87

Figure 3.7 Shows the different test sections material of same diameter 4mm (copper, aluminium and stainless steel) 87

Figure 3.8. Photograph of the Reservoir Tank 88

Figure 3.9. Photograph of the Magnetic gear pump 88

Figure 3.10. Photograph of the Hoffman Muller inverter 89

Figure 3.11. Photograph of the Electromagnetic flow meter 90

Figure 3.12. Photograph of the Differential Pressure Transducers 92

Figure 3.13. Photograph of the Refrigerated Bath Circulators 94

Figure 3.14. Photograph of the Digital Voltmeter and clamp meter 95

Figure 3.15. Snapshot of the WINCC software and SCADA SYSTEM to control the power supply 97

Figure 3.16. Photograph of the heater around the test section 97

Figure 3.17. Photograph of the Thermocouple calibrator 99

Figure 3.18. Thermocouple testing 100

Figure 3.19. Photograph of the Data acquisition system 101

Figure 3.20. Photograph of the PLC system attached with the SCADA system 102

Figure 3.21. Photograph of the grove on a test section 103

Figure 3.22. Installation of thermocouple 103

Figure 3.23. Photograph of connection. 104

Figure 3.24. Photograph of the heat transfer test rig 105

Figure 4.1. Shows the prepared nanofluids of all concentrations 111

Figure 4.2. FTIR spectra of Pristine GNP and PGGNP 112

Figure 4.3. Raman spectra of pristine GNP and PGGNP. 113

Figure 4.4. (a-f) TEM and (g-i) SEM images of PGGNP 114

Figure 4.5. FTIR spectra of Pristine GNP and TMP-treated GNP 115

Figure 4.6. Raman spectra of pristine GNP and TMP-treated GNP. 116

Figure 4.7. TEM images of TMP-treated GNP. 117

Figure 4.8. TEM images of Al_2O_3 at 0.1wt% 119

Figure 4.9. TEM images of SiO_2 at 0.1wt% 120

Figure 4.10. (a) Plot of absorbance versus wavelength for PGGNP-based water nanofluid at 0.1 wt% and (b) plot of colloidal stability of PGGNP in water. 121

Figure 4.11. (a) Plot of absorbance versus wavelength for TMP-treated GNP-based water coolant at 0.1 wt.% and (b) plot of colloidal stability of TMP-treated GNP in water. 122

Figure 4.12. (a) Plot of absorbance versus wavelength for Al_2O_3 based water nanofluid at 0.1 wt% and (b) plot of colloidal stability of Al_2O_3 in water. 124

Figure 4.13. (a) Plot of absorbance versus wavelength for SiO_2 based water nanofluid at 0.1 wt% and (b) plot of colloidal stability of SiO_2 in water. 125

Figure 4.14. Plots of viscosity versus shear rate at various concentrations and temperatures for PGGNP-water. 129

Figure 4.15. Plots of viscosity versus shear rate at various concentrations and temperatures for TMP-treated GNP. 130

Figure 4.16. Plots of viscosity versus shear rate at various concentrations and temperatures for Al_2O_3. 131

Figure 4.17. Plots of viscosity versus shear rate at various concentrations and temperatures for SiO_2. 132

Figure 4.18. Thermal conductivity of (a) PGGNP-water, (b) TMP-treated GNP, (c) Al_2O_3 and (d) SiO_2 as a function of concentration and temperature 134

Figure 4.19. Thermal conductivity ratios of (a) PGGNP-water, (b) TMP-treated GNP, (c) Al_2O_3 and (d) SiO_2 with different concentrations and temperatures. 136

Figure 5.1. Schematic of the (a) resistances inside the test section and (b) control volume around the mean fluid temperature 138

Figure 5.2. A non-insulated tube and its thermal resistance diagram 142

Figure 5.3. Outer insulation and surrounding temperature at different velocity for the water run..... 143

Figure 5.4 Measured average Nusselt number and the prediction correlations for distilled water versus the velocity at different heat fluxes; (a) 18565 W/m^2 (b) 23870 W/m^2 147

Figure 5.5. Friction factor as a function of velocity for distilled water 147

Figure 5.6. Heat transfer coefficient as a function of velocity for two different water runs at two different heat fluxes of (a) 18565 W/m^2 and (b) 23870 W/m^2. 149

Figure 5.7. Frictional head loss as a function of velocity for two different DW runs .. 150

Figure 6.1. The effects of Reynolds number and concentration of PGGNP-Water on the convective heat transfer coefficient at inlet temperature of 30°C and input heat of (a) 23870 W/m^2 and (b) 18565 W/m^2. 153

Figure 6.2. The effects of Reynolds number and concentration of TMP-treated GNP on the convective heat transfer coefficient at inlet temperature of 30^{0}C at input power of (a) 23870 W/m^2 and (b) 18565 W/m^2. 155

Figure 6.3. The average Nusselt number of PGGNP-Water at different concentrations and Reynolds number at input of (a) 23870 W/m^2 and (b) 18565 W/m^2. 157

Figure 6.4. The average Nusselt number of TMP-treated GNP at different concentrations and Reynolds number at input power of (a) 23870 W/m^2 and (b) 18565 W/m^2. 158

Figure 6.5. The effects of Reynolds number and concentration of Al_2O_3 on the convective heat transfer coefficient at inlet temperature of 30^0C and input power of (a) 23870 W/m^2 and (b) 18565 W/m^2 160

Figure 6.6. The effects of Reynolds number and concentration of SiO_2 on the convective heat transfer coefficient at inlet temperature of 30^0C and input power of (a) 23870 W/m^2 and (b) 18565 W/m^2 161

Figure 6.7. The average Nusselt number of Al_2O_3 at different concentrations and Reynolds number at input power of (a) 23870 W/m^2 and (b) 18565 W/m^2 163

Figure 6.8. The average Nusselt number of SiO_2 at different concentrations and Reynolds number at input power of (a) 23870 W/m^2 and (b) 18565 W/m^2. 164

Figure 6.9. The effects of diameter and velocity of nanofluids on the convective heat transfer coefficient at inlet temperature of 30^0C at input power of 23870 W/m^2. 165

Figure 6.10. The average Nusselt number of nanofluids at different velocities with input power of 23870 W/m^2 166

Figure 6.11. The effects of diameter and velocity of nanofluids on the convective heat transfer coefficient at inlet temperature of 30^0C and input power of 23870 W/m^2. 168

Figure 6.12. The average Nusselt number of nanofluids at different velocities with input power of 23870 W/m^2 169

Figure 6.13. The effects of diameter and velocity of nanofluids on the convective heat transfer coefficient at inlet temperature of 30^0C and input power of 23870 W/m^2. 170

Figure 6.14. The average Nusselt number of nanofluids at different velocities with input power of 23870 W/m^2 171

Figure 6.15. The effects of material and velocity of nanofluids on the convective heat transfer coefficient at inlet temperature of 30^0C at input power of 23870 W/m^2. 173

Figure 6.16. The average Nusselt number of nanofluids at different velocities with input power of 23870 W/m^2 174

Figure 6.17. The effects of material and velocity of nanofluids on the convective heat transfer coefficient at inlet temperature of 30^0C and input power of 23870 W/m^2. 176

Figure 6.18. The average Nusselt number of nanofluids at different velocities with input power of 23870 W/m^2 176

Figure 6.19. The effects of material and velocity of nanofluids on the convective heat transfer coefficient at inlet temperature of 30^0C and input power of 23870 W/m^2. 178

Figure 6.20. The average Nusselt number of nanofluids at different velocities with input power of 23870 W/m^2 178

Figure 6.21. Friction factor of PGGNP-Water at different velocities at inlet temperature of 30^{o}C and input power of (a) 23870 W/m^2 and (b) 18565 W/m^2 180

Figure 6.22. Effect of Reynolds number and concentration of TMP-treated GNP on the friction factor at inlet temperature of 30^{o}C with input power of (a) 23870 W/m^2 and (b) 18565 W/m^2. 181

Figure 6.23. Effect of Reynolds number and concentration of Al_2O_3 on the friction factor at inlet temperature of 30^{o}C with input power of (a) 23870 W/m^2 and (b) 18565 W/m^2. 182

Figure 6.24. Effect of Reynolds number and concentration of SiO_2 on the friction factor at inlet temperature of 30^{o}C with input power of (a) 23870 W/m^2 and (b) 18565 W/m^2. 183

Figure 6.25. Performance index of PGGNP-Water at different concentrations versus Reynolds number at input of (a) 23870 W/m^2 and (b) 18565 W/m^2 185

Figure 6.26. Performance index of TMP-treated GNP at different concentrations versus Reynolds number at input power of (a) 23870 W/m^2 and (b) 18565 W/m^2. 186

Figure 6.27. Performance index of Al_2O_3 at different concentrations versus Reynolds number at input power of (a) 23870 W/m^2 and (b) 18565 W/m^2. 187

Figure 6.28. Performance index of SiO_2 at different concentrations versus Reynolds number at input power of (a) 23870 W/m^2 and (b) 18565 W/m^2. 188

Figure 6.29. Pumping power of PGGNP-water at different concentrations for input power of (a) 23870 W/m^2 and (b) 18565 W/m^2. 190

Figure 6.30. Pumping power of TMP-treated GNP at different concentrations and temperatures at input power of (a) 23870 W/m^2 and (b) 18565 W/m^2. 191

Figure 6.31. Pumping power Al_2O_3 at different concentrations and temperatures at input power of (a) 23870 W/m^2 and (b) 18565 W/m^2. 192

Figure 6.32. Pumping power SiO_2 at different concentrations and temperatures at input power of (a) 23870 W/m^2 and (b) 18565 W/m^2. 193

Figure 6.33. Efficiency of loop for the PGGNP-Water at different concentrations and Reynolds number at input power of (a) 23870 W/m^2 and (b) 18565 W/m^2. 195

Figure 6.34. Efficiency of loop for the TMP-treated GNP at different concentrations and Reynolds number at input power of (a) 23870 W/m^2 and (b) 18565 W/m^2. 196

Figure 6.35. Efficiency of loop for the Al_2O_3 at different concentrations and Reynolds number at input power of (a) 23870 W/m^2 and (b) 18565 W/m^2. 197

Figure 6.36. Efficiency of loop for the SiO_2 at different concentrations and Reynolds number at input power of (a) 23870 W/m^2 and (b) 18565 W/m^2 198

Figure 6.37. 3D schematic view of the test sections. 200

Figure 6.38. Comparison of Nusselt numbers versus Reynolds numbers for water at three different grid distributions. 203

Figure 6.39. Comparison Nusselt numbers various Reynolds numbers obtained by two-phase mixture method and Gnielinski and Dittus-boelter equations at (a) q= 18565 W/m^2 (b) q=23870 W/m^2. 205

Figure 6.40. Comparison of the convective heat transfer coefficients at various Reynolds numbers and weight concentrations at (a) q= 18565 W/m^2 (b) q=23870 W/m^2. 207

Figure 6.41. Average Nusselt numbers various Reynolds numbers and weight concentrations at (a) q= 18565 W/m^2 (b) q=23870 W/m^2. 209

Figure 6.42. Effect of Reynolds number and concentration of PGGNP-water based water nanofluids on the pressure drop. 210

Figure A1. Temperature drop through the heated wall 253

Figure A2. 1/U as a function of u^n for the thermocouples (a) number 1, (b) number 2, (c) number 3, (d) number 4, (e) number 5 and (f) number 6. The calibration experiment was conducted with DW in test section of 2mm diameter at bulk temperature 30℃, and heat flux of 23870 W/m^2 256

Figure A3. 1/U as a function of u^n for the thermocouples (a) number 1, (b) number 2, (c) number 3, (d) number 4, (e) number 5 and (f) number 6. The calibration experiment was conducted with DW in test section of 2mm diameter at bulk temperature 30℃, and heat of flux 18565 W/m^2 257

Figure A4. 1/U as a function of u^n for the thermocouples (a) number 1, (b) number 2, (c) number 3, (d) number 4, (e) number 5 and (f) number 6. The calibration experiment was conducted with DW in test section of 4mm diameter, bulk temperature 30℃, and heat flux of 23870 W/m^2 258

Figure A5. 1/U as a function of u^n for the thermocouples (a) number 1, (b) number 2, (c) number 3, (d) number 4, (e) number 5 and (f) number 6. The calibration experiment was conducted with DW in test section of 4mm diameter at bulk temperature 30℃, and heat flux of 18565 W/m^2.....259

Figure A6. 1/U as a function of u^n for the thermocouples (a) number 1, (b) number 2, (c) number 3, (d) number 4, (e) number 5 and (f) number 6. The calibration experiment was conducted with DW in test section of 15mm diameter at bulk temperature 30℃, and heat flux of 23870 W/m^2.....260

Figure A7. 1/U as a function of u^n for the thermocouples (a) number 1, (b) number 2, (c) number 3, (d) number 4, (e) number 5 and (f) number 6. The calibration experiment was conducted with DW in test section of 15mm diameter at bulk temperature 30℃, and heat flux of 18565 W/m^2.....261

Figure C1. Variation of heat transfer coefficient with velocity for DW retest. 272

LIST OF TABLES

Table 2.1. Summary of INPBE results (Buorgiorno, 2009) 45

Table 2.2. Previous data for thermal conductivity of nanofluids 47

Table 2.3. Summary of experimental results for heat transfer performance of nanofluids 61

Table 3.1. Specifications and errors of the measuring instruments and sensors used in the present experiment. 85

Table 3.2. A summary of experimental conditions for heat transfer and pressure loss studies 85

Table 3.3. Technical specifications for V8 series inverters 90

Table 3.4. Technical specifications of Electromegnetic flow meter 91

Table 3.5. Flow meter calibration data 91

Table 3.6. Standard specifications of the Differential Pressure Transducers 92

Table 3.7. Calibration conditions 93

Table 3.8. Static pressure test 93

Table 3.9. Differential pressure test 93

Table 3.10. Specifications of the Refrigerated Bath 94

Table 3.11. Specifications of the Multimeter 95

Table 3.12. Specifications of the Clamp Meter 96

Table 3.13. Dimensions of the test section 102

Table 4.1. Nanoparticle specifications 107

Table 4.2. Fourier transform infrared interpretation of the functionalized GNP 111

Table 4.3. Fourier transform infrared interpretation of the functionalized GNP 115

Table 4.4. Zeta potential, average particle size distribution, mobility and polydispersity Index (PDI) of Al_2O_3 and SiO_2 in distilled water. 127

Table 4.5. Specific heat, Dynamic viscosity and density of the PGGNP-Water at the bulk temperature of 30^0C 136

Table 4.6. Specific heat, Dynamic viscosity and density of the TMP-treated GNP at the bulk temperature of 30^0C. 136

Table 4.7. Specific heat, Dynamic viscosity and density of the Al_2O_3 at the bulk temperature of 30^0C. 137

Table 4.8. Specific heat, Dynamic viscosity and density of the SiO_2 at the bulk temperature of 30^0C. 137

Table 5.1. Heat loss calculations 142

Table 5.2. Insulation details 144

Table 5.3. Uncertainty ranges. 148

Table 6.1. Summary of the effect of the size on the heat transfer performance and friction factor of nanofluids 171

Table 6.2. Summary of the effect of material on the heat transfer performance and friction factor of nanofluids 178

Table B1. Ranges and accuracies of instruments used 263

Table B2. Uncertainties of fluid properties 264

Table B3. Uncertainty ranges. 270

Table C1. Cleaning agent used for test rig. 271

LIST OF SYMBOLS AND ABBREVIATIONS

A	absorbency
AFM	Atomic force microscopy
ANNs	Artificial neural network
b	optical path (cm)
B	Optical path (cm)
c	molar concentration (mol/dm^3)
C_p	Specific heat capacity, J/kg K
$C_{1\varepsilon}$, $C_{2\varepsilon}$, $C_{3\varepsilon}$, σ_k, σ_ε	Model constants
CTAB	Cetyltrimethylammonium Bromide
CHF	Critical heat flux
CNT	Carbon nanotube
CVD	Chemical vapor deposition method
D	Tube diameter, m
DSC	Differential scanning calorimetry
DW	Distilled water
ECG	Epicatechin gallate
EDL	Electrical double layer
EGCG	Epigallocatechin gallate
f	Friction factor
FT-IR	Fourier transform infrared spectroscopy
G_b	generation of turbulence kinetic energy
GA	Gum Arabic
GO	Graphene oxide

GNP	Graphene nanoplatelets
GT	Green tea
GTPs	Green tea polyphenols
h	Convective heat transfer coefficient
HC	Hamilton-Crosser
I	Electrical current, A
k	Thermal conductivity, W/m.K
L	Tube length, m
MW-CNT	Multiwall carbon nanotube
NDG	Nitrogen-doped graphene
Nu	Nusselt number
P	Heater power, W
Pe	Péclet number
Pr	Prandtl number
PVD	Physical vapor deposition method
q″	Heat flux, W/m^2
Re	Reynolds number
rGO	reduced graphene oxide
SDBS	Sodium dodecyl benzene sulfonate
SDS	Sodium dodecyl sulfonate
SEM	Scanning electron microscopy
SL	Sodium Laurate
SSA	Specific surface area
SW-CNT	Single-wall carbon nanotube
T	Temperature, K

TEM	Transmission electron microscopy
THW	Transient hot-wire
TPS	Transient plane source
U	Mean velocity, m/s
V	Volts, V
v	Mean velocity, m/s
w	Water
W	Watt
wt%	weight percentage
X, Y, Z	Cartesian coordinates
x	Axial distance
XRD	X-ray diffraction
XPS	X-ray photoelectron spectroscopy

Greek

ΔP	pressure drop, Pa
wt%	weight percentage
ϕ	nanoparticle volumetric fraction
μ	viscosity, Pa.s
ε	Turbulent dissipation
ρ	density, kg/m^3
η	thermal performance factor
σ	Electrical conductivity

Subscripts

avg	average
b	bulk

avg	average
b	bulk
bf	base fluid
i	inner
in	inlet
m	mean
nf	nanofluid
np	nanoparticle
o	outer
out	outlet
w	wall

LIST OF APPENDICES

APPENDIX A: CALIBRATION METHODS 240

APPENDIX B: UNCERTAINTY ANALYSIS 249

APPENDIX C: CLEANING OF THE TEST SECTION 257

CHAPTER 1: INTRODUCTION

1.1 Background

Nanofluids are suspensions obtained from dispersing different nanoparticles in host fluids to enhance thermal properties (Eastman, Choi, Li, Thompson, & Lee, 1997; Ghozatloo, Rashidi, & Shariaty-Niassar, 2014; Hindawi, 2014; M. Mehrali et al., 2014; Wei, Y. & Xie, 2012). These are next-generation heat transfer fluids and introduced as heat exchanging fluids. It has better thermal properties than conventional heat transfer fluids (Hassan et al., 2013; Sadeghinezhad, E. et al., 2014; Sadri et al., 2014b; Witharana, Sanjeeva, Palabiyik, Musina, & Ding, 2013; Yang, Y., Zhang, Grulke, Anderson, & Wu, 2005). Over the past two decades, nanofluids have exhibited remarkable improvement in thermal conductivity, stability, and heat transfer coefficients which could reduce overall plant power consumption and costs on application in heat exchangers. Nanofluids have great application potential in several fields. Nanofluids are increasingly utilized in different heat exchangers to optimize energy consumption (Hindawi, 2014). Hence, discovery of suitable nanofluids having improved heat transfer properties and high thermal conductivity has become challenging (Chen, Haisheng, Witharana, Jin, Kim, & Ding, 2009; Kakaç & Pramuanjaroenkij, 2009; M. Mehrali et al., 2014; Mangrulkar C.K. & Kriplani V.M., 2013; Taylor, R. A. & Phelan, 2009; Togun et al., 2014; Yang, J.-C., Li, Zhou, He, & Jiang, 2012). Several studies have reported the results of thermal conductivity of metaloxide based water nanofluids [e.g., aluminum oxide (Al_2O_3), SiO_2, TiO_2, and copper oxide (CuO)] in the last decade. These studies have explored the evolution of thermal conductivity of suspensions with solid content. Thermal conductivity enhancement of nanofluids depends on adding nanoparticles and the nanoparticle aspect ratio (Halelfadla, Estelléb, & Maréa, 2014). More common nanoparticles and basefluids have exploited the synthesis operation are

presented in Figure 1.1. However, adding nanoparticles increases viscosity of nanofluids which limits the thermal benefits of nanofluids through enhanced pumping power in the systems. Along with the thermal behavior of nanofluids, the most important issue is the stability of nanofluids; achieving the desired stability remains challenging today (Hindawi, 2014). Most investigations have focused on the suspension stability of nanofluids with no conclusive results. Several researchers have investigated the addition of gum arabic, gum tragachan, cetyl trimethylammonium bromide (CTAB), and sodium dodecylbenzenesulfonate (SDBS) surfactants as well as controlling of pH suspension (Barber, Brutin, & Tadrist, 2011; Mahboobeh, S.S. Sara, A. Hossein, & K.G Elaheh, 2013; Nkurikiyimfura, Wang, & Pan, 2013). Adding surfactants and modifying nanoparticle surfaces effectively could improve stability of the nanofluids based on steric hindrance and electrostatic repulsion among nanoparticles (Kim, Y. J., Ma, & Yu, 2010; Shanthi, Shanmuga, & Velraj, 2012; Wang, B., Wang, Lou, & Hao, 2012). Adding surfactants is simple and convenient and is thus attractive in practical applications. Unfortunately, maintaining long-term stability of nanofluids with increased concentrations become difficult because steric hindrance and electrostatic repulsion lose their effects when the distances among nanoparticles become shorter (Goodarzi et al., 2014; Gu, Hou, Lu, Wang, & Chen, 2013; Harikrishnan, Magesh, & Kalaiselvam, 2013; Seon & Kim, 2011). Decreasing nanofluid concentration is the best approach to maintain good fluidity. Recently, significant investigations on the use of carbon-based nanomaterials such as, single-wall carbon nanotube, multi-wall carbon nanotube, graphene oxide and graphene nanoplatelets (GNP) to make nanofluids were reported in the literature (Sharma, Tiwari, & Dixit, 2016; Yarmand et al., 2015). New research specifies that graphene nanofluids could provide higher thermal conductivity enhancement in comparison to other tested nanofluids (Sharma et al., 2016). Graphene is an allotrope of carbon atoms which has drawn attention of researchers recently due to

its superior properties, such as high elastic modulus, good electrical conductivity, good thermal conductivity, and self-lubricating behavior (Nikkhah et al., 2015; Tabandeh-Khorshid, Omrani, Menezes, & Rohatgi; Zhao, Yang, Li, Zhang, & Li, 2016). In the last few years, a significant number of studies have been conducted with graphene due to its unique thermal, electrical, optical, mechanical and other favorable characteristics. Characterization of graphene provides an important part of graphene research and involves measurements based on various spectroscopic and microscopic techniques (Rao, C. N. R. & Sood, 2013).

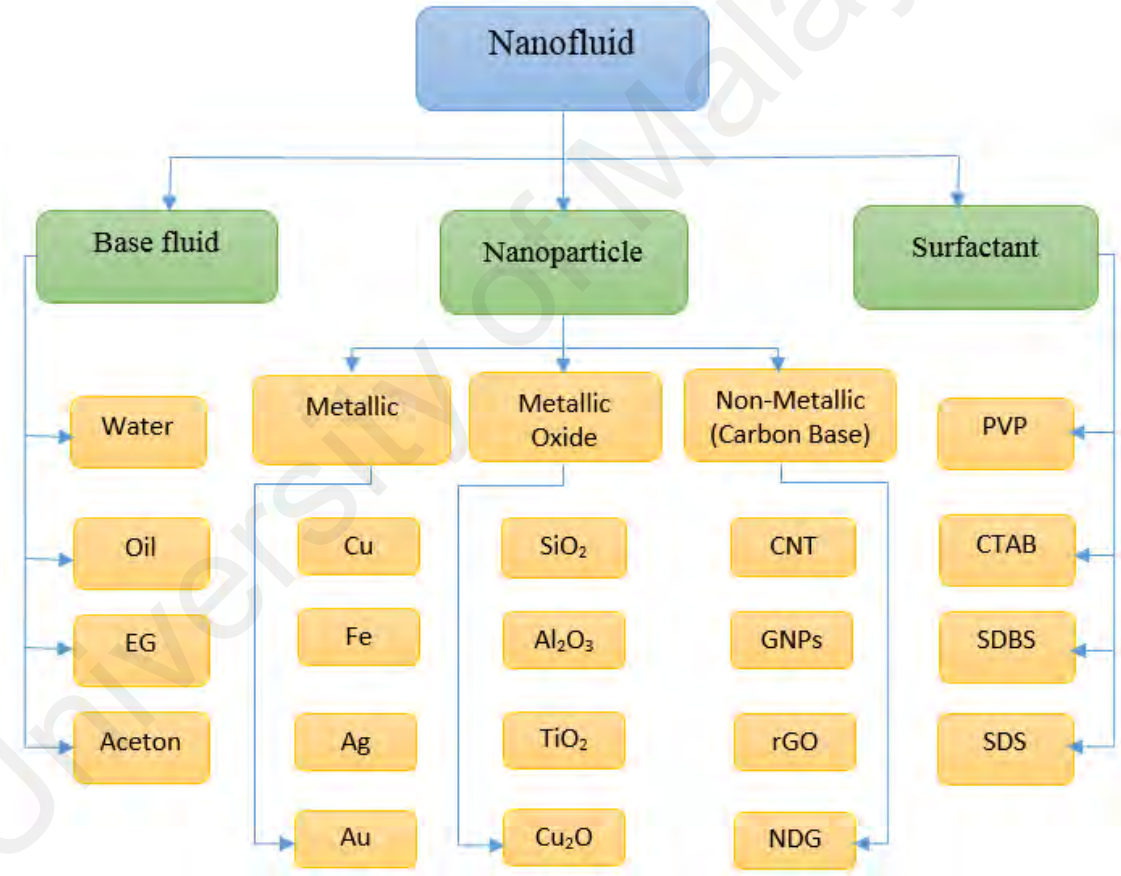

Figure 1.1. Common base fluids, nanoparticles, and surfactants for synthesizing nanofluids.

1.2 Development of nanofluids

Norio Taniguchi first used the term "nanotechnology" in 1974. He described nanotechnology as technology that engineers materials at the nanometer size. Choi

(Choi, S.U.S & Eastman, 1995) coined the term "nanofluid" in 1995 to describe this combination. The main focus of nanofluid research since then has been to develop superior heat transfer fluids (Taylor, R. A. & Phelan, 2009; Wu & Zhao, 2013). Nanofluids have become established in the history of nanoscience and have therefore attracted the attention of researchers around the globe. Nanofluid research has expanded over the years, as evidenced by the fact that studies numbered only 10 research papers in 2001 and grew to 175 in 2006 and 700 in 2011 (Mahian, Kianifar, Kalogirou, Pop, & Wongwises, 2013; S. Mukherjee & S. Paria, 2013; Taylor, R. et al., 2013; Tie, Li, & Xuan, 2014).

Modern nanotechnology has enabled the production of average-sized (below 100 nm) metallic and nonmetallic nanoparticles. The mechanical, optical, electrical, magnetic, and thermal properties of nanoparticles are better than those of conventional bulk materials of coarse grain structures (Kamiński & Ossowski, 2014; Karimipour et al., 2014). Recognizing the opportunity to apply nanotechnology in thermal engineering, Stephen Choi and his colleagues at the Argonne National Laboratory (ANL) proposed the concept of nanofluids in 1994 and investigated issues related to fundamentals and applications of nanofluids. Researchers from Japan and Germany also published articles that describe fluids which resemble the concept of nanofluids developed at ANL. Researchers from Japan have (Cowan, 1963) dispersed Al_2O_3, SiO_2, and TiO_2 by adding acid (HCl) or base (NaOH) (Choi, 1995; Dehkordi, 2011; Wei, Yu & Huaqing, 2012) to the base liquids. Abrasion-related properties are more favorable than conventional solid/fluid mixtures. Successful employment of nanofluids supports the current trend towards component miniaturization by enabling the design of small and light heat exchange systems. Yu (Yu.W. France, D, & J.S. Choi, 2008) discussed the properties of nanofluids and future challenges. Keblinski et al. (Keblinski, P., Phillpot, Choi, &

Eastman, 2002) studied the heat flow in nanoparticle suspensions. The research showed that the nanofluids exhibit high thermal conductivity even at low concentrations of suspended nanoparticles. For example, the experiments exhibited an increase in thermal conductivity by dispersing less than 1% volume fraction of copper (Cu) nanoparticles or carbon nanotubes (CNT) in ethylene glycol or oil by 40% and 150%, respectively (Abareshi, Goharshadi, Mojtaba Zebarjad, Khandan Fadafan, & Youssefi, 2010; Sadri et al., 2014b). The research also showed that nanofluid technology provides opportunities for developing nanotechnology-based coolants for various innovative engineering and medical applications (Choi, S.U.S., 209; R. Sadri et al., 2014).

1.3 Potential features of nanofluids

Nanofluids have uncommon features that are essential for various engineering applications. These special qualities include (Al-Nimr & Al-Dafaie, 2014; Murshed & Nieto de Castro, 2014; Peyghambarzadeh, Hashemabadi, Chabi, & Salimi, 2014; Shanbedi, Heris, et al., 2015; Tie et al., 2014; Tuqa. Abdulrazzaq et al., 2013; Witharana, Sanjeeva et al., 2013; Xie, H. et al., 2002; Xing, Yu, & Wang, 2015; Zhang, Shao, Xu, & Tian, 2013):

- Ultrafast heat transfer ability
- Increased thermal conductivity and exceptional theoretical predictions
- Justified pumping power
- Enhanced stability over other colloids
- Superior lubrication
- Tolerable friction coefficient
- Acceptable erosion and clogging in microchannels

1.4 Applications of nanofluids

Nanofluids have been extensively used in various applications. Using of nanofluids is primarily driven by the potential to develop fluids with significantly increased conductive and convective heat transfer properties (Taylor, R. et al., 2013). Various researchers have reviewed nanofluids for heat transfer applications (Huminic & Huminic, 2012; Murshed, Nieto de Castro, Lourenço, Lopes, & Santos, 2011; Vajjha, Ravikanth S. & Das, 2012). For example, nanofluids can be used in several engineering applications in the automotive industry, medical arena, power plant cooling systems, and computers because of their enhanced properties as thermal transfer fluids (Kaufui & D.L Omar, 2010; Saidur, Kazi, Hossain, Rahman, & Mohammed, 2011). Nanofluids could be used in transportation, energy production, electronics systems (e.g., microprocessors and micro-electro-mechanical systems), and biotechnology. The number of companies that observe the potential of nanofluid technology and its focus for specific industrial applications have been increasing. In the transportation industry, nanocars (e.g., GM and Ford) are focusing on nanofluid research projects (Huminic & Huminic, 2012; Leong, Saidur, Kazi, & Mamun, 2010; Saidur, Leong, & Mohammad, 2011).

In 2008, Routbort (J. Routbort, 2009) started a project that used nanofluids for industrial cooling to save energy and decrease emissions. The restoration of cooling and heating water with nanofluids can conserve 1 trillion Btu of energy in the U.S.A Employing nanofluids in closed-loop cooling cycles can save approximately 10 to 30 trillion Btu per year in the U.S.A electric power industry, which is equivalent to the annual energy consumption of approximately 50,000 to 150,000 households. Associated emission reduction will approximately be 5.6 million metric tons of carbon dioxide, 8,600 metric tons of nitrogen oxides, and 21,000 metric tons of sulfur dioxide.

Various industrial processes for Michelin tire plants in North America are constrained by the lack of facilities to efficiently cool rubber during processing, which requires over 2 million gallons of heat transfer fluids. Michelin aims to increase the productivity of its rubber processing plants by 10% if sufficient water-based nanofluids can be developed and produced in a cost-effective manner (Kaufui & D.L Omar, 2010; Yu, W. et al., 2010).

Han et al. (Han, Z. H., F. Y. Cao, & B. Yang, 2008) used phase change materials as nanoparticles in nanofluids to synchronously increase effective thermal conductivity and specific heat of the fluids. For example, a suspension of indium nanoparticles (melting temperature) in polyalphaolefin was synthesized using one-step nanoemulsification process. Temperature dependent behavior of the thermo-physical properties (i.e., thermal conductivity, viscosity, and specific heat) of the fluid were measured experimentally. The melting–freezing phase transition of the indium nanoparticles significantly augmented the effective specific heat of the fluid.

According to a report from MIT (2007), the total geothermal energy resources of the world exceeded 13000 ZJ. Currently, only 200 ZJ is extractable. However, over 2,000 ZJ can be extracted to supply the energy needs of the world for several millennia with technological improvements (Kaufui & D.L Omar, 2010). When extracting energy from the Earth's crust at a length that varies between 5 km to 10 km and temperature between 500 and 1000 °C, nanofluids could be used to cool pipes exposed to high temperatures. When drilling, nanofluids could cool drilling machinery and equipment under high friction and high temperature environments (Rahul & B.S. Kothawale, 2013). As fluid superconductors, the nanofluids could be used to extract energy from the Earth's core and process it in a pressurized water reactor power plant system to generate large amounts of work energy (Kaufui & D.L Omar, 2010).

Experimental data obtained by using nanofluids in commercial heat exchangers confirm that flow type (i.e., laminar or turbulent) inside heat exchanging equipment is essential to the effectiveness of a nanofluid. Using nanofluids when the heat exchanger operates under turbulent conditions is beneficial only if the increase in thermal conductivity is accompanied by a marginal increase in viscosity; this condition is difficult to achieve. However, the disadvantage of using nanofluids when the heat exchanger operates under laminar conditions is the high costs and potential suspension instability. The empirical correlations used to characterize the heat transfer processes are reliable for convective heat transfer coefficient prediction of nanofluids provided the accurate values of physical properties are obtained (Gupta, H. K., G.D Agrawal, & J. Mathur, 2012; Pantzali, A.A. Mouza, & S.V. Paras, 2009; Saidur, Leong, et al., 2011). Therefore, substituting conventional fluids with nanofluids in industrial heat exchangers is unsuitable if large volumes of nanofluids are involved and turbulent flow is developed. However, using nanofluids instead of conventional fluids is advantageous in micro-scale equipment with increased thermal duties and under laminar flow. In any case, the nanofluid properties should be defined carefully to evaluate their effectiveness in specific heat exchangers (Ahmadreza.Abbasi. Baharanchi, 2013; Huminic & Huminic, 2012).

All methods used to characterize nanofluid stability suggest that mixing nanoparticles of different types and potentials produces a synergistic effect that allows low-stability particles to remain suspended within fluid domains with high resultant surface charge density. Moreover, the results give rise to other important issues related to suspension stability (e.g., time and sonication methods and devices used for particle dispersion). The rheological study reveals noticeable differences in viscosity and shear stress values among different ratios of nanoparticle elements at specific weight percentages.

This study serves as a foundation to explore possibilities in improving the thermo-physical properties of selected nanofluids by tuning particle suspension stability in fluid mediums (Chang, Chen, Jwo, & Chen, 2009; Lee, D., Kim, & Kim, 2006). The persisting challenge inherent in these techniques is achieving the mass production level, which is hindered by stringent requirements and environments. Thus, combining particles of different types and characteristics to enhance the properties of nanofluids allows the integration of nanoparticles via different routes to alleviate deficiencies/drawbacks associated to low stability particles. The approach is viable for small amounts of particles with enhanced surface properties produced by laboratory equipment to act as additives and improve the stability of commercially produced TiO_2 nanoparticles synthesized near IEPs. Careful mixtures of these particles at a stable state (away from pH of IEP) could potentially form favorable aggregation and improve nanofluid properties to suit specific applications, especially within the thermal engineering domain.

In summary, much ground has been covered on NF synthesis, but the main issues remain unresolved. The stability of nanofluids at high temperatures remains a challenge, and several new challenges are derived from emerging applications. The stabilizing agents of a nanofluid should enable long-term and high-temperature stability (Taylor, R. et al., 2013). Barriers in application are due to inconsistent results, poor characterization of suspensions, and lack of theoretical understanding of mechanisms. Suspended nanoparticles in various base fluids could alter the fluid flow and heat transfer characteristics of base fluids (Choi, U. S. S., 1995).

Simple, scalable, and environmentally acceptable approaches for synthesizing nanofluids are still being developed to consistently meet the product specifications. Recent progress on the one-step approach is promising. However, further investigations

should be conducted to bring nanofluid synthesis to a state where production can be scaled up.

1.5 Objectives of the present research

The main objectives of this research can be summarized as follows:

1. To develop new types of graphene nanoplatelets by covalent modification techniques.
2. To investigate the thermo-physical properties of the developed nanofluids and their characterization.
3. To investigate experimentally nanomaterials and size effects on the heat transfer performance of nanofluids in a circular tube heat exchanger of different tube materials and dimensions.
4. Simulation of the heat transfer to nanofluids in pipe flow and compare the numerical data with the experimental results for validation.

1.6 Layout of thesis

The thesis starts with a look at the different mechanisms of energy transport in nanofluids, followed by a summary of previous literature review of thermo-physical properties, stability, convective heat transfer and pressure drop of nanofluids. This is followed by part of the literature survey presented in Chapter 2. In Chapter 3 characterization method, instruments, the experimental setup, test section, calibration of the instruments are discussed. The preparation methods and thermo-physical properties of the prepared PGGNP-water, TMP-treated GNP, Al_2O_3 and SiO_2 nanofluids are discussed in Chapter 4. The method of data reduction, uncertainty analysis of the experimental set-up and validation of the test sections are well discussed in Chapter 5. Heat transfer and friction factor results are discussed in Chapter 6 and they are followed by the performance evaluation of the prepared nanofluids. The Chapter 7 contains a summary of the work done and proposed recommendations for future work. Appendix

A contains discussion about calibration of the test section, from which the current setup is based. Appendix B describes the uncertainty analysis and in the last Appendix C the cleaning procedure is elucidated.

CHAPTER 2: LITERATURE REVIEW

2.1 Background

Throughout history, people worked on the subject of heat transfer phenomenon for a better heat transfer performance, which directly affects the standard of their life. With the development of heat engines, heat pumps and similar devices the requirement for a better heat transfer became more important. Heat exchanger devices, heat transfer fluids or other components related to heat transfer were invented and improved with thriving technology. Usage of more compact, larger heat transfer area heat transfer devices are common in today's industry. However, heat transfer requirements of these devices are becoming larger while their sizes are becoming smaller. At this point, increasing the heat transfer area of a device may no longer be a solution because the practical limitations of manufacturing smaller channels or components can be a problem with usage of conventional methods. In this chapter, a literature survey on the studies about the different preparation methods, thermo-physical properties of nanofluid, stability measurement of nanofluids and forced convection heat transfer with nanofluids are presented.

2.2 Preparation of nanofluids

Preparation of nanofluids is the important and first step in the use of nanoparticles to improve the thermal conductivity of nanofluids. Nanofluids are primarily prepared via two processes: two-step preparation and one-step preparation.

2.2.1 Two-step method

Several researchers employed the two-step method to prepare nanofluids (Eastman et al., 1997; Ghozatloo, Shariaty-Niasar, & Rashidi, 2013; Nikkam et al., 2014; Suresh, S., Venkitaraj, Selvakumar, & Chandrasekar, 2011). The method utilized nanoparticles,

nanofibers, nanotubes, and other nanomaterials, which are initially produced as dry powders via chemical or physical methods.

This method is extensively used in synthesizing nanofluids by mixing base fluids with commercially-available nanopowders obtained from different mechanical, physical and chemical routes (e.g., milling, grinding, and sol-gel and vapor phase methods). Ultrasonic vibrators or high shear mixing devices are generally used to stir nanopowders with host fluids. Frequent use of ultrasonication or stirring decreases particle agglomeration (Chung, S. J. et al., 2009). Agglomeration is a major issue in synthesizing nanofluids (Wang, X. Q. & A.S. Mujumdar, 2008). The two-step method is the most economical method for large-scale production of nanofluids because nanopowder synthesis techniques have already been scaled up to industrial production levels (Ponmani, William, Samuel, Nagarajan, & Sangwai, 2014; Wei, Yu & Huaqing, 2012). Nanoparticles tend to aggregate because of high surface area and activity (Hindawi, 2014). Researchers suggest (Eastman, Choi, Li, Yu, & Thompson, 2001) that the two-step method is more suitable for preparing nanofluids with oxide nanoparticles than those with metallic nanoparticles. Stability is a significant issue for this method as the powders aggregate easily because of the strong van der Waals force among nanoparticles. Despite its disadvantages, the method is recognized as the most economical process for producing nanofluids (Mukherjee & Paria, 2013). Figure 2.1 shows the two-step method.

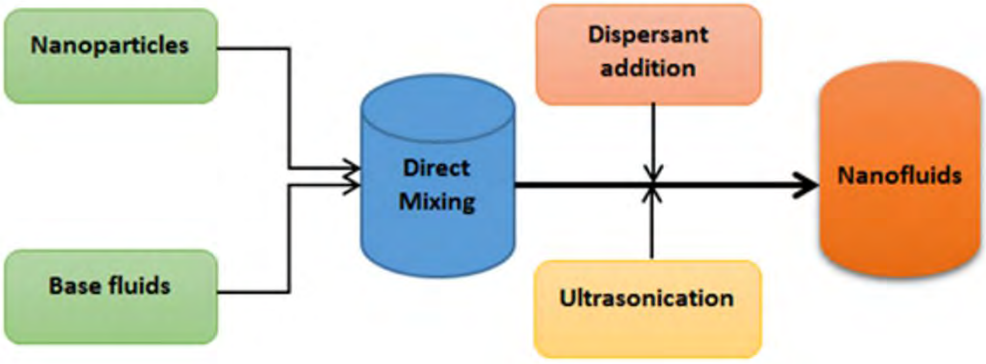

Figure 2.1. Two-step preparation process of nanofluids (S. Mukherjee & S. Paria, 2013), reproduced with permission from principal author and publishers IOSR JMCE

Preparation of stable nanofluids is an important area in nanofluid research and application (Manimaran, K. Palaniradja, N. Alagumurthi, S. Sendhilnathan, & J. Hussain, 2014). Eastman (Eastman et al., 2001) employed the two-step method to prepare nanofluids and observed that nanometer-sized Cu particles dispersed in ethylene glycol have higher effective thermal conductivity than those dispersed in pure ethylene glycol. The method may be economical, but it presents drying, storage, and transportation issues. Issues in agglomeration and clogging also decrease the thermal conductivity of nanofluids. The advantage of this method is that the nanofluids could be prepared on a large scale. However, nanoparticle aggregations are difficult to break up under ultrasonication or stirring. Thus, stability and thermal conductivity of nanofluids prepared through dispersion are usually not ideal (Haitao. Zhu, Dongxiao. Han, Zhaoguo. Meng, Daxiong. Wu, & Zhang, 2011).

2.2.2 One-step method

Advanced techniques are developed to produce nanofluids via one-step method because of the difficulty in preparing stable nanofluids via the two-step method. The one-step method includes the direct evaporation and condensation method, submerged-arc nanoparticle synthesis system (SANSS), and laser ablation methods (Das, S.K , Choi, Yu, & Pradeep, 2007; Haitao. Zhu et al., 2011; Lo, T.T Tsung, & L.C Chen,

2005), in which metals are vaporized using physical technology and cooled into liquids to obtain nanofluids. These physical methods have excellent control over particle sizes and produce stable nanofluids.

The one-step method involves simultaneously producing and dispersing particles in fluids (Wei, Yu & Huaqing, 2012). The method includes the chemical liquid deposition method and vapor deposition method. Several researchers have used this method to prepare nanofluids (De Robertis et al., 2012; Jamal-Abad, Zamzamian, & Dehghan, 2013; Munkhbayar, Tanshen, Jeoun, Chung, & Jeong, 2013; Paul, Sarkar, Pal, Das, & Manna, 2012; Singh, A. K. & V. S. Raykar, 2008; Yang, L., Du, Niu, Li, & Zhang, 2011; Zhu, H.-t., Lin, & Yin, 2004). Drying, storage, transportation, and nanoparticle dispersion are avoided in this method to minimize nanoparticle agglomeration and increase fluid stability. The method prepares uniformly dispersed nanoparticles, which are stably suspended in base fluids. The method reduces production costs (Zhu, H.-t. et al., 2004). Vacuum-SANSS prepares nanofluids using different dielectric liquids. Different morphologies are mainly influenced and determined by the various thermal conductivity properties of dielectric liquids. The prepared nanoparticles exhibit needle-like, polygonal, square, and circular morphological shapes. The method avoids undesired particle aggregation fairly well (Wei, Yu & Huaqing, 2012). However, the most important disadvantage of the method is that residual reactants remain in the nanofluids because of incomplete reaction or stabilization. Explaining the nanoparticle effect is difficult without eliminating this impurity effect. Furthermore, a one-step chemical *s*olution method (CSM) has recently been developed to create nanofluids by design; CSM can synthesize nanofluids of various microstructures and has successfully produced nine kinds of nanofluids (L.Q. Wang & Wei, 2009; Wang, L. Q. & Quintard, 2009; Wei, X. & Wang, 2010; Wei, X. H., H.T. Zhu, T.T. Kong, & Wang,

2009). Nanofluids synthesized by CSM have higher conductivity enhancement and better stability than those synthesized by other methods. CSM is also distinguished from other methods by its controllability. However, synthesizing nanofluids on a large scale is difficult when employing the one-step method. The nanofluid microstructure can be varied and manipulated by adjusting synthesis parameters [e.g., temperature, acidity (pH), ultrasonic and microwave irradiation, and reactant and additive types and concentrations] and the order in which the additives are added to the solution (L.Q. Wang & Wei, 2009; Wang, L. Q. & Quintard, 2009; Wei, X. & Wang, 2010).

2.3 Stability of nanofluids

Surfactants enhance nanoparticle stability in fluids. However, surfactant functionality under high temperatures is a major concern, especially for high-temperature applications. The sedimentation method, also called the settling bed, is the most decisive and extensively used technique for evaluating the stability of a nanofluid (Witharana, S. , C. Hodges, D. Xu, X. Lai, & Y. Ding, 2012; Witharana, Sanjeeva et al., 2013). In this method, light absorbance is measured or the bed height is visually monitored over a certain period of time. The main drawback of using this method on fairly slow settling suspension is the long observation time; a faster technique involves the time-resolved measurement of the zeta potential of the sample. Another disadvantage of this method is that it restricts the viscosity and particle concentration of samples.

The main challenge in preparing nanofluids is their poor stability caused by the formation of agglomerates, which are generated by high surface areas and strong van der Waals forces among nanoparticles. The stability of nanofluids is essential in practical applications because the thermo-physical properties of unstable fluids change through time (Bianco, Manca, & Nardini, 2014; Haghighi et al., 2013). Although various methods have been developed to prepare nanofluids, these methods all have

instability problems caused by particle agglomeration in base fluids. Stability requires uniformly dispersed nanoparticles in the base fluid. The thermal and electrical properties of nanofluids are enhanced when the nanofluids are stable (Philip & Shima, 2012; Ponmani et al., 2014). Nanoparticle agglomeration not only settles and clogs microchannels, but also decreases the thermal conductivity of nanofluids (M.P. Beck, Y.H. Yuan, P. Warrier, & Teja, 2010). Thus, the stability of nanofluids should be investigated because it significantly influences the properties of nanofluids for application; the influencing factors in the dispersion stability of nanofluids should also be studied and analyzed (Sarkar, S., Ganguly, & Biswas, 2012; Sarkar, S., Ganguly, Dalal, Saha, & Chakraborty, 2013).

Colloidal dispersions have been investigated through particle motion analysis under various flow conditions and sedimentation characteristics studies on suspended nanoparticles in base fluids to prepare stable nanofluids (Wasan, Nikolov, & Moudgil, 2005). Colloid stability in water is best studied using the Derjaguin–Landau–Verwey–Overbeek (DLVO) theory (Deryaguin & L. Landac, 1941; Overbeek, 1952; Rao, Y., 2010b; Verwey & Overbeek, 1948). Although a recently proposed extended DLVO theory describes the stability of nanofluids well, a good theoretical framework and analytical tools that could develop stable nanofluids are still lacking (El-Brolossy & Saber, 2013; Rao, Y., 2010b). Nanofluids have recently been reported to be more stable than micrometer-sized particle suspensions because of vigorous Brownian motion of suspended nanoparticles in base fluids (Hwang, Yujin et al., 2008; Tantra, Schulze, & Quincey, 2010). Among the various nanofluid preparation methods, adding surfactants is efficient in homogeneously dispersing nanoparticles in base fluids. Surfactants [e.g., sodium dodecyl sulfate (SDS)] cause electrostatic repulsion among surfactant-coated nanoparticles, which significantly decreases particle agglomeration because of the van

der Waals forces of attraction (Fendler, 2001; Tantra et al., 2010).

Low costs, long-term stability, and good fluidity are the three most significant preconditions for the nanofluids toward practical applications in the heat transport field (Lee, K.J. , S.-H. Yoon, & Jang, 2007). Figure 2.2 shows nanofluid samples where one is visually stable, while the other shows that particles are visibly separated from the liquid. Stable nanofluids are not clearly defined. Nevertheless, nanofluids are widely agreed to be stable when they remain as a single entity for a considerable period of time (i.e., usually for three consecutive months or more from the preparation date) (Rao, Y., 2010b; Sarkar, S. et al., 2013).

Figure 2.2. Stable (left) and unstable (right) nanofluids

Gravitational force causes particles to separate from the liquid and settle on the bottom. The settling theory of Stoke in Equation 2.1 explains particle settling when gravitational acceleration and viscous forces act on particles. For heat transfer applications, the nanoparticles are denser than the working liquid $(\rho_s > \rho)$ and settle with time (Hwang, Yujin et al., 2008; Kallay & Å½alac, 2002; Witharana, S. , 2011). However, this effect is counter-balanced by the small sizes of the nanoparticles *(x)*,

which result in small settling velocities *(U_t)* and large time scales. Problems occur when nanoparticles flock together and form aggregates, which are heavy and settle quickly.

$$U_t = \frac{x^2(\rho_s - \rho)g}{18 * \mu} \qquad (2.1)$$

Settling is essential in various industrial sectors (e.g., petroleum, mining, and mineral). Fluids are either stationary or moving in heat transfer equipment. The probability of particles settling on the tube in circulating nanofluids (i.e., forced convection in tubes) is low because of mixing. However, the probability is high in natural convection and pool boiling environments because of the stationary nature of the bulk fluid. Thus, settled particles clog fluid channels and add thermal wall resistance where wall materials are highly thermally conductive. Ultimately, nanofluids could diminish the system instead of enhancing it (Witharana, Sanjeeva et al., 2013). Therefore, the increase in critical heat flux is proven because of the systematic deposition of nanoparticles on heated surfaces. The question on how to stabilize nanofluids for heat transfer applications remains. A nanofluid collapses as a result of particle settling, which in turn could be a consequence of undesired aggregation. The interaction among suspended particles should be examined to further explore this condition.

Most researchers who employed electrostatic stabilization (pH regulation) avoided working at the iso electric point (IEP) vicinity of the particle. Extensive agglomeration is undesirable because of the adverse effects of high viscosity and low thermal conductivity enhancement within the thermal management system. These two characteristics are the most difficult to address and have attracted several researchers in

the industry and the academe (Ghadimi, Saidur, & Metselaar, 2011; Kallay & Å½alac, 2002; Mondragón, 2012; Rao, Y., 2010a). Accurate properties of nanofluids (e.g., effective thermal conductivity, particle size, and dispersion stability) should be measured and analyzed for their practical applications. Dispersion stability should be evaluated by measuring the exact amount of suspended and settled nanoparticles in the base fluid over time. Several methods are used to evaluate the dispersion stability of nanofluids (Lee, J., Han, & Koo, 2014).

Hwang et al. (Hwang, Y. et al., 2007) evaluated the stability of nanofluids by using UV-vis. A spectrophotometer with multiwalled carbon nanotubes (MWCNT) and Fullerene/oil from absorption and particle concentration exhibited a linear relation. The relative nanofluid stability was estimated from this relation. Wang et al. (Wang, X. J., X. Li, & Yang, 2009) measured the stability of nanofluids using a Malvern ZS Nano S analyzer (DLS), alumina, and Cu/water. A well-dispersed suspension was obtained with high surface charge density. Chen et al. (Chen, G., W. Yu, D. Singh, D. Cookson, & Roubort, 2008) employed small angle X-ray scattering with Ludox. When analyzing X-ray scattering, particles in the liquid are complicated by the interference among X-rays that are elastically scattered from individual particles. Wensel et al. (Wensel, J. et al., 2008) evaluated the stability of nanofluids by visually inspecting the dispersion stability of nanofluids with nanotubes and metal oxide particles. Chiesa and Simonsen (Chiesa & A.J. Simonsen, 2007) utilized transmission electron microscopy (TEM) and alumina/oil, and obtained stable nanofluids when the nanoparticles were well distributed.

Chang (Chung, K. L., C.L. Hung, & H.T. Su, 2004) investigated the effect of additional magnetic field on the stability of CuO nanofluid (60 nm). Nanofluids were prepared by self-developed ASNSS, and the particles inside the CuO nanofluid became unstable within a short period of time. The repulsion of the static electric charge among

suspension particles decreased and enabled them to agglomerate. Strong magnetic fields contributed to coarser particles than those formed under weak magnetic fields. Long permeance times required short periods for nanoparticle agglomeration and complete precipitation under magnetic fields. However, the permeance frequency level had no apparent effect on nanoparticle suspension. The repulsion force among particles decreased because of additional magnetic fields, which caused electric potential to drop and allowed nanoparticles to form aggregates; further details are presented in (Chung, K. L. et al., 2004; Mahian, Mahmud, & Heris, 2012).

Yujin (Hwang, Yujin et al., 2008) employed the one-step method to enhance nanoparticle dispersion in the base fluid. A modified magnetron sputtering system was utilized. Sputtered Ag nanoparticles were directly collided with thin films of silicon oil formed on a rolling drum (Figure 2.3) for 20 min. The target substrate was a rotating drum dipped into a reservoir of silicon oil. Rotational speed was from 0 rpm to 10 rpm. Distance between Ag sputtering target and drum was fixed at 8 cm. Sputtered Ag particles directly dispersed in thin films of silicon oil formed on the rotating drum. The average diameter of Ag nanoparticles was 3 nm. No sedimentation was observed for 60 days after producing Ag–silicon oil nanofluids using the modified magnetron sputtering system, which indicates the long-term stability of prepared Ag–silicon oil NF.

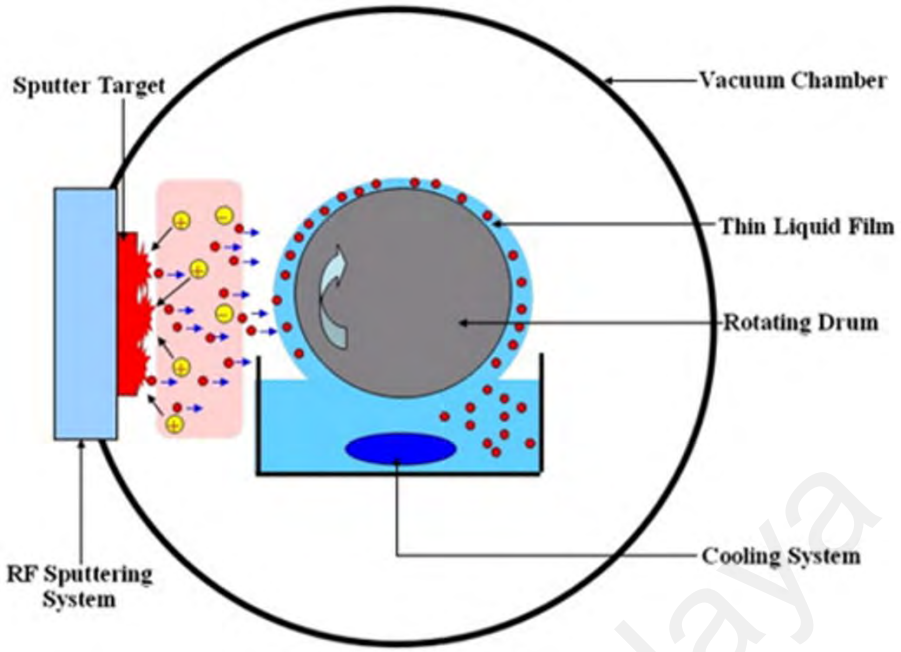

Figure 2.3. Schematic diagram of the modified magnetron sputtering system that produced nanofluids (Hwang, Yujin et al., 2008), reproduced with permission from elsevier (license number 3499320311083)

Sanjeeva et al. (Witharana, Sanjeeva et al., 2013) measured the stability of TiO_2, Al_2O_3, and ZnO nanofluids. Ultrasonication was applied at 37 kHz to break agglomerates using a digital sonicator. The two-step method was utilized to prepare nanofluids. Dispersion characteristics of suspensions were evaluated through visual inspection, particle size measurement, and zeta potential analysis. Particle size and zeta potential measurements were collected using a zetasizer nano ZS device. Titrations were performed at 20 °C. Deposit thicknesses at the container bottoms (vials) were measured a month after sonication using a meter ruler with small gradations of 1 mm (Xuan, Y. & Li, 2000). Propylene glycol (PG)-based nanofluids exhibited good overall stability for all different concentrations in TiO_2 at 1, 6, and 9 wt%. All samples were sonicated for 16 h. Al_2O_3 nanofluids were more stable than TiO_2 nanofluids. However, increasing their particle concentrations up to 6 wt% and 9 wt% decreased stability and generated thin sediments just after two days; Al_2O_3 nanofluids became stable after two months with base fluids PG and ethylene glycol (EG). Figure 2.4 shows that Al_2O_3–WEG exhibited

tremendously high zeta potential at 100 mV when pH < 6. Except for the interval 8.5 < pH < 10.5, the nanofluid should be stable except for an interval of 8.5 < pH < 10.5. Al_2O_3–WPG nanofluids yielded maximum zeta potential at pH 6. Therefore, WEG- and WPG-based Al_2O_3 nanofluids should exhibit the best stability at pH < 6.

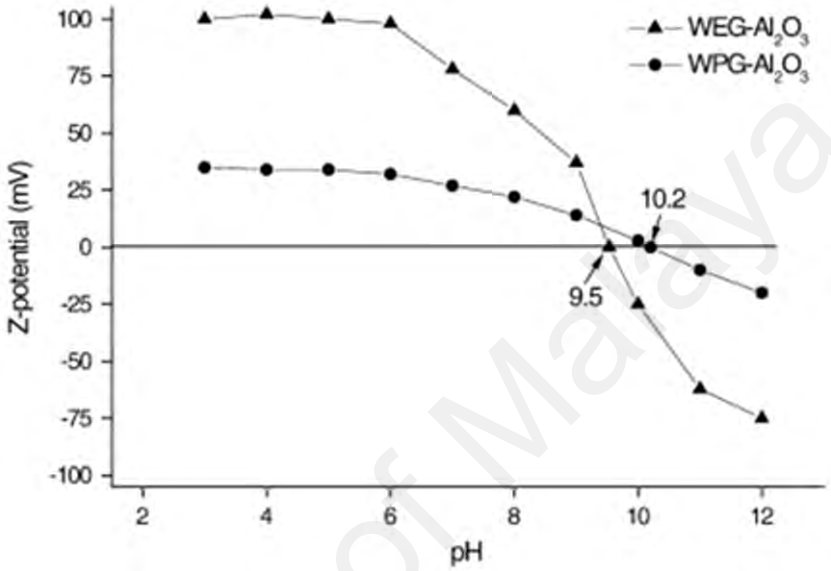

Figure 2.4. Zeta potential curves for 1 wt% suspension of Al_2O_3 in WEG and WPG at 20 °C (Witharana, Sanjeeva et al., 2013), reproduced with permission from elsevier (license number 3499320407975)

ZnO became stable after two months with PG-based fluid at particle concentrations of 1 wt%. Daylight caused color change in all glycol-based TiO_2 suspensions. Daylight also caused particle agglomeration in PG-based Al_2O_3 and TiO_2 samples (Witharana, Sanjeeva et al., 2013). Li (Li, D. & W. Fang, 2012) prepared a series of surface-coated silver nanoparticles using dialkyl dithiophosphates with different hydrocarbon chain lengths (C12, C16, C18) as efficient bonding ligands. Silver-kerosene nanofluids were thermally oxidized in an isothermal apparatus after preparation and characterization. The thermal stabilities of silver nanofluids of AgDDP12 and kerosene were monitored through UV-vis spectral analysis. Consequently, the silver nanofluids became stable for

a certain time limit at high temperatures because of the ligand surface coating. Thus, silver nanoparticles with good oil dispersion and surface coated by dithiophosphates could prepare oil-based nanofluids, which favors thermal oxidation stability of oil at high temperatures. Ponmani et al. (Ponmani et al., 2014) observed ZnO and CuO nanofluids with varying concentrations of nanoparticles (0.1, 0.3, and 0.5 wt%) prepared using the two-step method in 0.4 wt% of xanthan gum (XG) aqueous solution. The XG aqueous solution formed a jelly-like structure around the nanoparticles and kept them suspended. CuO nanofluid was more stable than ZnO nanofluid in the same base system. Jian et al. (Liu, Wang, Zhang, Fang, & Zhang, 2014) evaluated the thermal stability of ionic liquid 1-hexyl-3-methylimidazolium tetrafluoroborate [HMIM]BF_4 and its graphene (GE)-dispersed nanofluids using thermogravimetric analysis. Figure 2.5 shows the thermal decomposition profiles that were obtained. Initial decomposition temperature (T_{onset}) of [HMIM]BF_4 was 440.6 °C, which indicates good thermal stability. Moreover, T_{onset} of GE-dispersed ionanofluids was 438 and 437.7 °C at GE loadings of 0.03 and 0.06 wt%, respectively; these temperatures were close to that of [HMIM]BF_4. Adding GE into ionic liquid changed thermal stability only slightly. [HMIM]BF_4 and its GE-dispersed nanofluids exhibited high thermal stability because of their initial decomposition temperature at 440 °C. Thermal conductivity of [HMIM]BF_4 and the ionanofluids linearly increased as temperature increased from 25 °C to 200 °C. The high decomposition temperature of [HMIM]BF_4 and its GE-dispersed ionanofluids indicated that they were suitable for use as HTFs in medium- and high-temperature heat transfer systems.

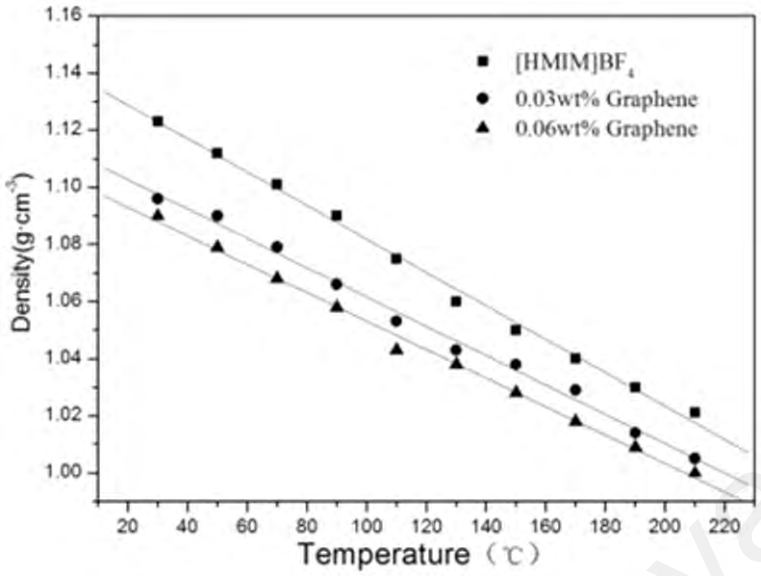

Figure 2.5. Thermal decomposition profiles of [HMIM]BF_4 and GE-dispersed ionanofluids at mass fractions of 0.03% and 0.06%, respectively (Liu, J. et al., 2014), reproduced with permission from elsevier (license number 3499320145610)

Sandip (Sarkar, S. et al., 2013) measured the stability of Cu–water and Al_2O_3–water nanofluids using dynamic mode decomposition (DMD). The DMD is a modal decomposition method based on spectral analysis operator. The method approximates the modes of the Koopman operator and is adjoint of the Perron–Frobenius operator. The work was the first attempt to analyze mixed convective stability of nanofluid flow past a square cylinder through DMD. Phase portrait of real and complex DMDs exhibited trajectories with concentric circles. Real and complex parts of most dominant eigenmodes for both nanofluids exhibited 90° phase differences. Energy content in Cu–water nanofluids was higher than that of Al_2O_3–water nanofluids. Lamas (Lamas, Abreu, Fonseca, Martins, & Oliveira, 2012) used an innovative technique to quantitatively characterize the colloidal stability of MWCNT-based water nanofluids. The method evaluates colloidal dispersion of suspensions by applying a centrifugal field. Analytical centrifuge is an effortless and undemanding method of estimating the shelf life of suspensions (Lerche, 2002). The method accelerates demixing and evaluates concentration changes by detecting transmission profiles along the entire sample height.

Measuring the settling velocity at high relative centrifugal force (RCF = centrifugal acceleration/earth acceleration) ensures that the constant of proportionality can be identified with the demixing phenomenon, and the results can be extrapolated to gravity conditions (RCF = 1). Consequently, the colloid shelf life can be estimated directly. Functionalized MWCNT (D20–40 L10–30) suspended in DW-60% EG provides the highest stabilization, which requires almost 50 years to fully settle. The settling velocity of MWCNT-based nanofluids decreased as aspect ratio and nanoparticle concentration (ref) increased (Lamas et al., 2012). Rosa (Mondragon, Julia, Barba, & Jarque, 2012) characterized silica–water nanofluid, and the BS technique was employed for stability light backscattering. The amount of light backscattered by the NF from an incident laser beam was measured using a Turbiscan Lab Expert (Formulaction SA, France). Measurements were based on the multiple light scattering theory. Backscattering profiles for each nanofluid were obtained along the cell height. Measurements were collected at different time intervals of up to 48 h to analyze the stability of nanofluids. Singh et al. (Singh, D. K., D.K. Pandey, R.R. Yadav, & Singh, 2012) considered the formation of zinc oxide nanofluid in a polyvinyl alcohol solution using sonication. Fedele et al. (Fedele, L. Colla, S. Bobbo, S. Barison, & Agresti, 2011) examined the stability of water-based nanofluids that contain various nanoparticles [i.e., TiO_2, CuO, carbon nanohorns in polyethylene glycol (PEG) and water, and SDS as surfactants] using a DLS apparatus. Both PEG and SDS were good dispersants for nanofluids. Chung et al. (Chung, S. J. et al., 2009) studied the effect of ultrasonic dispersion in forming zinc oxide nanofluid in water using the two-step method. Hwang et al. (Hwang, Yujin et al., 2008) investigated various physical techniques for dispersing carbon black and silver nanoparticles in nanofluids using the two-step method.

Meng (Meng, Wu, Wang, Zhu, & Li, 2012) produced CNT glycol nanofluids whose sizes and morphologies were examined using TEM, JEM-2000EX at an acceleration

voltage of 160 kV. UV-Vis-NIR spectroscopy of CNT glycol nanofluids was recorded on a Cary 500 spectrophotometer from 200 nm to 2500 nm. CNTs were treated by oxidation with HNO_3. CNTs were broken into short and less twisted shreds after HNO_3 treatment, which resulted in high stability and enhanced dispersion. The prepared nanofluids could remain stable for more than two months without sedimentation.

Pang (Pang & Y.T. Kang, 2012) prepared the nanofluids using the two-step method. Al_2O_3 nanoparticles with sizes from 40 nm to 50 nm were used with base fluid $H_2O/CH_3OH/NaCl$ to produce nanofluids with particle concentrations of 0.1 vol%. Dispersion stability of $H_2O/CH_3OH/NaCl$-based Al_2O_3 (0.1 vol%) nanofluids deteriorated a week after preparation. Thermal conductivity of nanofluids were highly enhanced at 6.3% for concentrations of 10 wt% NaCl, 40 vol% CH_3OH, and 0.1 vol% Al_2O_3 nanoparticles.

Lee et al. (Lee, S. W., Park, Kang, Bang, & Kim, 2011) inspected thermo-physical properties of SiC/DIW nanofluids in high-temperature heat transfer applications. SiC nanofluids were prepared in-house, and the shapes and sizes of SiC nanoparticles were checked. Therefore, the isoelectric point (IEP) was identified at pH 6 for SiC dispersion stability, and the pH control maintained the stability.

Zhu et al. (Zhu, D. et al., 2009) investigated dispersion behavior and thermal conductivity of Al_2O_3 –water nanofluid under different pH values and SDBS concentrations. Zeta potential and particle size were measured, and DLVO theory was used to calculate attractive and repulsive potentials. Thermal conductivity was measured using a hot disk thermal constant analyzer. Stability and thermal conductivity enhancements for Al_2O_3–H_2O nanofluids significantly depended on pH values and different SDBS dispersant concentrations of nanosuspensions; optimal pH values and SDBS concentrations resulted in the best dispersion behavior and highest thermal

conductivity. Yurong et al. (He et al., 2007) investigated stable aqueous TiO_2 nanofluids with different particle (agglomerate) sizes and concentrations, which were formulated and measured for static thermal conductivity and rheological behavior. Their work focused on forced convective heat transfer of TiO_2 nanofluids. The nanofluids were measured for heat transfer and flow behavior when they flowed upward through a vertical pipe in both laminar and turbulent flow regimes. The authors claimed that TiO_2 nanofluids have excellent stability even without using any stabilizer, and metal oxides (e.g., TiO_2 nanoparticles) were more chemically stable than their metallic counterparts.

Witharana (Witharana, S., H. Chen, & Y. Ding, 2011) investigated the structural stability of EG-based TiO_2 nanoparticles prepared from the two-step method to study the dependence of shear stability of nanofluids on temperature, particle loading, and shear rate. The nanofluids were stable for two months with no visible separation, which indicated long-term aggregate stability. Moreover, light scattering data obtained from the Malvern zetasizer-nano device showed that the suspended particles were approximately 130 nm. Aggregates in quiescent flow fields were stable at temperatures of up to 60 °C. Shear stability data showed that the aggregates were sufficiently stable over a range of rigorous shear rates and temperatures.

Haghighi et al. (Haghighi et al., 2013) studied the shelf stability of Al_2O_3 nanofluids, including three DW-based clays with concentrations of 9 wt% for types (I) and (II) and 1.75 wt% for type (III); DW-based Al_2O_3 (9 wt%) and EG-based CeO_2 (1 and 2 wt%) were evaluated. The results showed that nanofluids with low solid particle loading demonstrated slightly better stability than concentrated nanofluids. DW–Al_2O_3 nanofluid was reasonably stable and were promising candidates for practical applications. Thermal conductivity and viscosity of Al_2O_3 as a nanofluid with good

shelf stability were measured from 20 °C to 40 °C, and the results were on average 8% and 23.5% higher than DW, respectively.

Munkhbayar et al. (Munkhbayar, Bat-Erdene, Sarangerel, & Ochirkhuyag, 2013) measured the stability and thermal conductivity of silver-based aqueous nanofluids (1 wt%, 2 wt%, and 3 wt%) from 300 nm to 800 nm and from 20 °C to 40 °C. Consequently, silver nanoparticles ground by a 1 mm ball size dispersed in an aqueous solution (1 wt%) exhibited the highest thermal conductivity (621 W/mK) (Corrected) and was greater than that of the nanofluids prepared under other conditions at 40 °C.

Sundar et al. (Sundar, L. Syam, Farooky, Sarada, & Singh, 2013) conducted stability experiments for Al_2O_3 and CuO nanofluids in 50:50% of EG/W-based fluid at volume concentrations of 0.2%, 0.4%, and 0.8%. The solution was kept in an ultrasonic bath for approximately 2 h to uniformly disperse the nanoparticles in the base fluid. No surfactant was used in the base fluid. Stable colloidal suspensions of Al_2O_3 and CuO nanofluids were obtained. In comparison with the base fluid, thermal conductivity enhancement varied from 9.8% to 17.89% for Al_2O_3 nanofluid and from 15.6% to 24.56% for CuO nanofluids under a temperature range of 15 °C to 50 °C at 0.8% volume concentration.

Lee et al. (Lee, J. H., Lee, & Jeong, 2013) indicated that pH is essential to colloidal stability of oxide nanoparticles. The effects of pressure on the critical heat flux were investigated in a pool of water-based nanofluids of magnetite (Fe_3O_4) and alumina (Al_2O_3) nanoparticles using Ni–Cr wire. Zeta potential for magnetite–water nanofluid (MWNF) at high nanoparticle concentrations and 3 h of sonication in an ultrasonic vessel was immediately measured after colloid preparation and again after the nanofluid was preserved for 24 h. All nanofluids utilized in the experiments were stable.

Habibzadeh et al. (Habibzadeh et al., 2010) reported that large relative surface areas of nanoparticles not only significantly improved heat transfer capabilities, but also increased nanofluid suspension stability. SnO_2 nanofluids were prepared by dispersing tin dioxide nanoparticles in DI water as the base fluid (Habibzadeh et al., 2010). A microwave-induced combustion synthesis method was used to prepare SnO_2 nanoparticles. Nanofluids were ultrasonicated for dispersion. The nanofluid prepared by SnO_2 nanoparticles synthesized at $\Phi = 1.0$ (SN1.0) with high surface area and low aggregation ratio. Thus, fine crystallite sizes were the most stable nanofluid. Phuoc (Phuoc, Massoudi, & Chen, 2011) used chitosan to stabilize MWCNTS dispersed in deionized water (Phuoc et al., 2011). The weight fraction of chitosan was 0.2 wt%. The nanofluids prepared without chitosan were unstable. Solids precipitated quickly and settled at the bottom of the vial approximately 30 min after preparation. The fluid stabilized at 0.2 wt% chitosan and remained stable for months.

Nikkam et al. (Nikkam et al., 2014) studied the heat transfer application of nanofluids that consist of Cu nanoparticles in diethylene glycol-based liquid. This work employed the one-step (microwave-assisted) method to overcome challenges in the stability of nanofluids. Cu nanofluids that were synthesized using this method were colloidally stable for several weeks with no precipitation. Maximum enhancement value of 7.2% was obtained for Cu nanofluid at 1.6 wt% concentration, while a viscosity increase of 5.2% was observed for the same nanofluid at 1.6 wt%. Salma et al. (Halelfadl, Maré, & Estellé, 2014) analyzed the thermo-physical properties of water-based nanofluids that contain CNTs stabilized by sodium dodecyl benzene sulfonate (SDBS) as surfactants. The influence of particle concentrations from 0.0055% to 0.278% and temperatures from 20 °C to 40 °C on thermal conductivity was reported. An increase in thermal conductivity with nanoparticle volume fraction and temperature was observed (Lee, S. W. et al., 2011; Mukherjee & Paria, 2013; Taylor, R. et al., 2013)

2.4 Effects of pH on stability of nanofluids

pH, which is related to electrostatic charge on the particle surface, is a key parameter in determining colloidal stability or stable nanoparticle dispersion. pH can be interpreted and quantified as zeta potential. pH values must be far from IEP to maintain the stability, which is the pH at which a particle surface carries no net electrical charge (zero zeta potential). Therefore, particle precipitation and agglomeration occur in colloidal dispersion because no sufficient repulsive forces exist among particles. The absolute value of the zeta potential of the particle surface increases as pH values change from IEPs; interaction among particles because of the electrical double layer becomes sufficient in preventing attraction and collision among particles caused by Brownian motion (Lee, S. W. et al., 2011; Taylor, R. et al., 2013). A common challenge in using nanofluids is maintaining nanoparticle suspension within the fluid (Salman, Mohammed, Munisamy, & Kherbeet, 2013; Udbhav.Ojha, Sumitesh. Das, & Subhrakanti. Chakraborty, 2010; Wang, X. J., Li, Xu, & Zhu, 2014). According to the DLVO theory, pH influences nanoparticle aggregation (Carine.T. Wamkam, Michael. K. Opoku, Haiping. Hong, & Pauline, 2011). Thermal conductivity of prepared nanofluids was enhanced with base fluids of different pH values. Anoop (Anoop, Sundararajan, & Sarit Das., 2009) achieved suspension of Al_2O_3 particles for several weeks by altering the pH values of the nanofluid. Keeping the nanofluid away from its IEP, or the point where zero net charge is present between the particles and the bulk fluid, ensured that the particles were kept in suspension by the electrostatic repulsive force among them. pH values of 1, 2, 4, and 6 wt% were 6.5, 6, 5.5, and 5, respectively (Haddad, Abid, Oztop, & Mataoui, 2014). Moreover, researchers have made a number of observations that could be explained by existing colloidal science literature. For example, Wamkam et al. (Wamkam, M.K. Opoku, H. Hong, & Smith, 2011) were unable to obtain thermal conductivity enhancements below a pH value of 4.5, which

coincided with the IEP of their study, because of different crystalline phases of titanium dioxide (i.e., anatase and rutile). The different structures of each phase resulted in significant variance in surface properties. Rutile has an IEP of 6.5 pH units, whereas anatase has an IEP of 4.5 pH units (Diebold, 2003). Thus, the anomalous behavior observed by Wamkam (Wamkam et al., 2011) was due to the anatase phase used in their study. Xie et al. (Xie, H. et al., 2002) reported that enhanced thermal conductivity ratio decreased pH value increased from 2 to 12 in Al_2O_3 nanofluids. Li et al. (Li, X. F. et al., 2008) showed that thermal conductivity ratio increased as pH value increased from 3 to 9.5 in a CuO–H_2O system. Lee et al. (Lee, D. et al., 2006) showed that effective thermal conductivity (Keff) increased by a factor of 3 as pH decreased from 8 to 3 in CuO–water nanofluids. Timofeeva et al. (Yu, W. et al., 2010) studied pH variation between 5.5 and 10.3 and observed a significant (34%) viscosity drop for silicon carbide (SiC)/water nanofluids, while thermal conductivity was unaffected and remained within the experimental uncertainty.

Thermal conductivity enhancements in nanofluids are significantly pH dependent. Wang (Wang, X. J. et al., 2009) obtained approximately 6% difference in thermal conductivity enhancement of Cu–H_2O between pH values of 3.30 to 9. Li (Li, Y. H., W. Qu, & Feng, 2008) observed a similar difference (~6%) between pH values of 3 to 9 for the Cu–H_2O system. In both cases, maximum thermal conductivity enhancements were obtained at pH value in which the greatest zeta potential for Cu–H_2O systems was observed (45 mV). Furthermore, thermal conductivity of water was virtually constant for all tested pH values in both studies. Thus, the surface charge or its indirect effects (e.g., agglomeration) is key in enhancing thermal conductivity of stationary nanofluids (Ismay, Doroodchi, & Moghtaderi, 2013).

Carine et al. (Carine.T. Wamkam et al., 2011) studied pH effects on thermal conductivity, zeta potential, particle size, and viscosity of nanofluids that contain TiO_2 and ZrO_2 using the Toledo model SevenEasy S20 pH meter. NF stability was influenced by pH values and IEP. Figure 2.6 shows ZrO_2 nanoparticle zeta potential and average particle size versus varying pH values. IEP (zero charge) was observed at approximately pH 6. The average particle size distribution was almost symmetrical, and the maximum size was near IEP. When pH increase or decrease and shifted away from IEP, average particle size significantly decreased from 1200 nm to 100 nm. Decreased particle size indicated that the particles were less aggregated. Repulsive forces among metal oxides at IEP are zero, and nanoparticles are coagulated at pH value below this point (Figure 2.6). According to the DLVO theory, nanoparticles become unstable when pH equals or nears IEP. They then form aggregates, cluster, and then precipitate.

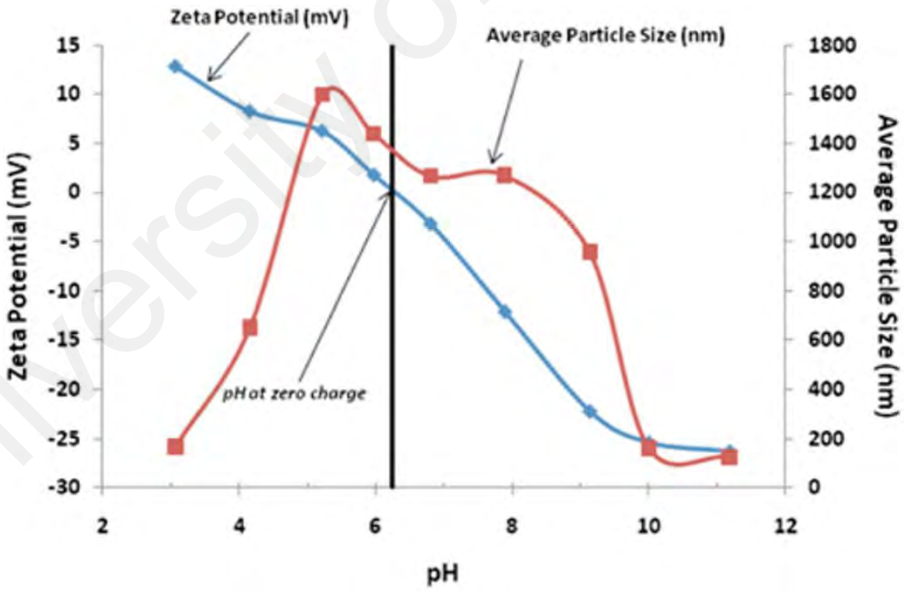

Figure 2.6. Zeta potential and average particle size of nanoparticles vs different pH values of ZrO_2 (Carine.T. Wamkam et al., 2011), Reproduced with permission from Susann Brailey, Manager, Rights and Permissions AIP Publishing LLC

Maryam et al. (Abareshi et al., 2010) studied magnetic Fe_3O_4 nanoparticles synthesized using the co-precipitation method at different pH values. X-ray

diffraction (XRD), Fourier transform infrared spectroscopy, and TEM techniques were used to characterize nanoparticle structure, purity, and size. Magnetic properties were evaluated using a vibrating sample magnetometer. Fe_3O_4 nanoparticles were dispersed with tetramethyl ammonium hydroxide into deionized water to obtain nanofluids. The experiments were conducted under different initial pH values of iron salt solutions to obtain the final pH value in forming Fe_3O_4 nanoparticles (Haddad et al., 2014). Characteristic peaks of magnetite were (2 2 0), (3 1 1), (4 0 0), (4 2 2), (5 1 1), and (4 0 0). XRD patterns show that initial pH of iron salt solutions and final pH values are essential to Fe_3O_4 nanoparticle crystallinity. Although the crystal structure of Fe_3O_4 nanoparticles did not change, reflection peaks from the MN1 to MN4 samples sharpened and narrowed, which indicated improved crystallinity. Thus, changing the final pH (from 10.5 to 9.5) and increasing the initial pH of the iron salt solution (from 1 to 1.5) significantly improved Fe_3O_4 nanoparticle crystallinity. Zhu (Zhu, D. S., 2009) investigated the dispersion behavior and thermal conductivity of Al_2O_3–water nanofluids under different pH levels. For all the experiments, 0.1 wt% alumina nanofluid concentration was used. Analytical grade hydrochloric acid (HCl) and sodium hydroxide (NaOH) were used to control the pH level of the nanofluid (Zhu, D. S., 2009). An ionic surfactant, SDBS, was added to the mixture and mixed in an ultrasonicator to assist in the initial nanoparticle dispersion. The optimum pH value of alumina nanofluids with SDBS as surfactants was 8, which is the point of greatest zeta potential. In this case, particles have the highest electrostatic repulsive forces, which keep them in suspension. Thermal conductivity of alumina nanofluid was measured using the transient plane source method. pH values of thermal conductivity increased from 3.0 to between 8.0 and 9.0. Al_2O_3 nanoparticles coagulated as pH level of the nanofluid increased further away from the point of zero change, the point where no repulsive forces existed among the nanoparticles. Consequently, hydration forces were

strong among the particles. Increased hydration forces enhanced nanoparticle mobility. The mobility of the nanoparticles created microscopic motions that caused microconvection and enhanced the heat transfer process (David Martinez, 2009). Ismay (Ismay et al., 2013) prepared the water-based titania nanofluids. The crystalline phase was confirmed by analyzing zeta potential variation with pH. Thermal conductivity enhancement was improved by 2% because of pH with large spikes of enhancement observed as fluid pH approached the IEP of TiO_2. Ding et al (Yulong Ding, 2006), studded the heat transfer behaviour of aqueous suspensions of multi-walled carbon nanotubes (CNT nanofluids), they compared the axial profiles as shown in Figure 2.7, at two Reynolds numbers, of the convective heat transfer coefficient under two pH conditions. The convective heat transfer coefficient at pH = 6 was slightly higher than that at pH = 10.5. It is unclear if the effect of pH is actually very small under other pH conditions. If the small effect of pH is proven, excellent opportunities will be provided for future industrial taking-up of the technology as both very acidic and basic suspensions would increase both the capital and operating costs and also have significant safety implications.

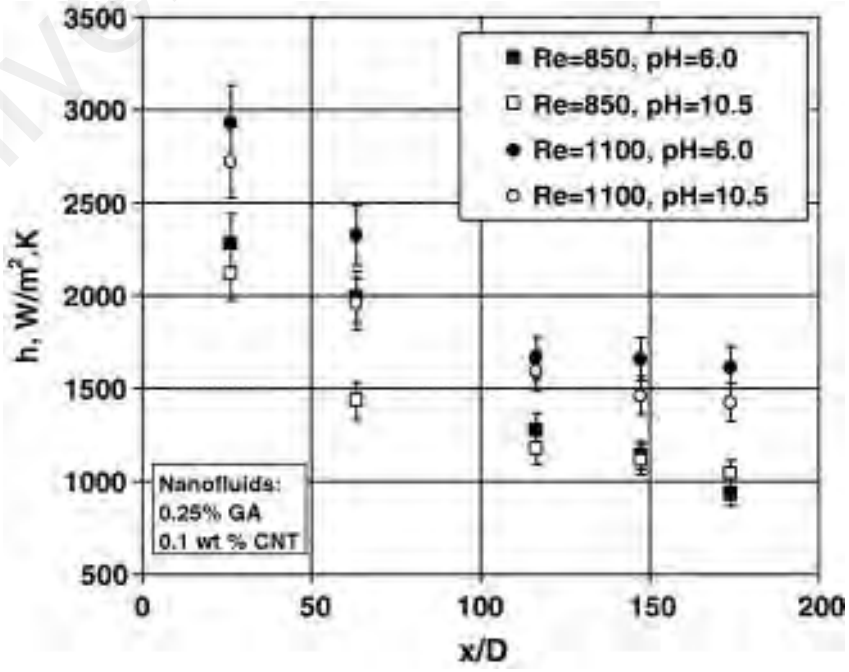

Figure 2.7. Effect of pH on the convective heat transfer (Yulong Ding, 2006).

Xie (Xie, H., 2002) studied the effect of the pH of the mixture, specific area of Al_2O_3 particles, crystalline phase in solid state, and thermal conductivity of base fluid. Thermal conductivity of Al_2O_3 nanofluid increased by increasing the difference between the pH value of the aqueous suspension (i.e., pH at which a particular molecule carries no electric charge) and IEP. Abbasian and Amani (Abbasian Arani & J. Amani, 2012) dispersed TiO_2 nanoparticles in distilled water using an ultrasonic vibrator with magnetic stirrer and stirred for approximately 3 h to break down nanoparticle agglomeration. CTAB surfactants were added at extremely low concentration (approximately 0.01%) to hinder the thermo-physical properties of the nanofluid. Therefore, pH values were between 5.62 and 7 (IEP of TiO_2 was 2.9). Fedele et al. (Laura. Fedele, Laura. Colla, & Bobbo, 2012) sonicated TiO_2 nanofluid at 35 wt% after adding distilled water at a weighed amount. The average nanoparticle dimension in the suspension was analyzed using the dynamic light scattering method. The mean diameter of TiO_2 was 76 nm at 1 wt%, 72 nm at 10 wt%, and 73 nm at 20 wt%. The nanofluids were stable at these compositions in the absence of particle aggregates. TiO_2–water nanofluid zeta potential was approximately 55 mV; the empirical limit in which colloidal suspension should be stable is only 30 mV. pH values were 1.86 for 35 wt%, 2.24 for 20 wt%, 2.37 for 10 wt%, and 3.07 for 1 wt%. Vahid et al. (Iranidokht, Hamian, Mohammadi, & Shafii, 2013) investigated the thermal conductivity of Cu–TiO_2–EG and Al_2O_3–TiO_2–EG mixed nanofluids (MN). Thermal conductivity was measured and compared with those of single particle nanofluids (SPN). After changing the pH, thermal conductivity enhancement of Cu–EG nanofluids was 4.7% at 0.1 vol% and 37% at 2 vol%. In all volume fractions, changing the pH and using surfactants increased thermal conductivity because of ion agglomeration on the nanoparticle surface. Therefore, the maximum thermal conductivity enhancement obtained for Al_2O_3–EG

nanofluid was 13% at 2.0 vol%. Furthermore, pH variation from neutral pH further enhanced thermal conductivity. At 0.1%, 0.5%, 1%, and 2 vol% nanoparticles, thermal conductivity enhancements were 0.7%, 3.2%, 7.7%, and 11.5% before pH change and 1.3%, 4.3%, 8.2%, and 13% after pH change, respectively. Thermal conductivities of all SPNs and MNs were dependent on pH values. In neutral pH, a significant difference exists between experimented thermal conductivity and estimated MN values. This difference can be decreased to a minimum by changing the pH and using SDBS as surfactant. Therefore, pH influence on various physical parameters (e.g., thermal conductivity, zeta potential, viscosity) of nanofluids should be examined further. Knowledge on the physical properties and behavior of such nanofluids at various pH values is invaluable in analyzing and synthesizing novel nanofluids (Carine.T. Wamkam et al., 2011).

2.5 Thermal and rheological properties of nanofluids

Dispersing solids in fluids to enhance thermal conductivity is an old concept. For more than 100 years, scientists and engineers have made great efforts to enhance the inherently poor thermal conductivity of liquids by adding solid particles. Maxwell and Yang (Maxwell, 1873a; Wen, Ding, Cui, & Wang, 2004; Yang, YiJun, 2011) presented a theoretical model for predicting thermal conductivity increase in solid dispersed liquids. However, particle size was limited to micrometer or millimeter, and solid particle concentrations were low because these particles settled easily. In the past decades, more than 300 research groups and companies have focused on nanofluid research because of its potential to enhance heat transfer rates. Tremendous thermal conductivity enhancement was observed (Gu et al., 2013; Mehrali, M et al., 2014; R. Sadri et al., 2014; Saidur, Leong, et al., 2011; Wang, B.-X., Zhou, L.-P., & Peng, X.-F., 2003). Further, the heat transfer properties of GNP are expected to be much different

from zero dimensional nanoparticles and one dimensional carbon materials. GNP is an excellent thermal conductor, so a GNP nanofluid is expected to display a significant thermal conductivity enhancement. In addition, synthesizing graphene nanoparticles is relatively easy and cost effective. Small variation of properties of graphene has been reported due to different methods used to manufacture one layer or multi-layer graphene such as, exfoliation of graphene oxide layer, deposition with chemical vapor and mechanical cleavage, etc. . Experimental investigation has revealed that the thermal conductivity and heat transfer properties of one layer graphene are higher than CNT. The conventional theory of Maxwell or the Hamilton–Crosser (H–C) model could not predict anomalous enhanced thermal conductivity. Several mechanisms (Keblinski, P. , S.R. Phillpot, S.U.S. Choi, & Eastman, 2002) have been proposed to explain the thermal transport properties of nanofluids. However, these models exhibited large discrepancies among themselves, significantly restricting their applicability. In the nineteenth century, Maxwell (Maxwell, 1873b) proposed an effective medium model for thermal conductivity of suspensions. The model clearly indicated that thermal conductivity of solid and liquid mixtures is higher than that of base liquids, which makes solid and liquid mixtures potential candidates for heat transfer fluids. Solids have higher thermal conductivity than liquids. However, the problems associated with using solid and liquid mixtures as heat transfer fluids include sedimentation, clogging, fouling, erosion, and excessive pressure drop. These problems have been solved with the introduction of nanotechnology. Thus, the addition of different nanoparticles into heat transfer fluids has attracted researchers. Several formulas have been introduced and extensively employed by researchers to calculate thermal conductivity of different nanofluids. According to Duangsongsuk (Duangthongsuk, W. & Wongwises), although measured thermal conductivity exhibited relatively high deviation from published correlations, a comparative study on the Nusselt (Nu) number based on both approaches provided

relatively similar results. Thus, changes in thermal conductivity exhibit a less profound effect on modulating the transport behavior of nanofluids. The series of models for calculating the thermal conductivity of nanofluids is as follows: Equation developed by Hamilton and Crosser (Hamilton & Crosser, (1962)):

$$\frac{\lambda_{nf}}{\lambda_w} = \left[\frac{\lambda_p+(n-1)\lambda_w-(n-1)\phi(\lambda_w-\lambda_p)}{\lambda_p+(n-1)\lambda_w+\phi(\lambda_w-\lambda_p)}\right] \quad (2.2)$$

$$n = 3/\psi \quad (2.3)$$

where n and ψ represent the shape factor and sphericity of the particle. Sphericity determines the ratio of the equivalent surface area of the sphere to that of the surface area of a particle with identical volume. A spherical shape has a sphericity measurement of 1, while a cylindrical shape constitutes half of the surface of the equivalent spherical shape. λ_p, λ_{nf} and λ_w denote the thermal conductivities of nanoparticle, Nanofluid and base fluid, respectively; ϕ signifies particle volume concentration.

Equation (2.4) developed by Yu and Choi (Yu, W. & Choi):

$$\frac{\lambda_{nf}}{\lambda_w} = \left[\frac{\lambda_p+2\lambda_w+2\phi(\lambda_w-\lambda_p)(1+\beta)^3}{\lambda_p+2\lambda_w-2\phi(\lambda_w-\lambda_p)(1+\beta)^3}\right] \quad (2.4)$$

where β denotes the ratio of the nanolayer thickness to the original particle radius. β is taken as 0.1 for calculating the thermal conductivity of the nanofluid.

Equation developed by Wasp (Wasp):

$$\frac{\lambda_{nf}}{\lambda_w} = \left[\frac{\lambda_p+2\lambda_w-2\phi(\lambda_w-\lambda_p)}{\lambda_p+2\lambda_w+\phi(\lambda_w-\lambda_p)}\right] \quad (2.5)$$

Equation by Murshed et al. (Murshed, Leong, & Yang):

$$\lambda_{nf} = \frac{1}{4}\left[(3\phi - 1)k_p + (2 - 3\phi)\lambda_w\right] + \frac{\lambda_w}{4}\sqrt{\Delta} \quad (2.6)$$

where

$$\Delta = \left[(3\phi - 1)^2\left(\lambda_p/\lambda_w\right)^2 + (2 - 3\phi)^2 + 2(2 + 9\phi - 9\phi^2)\left(\lambda_p/\lambda_w\right)\right] \quad (2.7)$$

Equation by Timofeeva et al. (Timofeeva, Gavrilov, McCloskey, & Tolmachev):

$$\frac{\lambda_{nf}}{\lambda_w} = (1 + 3\phi) \quad (2.8)$$

Equation by cocaine [57]:

$$\frac{\lambda_{nf}}{\lambda_w} = 1 + 4.4RE^{0.4}Pr^{0.66}\left(\frac{T}{T_{fr}}\right)^{10}\left(\frac{\lambda_s}{\lambda_w}\right)^{0.03}\phi^{0.66} \quad (2.9)$$

where *Re* is the nanoparticle Reynolds number, *Pr* is the Prandtl number of the base liquid, *T* is the nanofluid (NF) temperature, and T_{fr} is the freezing point of the base liquid. The Reynolds number is defined as $Re = (\rho_w u_B d_p)/\mu_w$, where ρ_W and μ_W are the mass density and dynamic viscosity of the base fluid, respectively, and dp and u_B are the nanoparticle diameter and Brownian velocity, respectively. Once u_B is calculated as the ratio between dp and the time required to cover distance $\tau_D = (d_p)^2/6D$ (Keblinki et al. (Keblinski, P. et al., 2002)) where *D* stands for the Einstein diffusion coefficient and the nanoparticle Reynolds number is given by Equation (2.10).

$$Re = \frac{2\rho_w K_b T}{\pi \mu_f^2 d_p} \quad (2.10)$$

where k_b=1.38066 x 10^{-23} J/K is the Boltzmann's constant. All physical properties in Equations (9) and (10) are calculated at NF temperature *T*.

Efficiency of heat transfer performance of fluids is improved by enhancing thermal conductivity and heat transfer properties. Nanostructures typically have higher thermal conductivity than conventional fluids (e.g., water, ethylene glycol, and transformer oil) and microstructures; thus, utilizing nanostructures as base fluids has been proposed (Ghozatloo et al., 2013). Heat transfer performance of fluids is improved by adding nanostructures, which should be stable in the fluid. Graphene has an extremely high thermal conductivity of approximately 5000 W/Mk (corrected) (Alexander et al., 2008). Thus, thermal conductivity behavior would be interesting to study as a two-dimensional structure (Chandrasekar, Suresh, & Senthilkumar, 2012; Mehrali, Mohammad, Sadeghinezhad, Emad, Tahan Latibari, Sara, Mehrali, Mehdi, Togun, Hussein, & Zubir, M. N. M., 2014; Sadeghinezhad, emad et al., 2014b; Tessy Theres Baby, 2010).

The degree of thermal conductivity enhancement is inconsistent with research on thermal properties of nanofluids. Researchers have observed abnormal thermal conductivity enhancement in nanofluids. However, when they tested the same type of nanofluids from the same source during the International Nanofluid Property Benchmark Exercise (INPBE), researchers observed no abnormal thermal conductivity enhancement. Table 2.1 shows the reproduced results, and Table 2.2 summarizes the results of thermal conductivity measurement from different research centers in the past 15 years. Earlier measurements by several investigators indicated that the thermal conductivity of nanofluids could be influenced by several parameters in the colloid system. Such parameters are base fluid type, particle size, particle shape, pH value in aqueous fluids, and temperature. Xie et al. (Xie, H., Lee, & Youn, 2003) reported the

effect of base fluid on thermal conductivity of nanofluids. They dispersed treated CNT in three different base fluids (i.e., decene, distilled water, and ethylene glycol). Decene-based nanofluids have the highest enhancement in thermal conductivity, followed by ethylene glycol-based nanofluids, and distilled water-based nanofluids have the least enhancement. Li and Peterson (Li, C. & Peterson, 2006) documented the effect of particle size on thermal conductivity enhancement. They showed that 36 nm Al_2O_3 in water had larger thermal conductivity enhancement than 47 nm Al_2O_3 in water, especially at high temperatures (35.5 °C); however, the difference between these two nanofluids is indistinguishable at 28 °C. Chen and Yang (Chen, H. & Yang, 2008) observed that aqueous suspension of titanate nanotubes (aspect ratio is approximately 10) have higher thermal conductivity enhancement than that predicted by the Hamilton–Cross model. Timofeeva et al. (Timofeeva, Routbort, & Singh, 2009) reported that the effective thermal conductivity predicted by the Hamilton–Cross model is significantly diminished by interfacial effects proportional to the total surface area of nanoparticles; the results were consistent with the prediction of the Hamilton–Cross model for spherical particles. Timofeeva et al. (Timofeeva et al., 2009) also discussed the pH effects on their samples. Acidic environments (pH < 7) are suitable for most nanoparticles. Figure 2.8 (a) demonstrates the thermal conductivity enhancement of TiO2–EG nanofluid. Changing pH also had a favorable impact on TiO2–EG nanofluid thermal conductivity. The enhancement of thermal conductivity for TiO2–EG nanofluid after changing the pH in 2 vol% was 18%, which shows 2.5% more increment compared to unchanged pH case. Similarly, in 0.5 vol% after changing pH thermal conductivity enhancement was 7.1%, which shows 0.7% more increment compared to previous case. Figure 2.8(b) shows two studies by Mauro et al (Lomascolo, Colangelo, Milanese, & de Risi, 2015) on Al_2O_3–water nanofluids of various pH values, and investigates CuO–water nanofluids of two pH values (3 and 6). In particular the researcher explains the

dependence of thermal conductivity on the solution pH, assuming that an increase in difference between isoelectric point of the Al_2O_3 particle and pH value of the solution increases the mobility of particles, which, as a consequence, increases the micro-convection effect of heat. In order to improve the thermal performance of the solar collector Goudarzi et al (Goudarzi, Nejati, Shojaeizadeh, & Asadi Yousef-abad, 2015) used nanofluids at various pH values as base fluids. Water based CuO nanofluid was used as the working fluid. After the preparing of this nanofluid at 0.1 wt.% of nanoparticles, its pH was set at three different values (3, 6 and 10.5). Figure 2.8 (c) indicates the efficiencies of the solar collector with nanofluid at these three pH values in 0.0083 kg/s mass flow rate of fluid, versus the reduced temperature parameter, (Ti-Ta)/Ib. It can be seen that the collector efficiency decreases with increase in the value of pH. This behavior can be explained by comparing of the pH of the nanofluid with the pH of isoelectric point of nanoparticles. The pH of isoelectric point for CuO is 9.5. Thus the efficiency of the solar collector at pH = 3 was higher than that for pH = 10.5 by about 108%.

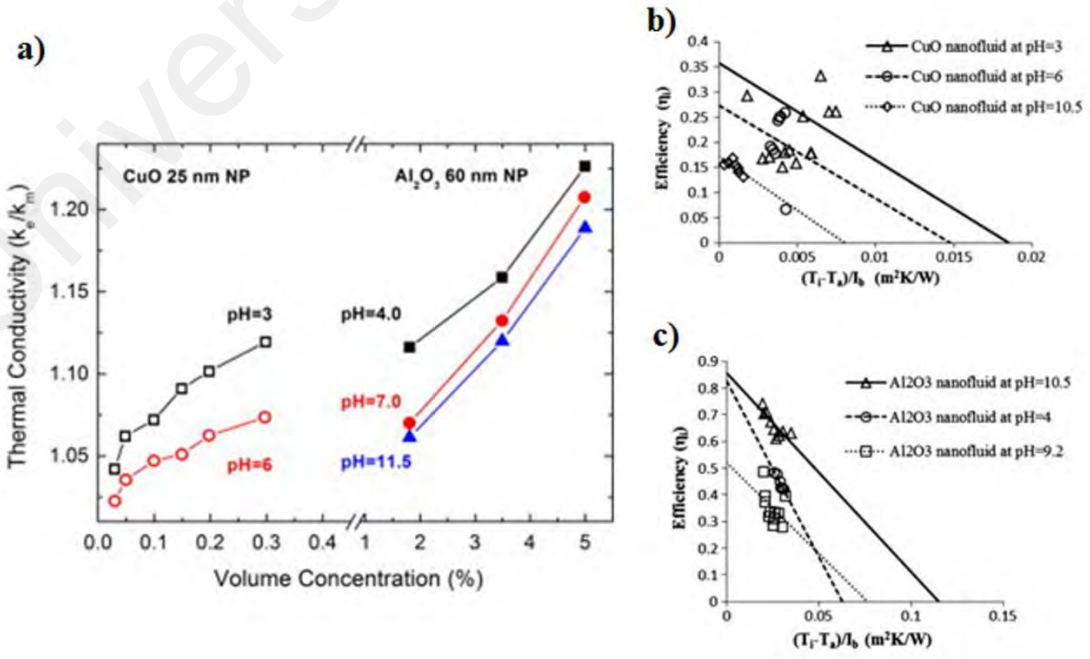

Figure 2.8. (a) Thermal conductivity enhancement of TiO2eEG nanofluid with pH of 9.5 and SDBS mass fraction of 1%, (b) Fig. 2.10. ke/k0 As a function of volume concentration, for various nanofluids. Role of pH. Right side: Al_2O_3 60 nm NP in water; left side CuO 25 nm NPs in water, (c) The efficiency of the cylindrical solar collector with CuO nanofluid at three different pH values (Goudarzi et al., 2015; Iranidokht et al., 2013; Lomascolo et al., 2015)

Several studies have reported on the effect of temperature on thermal conductivity of nanofluids. Chen and Yang (Chen, H. & Yang, 2008) reported that thermal conductivity increases with the increase of the temperature of the nanofluid. This conclusion is similar with that of Li and Peterson (Li, C. & Peterson, 2006), who found that thermal conductivity significantly increases with small increases in temperature. A total of 6% volume fraction of CuO nanoparticle/distilled water suspension increased the effective thermal conductivity by 1.52 times that of pure distilled water, and 10% Al_2O_3 nanoparticle/distilled water suspension increased the effective thermal conductivity by a factor of 1.3 at 34 °C. However, some researchers documented that thermal conductivity increased only slightly as the temperature of nanofluids increased slightly. Chon and Kihm (Chon & Kihm, 2005) observed a lesser increase in thermal conductivity than that of Das at the same temperature range. Thermal conductivity increase at different temperatures is affected by particle size in the colloid system. Small particle size in the nanofluids result in large thermal conductivity increase at high temperatures, whereas large particles in the nanofluids result in small thermal conductivity increase at high temperatures. However, Timofeeva et al. (Timofeeva, Gavrilov, McCloskey, & Tolmachev, 2007) argued that thermal conductivity enhancement of nanofluids relative to base fluids at elevated temperatures is independent of temperature by investigating both water- and EG-based nanofluids.

Table 2.1. Summary of INPBE results (Buorgiorno, 2009)

Sample description	Measured k (W/mK)	Measured k/kf	Predicted k/kf Lower bound	Predicted k/kf Lower bound
Alumina nanorods (80 × 10 nm^2), 1 vol% in DI water	0.627±0..013	1.036±0.00 4	1.024	1.086
DI water	0.609±0..003	n/a	n/a	n/a
Alumina nanoparticles (10 nm), 1 vol% in PAO+surfactant	0.162±0..004	1.039±0.00 3	1.027	1.03

Alumina nanoparticles (10 nm), 3 vol% in PAO+surfactant	0.174±0..005	4	1.121±0.00	1.083	1.092
Alumina nanorods (80 × 10 nm^2), 1 vol% in PAO+surfactant	0.164±0..005	3	1.051±0.00	1.07	1.116
Alumina nanorods (80 × 10 nm^2), 3 vol% in PAO+surfactant	0.182±0..006	5	1.176±0.00	1.211	1.354
PAO+surfactant	0.156±0..005		n/a	n/a	n/a
Gold nanoparticles (10 nm), 0.001 vol% in water +stabilizer	0.613±0..005	3	1.007±0.00	1	1
water+stabilizer	0.604±0..003		n/a	n/a	n/a
Silica nanoparticles (22 nm), 31 vol% in water+stabilizer	0.729±0..007	0	1.204±0.01	1.008	1.312
DI water	0.604±0..002		n/a	n/a	n/a
Mn–Zn ferrite nanoparticles (7 nm), 0.17 vol% in water +stabilizer	0.459±0..005	8	1.003±0.00	1	1.004
water+stabilizer	0.455±0..005		n/a	n/a	n/a

Table 2.2. Previous data for thermal conductivity of nanofluids

Investigator	Particle size and shape	Base Fluids	Observations
Choi and Eastman (Choi, S.U.S & Eastman, 1995)	Cu (0.3,0.5,1.0) sphere size is unknown	Water	5% to 20% VF, 10% to 250% improvement
Eastman et al. (Eastman et al., 2001)	Cu sphere 10 nm	EG	0.1% to 0.25% VF, 2% to 40% improvement
	CuO sphere 35 nm	EG	1% to 4% VF, 5% to 22% improvement
	Al_2O_3 sphere size is unknown	EG	1% to 3% VF, 2% to 14%
Garg et al. (Garg et al., 2008)	CuO sphere 200 nm	EG	0.4% to 2.00% VF, 2% to 12.5% improvement
Chen and Wang (Chen, H. & Yang, 2008)	TiO_2 tube shape 10 nm × 100 nm 20 °C	water	0.25% to 0.6% VF, 2.5% to 4% improvement
	TiO_2 tube shape 10 nm × 100 nm 40 °C	water	0.25% to 0.6% VF, 4% to 5.5% improvement
Xie et al. (Xie, H. et al., 2003)	Treated CNT sphere 50 nm	Decene	0.25% to 1.0% VF, 5% to 20% improvement
	Treated CNT sphere 50 nm	Distilled water	0.4% to 1.0% VF, 3% to 7% improvement
	Treated CNT sphere 50 nm	EG	0.25% to 1.0% VF 3% to 12% improvement
Das et al. (Das, S. K., Putra, Thiesen, & Roetzel, 2003)	Al_2O_3 sphere 38.4 nm	Water	1.0% to 4.0% VF, 2% to 8% improvement
	CuO sphere 23.6 nm	Water	1.0% to 4.0% VF 7% to 14% improvement
Patel et al.	Au thiolate sphere 3	Water	0.005% to 0.011% VF 2.2% to

(Patel et al., 2003)	nm to 4 nm 29 °C		6.2% improvement
	Au thiolate sphere 3 nm to 4 nm 40 °C	Water	0.005% to 0.011% VF, 5% to 9.2% improvement
	Au thiolate sphere 3 nm to 4 nm 50 °C	Water	0.005% to 0.011% VF, 6.8% to 11% improvement
	Ag thiolate sphere 10 nm to 20 nm 30 °C	Water	0.001%VF 3%
	Ag thiolate sphere 10 nm to 20 nm 40 °C	Water	0.001%VF 7%
	Ag thiolate sphere 1020 nm 50 °C	Water	0.001%VF11%
Murshed et al. (Murshed, Leong, & Yang, 2005)	TiO_2 sphere 15 nm	Water	1% to 5% VF, 18% to 29.7% improvement
	TiO_2 tube shape 10 nm × 40 nm	Water	1% to 5% VF, 22% to 32.8% improvement
Das et al., Xie et al. (Das, S. K., Choi, & Yu, 2008; Xie, Wang, Xi, & Liu, 2002)	SiC sphere 26 nm	Distilled water	1.5% to 4.2% VF, 5% to 15% improvement
	SiC sphere 600 nm	Distilled water	1.0% to 4.0% VF, 6.5% to 22% improvement
Choi et al. (Chon & Kihm, 2005; Das, S. K. et al., 2008)	Al_2O_3 sphere 11 nm	Water	1% VF 22%
	Al_2O_3 sphere 47 nm	Water	1% VF 7%
	Al_2O_3 sphere 150 nm	Water	1% VF 2%
Xuan and Li, Das et al. (Das, S. K. et al., 2008; Xuan, Y. & Li, 2000)	Cu sphere 100 nm	Transformer oil	2.2% to 7.6% VF, 12% to 42% improvement

Bouriorno (Buorgiorno, 2009) launched the INPBE, and 34 research centers around the globe participated in the program. Four different nanofluid samples were procured and sent to the centers. The centers were made to adhere to the same sample handling protocol. Measured data were organized by MIT. Nan's modified Maxwell's model was employed to predict the thermal conductivity ratio of nanofluids (W. Nan, R. Birringer, D. R. Clarke, & H. Gleiter, 1997). The model determined the effects of particle geometry and finite interfacial resistance. The expression of the model is presented in Equation (2.11).

$$\frac{k}{k_f} = \frac{3 + j\,[2b_{11}(1 - L_{11}) + b_{33}(1 - L_{33})]}{3 - j\,(2b_{11}L_{11} + b_{33}L_{33})} \qquad (2.11)$$

where represent particles shaped as prolate ellipsoids with principal axes $a_{11} = a_{22} < a_{33}$

$$L_{11} = \frac{p^2}{2(p^2 - 1)} \quad \frac{p}{2(p^2 - 1)^{3/2}} \quad \cosh^{-1} p,$$

$$L_{33} = 1 - 2L_{11},\ p = a_{33}/a_{11},$$

$$b_{ii} = \frac{k_{ii}^{c} - k_f}{k_f + L_{ii}(k_{ii}^{c} - k_f)}$$

$$, \quad k_{ii}^{c} = \frac{k_p}{1 + \gamma L_{ii}}$$

k_p/k_f

$$\gamma = (2 + 1/p)\, R_{bd} k_f / (a_{11}/2)$$

R_{bd} is the (Kapitza) interfacial thermal resistance. The upper bound of this prediction neglected interfacial thermal resistance ($R_{bd} = 0$), while the lower bound used a typical value of interfacial resistance (10^{-8} m^2 K/W). The final results showed that thermal conductivity enhancement of nanofluids is predicted by the lower bound theory with a < 17% error, while the upper bound theory predicts 90% of data with a < 18% error. Shape size has a key function in thermal conductivity enhancement of nanofluids. Thermal conductivity of nanofluids has been thoroughly investigated, but discrepancies still exist. The nature of particles, heat transfer fluid, and particle size and distribution affect the physical properties of nanofluid. The nanofluid synthesis process should be standardized and fully understood. Measurement methods also strongly influence the results of measured physical properties.

Theoretical mechanisms have been proposed to explain anomalous effective thermal conductivity enhancement. These mechanisms include the Brownian motion of particles, nanolayer structure at the interface nanoparticle medium, and nanoparticle clustering or agglomeration (Lamas, Abreu, Fonseca, Martins, & Oliveira, 2014). Keblinski et al. (Keblinski, P. et al., 2002) proposed to neglect the Brownian motion because the theoretical Brownian diffusion of nanoparticles is slower than thermal diffusion of the base fluid. Moreover, researchers observed from experimental studies that the dependence of thermal conductivity enhancement on Brownian mechanisms is negligible because they simply follow the temperature behavior of the base fluid. The nanolayer theory states that liquid molecules near solid surfaces become more organized than bulk liquids and form a solid-like layer that enhances heat conduction through the

medium. However, Kapitza resistance at the nanoparticle medium interface could negatively affect possible enhancements from the nanolayer structure. A recent benchmark study suggested that effective thermal conductivity of nanofluids depends on the effective medium theory, which states that spatial distribution of particles in the medium is the key to observed enhancements (Lamas et al., 2014). The most commonly studied nanoparticles in thermal nanofluid engineering include Cu, CuO, Al_2O_3, and CNTs (Li, F.-C. et al., 2013; Ponmozhi et al., 2009). CNT-based nanofluids exhibit the highest enhancement on effective thermal conductivity under the same experimental conditions (Evans, William et al., 2008). This condition is explained by the high thermal conductivity and geometrical aspect of individual CNTs (Hasselman & Johnson, 1987; Lamas et al., 2014).

Phuoc et al. (Phuoc et al., 2011) prepared the nanofluids by dispersing MWCNTs in deionized water (DW). Thermal conductivity enhanced from 2.3% to 13% for nanofluids with 0.5 wt% to 3 wt% MWCNTs (0.24 vol% to 1.43 vol%). Choi et al. (Choi, S.U.S. , Z.G. Zang, W. Yu, F.E. Lookwood, & Grulke, 2001) reported significant enhancements for MWCNTs (mean diameter: 25 nm and length: 50 μm) in oil suspension at room temperature. Thermal conductivity increased by more than 160% at 1% volume fraction compared with that of the base fluid. Ding et al. (Ding, Alias, Wen, & Williams, 2006) reported a maximum enhancement of 79% at 1 wt% MWCNT dispersed in water with SDBS as surfactant. Assael et al. (Assael, C.F. Chen, I. Metaxa, & Wakeham, 2004) observed thermal conductivity enhancement of 38% for 0.6 vol% CNTs in water stabilized by SDS and CTAB. Ghozatloo (Ghozatloo et al., 2013) investigated the thermal conductivity of functionalized graphene nanofluids prepared via the alkaline method. Nanosheet graphene was synthesized using chemical vapor deposition (CVD). Thermal conductivity enhancement was 13.5% for sample 1 (0.05

wt%) and 12.5% for sample 2 (0.03 wt%) at 25 °C; sample 1 increased to 17% at 50 °C. Feng et al. (Li, F.-C. et al., 2013) prepared viscoelastic fluid-based nanofluids (VFBN) using viscoelastic aqueous solution of cetyltrimethyl ammonium chloride/sodium salicylate as base fluid and MWCNTs as nanoparticles. The experimental thermal conductivities of the tested VFBNs were significantly higher than those of corresponding base fluids. These thermal conductivites increased as particle volume fraction and fluid temperature increased, which demonstrated potential for heat transfer enhancement. With significantly increasing thermal loads in microelectronics and higher-powered automobiles, the need for high performance cooling fluids increases each year. Conventional approaches that use extended surfaces require additional pumping power and have been assumed to have reached their limits. Various attempts have been made to increase the thermal conductivity of the fluid itself (Lee, D. et al., 2006). Choi (Choi, 1995) presented the possibility of using a new type of fluid-containing nanoparticles in 1995, and large enhancements that exceed 100% in effective thermal conductivity (*K*eff) of these fluids were reported. This prospect for fluids and nanofluid enhancement triggered researchers to determine the best combinations of particles and solvents (Choi, S. U. S., Zhang, Yu, Lockwood, & Grulke, 2001; Eastman et al., 2001; Lee, Choi, Li, & Eastman, 1999; Murshed et al., 2005; Patel et al., 2003; Timofeeva et al., 2007; Timofeeva et al., 2009; Tu, Dinh, & Theofanous, 2004; Wen & Ding, 2005; Xie et al., 2002; Xuan, Li, & Hu, 2003; Xuan, Y. & Li, 2000; You, Kim, & Kim, 2003) and to clarify governing mechanisms (Jang & Choi, 2004; Keblinski, P. et al., 2002; Kumar et al., 2004; Wang, Zhou, L. P., & Peng, X. F., 2003).

Different mechanisms have been proposed to explain thermal transport enhancement, including interfacial resistance, nanoparticle motion, liquid layering at particle liquid interface, and nanoparticle clustering (Eastman, Phillpot, Choi, & Keblinski, 2004).

Nanoparticle motion (Brownian motion) (Bhattacharya, Saha, Yadav, Phelan, & Prasher, 2004; Chon & Kihm, 2005; Koo & Kleinstreuer, 2004; Krishnamurthy, Bhattacharya, Phelan, & Prasher, 2006; Prasher, Bhattacharya, & Phelan, 2005, 2006; Wong, K. F. V. & Kurma, 2008), and nanoparticle clustering (Hong, K. S., Hong, & Yang, 2006; Lee, D. et al., 2006; Prasher, Phelan, & Bhattacharya, 2006; Wang, B.-X. et al., 2003; Xuan et al., 2003; Yu, W. & Choi, 2004) have attracted the most attention.

Keblinski et al. (Keblinski, P. et al., 2002) proposed three conceivable mechanisms that are important for abnormal increases (i.e., Brownian motion, liquid layering, and ballistic phonon transport). These mechanisms provide insight into the most important factor that affects effective thermal conductivity (K_{eff}). Although the effect of Brownian motion was shown to be negligible through a scaling analysis, a few researchers still argue its influence. For example, (Jang & Choi, 2004) and (Kumar et al., 2004) derived their own formulas to consider the nanoconvection caused by Brownian motion. Both predicted K_{eff} well using different equations (Kumar et al., 2004). Both also disregarded metal oxide particles to validate the high aggregation in the Brownian models (Jang & Choi, 2004; Kumar et al., 2004; Lee, D. et al., 2006). Aggregate particles move more slowly than isolated particles. Thus, mobility equivalent size (often called hydrodynamic size) should be used instead of primary particle size.

Researchers (Keblinski, P. et al., 2002; Xue & Xu, 2005; Yu, W. & Choi, 2004) claimed that liquid layering at the particle liquid interface is the most important mechanism and supported its validity by predicting K_{eff} using their models. Estimations were based on arbitrarily assumed values for thermal conductivity and thickness of the interfacial layer. Furthermore, theories and experimental data that quantitatively discuss ballistic phonon transport are unavailable. Two groups (Patel et al., 2003; Xie, H. et al., 2002) added another important factor (i.e., surface chemical effect), which is not understood by all pre-existing models. Xie (Xie, H. et al., 2002) presented that a simple

acid treatment of CNTs enhanced the suspension stability of CNT in water. This enhancement was attributed to hydrophobic-to-hydrophilic conversion of the surface nature because of the generation of a hydroxyl group. Patel and Das (Patel et al., 2003) reported that 4 nm Au nanoparticles coated in covalent chains of toluene were approximately 50 times less effective for heat transport than 10 mm to 20 nm uncoated nanoparticles in water. This finding is the exact opposite of the conventional size effect (Jang & Choi, 2004; Kumar et al., 2004; Lee, D. et al., 2006; Xie et al., 2002).

The hypothesis of thermal transport enhancement because of Brownian motion was theoretically and experimentally proven as inconclusive (Evans, W., Fish, & Keblinski, 2006; Keblinski, P. & Thomin, 2006; Vladkov & Barrat, 2006). Nanoparticle aggregation (clusters) plays a significant role in the thermal transport in nanofluids. A light scattering method shows that cluster size (caused by aggregation) in Fe-ethylene glycol nanofluids increased from 1 micron to 2.4 microns after sonication during a 50 min waiting time (Hong, K. S. et al., 2006). Thermal conductivity is enhanced in aggregates/clusters, especially for highly conducting particles, by the percolation effect. However, sedimentation will increasingly occur when aggregate size exceeds the threshold value. Small particle size and short distance among particles increase aggregation probability. Low pH values imply high surface potential and, consequently, high repulsive energy and less aggregation (Gharagozloo, Eaton, & Goodson, 2008; Krishnamurthy et al., 2006; Lee, D. et al., 2006; Wensel, J. et al., 2008; Williams, Bang, Forrest, Hu, & Buongiorno, 2007).

According to the DLVO theory, *p*H notably influences nanoparticle aggregation. The high surface energy of nanoparticles allows for easy coagulation and difficult dispersion in the base fluid. This condition changes the morphology and volume fraction of the nanoparticles, which cause low fluidity (Keblinski, P. & Thomin, 2006; Lee, D. et al., 2006; Li, X. F. et al., 2008). Therefore, controlling the coagulation of nanoparticles in

the nanofluid is a primary issue to exploit their potential benefits and applications. In nanofluids, controlling nanoparticle coagulation significantly evaluates dispersion stability behavior (Li, X. F. et al., 2008; Nguyen et al., 2007).

Keblinski (Keblinski, P., Prasher, & Eapen, 2008) argued that the conventional method of comparing the measured thermal conductance of nanofluid with the classical effective medium theory has generated misconception among researchers. Therefore, he revised the existing concept by introducing upper and lower bounds for the property based on the work of Hashin–Shtrikman (Hashin & Shtrikman, 1962a 1963) to reflect a realistic theoretical prediction that represents the experimental data. The bound was constructed as mathematical inequality in which the lower bound reflects a set of well-dispersed nanoparticles in a fluid matrix, which corresponds to the Hamilton–Crosser theory based on the work of Maxwell on well-dispersed particles (Hamilton & Crosser, (1962) ; Maxwell, 1881). The upper bound describes large pockets of fluid separated by linked, chain-forming, or clustered nanoparticles. The bounds do not provide precise mechanisms of thermal conductance but sets restrictive limits based on the volume fraction alone. Adopting this concept could eliminate abnormal or anomalous concepts from NF research on thermal conductivity enhancement of nanofluid.

The rheological properties of colloids have been extensively studied in the past century. Einstein proposed a theoretical equation to predict viscosity of very diluted colloid systems (less than 1% by volume). Researchers have attempted to improve viscosity models for colloids. The hydrodynamic interaction among particles becomes important as concentration increases because fluid disturbance around one particle interacts with that around other particles. Batchelor (Batchelor, 1977) considered this factor and proposed an improved model to predict colloid viscosity at relatively high concentrations. Multiple particle colloids become important as concentrations further increase; this finding has not been analyzed rigorously. Krieger (Krieger & Dougherty,

1959) proposed a semi-empirical correlation for shear viscosity in 1959 to cover the entire range of concentrations. Researchers (Abdulagatov & Azizov, 2006; Goodwin & Hughes, 2000; Larson, 2005) experimentally investigated the rheological properties of colloids. Olhero and Ferreira (Olhero & Ferreira, 2004) investigated particle size and distribution effects on colloid viscosity. Fine particle sizes resulted in high viscosity, whereas large particle distribution decreased viscosity. However, the rheological properties of nanofluids have rarely been examined.

The results from different centers are inconsistent. The rheological property of nanofluids depends on synthesis methods of nanofluids and colloid particle size and distribution. Chen (Chen, H., Ding, & Tan, 2007) obtained viscosity measurements of TiO_2 particles in EG for low nanoparticle concentrations. Nanofluids behaved as Newtonian fluids, and viscosity is a strong function of concentration and temperature. The viscosity increase of colloids was larger than the value predicted by Einstein, and the value was fitted by the modified Krieger–Dougherty equation. Prasher et al. (Prasher, Song, Wang, & Phelan, 2006) investigated viscosity of alumina in PG at various shear rates, temperatures, and concentrations. nanofluids also behaved as Newtonian fluids, and relative increases in viscosity were independent of temperature. The viscosity of nanofluids increased as the volume percentage of nanoparticles increased. Several researchers also investigated the effect of particle shapes. Kwak et al. (Kwak & Kim, 2005) conducted experiments on 10 nm to 30 nm CuO nanoparticles with an aspect ratio of 3 in EG. Nanofluids at low concentrations displayed the non-Newtonian effect; shears decrease as shear rates increase.

Nanofluid viscosity is generally governed by particle size and morphological structure for specific nanoparticle loading; small and high length-to-width ratio particles yield high value (Jia-Fei, Zhong-Yang, Ming-Jiang, & Ke-Fa, 2009). Nanofluids with

pH close to the IEP of the particle exhibit the highest viscosity because of substantial particle agglomeration. However, viscosity can reach its maximum at pH value at the highest particle charge density depending on particle size (Jia-Fei et al., 2009). Furthermore, aside from pH adjustment, the addition of surfactant modifies the rheological properties of nanofluids (Xian-Ju & Xin-Fang, 2009). Classifying nanofluids as non-Newtonian fluids is an intensely debated subject within the academic field (Chen, H. et al., 2007; Lee, J.-H. et al., 2008; Prasher, Song, et al., 2006). The contradictory findings suggest several inconclusive issues that pertain to the inherent properties of nanofluids. Table 2 shows that available experimental data from different research groups vary extensively and should be investigated further.

2.6 Heat transfer performance

The enhancement of the heat transfer coefficient is a better indicator than thermal conductivity enhancement for nanofluids used in the design of heat exchange equipment. Researchers have investigated heat transfer performance and flow characteristics of various nanofluids with different nanoparticles and base fluid materials (Albadr, Tayal, & Alasadi, 2013; Kakaç & Pramuanjaroenkij, 2009; Sonawane, Khedkar, & Wasewar, 2013).

Results on heat transfer performance of nanofluids differ from one research center to another. Heat transfer performance in nanofluids has two major schools of thought. The first school of thought claims that significant increases in heat transfer coefficient can be achieved without sacrificing pumping power; the school is led by (ref name) (Choi, S. U. S. et al., 2001). The second school of thought claims that heat transfer coefficient enhancement is limited, and enhancement is offset by increasing pumping power. The second school of thought is represented by (Williams, Buongiorno, & Hu, 2008) from MIT and by (Kabelec, S. & Kuhnke, 2006) from Helmut Schmidt University. Table 2.3

lists the results of both groups.

Majority of earlier investigation on nanofluid regarding thermophysical properties and heat transfer coefficient was done on single nanoparticles; based on them, graphene based nanofluids provided the best heat transfer coefficient. Synthesis of nanocomposite and preparation of nanofluid based on nanocomposite are very new and interesting topic for researcher (Amiri , Shanbedi. M, Eshghi. H, Heris. S.Z, & M., 2012; Jha & Ramaprabhu, 2008; T.T & R. Sundara., 2011; Tabandeh-Khorshid et al.). Suresh et al (S, K, P, & M, 2012) used Hybrid nanofluids of Al_2O_3–Cu and investigated the results experimentally. They reported that about 14% enhancement in Nusselt number for laminar flow was achieved in comparison with pure water. Sunder et al (S et al., 2012) synthesized MWCNT-Fe3O4 nanocomposite and prepared hybrid nanofluid and achieved 31% improvement in Nusselt number at 0.3% volume concentration and at Reynolds number of 22,000. However, the nusselt number and heat transfer coefficient of a nanofluid also depends on a number of other factors, such as thermal conductivity and specific heat capacity of the base fluid and nanoparticles, the flow pattern, the viscosity of the nanofluid, the concentration of the suspended nanoparticles, the dimensions and the shape of the particles as well as the flow structure (M. Memari, A. Golmakani, & A.M. Dehkordi, 2011; W. Azmi, K. Sharma, P. Sarma, R. Mamat, & S. Anuar, 2014). Only a limited investigations have been performed on the dependence of the convective heat transfer of carbon-based nanofluids on relevant thermophysical properties.

Shriram et al. (Sonawane et al., 2013) studied the heat transfer characteristics of Al_2O_3–water nanofluids as coolants used in concentric tube heat exchanger. The experiments were conducted in a wide range of Reynolds numbers and nanoparticle volume concentrations. For the same range of Reynolds numbers, adding nanoparticles

to the base fluid enhanced heat transfer performance, which resulted in higher heat transfer coefficients than that of the base fluid. Khairul et al. (Khairul et al., 2014) studied the effects of water and CuO–water nanofluids in a corrugated plate heat exchanger. The heat transfer coefficient of CuO–water nanofluids increased from approximately 18.50% to 27.20% compared with nanoparticle volume concentration of water from 0.50% to 1.50%. Increments of particle volume fraction and volume flow rate also enhanced the friction factor, which resulted in high pressure drop and pumping power. Yang et al. (Yanga et al., 2013) studied the heat transfer performance of viscoelastic fluids, water-based Cu nanofluid and viscoelastic-fluid-based Cu nanofluid in a circular pipe at a Peclet number of 40000. Significant enhancement was observed in local convective heat transfer performance. Heat transfer enhancement rates increased as the volume fraction of nanoparticles and fluid temperature increased. The Brownian motion and decreased thermal boundary layer are the two main factors in enhancing heat transfer performance.

Razi et al. (Razi, Akhavan-Behabadi, & Saeedinia, 2011) studied heat transfer and pressure drop characteristics of the pure base oil and CuO-base oil nanofluid flow inside the round tube and flattened tubes under constant heat flux. Five round copper tubes of 12.7 mm outer diameter, 0.6 mm wall thickness and 1200 mm length are selected. Four tubes of them are flattened into oblong shapes with internal heights of 9.6 mm, 8.3 mm, 7.5 mm, and 6.3 mm and the fifth one is used as a round tube. he experimental system used in this study was shown schematically in Figure 2.9.

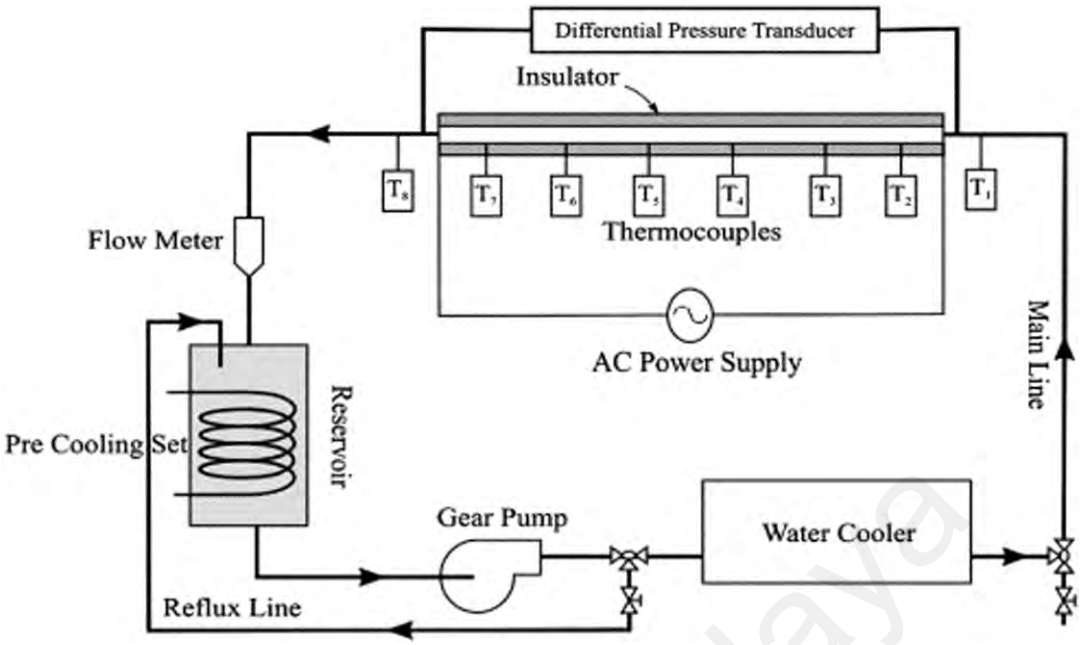

Figure 2.9. Experimental setup for the study of the flow and heat transfer characteristics of the CuO-base oil nanofluid flow inside the round tube and flattened tubes under constant heat flux (Razi et al., 2011)

To evaluate the overall performance of the two enhanced heat transfer techniques utilized, a new parameter called "performance index" was defined to consider both heat transfer and pressure drop characteristics, simultaneously.

Experimental results showed that, for a given flattened tube and at a same flow conditions, there is a noticeable increase in heat transfer coefficient as well as pressure drop of nanofluids compared to that of base liquid. Also, at the same flow conditions and for a given nanofluid with constant particle concentration, flattened tubes enhance the heat transfer rates compared to that of the round tube, significantly. As the tube profile is more flattened, this enhancement is more pronounced. The same enhancement trend in pressure drop is seen when the tube profile is becoming more flattened.

Table 2.3. Summary of experimental results for heat transfer performance of nanofluids

Investigator	Particle size and shape	Base fluids	Observations
Williams et al. (Williams et al., 2008)	Al_2O_3 sphere size	water	No Nu increase was observed
Kabelec and Kuhnke (Kabelec, S. & Anoop, 2008)	Al_2O_3sphere size	water	Heat transfer coefficient in the turbulent regime does not exhibit any remarkable increase that exceeds measurement uncertainty
Wen and Ding (Wen & Ding, 2004)	Al_2O_3 sphere 30 nm	water	0.6% VF Re=1050 x/D from 25 to 155 1.3% to 12.5% increase in h
	Al_2O_3 sphere 30 nm		Higher h improvement in lower x/D value (close to entry region)
	Al_2O_3 sphere 30 nm	water	0.6% VF Re=1050 x/D from 25 to 155 1.3% to 9.5% increase in h

	Al_2O_3 sphere 30 nm	water	Higher h increase in lower x/D value (close to entry region)
Zeinali et al. (Zeinali Heris, Etemad, & Nasr Esfahany, 2006)	Al_2O_3 sphere 20 nm	DI water	Re=650 to 2050, 0.2% to 3.0%VF 10% to 35% increase in h
Xuan et al. (Xuan, Y. M., Li, & Wang, 2003)	Cu sphere under 100 nm		Re=10000, 0.3% to 2.0%VF 1% to 27% increase in Nu Re=15000, 0.3% to 2.0%VF 1% to 39% increase in Nu Re=17500, 0.3% to 2.0%VF 1% to 39% increase in Nu
		DI water	Re=20000, 0.3% to 2.0%VF 1% to 38% increase in Nu
Yulong et al. (Yulong Ding, 2006)	MCNT-twisted string size unknown 2.5 wt% GA stabilizer	Distilled water	Re=800, 0.1% to 0.5%wt 10% to 350% increase in h at different locations Acidic (PH=6) has higher increase in h than PH=10.5
Phelan and Lai (Phelan & Lai, 2009)	Al_2O_3 sphere 20 nm to 56 nm	water	Re=22 to 900, 0.2% to 1%VF, 3% to 59% increase in Nu Higher Re higher increase in Nu Higher VF higher increase in Nu

After Choi and Eastman announced that thermal conductivity of base fluids significantly increases with the addition of nanosized solid particles, researchers have begun to work on heat transfer performance of nanofluids in pipe flow, including both natural and forced convection. Wen and Ding (Wen & Ding, 2006) investigated natural convection of titanium oxide nanofluids in pipe flow, which decreased by approximately 30% because of increased thermal conductivity and viscosity and particle–surface interaction. Natural convection exhibited negative results and limited application. Thus, researchers focused on forced convection with nanofluids. Lee et al. (Xuan, Y. M. et al., 2003) documented approximately 39% of Nu enhancement for 2.0% volume Cu particle

in water at 10,000 < Re < 25,000 flow regimes in 2003. The percentage increase in Nu highly depended on the percentage of nanoparticles, and a new correlation for turbulent nanofluid heat transfer inside pipes was suggested;

$$Nu_{nf} = 0.4328\,(1.0+11.285\phi^{0.754}\,Pe_d^{0.218})\,\mathrm{Re}_{nf}^{0.333}\,\mathrm{Pr}^{0.4} \quad \text{(for laminar flow)} \qquad (2.12)$$

$$Nu_{nf} = 0.0059\,(1.0+7.6286\,\phi^{0.6886}\,Pe_d^{0.001})\,\mathrm{Re}_{nf}^{0.9238}\,\mathrm{Pr}^{0.4} \quad \text{(for turbulent flow)} \qquad (2.13)$$

However, the correlation does not apply to all experiments. Cho (Cho, 1998) showed a different percentage increase in Nu number for a similar range of Reynolds number. Only a 12% increase was observed in Nu for 3.16% volume percentage of TiO_2 in water. Particle size, material, and volume fraction clearly influence the Nu number in turbulence flow. We cannot conclude a correlation for all kinds of nanofluids for forced convection in turbulent pipe flow.

Kablec and Wen (Kabelec, S. & Anoop, 2008; Wen & Ding, 2006) measured the local heat transfer coefficients of various types of nanofluids in developing laminar pipe flow. The heat transfer coefficient significantly increased depending on particle shape. For example, the spherical Al_2O_3 exhibited the smallest enhancement, and titanium dioxide nanotubes with an aspect ratio of 10 showed a 20% to 30% increase in heat transfer coefficient in the developing region. Both enhancements in the developing region decreased as the flow approached the fully developed region. An abnormal heat transfer coefficient increase of up to 400% was also observed for CNTs. Justifying the application of these nanofluids in real applications is difficult because the increase was irregular and limited to a very small developing region. Kablec and Anoop (Kabelec, S. & Anoop, 2008) observed similar heat transfer enhancement in the developing region. Their results suggested that the increase in heat transfer coefficient strongly depended

on particle size; small particles had superior heat transfer coefficient improvement, whereas large particles had less improvement. Timofeeva et al. (Timofeeva et al., 2007) from the ANL different results. Their experimental results illustrated that the enhancement in heat transfer coefficient in laminar developing region increased with the increase of particle size in the nanofluids. Both results were based on spherical nanoparticles. Hwang et al. (Hwang, K., Jang, & Choi, 2009) observed an 8% heat transfer coefficient increase for 0.3% Al_2O_3 in water. According to Choi, thermal conductivity enhancement was observed in their samples. Thus, heat transfer coefficient increase can be offset by thermal conductivity increase when converted to a non-dimensional Nu number.

Williams et al. (Williams et al., 2008) investigated Al_2O_3 and ZrO_2 in water in a horizontal pipe flow with constant heat flux boundary conditions. The classic Dittus–Boelter correlation can be used to predict the Nu number of nanofluids in the turbulence region ($9{,}000 < Re < 63{,}000$) by substituting the properties of nanofluids into the equation. No new mechanisms were observed in heat transfer for nanofluids in the turbulence region. Kablec and Anoop (Kabelec, S. & Anoop, 2008) obtained the same results regarding heat transfer to nanofluids in the turbulence region. They were unable to identify remarkable increases in thermal performance of nanofluids compared with the performance of the base fluid. Sommers and Yerkes (Sommers & Yerkes, 2010) observed similar results in the transitional region ($2{,}000 < Re < 4{,}600$) in 2010; the increase of the Nu number was very limited. Nanofluids underwent discoloration after the experiments, which remains an unexplained phenomenon. Ulzie et al. (Ulzie Rea, Tom McKrell, Lin-wen Hu, & Buongiorno, 2008) used Al_2O_3 in water and ZrO_2 in water nanofluids and tested them in thermally developing laminar flow. They documented that the measured Nu numbers matched the analytical solutions of the local

Nu numbers. The results in the laminar flow region suggest that these nanofluids behaved as homogeneous mixtures. Consequently, heat transfer coefficient enhancement is not abnormal and is simply caused by different mixture properties of the nanofluids with respect to the base fluid. Hong et al. (Hong, Yang, & Choi, 2005) tested nanoparticle suspensions in organic fluid (auto transmission oils), which presented minor changes in the heat transfer coefficient and Nu number compared with those of base fluids in the laminar developing region. The results were inconsistent with the correlation developed by Xuan et al. (Xuan, Y. M. et al., 2003). However, the Xuan and Li correlation predicted higher results than the experimental results of Yang (Yang, YiJun, 2011). Several researchers from the industrial field conducted experimental measurements on nanofluids. Incropera et al. (Incropera, Lavine, & DeWitt, 2011) employed nanofluids in electronic cooling systems. Prasher et al. (Prasher, Song, et al., 2006) studied the use of nanofluids in electronic cooling and micro-channel heat transfer; nanofluids were found to be unsuitable. Schroeder and Morris (Schroeder & Morris, 2010) revealed that CuO–water and Al_2O_3–water nanofluids were unsuitable for magnetic resonance imaging heat exchangers and cold plate systems because of limited improvements in heat transfer performance, large pumping power requirement, health risks, and handling difficulties.

2.7 Friction loss of nanofluids

Heat transfer enhancement in thermal systems can be achieved through several techniques, including geometry reconfiguration, cooling fluid changes, and swirl generator insertion.

Researchers have conducted experimental and numerical investigations to improve the heat transfer performance and pressure drop of nanofluids with various nanoparticle

volume concentrations in laminar and turbulent flow regimes (M.S Youssef, A.A Aly, & E.B Zeidan, 2012; Sarkar, J., 2011; Tuqa. Abdulrazzaq et al., 2013).

The application of nanofluids also decreased friction and wear, parasitic losses, and operation of components such as pumps and compressors, subsequently leading to more than 6% fuel savings. Considerable savings could be obtained in the future (Choi, C., H.S Yoo, & J.M Oh, 2008; Rahul & B.S. Kothawale, 2013; Sundar, L. Syam, Singh, & Sousa, 2014). Sundar et al. (Sundar, L.S. et al., 2012) obtained 30.96% and 10.01% heat transfer and friction factor enhancement with 0.6% volume concentration of Fe3O4 NF at a Reynolds number of 22,000 (Kazi, Duffy, & Chen, 2014).

Duangthongsuk and Wongwises (Duangthongsuk, W. & S. Wongwises, 2010) presented that pressure drop with nanofluids was slightly higher than with base fluids and increased as volume concentration increased. Furthermore Duangthongsuk and Wongwises (Daungthongsuk & Wongwises, 2007) investigated the effect of thermophysical properties models on prediction of the heat transfer coefficient and also reported the heat transfer performance and friction characteristics of nanofluid under turbulent flow conditions. The 0.2 vol% TiO2 naoparticles are used to disperse in the water. The experimental apparatus (Figure 2.10) used in this experiment consists of a test section, two receiver tanks, a magnetic gear pump, a hot water pump, a cooler tank, a hot water tank and a collection tank. The test section is a 1.5 m long counter flow horizontal double-tube heat exchanger with nanofluid flowing inside the tube while hot water flows in the annular. The experiments were performed within the following ranges: the Reynolds number of the nanofluid varies in the approximate range of 3000‑18,000, the temperature of the nanofluid is 15^0C, 20^0C and 25^0C, the mass flow rates of the hot water are 3 lpm and 4.5 lpm, the temperature of the hot water is 35^0C, 40^0C, 45^0C and 50^0C. The researchers found that the various thermophysical models have no

significant effect on the predicted values of Nusselt number of the nanofluid. The results also indicated that the heat transfer coefficient of nanofluid is slightly greater than that of water by approximately 6-11%. The heat transfer coefficient of the nanofluid increases with an increase in the mass flow rate of the hot water and nanofluid, and increases with a decrease in the nanofluid temperature, and the temperature of the heating fluid has no significant effect on the heat transfer coefficient of the nanofluid. Finally, the use of the nanofluid has little penalty in pressure drop.

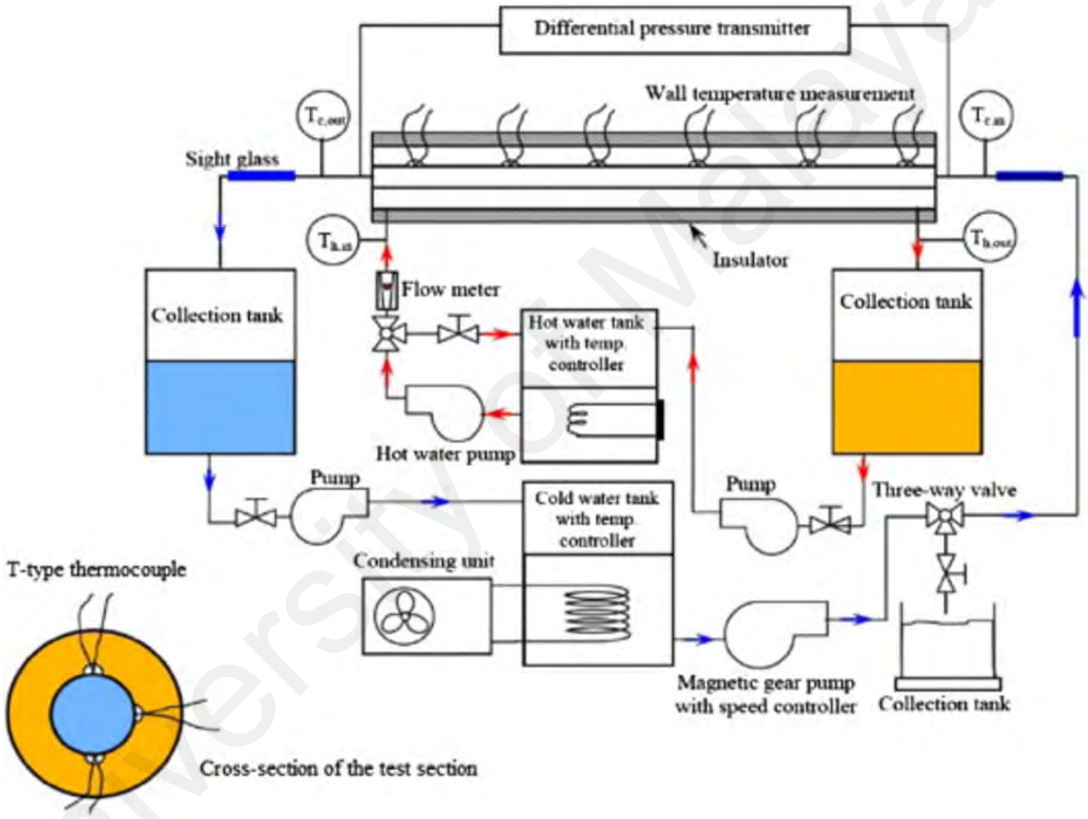

Figure 2.10. Experimental setup for the study of the flow and heat transfer characteristics of the TiO2/water nanofluid flow inside horizontal double-tube heat exchanger under turbulent flow (Duangthongsuk and Wongwises)

Teng et al. (Teng, Y.H. Hung, C.S. Jwo, Chen, & L.Y. Jeng, 2011) reported that pressure drop enhancement for titanium dioxide (TiO_2) nanofluid in circular pipes was low under turbulent flow conditions and high under laminar flow conditions. Sajadi and Kazemi (Sajadi & M.H. Kazemi, 2011) recently investigated the turbulent heat transfer

behavior of TiO_2 nanofluids in circular pipes under fully developed turbulent regime for various volumetric concentrations. The pressure drop of nanofluid was slightly higher than that of base fluids and increased as volume concentration increased. Vajjha et al. (Vajjha, R. S., D. K. Das, & D. P. Kulkarni, 2010) reported that pressure loss of nanofluids increased as volume concentration increased, and the increase of pressure loss for 10% Al_2O_3 nanofluid was approximately 4.7 times that of the base fluid (corrected). Duangthongsuk and Wongwises (Duangthongsuk, W. & S. Wongwises, 2008) disclosed that the pressure drop of nanofluids was very close to that of the base fluid. Sunder et al. (Sundar, L. Syam et al., 2014) synthesized MWCNT–Fe_3O_4 nanocomposite powder via the in situ method. Enhancement in the friction factor for 0.3% of MWCNT–Fe_3O_4 hybrid nanofluid was 1.11 times and 1.18 times at Reynolds numbers of 3000 and 22,000, respectively, compared with water. The pressure drop caused by increased friction for a particular Reynolds number and temperature was relatively negligible compared with the benefits of heat transfer enhancement. The developed Nu number and friction factor correlations were; (numbered)

$$Nu = 0.0215\, Re^{0.8} Pr^{0.5} (1+\varphi)^{0.78} \quad (2.14)$$

$$fReg = 0.3108 Re^{-0.245} (1+\varphi)^{0.42} \quad (2.15)$$

Li and Xuan (Li, Q. & Xuan, 2002) observed that the friction factors of the nanofluids coincided with those of water and the nanofluid with low volume fractions incurred almost no augmentation of the pressure drop. Sundar et al. (Sundar, L.S , K.V Sharma, & S. Parveen, 2009) obtained 2.25% heat transfer enhancement and 1.42% friction factor for Al_2O_3 NF in a tube. Ulzie et al. (Rea, McKrell, Hu, & Buongiorno, 2009) investigated heat transfer and viscous pressure loss for alumina–water and zirconia–water nanofluids in a flow loop with a vertically heated tube. Heat transfer coefficients

in the entrance and fully developed regions increased by 17% and 27%, respectively, for alumina–water nanofluid at 6 vol% with respect to pure water. The measured pressure loss for the nanofluids was generally higher than that for pure water.

Fotukian and Esfahany (Fotukain & M. N. Esfahany, 2010) indicated that the maximum increase in the pressure drop was approximately 20% for nanofluids. Suresh et al. (Suresh, S. , K.P. Venkitaraj, P. Selvakumar, & Chandrasekar, 2012) experimented on fully developed laminar convective heat transfer and pressure drop characteristics through a uniformly heated circular tube using Al_2O_3–Cu/water hybrid nanofluid. The maximum enhancement of the Nu number was 13.56% at a Reynolds number of 1,730 in comparison with the Nu number of water. Heyhat et al. (Heyhat, Kowsary, Rashidi, Momenpour, & Amrollahi, 2013) studied the heat transfer coefficient and friction factor of Al_2O_3–water nanofluids with volume concentrations of 0.1 vol% to 2 vol%; the heat transfer coefficient increased by approximately 32% in the fully developed region at 2 vol% nanofluid. The measured pressure loss for the nanofluids was generally higher than that for pure water. The pressure drop of nanofluids increased as volume fraction increased. The maximum pressure drop was approximately 5.7 times higher than that of pure water, which occurred at the highest volume fraction of NF (2%) at a Reynolds number of 360. This condition was caused by increased viscosity of nanofluids, which implies that nanofluids incur large penalties in the pressure drop for laminar flow regimes. Tiwari et al. (Tiwari, Ghosh, & Sarkar, 2013) studied the convective heat transfer performance and pressure drop characteristics of CeO_2/water nanofluid flowing in a plate heat exchanger. The pressure drop of the nanofluid was approximately similar to that of water at the optimum volume concentration, which suggests that the nanofluid provides significant heat transfer improvement with no penalty of pump power at optimum volume concentration and may be suitable for practical applications.

Most of the experimental studies showed that the pressure drop of the nanofluids fairly matched the values predicted from conventional correlations of base fluids for both laminar and turbulent flows. Therefore, the conventional friction factor correlation can be used to predict the pressure drop of nanofluid. However, the conventional correlation is not suitable for heat transfer coefficient of nanofluids. Thus, various correlations have been suggested for the Nu number for both laminar and turbulent flows. A common correlation for nanofluid heat transfer and friction factor in a tube with inserts should be developed (Meriläinen et al., 2013; Sundar, L.S et al., 2009). Further investigations should be conducted to develop a generalized Nu number and friction factor correlations for nanofluid in a tube with inserts.

In recent years, researchers have gradually shifted their attention to the use of carbon allotrope based nanofluids (S.A. Angayarkanni & J. Philip, 2015; Sadri et al., 2014a; Solangi et al., 2015). This is largely due to the ability to address the persisting issues on maintaining the long term stability as well as the exploitation of much effective stabilizing mechanism that uses substances highly benign to the environment, low in molecular weight, as well as requiring low amount in comparison to the conventional approaches (Liu, Y. et al., 2014). A large number of scientific research papers have been published investigating the effect of stable carbon based colloidal systems in changing the physicochemical properties of the host fluid as well as its role in improving different mode of heat transfer processes (Arzani, Amiri, Kazi, Chew, & Badarudin, 2015; Gupta, S. S. et al., 2011; Han, D., Meng, Wu, Zhang, & Zhu, 2011; Lee, Kyung Jin, Yoon, & Jang, 2007; Lee, S. W., Kim, & Bang, 2013; Nasiri, Shariaty-Niasar, Rashidi, & Khodafarin, 2012; Solangi et al., 2015; Zheng et al., 2011). On this note, it is worthy to highlight that a significant rise in thermal conductivity enhancement was reported with the addition of very low particle loading while incurring minimal penalty to the rheological performances (Amiri, Sadri, Shanbedi, Ahmadi, Chew, et al.,

2015; Amiri, Sadri, Shanbedi, Ahmadi, Kazi, et al., 2015; Shanbedi, Heris, et al., 2015; Zubir et al., 2015). It was also discovered that substances containing phenolic components served as effective carbon allotrope stabilizer which interact via π-π aromatic stacking between benzene ring structures while abundance of oxygen based groups provide the necessary hydrophilic feature to maintain the solubility of carbon allotropes in aqueous solvent (Solangi et al., 2015; Zheng et al., 2011). Further, in the light of the π-π interaction, several Polycyclic Aromatic Hydrocarbons (PAH) derivatives have also been reported to be used as stabilizer to effectively isolate CNT and other carbon allotropes in aqueous solution although there were concerns on the prolonged health issues to both environment and humans (Firme III & Bandaru, 2010; Murakami & Nakashima, 2006; Nakashima, Tomonari, & Murakami, 2002; Zhou et al., 2014). It was also evident that the flourishing increase in the number of publications related to the study of carbon based nanofluid in physical heat transfer processes (i.e. convection, boiling and radiation) was highly attributed to the above resolved solubility issues (Ding et al., 2006; Han, Z. & Fina, 2011).

Majority of earlier investigation on nanofluid regarding thermophysical properties and heat transfer coefficient was done on single nanoparticles; based on them, graphene based nanofluids provided the best heat transfer coefficient. Synthesis of nanocomposite and preparation of nanofluid based on nanocomposite are very new and interesting topic for researcher (Amiri et al., 2012; Jha & Ramaprabhu, 2008; T.T & R. Sundara., 2011; Tabandeh-Khorshid et al.). Suresh et al (S et al., 2012) used Hybrid nanofluids of Al_2O_3–Cu and investigated the results experimentally. They reported that about 14% enhancement in Nusselt number for laminar flow was achieved in comparison with pure water. Sunder et al (S et al., 2012) synthesized MWCNT-Fe3O4 nanocomposite and prepared hybrid nanofluid and achieved 31% improvement in Nusselt number at 0.3%

volume concentration and at Reynolds number of 22,000. However, the nusselt number and heat transfer coefficient of a nanofluid also depends on a number of other factors, such as thermal conductivity and specific heat capacity of the base fluid and nanoparticles, the flow pattern, the viscosity of the nanofluid, the concentration of the suspended nanoparticles, the dimensions and the shape of the particles as well as the flow structure (M. Memari et al., 2011; W. Azmi et al., 2014). Only a limited investigations have been performed on the dependence of the convective heat transfer of carbon-based nanofluids on relevant thermophysical properties.

2.8 Summary

Nowadays, more than ever before, cooling and heating are the most pressing challenges of many technologies. Nanofluids are promising for heat transfer enhancement due to their high thermal conductivity. Presently, discrepancy exists in nanofluid thermal conductivity data in the literature, and enhancement mechanisms have not been fully understood yet. The major efforts are: to determine methods to characterize a nanoparticle colloid's mass loading, chemical constituents, particle size, and pH; to determine temperature and loading dependent viscosity and thermal conductivity; to determine convective heat transfer coefficient and viscous pressure losses in a heated horizontal tube. Nanofluids containing metal nanoparticles were found to be Newtonian, whereas nanofluids containing metal oxides as well as carbon nanotubes showed non-Newtonian, shear thinning behaviour. Since the interaction forces between particles usually decrease during flow conditions, the flow resistance is also decreased. With no significant interaction forces between the particles, separation of the particles in the form of sedimentation may occur and therefore, rheological studies could possibly provide more information about the stability of the nanofluids and also the interactions between the particles and fluid molecules.

In addition, literature shows that there is an enhancement in heat transfer when working with nanofluids. The enhancement mainly depends on the thermal conductivity and heat capacity of the base fluid and nanoparticles, the flow pattern, the viscosity and density of the nanofluid, the volume fraction of the suspended particles, the dimensions and the shape of these particles as well as on the flow structure. The thermal conductivity of the nanofluid is a function of both the thermal conductivity of the nanoparticle and base fluid as well as the volume fraction, surface area, shape of the nanoparticle, the distribution of the dispersed particles and the thermal conductivity of the nanolayer. Many studies were done on the convective heat transfer enhancement of nanofluids containing metallic oxide particles and only a few containing carbon based. The correlations were mainly developed for nanofluids containing metallic oxide particles and then only for the laminar or turbulent flow regime.

Studies on the friction factor in nanofluids indicate that there is a pressure increase which is also directly related to the particle concentration. The penalty in pumping power is the greatest in the laminar flow regime but decreases as one enters the turbulent flow regime due to the viscosity behavior of the nanofluids. The pumping power can be reduced by proper preparation of the nanofluid.

There has been very little literature reported on the pressure losses and heat transfer enhancement in the different flow regime for nanofluids. Thus a study on carbon based nanofluids in the turbulent flow regime and developing a correlation for prediction purposes is of a great interest.

CHAPTER 3: CHARACTERIZATION METHOD, INSTRUMENT AND EXPERIMENTAL SET-UP

3.1 Analysis methods

As stated earlier, it is important to be able to fully characterize the nanofluids specimen used for heat transfer enhancement study and the methods for finding these experimental results. Details of the methods are stated in the following sections.

3.1.1 Field emission scanning electron microscopy

Field emission scanning electron microscopy (FESEM) is utilized for inspecting topographies of specimens at very high magnifications using a piece of equipment called the scanning electron microscope. In FESEM inspection, a beam of electrons is focused on a spot volume of the specimen, resulting in the transfer of energy to the spot. These bombarding electrons, referred to as primary electrons, which dislodge electrons from the specimen itself. The dislodged electrons, also known as secondary electrons, are attracted and collected by a positively biased grid or detector, and then translated into a signal.

To produce the FESEM image, the electron beam is swept across the area being inspected, producing many such signals. These signals are then amplified, analyzed, and translated into images of the topography being inspected. Finally, the image is shown on a CRT screen. The energy of the primary electrons determines the quantity of secondary electrons collected during inspection. The emission of secondary electrons from the specimen increases as the energy of the primary electron beam increases, until a certain limit is reached. Beyond this limit, the collected secondary electrons diminish as the energy of the primary beam is increased, because the primary beam is activating

electrons deep below the surface of the specimen. Electrons coming from such depths usually recombine before reaching the surface for emission.

Aside from secondary electrons, the primary electron beam results in the emission of backscattered (or reflected) electrons from the specimen. Backscattered electrons possess more energy than secondary electrons, and have a definite direction. As such, they cannot be collected by a secondary electron detector, unless the detector is directly in their path of travel. All emissions above 50 eV are considered to be backscattered electrons. Backscattered electron imaging is useful in distinguishing one material from another, since the yield of the collected backscattered electrons increases monotonically with the specimen's atomic number. Backscatter imaging can distinguish elements with atomic number differences of at least 3, i.e., materials with atomic number differences of at least 3 would appear with good contrast on the image. Field emission scanning electron microscopy (FESEM- CARL ZEISS- AURIGA 60) was used to observe the microstructures of the nano-particles.

3.1.2 Transmission electron microscopy

Transmission electron microscopy (TEM) is the primary technique to verify the dimensions of a single particle and to identify agglomerations of particles. The electron beam can be used to observe the features in the nanometer level. A major drawback to the use of TEM is that samples must be dried out of solution in order to be attached to the carbon matrix and place in the vacuum chamber of the TEM; therefore the particles are not exactly in the colloid state and agglomeration might occur during drying. However, TEM can be used in combination with dynamic light scattering to acquire exact sizing in nanofluid form. Another drawback of TEM is the cost and time investment needed to prepare and view the sample. It was decided to perform some

initial imaging as a feasibility study. Transmission electron microscopy (TEM) measurements were conducted on a CARL ZEISS-LIBRA120 microscope.

3.1.3 Fourier transform infrared spectroscopy

Fourier transform infrared spectroscopy (FT-IR) samples were prepared by grinding a very low concentration of dry material with potassium bromide (KBr) to form a very fine powder. This powder is then compressed into a thin pellet which can be analyzed. Functional groups on the basis of the graphene surface were analyzed by Fourier Transformation Infrared Spectrometer (Perkin Elmer-spectrum100 model FT-IR) at the wave ranges of 4000-400 cm^{-1}.

3.1.4 Raman

Raman spectroscopy is a spectroscopic technique used to observe vibrational, rotational, and other low-frequency modes in a system. It relies on inelastic scattering, or Raman scattering, of monochromatic light, usually from a laser in the visible, near infrared, or near ultraviolet range. The laser light interacts with molecular vibrations, phonons or other excitations in the system, resulting in the energy of the laser photons being shifted up or down. The shift in energy gives information about the vibrational modes in the system. Infrared spectroscopy yields similar, but complementary, information. Typically, a sample is illuminated with a laser beam. Electromagnetic radiation from the illuminated spot is collected with a lens and sent through a monochromator. Elastic scattered radiation at the wavelength corresponding to the laser line due, called elastic Rayleigh scattering, which is filtered out while the rest of the collected light is dispersed onto a detector by either a notch filter or a band pass filter. Thus Raman spectroscopy is used to provide a fingerprint by which molecules can be identified. Raman spectra were collected by using a Renishaw Invia Raman Microscope with laser excitation at 514nm.

3.1.5 Differential scanning calorimetry

Differential scanning calorimetry (DSC) is a powerful tool to measure the heat capacity of nanofluids. The difference in the amount of heat flow required for heating up a sample pan and reference pan are measured as a function of temperature. During the whole process, the sample and reference pans are maintained at nearly the same temperature throughout the experiment. The heat capacity of the reference pan is already known. By measuring the difference in heat flow, the heat capacity of the sample is obtained. If there are phase transitions happened in the sample pan, more or less heat will need to flow to it than the reference to maintain both at the same temperature, so endothermal or exothermal peaks are shown on the DSC curves, corresponding to melting or freezing, respectively. The phase transition temperatures and latent heats are determined according to the DSC curves. The heat capacities of nanofluids were obtained from a differential scanning calorimeter (METTLER TOLEDO 820C-Error ±0.25–1℃) at a heating rate of 5℃/min in purified nitrogen atmosphere.

3.1.6 Rheometer

Viscosity of nanofluids is one of the most critical parameters, which determines the quality of the heat transfer fluid. As with simple fluids, the viscosity of a nanofluid depends largely on the temperature (Mehrali, Mohammad, Sadeghinezhad, Emad, Tahan Latibari, Sara, Mehrali, Mehdi, Togun, Hussein, Zubir, M. N. M., et al., 2014). Moreover, the viscosity of nanofluids is measured at different RPMs of the rotor to investigate whether the nanofluids are Newtonian or non-Newtonian fluids. The rheological behavior of nanofluids with certain amount of nano sized particle was measured by an Anton Paar rheometer (Physica MCR 301). In order to verify the accuracy of viscometer as well as to assess the reliability of the experimental

procedures, the obtained values from water tests are validated by the equation (3.1), which could be the correlation for the dynamic viscosity of distilled water (Hagen, 1999):

$$\mu = e^{(1.12646-0.039638*T)/(1-0.00729769*T)}/10000 \quad (3.1)$$

Where, T is the temperature in Kelvin and μ is the viscosity in mPa.s.

3.1.7 UV-vis photo spectrometer

A UV-vis spectrum is a common procedure employed to study dispersibility of aqueous suspensions with sedimentation time. This procedure works based on various light wavelengths in which it could be absorbed or distributed by other substances in the nanofluids. The UV-vis spectra procedure follows the Beer-Lambert law, and shows the absorbance is directly proportional to the nanoparticle concentration in colloids. Although the stability of nanofluid is very important in order for practical application, the data of limited on estimating the stability of nanofluids (Mehrali, Mohammad, Sadeghinezhad, Emad, Tahan Latibari, Sara, Mehrali, Mehdi, Togun, Hussein, Zubir, M. N. M., et al., 2014). The zeta potentials of the nanofluids were measured by a zetasizer nano (Malvern instruments ltd., United Kingdom). The light transmission of all samples were measured with a Shimadzu UV spectrometer (UV-1800) operating between 190 and 1100 nm. The nanofluid solution was diluted with distilled water to allow sufficient transmission while each measurement was repeated three times to achieve a better accuracy.

3.1.8 Electrical conductivity

Electrical conductivity of the nanofluids both as functions of loading and fluid temperature were measured using a AB200 pH/Conductivity Meter (Fisher Scientific). The conductivity meter has a measuring range between 0 to 500mS/cm and a resolution

of 0.1%. Prior to the measurements, the meter was calibrated using the buffer solutions of known electrical conductivities. Measurements were taken by using ~40 ml of the nanofluid sample in a beaker which is located in an isothermal bath, with the conductivity probe immersed in it. At each temperature, the measurements were repeated 5 times, and the average value was taken.

3.1.9 KD2-Pro

An important property has been characterized in this study which is the thermal conductivity of the nanofluid. In order to select the desired fluids to be fully characterized, enhanced thermal conductivity is possibly the most important element in this study, because it points to the nanofluid with high heat transfer potential. There is an inexpensive commercially available system for the measurement of the thermal conductivity (Mehrali, Mohammad, Sadeghinezhad, Emad, Latibari, Sara Tahan, et al., 2014). The Decagon Devices KD2 thermal properties analyzer (KD2 Pro, Decagon Devices, Inc., USA), after some initial testing, it is used for all nanofluids at room temperature as a first check. In the following sections, the transient hot wire method, on which the KD2 operates, has been described in full along with the true thermal conductivity measurement apparatus. The accuracy of the KD2 is given as 5% by the manufacturer over a span of temperatures from 0 to 60℃. However it is found, through trial and error, that the KD2 operates very accurately if the probe is setup perfectly vertical and an isothermal bath is used to maintain the sample at 25℃. These techniques prevent convection problems and the external boundary effect problems as well. A schematic of the KD2 setup with the isothermal bath is shown in Figure 3.1.

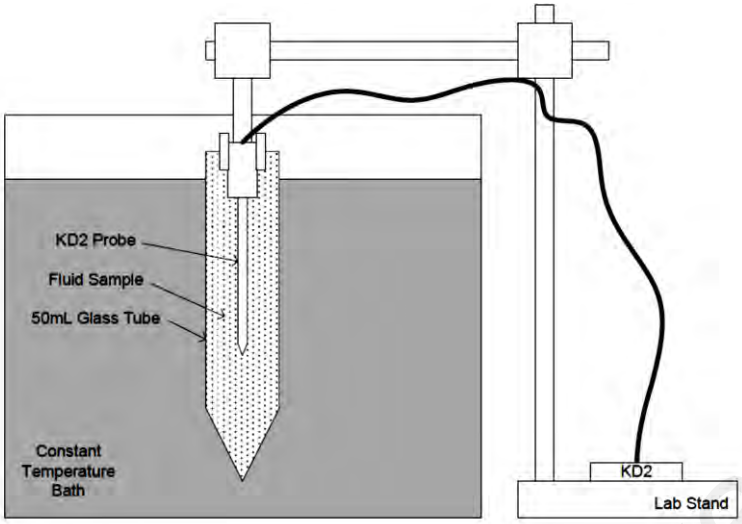

Figure 3.1. Schematic setup of KD2 thermal properties analyzer

Thermal conductivity measurements in this work were done based on THW method and the used analyzer device has 5% accuracy between 5°C and 50°C (Mehrali, Mohammad, Sadeghinezhad, Emad, Tahan Latibari, Sara, Mehrali, Mehdi, Togun, Hussein, Zubir, M. N. M., et al., 2014). The thermal conductivity measurement for distilled water are within 2-4% of previously reported data (Buongiorno et al., 2009; Ramires et al., 1995), as shown in Figure 3.2. The thermal conductivity measurements were repeated ten times and the average values were reported.

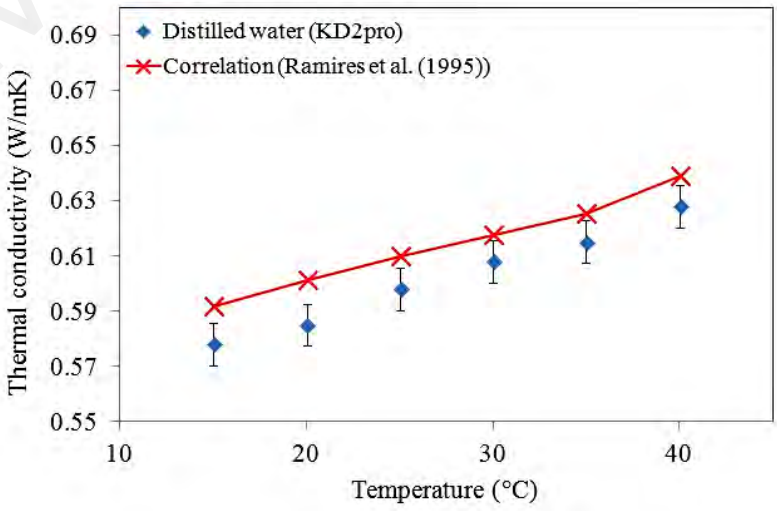

Figure 3.2. Comparison between distilled water and previous data

3.2 Description of the experiment

3.2.1 Experimental system

Figure 3.3 shows the schematic view of overall experimental set-up for the present work which consists of a flow loop, heated test section, cooling section, measuring instruments, data acquisition and control units. The flow loop includes a pump, a magnetic flow meter, a reservoir tank, a differential pressure transmitter, and a test section. This configuration closely resembles heat transfer in most heat exchangers to enable much clear representative of real engineering application. The nanofluids were pumped from a 20-L capacity stainless steel jacketed tank by a Cole-ParmerTM magnetic drive pump at a flow rate of 0-4 l/m, and the pump flow was controlled by a Hoffman MullerTM inverter. The flow rate and the pressure loss were measured using a N-FLO-25 Electromegnetic flow meter and a FoxboroTM differential pressure transmitter, respectively. In this experiment PLC control system was used and WINCC software was used for recording and analysis of the data.

A number of straight seamless test tubes (test sections) with the length of 1500 mm, (inner diameters: 2, 4, 15mm and outer diameter 6, 8,19mm) were used as the test sections. The test section was heated by using an Ultra-high-temperature heating flexible tape (Omega, USA) at a maximum power of 900 W, which was linked to a Variac transformer and a watt/amp meter. Six K- type thermocouples (Omega, Singapore) were mounted on the test section by using high temperature epoxy glue at 24cm equilateral axial distances on the outer surface of the test tube as schematically shown in (Figure 3.4). The positioning of the thermocouples was done at outer surface of the cylindrical tube in order to avoid boundary layer interruption originating from the thermocouple probe protruding into the conduit inner surface. As shown in Figure 3.5,

there exists a gap between the outer and the inner surface corresponding to the thickness of the conduit. In a pure conduction heat transfer, the inner surface can be described via the classical heat conduction equation. Further, two RTD (PT-100) sensors (Omega, Singapore) were inserted to obtain the bulk temperature at the inlet and outlet of the test section. All thermocouples and RTDs were calibrated via the use of Ametek temperature calibrator (AMETEK Test & Calibration Instruments, Denmark). The thermocouples and RTDs were connected to the SCADA system for the continuous monitoring and recording of the temperature data by a WINCC software at computer. To minimize the heat loss to the surroundings, a thick glass wool wrapping was implemented followed by rubber insulation dressing to provide maximum protection against heat loss to the surrounding. Three K-type thermocouples ware placed on the outermost surface of the insulation to calculate the heat loss. Furthermore, all piping and fittings were covered with rubber insulation to minimize transportation heat loss to achieve steady state temperature at the inlet and outlet of the test section. The comparative assessment between the input and output energy at different Re by using conventional expression ($Q = VI = \dot{m} C_p(T_{in} - T_{out})$) showed the average loss of approximately 3.96%, which is reasonable. It is believed that this low percentage of heat loss would not affect the overall heat transfer calculation process.

During the pipe flow experimental process, each sample was first poured into the stainless steel jacketed tank and circulated along the piping networks and measuring instruments using magnetic driven pump. The flow rate was maintained to correspond to the previous water run value in order to minimized the effect of pumping power and to reflect the actual contribution of the material property on the overall enhancement (if any) into the system. The cooling bath circulator was connected to the jacketed tank and

its temperature was adjusted until the bulk temperature complied with the predetermined criteria. In this test, the bulk temperature was maintained at 30^0C.

The relevant data were recorded after steady state condition was reached. The acquired raw data underwent series of rigorous analysis to obtain relevant property to describe the heat transfer performance. The surface, inlet and bulk temperature measurements were used along with the thermophysical property data to calculate heat transfer coefficient and Nusselt number which were plotted with respect to fluid bulk velocity/Reynolds Number for comparative assessment. The pressure drop over the test tube was measured by which the friction factor was calculated and plotted against flow velocity. To assess the reproducibility of the results the test section was thoroughly cleaned by using filtered and distilled water at the end of the sample test run and the experiment was repeated using distilled water at similar condition. Uncertainty analysis was conducted for both raw and derived parameters to ascertain the actual improvement in heat transfer under the present approach. However, considering the convection and convective heat transfer process, which occur simultaneously for the present case, further calibration test was needed to determine the exact temperature at the inner surface. Therefore, a Wilson plot was adopted to accomplish this task which is based on equating the resistance between different sections of the heat transfer direction and determining the inner surface temperature via mathematical manipulation. The inner diameter heat flux between different locations of the cross sectional direction was formulated as mentioned in Appendix A. A summary of experimental conditions for heat transfer and pressure loss studies is given in Table 3.2.

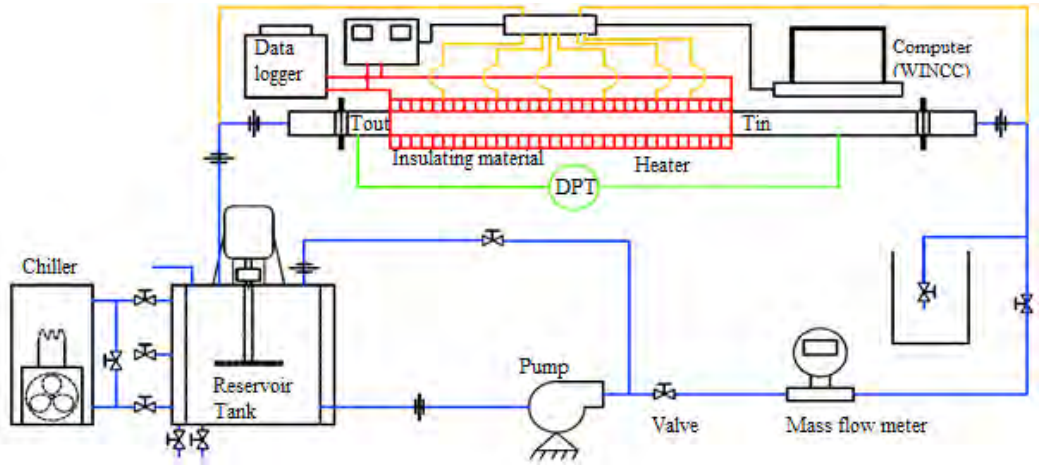

Figure 3.3. Schematic view of test section

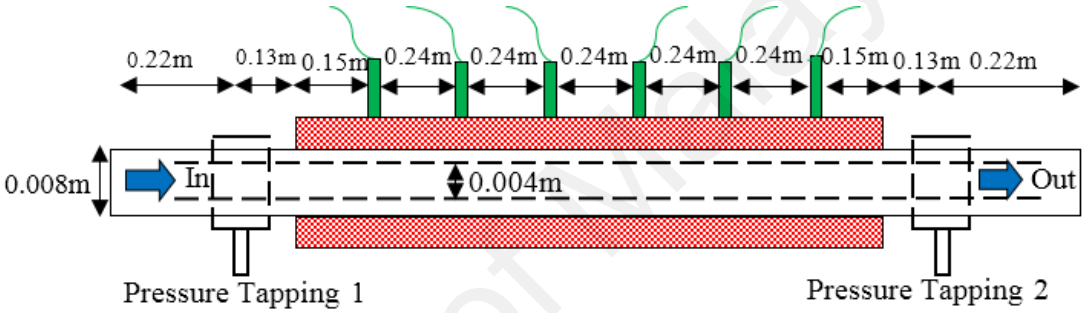

Figure 3.4. The schematic diagram of the experimental setup for the measurement of the convective heat transfer coefficient.

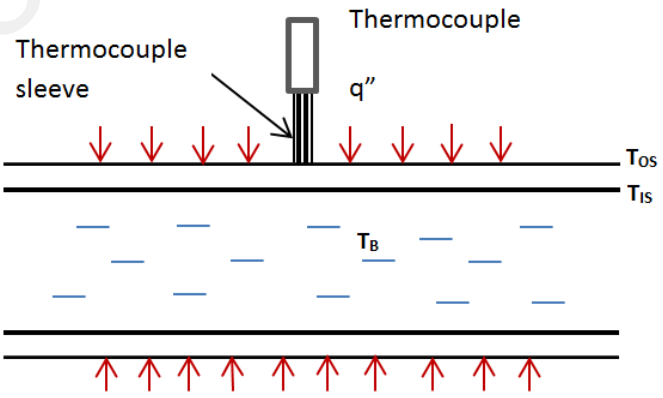

Figure 3.5. Schematic of temperature variation through heated wall

The specifications and the accuracy of the measuring instruments and sensors used in the present experimental setup are presented in Table 3.1.

Table 3.1. Specifications and errors of the measuring instruments and sensors used in the present experiment.

Measured parameter	Instrument and sensor type	Operating	Error
Surface temperature	Type K thermocouple	0-300℃	±0.1℃
Bulk Temperature	RTD (PT-100) sensor	0-200℃	±0.1℃
Fluid flow rate	Schmierer, Electromagnetic Flow Meter	0.03 m/s ~ 12 m/s	±0.5%
Fluid pressure drop	ALIADP, Differential Pressure Transmitter (DPT)	0-1500 kPa	±0.075%
Cooling unit	WiseCircu, DAIHAN Scientific, Refrigerated circulating bath	2.2 kW	±0.1℃

Table 3.2. A summary of experimental conditions for heat transfer and pressure loss studies

Nanofluids type	PGGNP-water, TMP-treated GNP, Al_2O_3 and SiO_2
Nanofluids concentrations	0.025, 0.050,0.075 and 0.1 wt%
Test sections diameters	2mm, 4mm and 15mm
Test section materials	Copper, Aluminum and Stainless steel

Heat supply	700W and 900W
Constant Heat flux	18565 W/m^2 and 23870 W/m^2
Velocity range	0.25-3 m/s
Bulk temperature	30^{o}C

3.2.2 Design and Construction

Some basic requirements are developed as design considerations for the convection loop. These requirements are generated in order to meet certain goals: some to satirist heat exchanger conditions, some to meet existing equipment and lab requirements, and finally some arbitrary conditions.

3.2.2.1 Test sections

In this experiment 5 different test sections of different diameters and materials were used as mentioned in Table 3.2. For investigating diametrical effect test sections were selected of stainless steel 316 material and their inner diameters were 2mm, 4mm and 15mm. Figure 3.6 shows the 3 different test sections of the same material with different diameters. Furthermore, for investigating material effect, the test sections were selected of same diameters with different materials (stainless steel, aluminium and copper). Therefore for material effect the diameter was selected 4mm. Figure 3.7 shows the 3 different test sections of same diameter with different materials.

Figure 3.6. Shows the different test sections diameters of stainless steel (2mm, 4mm and 15mm)

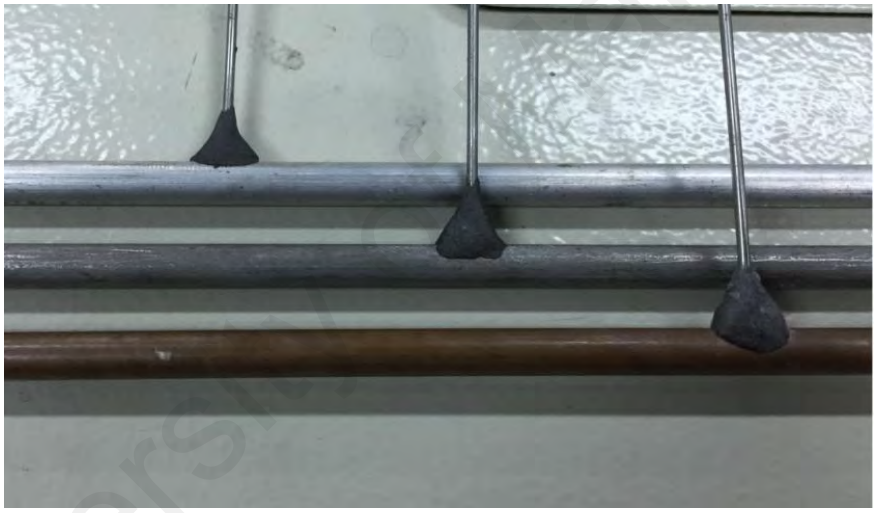

Figure 3.7 Shows the different test sections material of same diameter 4mm (copper, aluminium and stainless steel)

3.2.2.2 Reservoir Tank

The reservoir tank is a Jacketed Stainless steel of cylindrical shape with a capacity of 20 litters. The reservoir is kept 30 cm above the gear pump so that the gear pump will have adequate inlet flow to avoiding cavitation. At the bottom of the reservoir a piping connects to the gear pump while at the top a bypass line, return line and top stirrer for mixing fluid inside the tank as presented in Figure 3.8.

Figure 3.8. Photograph of the Reservoir Tank

3.2.2.3 Gear Pump

The gear pump used for the experiment is a Liquid flow sealed gear pump (Cole-Parmer magnetic drive pump), (see Figure 3.9). It is rated for a maximum flow of 120 LPM and Max Head is 8 M. This pump is capable of operating at variable speed with the maximum rated speed of 3200 RPM. The suction side of the pump is connected to the reservoir.

Figure 3.9. Photograph of the Magnetic gear pump

The pump is capable of operating with water up to 80℃, due to the shaft seal limitations. After rough estimation of the total loop pressure losses, assuming maximum 15mm inner diameter tubing, and from knowledge of the pump characteristic curve, it is found that the pump should be capable of producing around 52LPM.This will deliver a significantly turbulent flow rate for water at room temperature, up to Reynolds of 30,000. Therefore, the pump is deemed usable for the experiment.

3.2.2.4 Inverter

A Hoffman Muller inverter was used to control the speed of the pump as shown in Figure 3.10.

Figure 3.10. Photograph of the Hoffman Muller inverter

The specifications of the inverter are presented in Table 3.3.

Table 3.3. Technical specifications for V8 series inverters

Items	Contents
Model	HM-V8A11P5B
Input	AC, 1PH, 230V, 50/60HZ
Output	3PH, 1.5KW, 7A, 0-650HZ

3.2.2.5 Electromagnetic Flow Meter

N-FLO-25 Electromegnetic flow meter was used to measure fluid flow rate (see Figure 3.11). A magnetic flow meter (mag flowmeter) is a volumetric flow meter which does not have any moving parts and is ideal for wastewater applications or any dirty liquid which is conductive or water based. Magnetic flowmeters will generally not work with hydrocarbons, distilled water and many non-aqueous solutions. Magnetic flowmeters are also ideal for applications where low pressure drop and low maintenance are required.

Figure 3.11. Photograph of the Electromagnetic flow meter

The operation of a magnetic flow meter or mag meter is based upon Faraday's Law, which states that the voltage induced across any conductor as it moves right angles through a magnetic field is proportional to velocity of that conductor. The technical specifications are presented in Table 3.4.

Table 3.4. Technical specifications of Electromegnetic flow meter

Items	Contents
Model	N-FLO-25 Electromegnetic flow meter
Sensor range	DN10-DN3000
Operational pressure	PN 10 (1.0 MPa) for DN 15 to 300, Tri Clover
Measurement flow range	8 m^3/h
Measurement accuracy	±0.5%
Repeatability	0.1%
Environment temperature	-20-50℃
Minimum conductivity of measured liquid	$5\mu s/cm$
Lining	Teflon (PTFE)
Measuring electrodes	Hastelloy C4 standard

As stated above, the flow meters were supplied after calibration by the manufacturer, as shown in Table 3.5. Fluid viscosity can become an issue if the viscosity is higher than that of water. The deviation of the flow meter reading becomes an issue when the meter is running in the lower 25% of its operating range for fluids of viscosity less than 30 times that of water. Nanofluids used in the experimental investigation were typically only 5 times more viscous than water, therefore the calibration had not been an issue.

Table 3.5. Flow meter calibration data

Flow (m^3/hr)	Volume (L)	Actual (L)	Error (%)	Repeatability (%)
0.3	5.201	5.214	0.24	0.062
0.8	12.374	12.368	-0.05	0.105
1.60	20.871	20.787	-0.40	0.019

3.2.2.6 Differential Pressure Transducers

The smart FoxboroTM differential pressure transmitter (Model: IDP10-T22D21D-LIT) with accuracy of ±0.075% of span connected to the inlet and outlet of the test section was used in this test (see Figure 3.12).

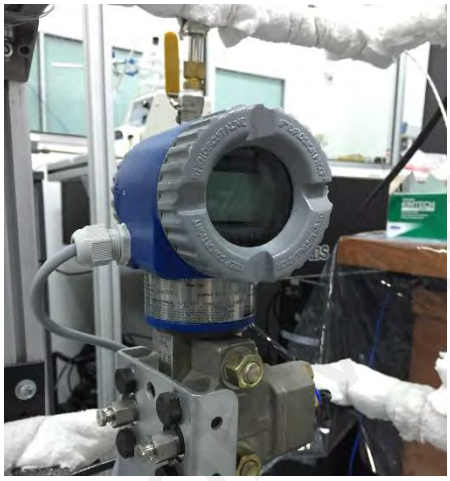

Figure 3.12. Photograph of the Differential Pressure Transducers

The standard specifications of the Differential Pressure Transducers are presented in Table 3.6. The calibration condition, static pressure test and differential pressure test are presented in Table 3.7 to Table 3.9, respectively.

Table 3.6. Standard specifications of the Differential Pressure Transducers

Items	Contents
Model	IDP10-T22D21D-LIT
Process Fluid	Liquid, Gas of Vapor
Application	Differential Pressure, Gauge Pressure, Absolute Pressure
Measuring Range	0 - 0.125 Kpa ~ 0 - 1.5 Kpa (Minimum) 0 - 4.0 Mpa ~ 0 - 1500.0 Kpa (Maximum)
Accuracy	± 0.075% of span
Stability	± 0.15% of URL for 2 years
Working	-25 to 95℃

Temperature	
Max. Pressure	1500 Kpa
Body material	SS 304
Diaphragm	SS 316L

Table 3.7. Calibration conditions

Ambient temperature	20℃	Relative humidity	60%
Grounding resistance	$> 200M\Omega$	Calibration range	0~50 KPa

Table 3.8. Static pressure test

Differential pressure value	Static pressure = 4.00 MPa			
	1 ATM	Error (%)	4 MPa	Error (%)
0.0 KPa	4.000 mA	0.000	4.012 mA	0.075
50.0 KPa	20.003 mA	0.019	20.000 mA	0.000

Table 3.9. Differential pressure test

D/P Value	output	Zero to F.S.	Error (%)	F.S. to Zero	Error (%)
0.0	4.000 mA	3.998 mA	-0.012	4.009 mA	0.056
12.5	8.000 mA	7.991 mA	-0.056	7.997 mA	-0.019
25.0	12.000 mA	11.992 mA	-0.050	11.992 mA	-0.050
37.5	16.000 mA	15.990 mA	-0.062	15.999 mA	-0.006
50.0	20.000 mA	19.997 mA	-0.019	19.992 mA	-0.050

3.2.2.7 Cooling unit

A Refrigerated Bath Circulator (DAIHAN-brand, WCR- P30) was used to balance the heat input and it is inside the jacketed tank (Figure 3.13). This refrigerated bath has:

1. RS232C Interface for Remote Monitoring and Controlling with PC
2. Stainless steel Bath (#304) for Superior Durability & High Thermal Efficiency.
3. Powerful Circulation Pump ensures temperature Uniformity: Internal and External Circulation.
4. Locking Mode Supported for Experimental Safety (Input to Jog-Shuttle can be Disabled)

Figure 3.13. Photograph of the Refrigerated Bath Circulators

The specification of the Refrigerated Bath are listed in Table 3.10.

Table 3.10. Specifications of the Refrigerated Bath

Items		Contents
Capacity & Models		30 L, WCR- P30
Temp. Range & Accuracy		-25℃~ +150℃, ±0.1℃
Temp. Resolution		0.1℃-Display, 0.1℃-Control
Temp. Uniformity & Probe		±0.2℃ at -10℃, PT100
Heating Power		2.2 kW
Refrigerator		7/8 HP
Cooling Capacity	at +20℃	631 W
	at 0℃	429 W
	at -20℃	284 W

Refrigerant	CFC	-Free(R-404A)	Refrigeration System

3.2.2.8 Digital multimeter and clamp meter

The Digital multimeter and clamp meter are the single most important piece of the data acquisition system. All of the voltage, current for heater and power supply were measured by these instruments (Figure 3.14). Voltmeter and clamp meter were purchased from Agilent and were calibrated by the manufacturer.

Figure 3.14. Photograph of the Digital Voltmeter and clamp meter

The full specifications for the voltmeter and clamp meter are available in the Table 3.11 and 3.12, respectively.

Table 3.11. Specifications of the Multimeter

Items	Contents
Model	Agilent, U1253B
Display	OLED
True RMS	AC + DC
Voltage	Up to 1000V AC, DC
Basic dcV accuracy	Up to 0.025%
Current	Up to 10 A
True RMS AC	50 V
Voltage	With 0.001V Resolution

	500 V With 0.01V Resolution
True RMS AC Current	5 A With 0.0001A Resolution
Resistance	Up to 500MΩ With 0.01nS Resolution

Table 3.12. Specifications of the Clamp Meter

Items	Contents
Model	Agilent, U1273A
Display	OLED
True RMS	AC + DC
Voltage	Up to 1000V AC, DC
Basic dcV accuracy	0.05% + 2 counts
Current	Up to 10 A (20 A for 30 s)
True RMS AC Voltage	30 V With 0.001V Resolution
	300 V With 0.01V Resolution
True RMS AC Current	3 A With 0.0001A Resolution
	10 A With 0.001A Resolution
Resistance	Up to 300 MΩ

3.2.2.9 Power Supply

A WINCC software was used to control the power supply and to record the data which was connected with the SCADA System. The maximum power output of 20A and output voltage of 0~260V was used to regulate the voltage. A Snapshot of the WINCC software and SCADA SYSTEM TO control the power supply is shown in Figure 3.15.

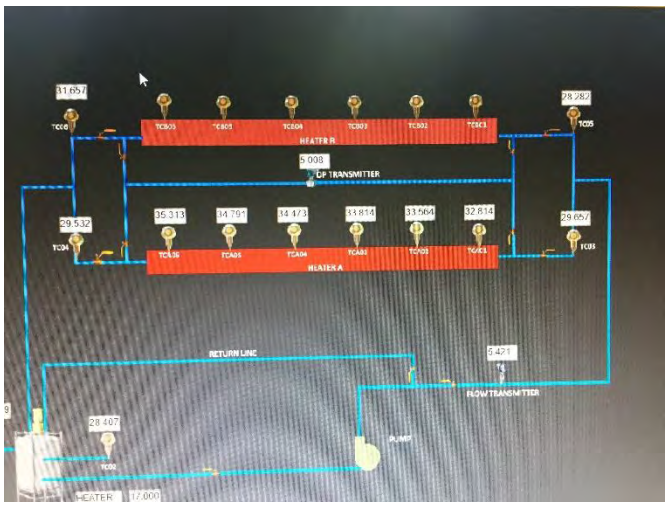

Figure 3.15. Snapshot of the WINCC software and SCADA SYSTEM to control the power supply

3.2.2.10 Heater

The test section is heated by an Ultra-High Temperature Heating Tapes (Omega, Modell: STH052-120) rapped around the outside of test section. The heater has specification of 940W, 13W/in^2, 240V, 1/2×12” size and maximum exposure temperature of 760℃. A photograph of the heater used in the experimental set-up is presented in Figure 3.16. This heater is then connected to PLC system for regulating the amount of heat input to the test section.

Figure 3.16. Photograph of the heater around the test section

This heating tapes are made from fine gage stranded resistance wires that are double insulated with braided Samox and knitted into flat tapes for maximum flexibility. A heavy insulated tape is made by taking a standard tape and braiding it between layers of Samox yarn. Flexible Heating Tapes and Cords are constructed from high quality resistance wire and braided insulation and are designed to provide use for a long life and high performance.

3.2.2.11 Thermocouple

Two different types of thermocouples were used for the experiment. The thermocouples used for the bulk fluid inlet and outlet (bulk) temperatures in respect to the test section are thermocouples from Omega (Model: PR-12-2-100-1/8-6-E-RP) with temperature range of -50 to 250°C. It is a RTD sensor (PT-100) thermocouple with 3mm sheath diameter and 100mm length. The tip of the thermocouple was inserted into the middle of the flow path of the fluid. The thermocouple is then attached to the data acquisition unit where the bulk temperature were recorded and analyzed. Another type of thermocouples used for surface temperature are type-K from Omega (Model: TJ36-CASS-032U-6). The metal transition barrel provides a solid mounting surface and the PFA insulated lead wire is a cost-effective solution for environmental temperatures to 260°C. This type-K thermocouple has 1mm sheath diameter and 150mm length. The thermocouples come specified from the manufacturer to have ±1℃ accuracy. All thermocouples are not calibrated in the technical sense and they are tested with standard temperatures to ensure no manufacturing or connection flaws are creating erroneous readings. The heat transfer results are directly affected by the temperature measurements. Thus, all the thermocouples (Type-K and RTD sensor) used in this experiment must be calibrated to determine their accuracy. The thermocouples are calibrated by two ways:

1. 650SE - Reference Temperature Calibrator

The system gives significant improvement in the calibration accuracy up to ±0.04°C with use of the external reference sensor. Axial homogeneity in the calibration well is important, as the typical thermo-sensitive element of a sensor can vary from 5mm to 60mm. The actual temperature in the well could inherently deviate from the ideal temperature as a function of the proximity to the bottom of the well Figure 3.17.

2. The thermocouples were immersed in well mixed boiling-water bath which was at 100.16°C for the laboratory pressure and a well-mixed ice-water bath maintained was at 0°C (see Figure 3.18).

Figure 3.17. Photograph of the Thermocouple calibrator

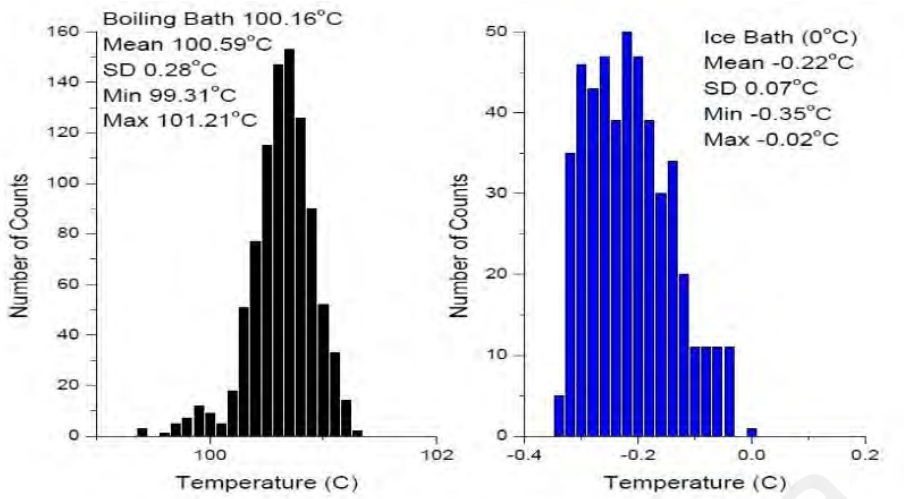

Figure 3.18. Thermocouple testing

3.2.2.12 Data logging system

The several types of data acquisition system are used for this experiment including Graphtec (midi logger gl220), Scada system (TK4H) and Multi Power monitor Figure 3.19. All this systems were connected to a PC for continuous data logging and monitoring.

Figure 3.19. Photograph of the Data acquisition system

All the type-K thermocouples are attached to the channels of PLC system. The PLC system was connected to computer to allow data upload in real time as well as remote configuration and real time data acquisition. The RTD sensors, flow meter and pressure transducer were attached to the PLC system. This PLC system was linked with computer where WINCC software was installed. The WINCC software was set to record the data at every one minute interval. Figure 3.20 shows the PLC system is shown attached with SCADA system.

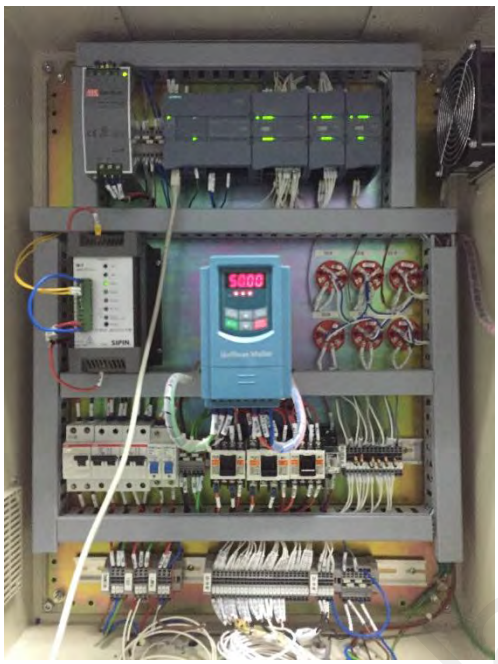

Figure 3.20. Photograph of the PLC system attached with the SCADA system

3.2.2.13 Test section

The heat transfer test section is the main part and it takes much effort to design properly. Test section was constructed by the Advanced Fluid dynamics lab, University of Malaya. The sectional view of the experimental test section is presented in table below and the major dimensions of the test section are tabulated in Table 3.13.

Table 3.13. Dimensions of the test section

Parameters	Values
Overall length	1500 mm
Inside diameter	15, 4 and 2mm
Outer diameter	19, 8 and 6mm
Wall thickness	2mm
Heating length	1300 mm
Thermal entry length	200 mm

The heat transfer test sections are straight stainless steel 316, copper and aluminium tube with the length of 1500mm. All the test sections, their sectional measurements are

presented in Table 3.13. Six grooves were cut along the tube length for holding the thermo-wells and the thermocouples. The grooves were cut as deep as possible while ensuring that the inside surface of the pipe was not disturbed. The distance between groove surface and inner surface of the tube was maintained at 1mm as shown in Figure 3.21.

Figure 3.21. Photograph of the grove on a test section

To keep thermocouple in location the thermo-well of 2mm outer diameter were installed and fixed with high temperature epoxy glue as shown in Figure 3.22.

High temp. Epoxy up to 200°C Thermo-wells installation

Figure 3.22. Installation of thermocouple

The thermocouple were installed inside the thermos-well and filled by thermo oil to confirm the uniform heating of the thermocouple sensor.

The thermocouples were calibrated to measure the surface temperature according to Equation (3.2).

$$T_W = T_{Tc} - \frac{\dot{q}}{\lambda/x} \qquad (3.2)$$

Details of the calibration are given in appendix and also the λ/x values of all the individual thermocouples are presented in appendix A. A Teflon flange was used to connect the test section to the test rig and reduce the heat loss, as shown in Figure 3.23.

Figure 3.23. Photograph of connection.

This experimental system is designed and constructed to conduct the experiments to investigate the convective heat transfer and pressure loss at constant heat flux in pipe flow. The flow regions investigated include thermally developing region in turbulent flow and the main test setup is depicted in. Figure 3.24 which shows the full image of heat transfer test rig.

Figure 3.24. Photograph of the heat transfer test rig

CHAPTER 4: NANOFLUIDS PREPARATION, EXPERIMENTS AND ANALYLSYS

4.1 Introduction

There are several methods used to prepare nanofluids. Many types of base fluids were examined to identify the stable combination of nanofluids. The goal is to find out how well commercially viable nanoparticles could be dispersed in heat transfer fluids. Therefore, the basefluid used in the present work was chosen distilled water. In this chapter the preparation and properties of the different nanofluids are discussed which were used in this study.

4.2 Nanofluids preparation

4.2.1 Chemical-assisted functionalization and preparation of PGGNP-water based nanofluids

Graphene nanoplatelets (GNPs) with an average thickness of 5–10 nanometers and a specific surface area of 50-750 m^2/g and it can be produced of different sizes, 1 to 50 microns. These interesting nanoparticles, including short stacks of platelet-shaped graphene sheets which are identical to those found in the walls of carbon nanotubes, but in a planar form. The GNPs have drawn a lot of interest due to their excellent electrical conductivity, high mechanical properties and the in-plane thermal conductivity of GNPs is reported to be as high as 3000-5000 W/m. Further, as this is a 2D material, the heat transfer properties are expected to be much different from the zero dimensional nanoparticles and one dimensional carbon nanotubes. Moreover, GNPs itself being an excellent thermal conductor, the graphene based nanofluids are normally expected to display significant thermal conductivity enhancement (Fang et al., 2013). The graphene nanoplates are also offered in granular form which could be dispersed in water, organic

solvents and polymers with the right choice of dispersion aids, equipment and techniques.

GNPs have special properties dependent on the number of layers, such as the saturable absorption, linear monochromatic optical contrasts and electric field assisted band gaps, which are not found in previously produced materials. These materials (Grade C, XG Sciences, Inc., USA) were used for the preparation of nanofluids. Each grade contains particles with a similar average thickness and specific surface area. Grade C particles have an average thickness of a few nanometers and a particle diameter of less than 2 μm. The average specific surface area is 750 m^2/g and all Specifications are shown in Table 4.1.

Table 4.1. Nanoparticle specifications

Particle	Graphene nanoplatelets (GNPs)
Color	Black granules/powder
Carbon content	>99.5
Bulk density	0.2-0.4 g/cm^3
Relative gravity	2.0-2.25 g/cm^3
Specific surface area	750 m^2/g
Particle diameter	2 μm
Peak in UV-vis spectrophotometer	265-270 nm
Thickness	2 nm
Thermal conductivity (parallel to surface)	3000 W/m.K
Thermal conductivity (perpendicular to surface)	6 W/mK
Electrical conductivity (parallel to surface)	10^7 siemens/m
Electrical conductivity (perpendicular to surface)	10^2 siemens/m

For this research pristine GNP with average surface area of 750 m^2/g and carbon purity over 95% was purchased from XG Sciences Company. All other chemicals were obtained from Sigma-Aldrich.

GNP is first covalently functionalized with carboxyl groups. Pristine GNP is sonicated with a mixture of H_2SO_4–HNO_3 acids in volume ratio of 3:1 for 12 h at 60 °C and then followed by stirring for 36h at the same condition to synthesize carboxylated GNP (GNP-COOH). The suspension was centrifuged at 11000 rpm with di-water to separate completely and supernatant reach pH around 3-4 simultaneously. The sample is then placed in the oven for 48 h at 50°C to dry. Then, in a typical experiment, 1 g GNP-COOH and 100ml propylene glycol was ultrasonicated for 10 min and then 13.4 ml H_2SO_4 was added drop by drop. The Mixture was sonicated for 8 hours and then placed on a magnetic stirrer for 12 h at 70°C. To increase reaction rate and based on the equilibrium law, the produced water in fischer esterification reaction has removed by evaporation of water. The equilibrium may be influenced by either removing water product from the reaction mixture and shifted in right side. The acid-catalyzed esterification of carboxylic acids with alcohols can give an ester. Eventually, the suspension result was centrifuged at 11000 rpm with anhydrous THF again and rinsed with ethanol and THF to remove not-reacted materials. The sample was then placed in the oven for 48 h at 60°C.

4.2.2 Chemical-assisted functionalization and preparation of TMP-treated nanofluids

Pristine GNP (average surface area of 750 m^2/g and purity over 95%) was purchased from XG Sciences Company. All other chemicals were obtained from Sigma-Aldrich. GNP is first covalently functionalized with carboxyl groups. Pristine GNP is sonicated with a mixture of H_2SO_4–HNO_3 acids in volume ratio of 3:1 for 12 h at 60 °C and then followed by string for 36h at same condition to synthesize carboxylated GNP (GNP-COOH). The suspension is centrifuged at 11000 rpm with di-water to separate completely and the supernatant reach PH around 3-4 simultaneously. The sample is then

placed in the oven for 4 days at 50 °C to dry it up. Then, in a typical experiment, 1 g GNP-COOH and 100ml Trimethylolpropane tris[poly(propylene glycol), amine terminated] ether (TMP) are sonicated for 10 min and then 13.4 ml H_2SO_4 was added drop by drop. The mixture sonicated for 8 hours and then placed on a magnetic stirrer for 12 h at 70 °C. To increase reaction rate and based on the equilibrium law, the produced water in fischer esterification reaction has removed by evaporation of water. The equilibrium may be influenced by either removing water product from the reaction mixture and shifted in right side. The acid-catalyzed esterification of carboxylic acids with alcohols can give an ester. Eventually, the suspension resulted is centrifuged at 11000 rpm with anhydrous Tetrahydrofuran (THF) again and rinsed with ethanol and THF to remove not-reacted materials. The sample is then placed in the oven for 48h at 60 °C.

4.2.3 Preparation of Al_2O_3 and SiO_2 nanofluids

For this study, Dry aluminum oxide and Silicon dioxide (Al_2O_3 nanopowder with particle size ~ 50 nm and SiO_2 nanopowder with particle size ~ 50 nm), acquired from sigma aldrich, and distilled water was used to prepare the nanofluids by two step method. The both nanofluids were characterized by zeta potential and transmission electron microscope (TEM). In order to break down the large agglomerates, ultrasonication was applied for 60 min to get homogenous distribution of nanoparticles. During the preparation of Al_2O_3 and SiO_2 nanofluids, the main concern is to get homogenous and uniform suspension of nanoparticles by minimizing the diameter of agglomerated nanoparticles. The agglomerated nanoparticles are settled with time leading to poor suspension stability. So, the amount of dispersant should be carefully selected. To determine the suitable amount of dispersant, four concentrations (0.025%, 0.05%, 0.075% and 0.1%) of each sample were prepared at pH 8. The method is

extensively used in synthesizing nanofluids by mixing base fluids with commercially available nanopowders obtained from different mechanical, physical and chemical routes (e.g., milling, grinding, and sol-gel and vapor phase methods). Frequent use of ultrasonication or stirring decreases particle agglomeration (Chung, S. J. et al., 2009). Agglomeration is a major issue in synthesizing nanofluids (Wang, X. Q. & A.S. Mujumdar, 2008). The two-step method is the most economical method for large-scale production of nanofluids because nanopowder synthesis techniques have already been scaled up to industrial production levels (Ponmani et al., 2014; Wei, Yu & Huaqing, 2012). Nanoparticles tend to aggregate because of high surface area and activity (Hindawi, 2014). Researchers suggest (Eastman et al., 2001) that the two-step method is more suitable for preparing nanofluids with oxide nanoparticles than those with metallic nanoparticles. The two step method is recognized as the most economical process for producing nanofluids (Mukherjee & Paria, 2013). Figure 4.1 shows the prepared nanofluids of all concentrations.

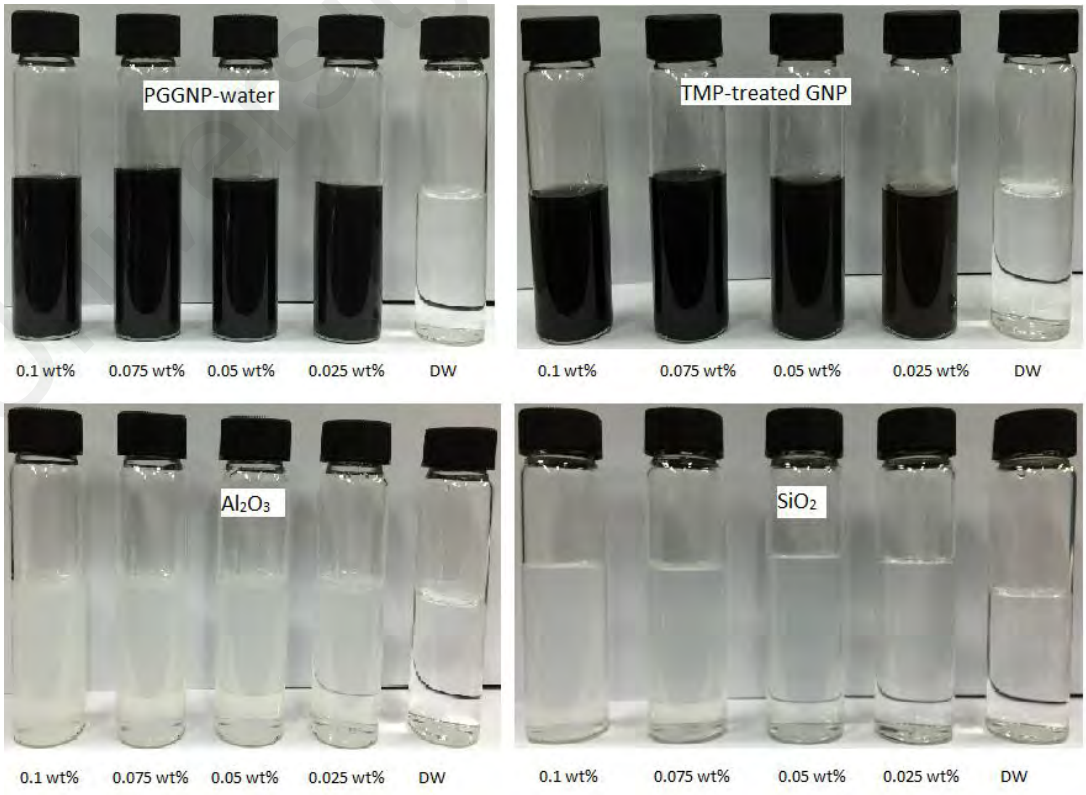

Figure 4.1. Shows the prepared nanofluids of all concentrations

4.3 Functionalization Analysis

4.3.1 Characterization of PGGNP-water

The FTIR spectra of the pristine GNP and PGGNP are shown in Figure 4.2. Obviously, in contrast to the pristine GNP, the PGGNP sample demonstrates clear cues of various functionalities groups. The detailed lists of peaks along with their interpretations are given in Table 4.2. The spectrum of PGGNP depict peaks at 1642 cm^{-1} and 1134 cm^{-1}, which could be attributed to the C=O and C–O stretching vibration. Also, another sharp peak at 1042 cm^{-1} is attributable to C–O stretching vibration of ester band, as a result of esterification of carboxylic acid groups on the main structure or edge of GNP with –OH band of PG. Thus, PG functionalization was confirmed by the appearance of peaks at 3403 cm^{-1}, 1453cm^{-1} and 1385 cm^{-1} for the O–H, COO^- stretching vibrations and CH_2 bending vibration, respectively. The peaks at 2931 and 2974cm^{-1} are in agreement with stretching vibration of C–H groups.

Table 4.2. Fourier transform infrared interpretation of the functionalized GNP

Peak(cm^{-1})	Interpretation
3403	O–H stretching vibration
2931 and 2974	C–H stretching vibration
1642	–C=O stretching vibration (Ester band)
1453	COO^- Stretching vibration
1385	CH_2 bending vibration
1134	C–O stretching vibration (carboxylic group)
1042	C–O stretching vibration (ester band)

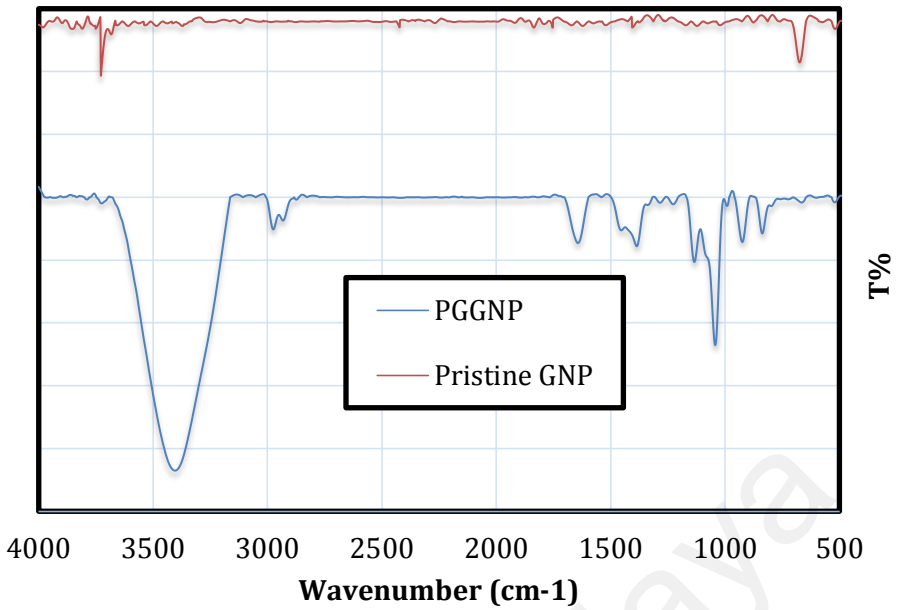

Figure 4.2. FTIR spectra of Pristine GNP and PGGNP

Raman spectral analyses of the PGGNP and as pristine GNP are shown in Figure 4.3. The Raman spectra of the both samples exhibit D and G bands, at around 1362cm^{-1} and 1592 cm^{-1} respectively. The D bands are related to the amorphous/disordered carbon (sp^3) and G bands to the graphitic carbon (sp^2). Increase in the I_D/I_G ratio means that number of sp^2 hybridized carbons changed to sp^3 hybridization carbons because of the covalent functionalization. However, it could be seen that intensity ratio of PGGNP sample is larger than that of the pristine GNP.

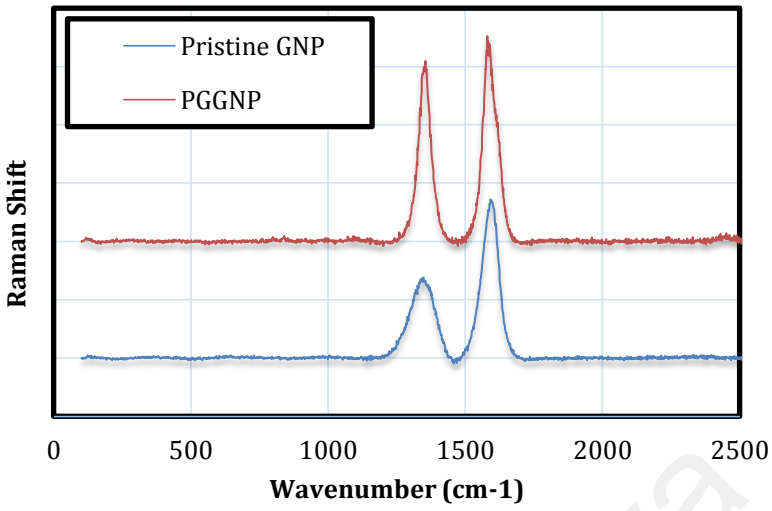

Figure 4.3. Raman spectra of pristine GNP and PGGNP.

Figure 4.4 illustrates the SEM and TEM images of pristine GNP and PGGNP. Although SEM and TEM images are not able to distinguish minute functional groups, but it can show the surface deterioration and wrinkles of the GNPs that formed as a result of PG functionalization. Overall, one can see some multi-layer GNP flakes with suitable and big grain size in images. According to the SEM and TEM results, the PGGNP papers preserved their shape and size. The marked changes in morphology and surface deterioration clearly can be seen in the SEM and TEM images. In particular, the lines seen in the TEM images are wrinkles on the GNP surface due to the inherent instability of 2D structures. The presence of these lines in PGGNP can be attributed to the enhancement of wrinkles (waviness) during the sonication procedure, resulting from the flexibility of GNP flakes after treatment.

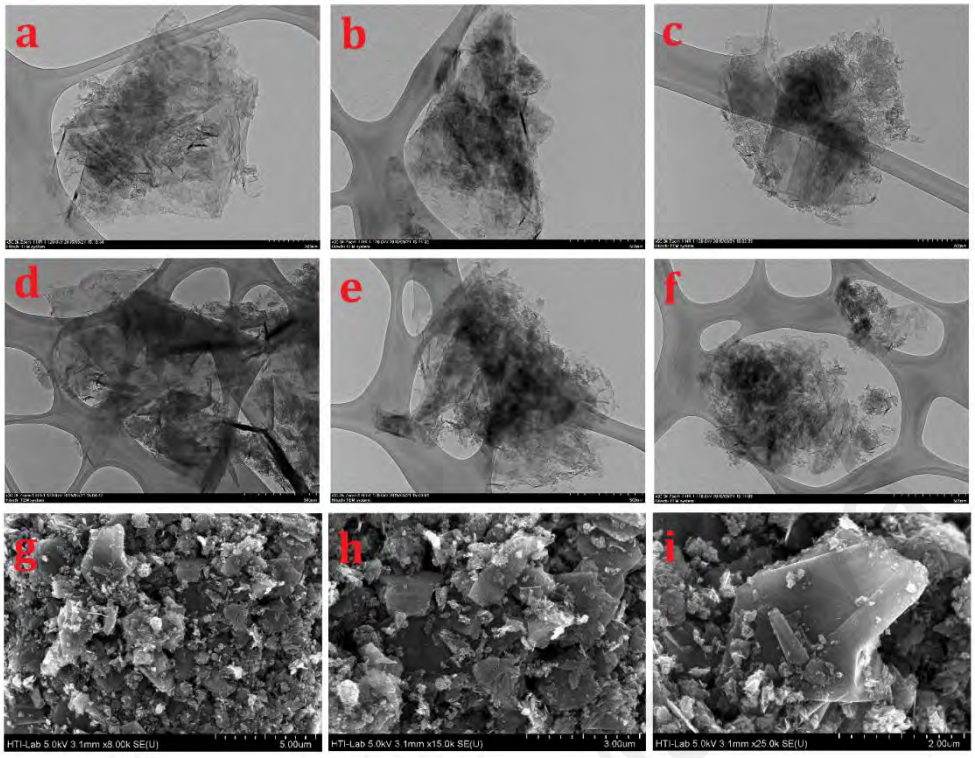

Figure 4.4. (a-f) TEM and (g-i) SEM images of PGGNP

4.3.2 TMP-treated GNP

The FTIR spectra of the pristine GNP and TMP-treated GNP are shown in Figure 4.5. Obviously, in contrast to the pristine GNP, the TMP-treated GNP sample shows clear cues of various functionalities groups. The detailed list of peaks along with their interpretations are listed in Table 4.3. The spectrum of TMP-treated GNP shows some peaks at 1637 cm^{-1} and 1105 cm^{-1}, which could be attributed to the C=O and C–O stretching vibration. Also, another small peak at 919 cm^{-1} is attributable to C–O stretching vibration of ester band, as a result of esterification of carboxylic acid groups on the main structure or edge of GNP with –OH band of TMP. Thus, TMP functionalization was confirmed by the appearance of peaks at 3430 cm^{-1} for O−H and N−H stretching vibration of primary amine/Symmetrical −NH stretching vibration. Also, the peaks at 2968 and 2876 cm^{-1} are in agreement with stretching vibration of C–H groups. Also, peak centered around 1575 cm^{-1} is attributable to the C=C stretching

vibration, as a result of the destruction of the main structure or open ends of GNP. TMP functionalization was further established by the appearance of peaks at 1463 cm^{-1} and 1375 cm^{-1} for the CH_2 and NH_2 bending vibrations, respectively.

Table 4.3. Fourier transform infrared interpretation of the functionalized GNP

Peak(cm^{-1})	Interpretation
3430	O − H and N − H stretching vibration of primary amine/Symmetrical − NH stretching vibration
2968 and 2876	C–H stretching vibration
1637	–C=O stretching vibration (Ester band)
1575	–C=C stretching vibration
1463	CH_2 bending vibration
1375	NH_2 bending vibration
1105	C–O stretching vibration
919	C–O stretching vibration (Ester band)

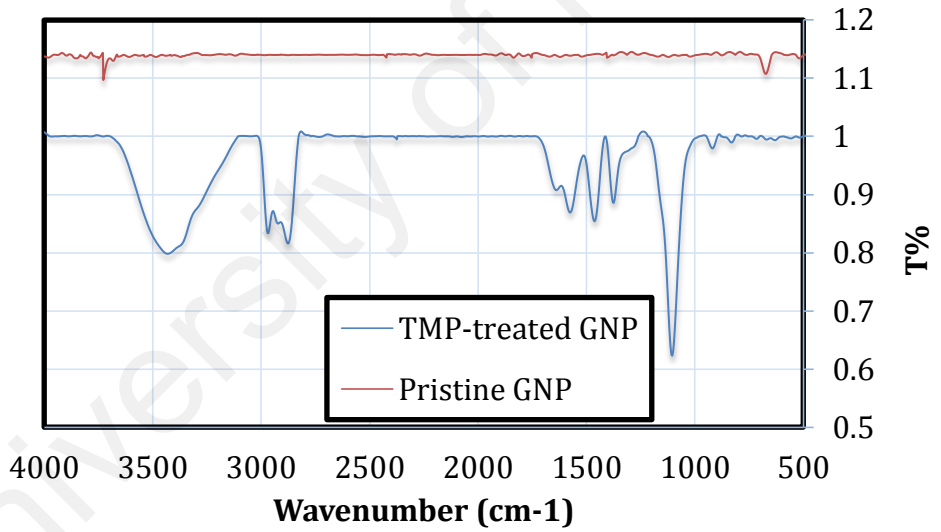

Figure 4.5. FTIR spectra of Pristine GNP and TMP-treated GNP

Raman spectral analysis of the TMP-treated GNP as well as pristine GNP are shown in Figure 4.6. The Raman spectra of the both samples exhibit D and G bands, at around 1362cm^{-1} and 1592 cm^{-1} respectively. The D bands are attributed to the amorphous/disordered carbon (sp^3) and G bands to the graphitic carbon (sp^2). Increase in the I_D/I_G ratio means that number of sp^2 hybridized carbons changed to

sp^3 hybridization carbons because of the covalent functionalization [20-21]. However, as could be seen intensity ratio of TMP-treated GNP sample is significantly larger than that of the pristine GNP. Note that TMP-treated GNP and pristine GNP show the I_D/I_G ratios of 0.92 and 0.51, which is in agreement with FTIR results.

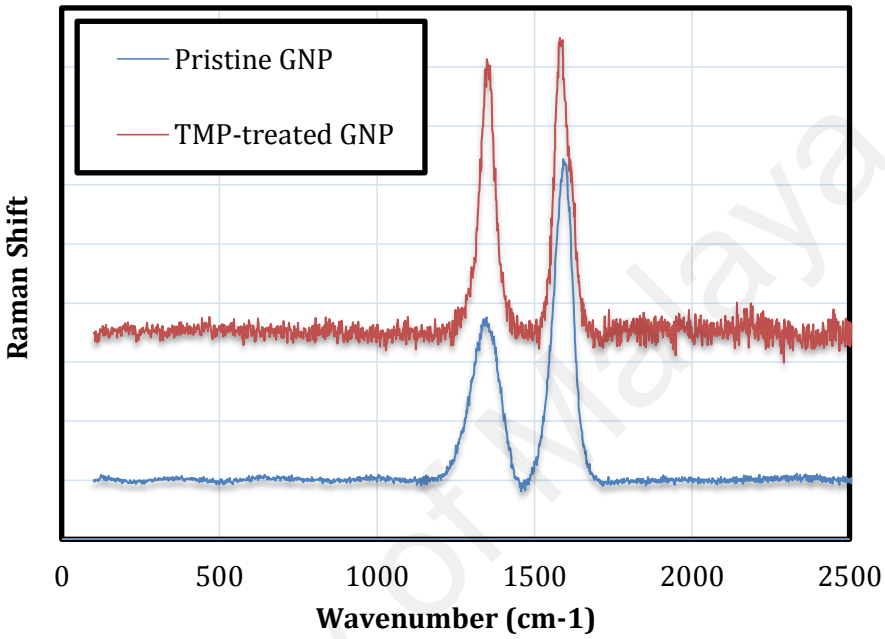

Figure 4.6. Raman spectra of pristine GNP and TMP-treated GNP.

Figure 4.7 illustrates the TEM images of pristine GNP and TMP-treated GNP. TEM images are able to show the surface deterioration and wrinkles of the GNPs that formed as a result of TMP functionalization. Overall, one can see some GNP sheets with large grain size in images. According to the TEM results, the TMP-treated GNP papers preserved their shape. Also, the lines seen in the TEM images are wrinkles on the GNP surface due to the inherent instability of 2D structures. The presence of these lines in TMP-treated GNP can be attributed to the enhancement of wrinkles (waviness) during the sonication procedure, resulting from the flexibility of GNP flakes after treatment. Note that functionalization can increase the wrinkles by increasing the wettability of surface.

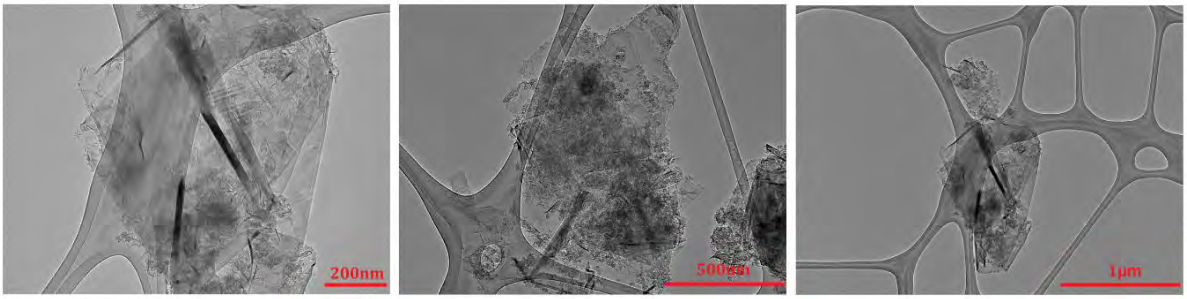

Figure 4.7. TEM images of TMP-treated GNP.

4.4 Characterization of Al_2O_3 and SiO_2

It is important to be able to fully characterize the nanofluids under inspection for heat transfer enhancement. The first steps are to quantify the composition, size and loading of the nanoparticles and search for impurities in the nanofluids. Tools utilized to characterize and qualify nanofluids for this study include neutron transmission electron microscopy (TEM) imaging, zeta potential.

4.4.1 Al_2O_3

The agglomeration of nanoparticles results in not only settlement and clogging but also the decrement of thermal conductivity of nanofluids. So, stability analysis is a matter of importance in context to its application. Sedimentation, centrifugation, spectral analysis and zeta potential analysis are the four basic methods for evaluating stability of nanofluids. The stability of nanofluids can be also detected by the electron and optical microscopes. Optical spectroscopy uses the interaction of light with matter as a function of wavelength or energy in order to obtain information about the material. Optical spectroscopy is attractive for materials characterization because it is fast, non-destructive and of high resolution. TEM is reckoned as the most important tool to determine the size distribution and the morphology of the synthesized nanoparticles. It uses electron beam to create the image of samples. Figure 4.8 depict, respectively, the

TEM images of 0.1 wt.% Al_2O_3/water nanofluid. As indicated in the TEM images (Fig. 4.8 a and b), the alumina nanoparticles are rectangle and rod-like in shape. However, the figures (Figure 4.8 c and d) portray that the sample with 0.1wt.% dispersant have the very minor agglomeration and they reached better suspension. Figure 4.8 presents TEM images after 1hr sonication. The sample is generally a much better dispersion. It can seen clearly that all particles are of same in size and their shize is below 50nm. In figure 4.8 From the TEM images, we find that the nanoparticles are spheres and have a broad size distribution. Another important aspect of the TEM is the ability to measure particle material content via the transmitted beam spectrum. This allows a distinction between large Al_2O_3 particles, debris or other impurities, and may show whether the Al_2O_3 particles are scouring and collecting surface material. In Figure 4.8 shows that the majority is Al_2O_3, indicating good purity of the sample and giving confidence in the above method of synthesis. For this study to get higher thermal conductivity no any surfactant was used.

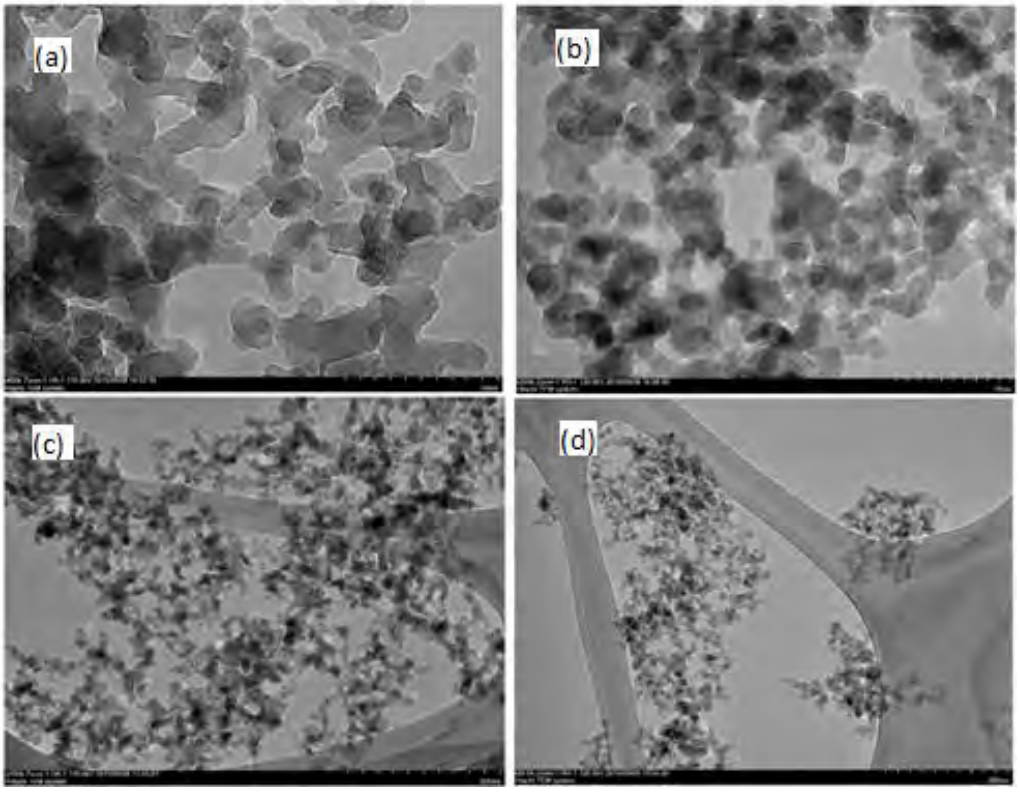

Figure 4.8. TEM images of Al_2O_3 at 0.1wt%

4.4.2 SiO_2

Figure 4.9 represents, the TEM images of 0.1 wt.% SiO_2/water nanofluid. As indicated in the TEM images (Fig.4.9 a and b), the silica nanoparticles are round and rod-like in shape. However, the figures (Figure 4.9 c and d) portray that the sample with 0.1wt.% dispersant have the very minor agglomeration and they reached better suspension. It can see clearly that all particles are of same in size and their size is below 50nm. Figure 4.9 presents TEM images after 1hr sonication. The sample is generally a much better dispersion. In figure 4.9 From the TEM images, we find that the nanoparticles are spheres and have a broad size distribution. To achieve the higher thermal conductivity no any surfactant was used for this work. Another important aspect of the TEM is the ability to measure particle material content via the transmitted beam spectrum. This allows a distinction between large SiO_2 and Al_2O_3 particles, debris or other impurities, and may show whether the SiO_2 and Al_2O_3 particles are scouring and collecting surface material. In Figure 4.8 and 4.9 shows that the majority of the SiO_2 and Al_2O_3, indicating good purity of the sample and giving confidence in the above method of synthesis.

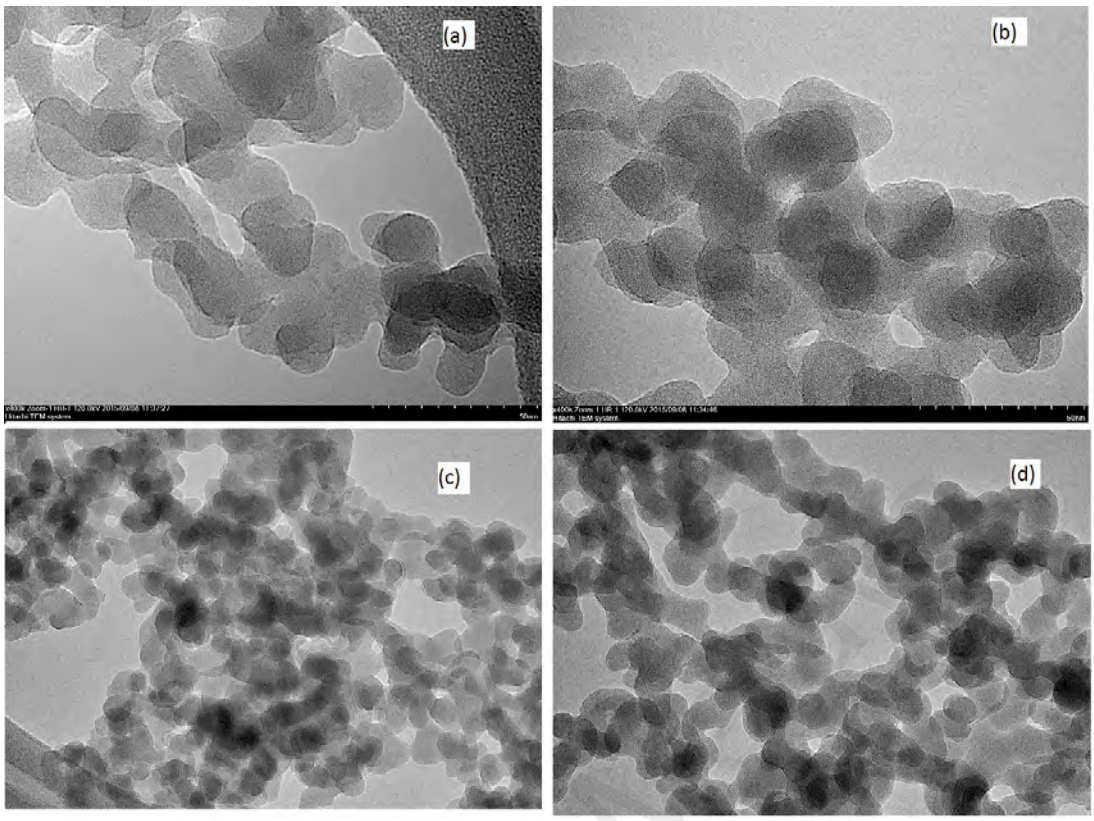

Figure 4.9. TEM images of SiO_2 at 0.1wt%

4.5 Stability

4.5.1 PGGNP-water

Plot of absorbance versus wavelength for highest concentrated colloidal solution in water was studied to trace the presence of specific particle within the binary system (Figure 4.10a). Figure 4.10b shows the plot of absorbance intensity versus wavelength for the PGGNP in water taken at specific period of time (34 days). It depicts the appreciably higher dispersibility of PGGNP in aqueous media. The measurement was carried out at peak wavelength of PGGNP-water to trace the alteration in the intensity which can be further used to describe the suspension stability at the constant weight fraction of PGGNP. It can be seen that the colloidal mixture show a downward trend of relative concentration as the time progressed, indicating that the level of particle concentration and thus the stability subsided. Also, the relative concentration (absorbance intensity) including PGGNP-based water shows the low amount of

sediment. The easily-miscible PG functionalities in water may explain the higher dispersion of the functionalized graphite as compared with others.

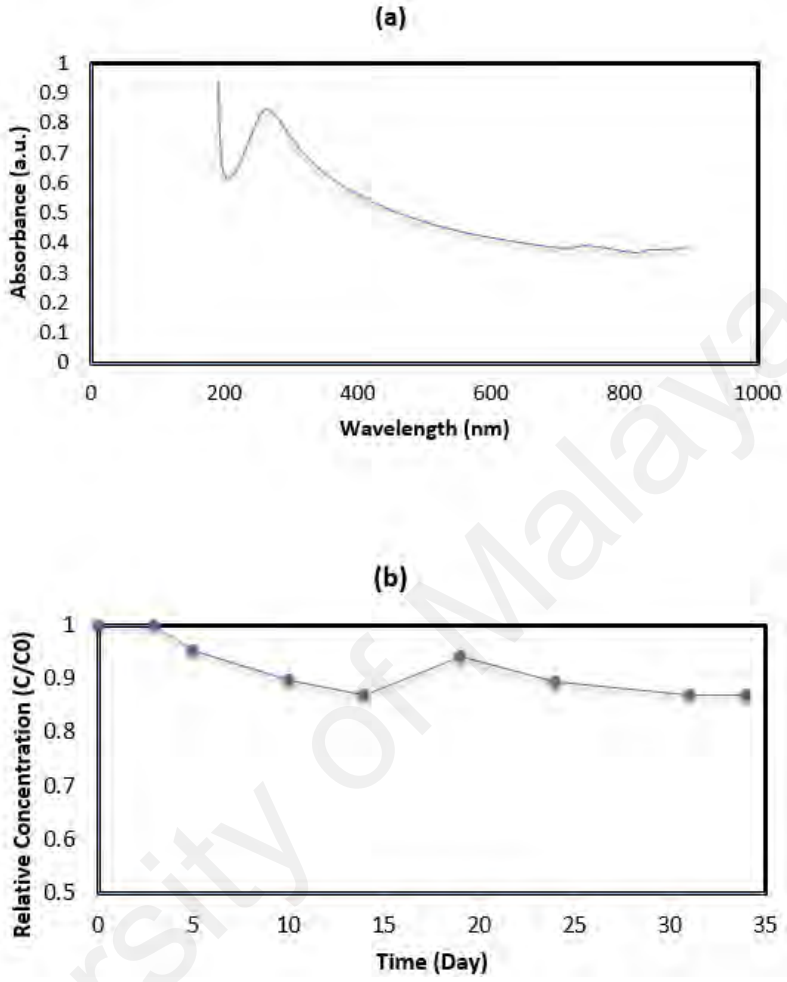

Figure 4.10. (a) Plot of absorbance versus wavelength for PGGNP-based water nanofluid at 0.1 wt% and (b) plot of colloidal stability of PGGNP in water.

4.5.2 TMP-treated GNP

Plot of absorbance versus wavelength for highest concentrated colloidal solution in aqueous media was investigated for presenting the specific particle within the binary system (Figure 4.11a). Figure 4.11b shows the plot of absorbance intensity versus wavelength for the TMP-treated GNP in water taken at specific period of time (34 days). It depicts the noticeably higher dispersibility of TMP-treated GNP in water as the main basefluid. The measurement was carried out at peak wavelength of TMP-treated

GNP/water coolants to trace the alteration in the intensity which can be further used to describe the suspension stability at the constant weight fraction of nanoparticles. It can be seen that the colloidal mixture show a gradual downward trend of relative concentration with time, indicating that the level of particle concentration and thus the stability subsided, surprisingly less than 12% sediment. Also, the relative concentration (absorbance intensity) including TMP-treated GNP-based water coolant shows the low amount of sediment (maximum of sediment was 12%). The easily-miscible TMP functionalities in water may explain the higher dispersion of the functionalized GNP flakes.

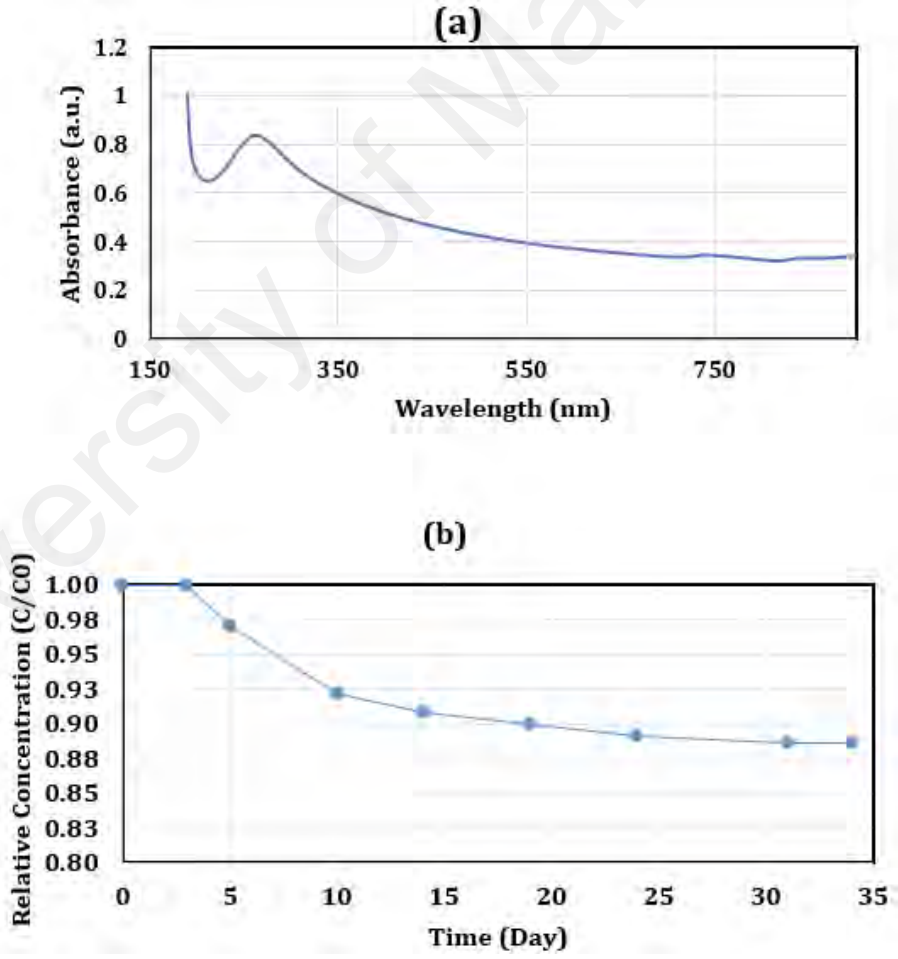

Figure 4.11. (a) Plot of absorbance versus wavelength for TMP-treated GNP-based water coolant at 0.1 wt.% and (b) plot of colloidal stability of TMP-treated GNP in water.

4.5.3 Al_2O_3

The stable homogeneous Al_2O_3 nanofluids were prepared for this study without using any surfactant. Plot of absorbance versus wavelength for highest concentrated colloidal solution in water was studied to trace the presence of specific particle within the binary system (figure 4.12). Figure 4.12b shows the plot of absorbance intensity versus wavelength for the Al_2O_3/water taken at specific period of time (31 days). It depicts the appreciably higher dispersibility of Al_2O_3 in aqueous media.

The measurement was carried out at peak wavelength of Al_2O_3 to trace the alteration in the intensity which can be further used to describe the suspension stability at the constant weight fraction of Al_2O_3. It can be seen that the colloidal mixture show a downward trend of relative concentration as the time progressed, indicating that the level of particle concentration and thus the stability subsided. Also, the relative concentration (absorbance intensity) including Al_2O_3 based water shows the low amount of sediment. The easily-miscible Al_2O_3 in water may explain the higher dispersion of the Al_2O_3 nanoparticle as compared with others.

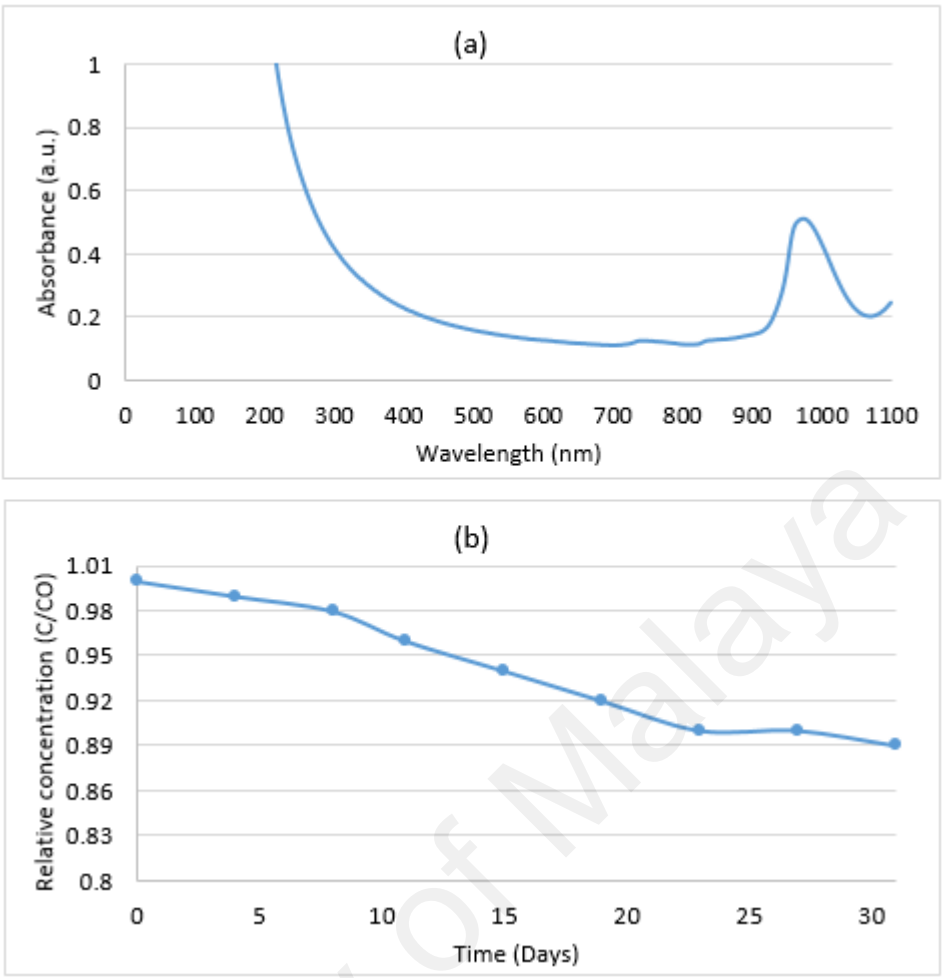

Figure 4.12. (a) Plot of absorbance versus wavelength for Al_2O_3 based water nanofluid at 0.1 wt% and (b) plot of colloidal stability of Al_2O_3 in water.

4.5.4 SiO_2

The stable homogeneous SiO_2 nanofluids were prepared for this study without using any surfactant. Plot of absorbance versus wavelength for highest concentrated colloidal solution in water was studied to trace the presence of specific particle within the binary system (figure 4.13a). Figure 4.13b shows the plot of absorbance intensity versus wavelength for the SiO_2/water taken at specific period of time (31 days). It depicts the appreciably higher dispersibility of SiO_2 in aqueous media. The measurement was carried out at peak wavelength of SiO_2 to trace the alteration in the intensity which can be further used to describe the suspension stability at the constant weight fraction of SiO_2. It can be seen that the colloidal mixture shows a downward trend of relative

concentration as the time progressed, indicating that the level of particle concentration and thus the stability subsided. Also, the relative concentration (absorbance intensity) including SiO_2 based water shows the low amount of sediment. The easily-miscible SiO_2 in water may explain the higher dispersion of the SiO_2 nanoparticle as compared with others.

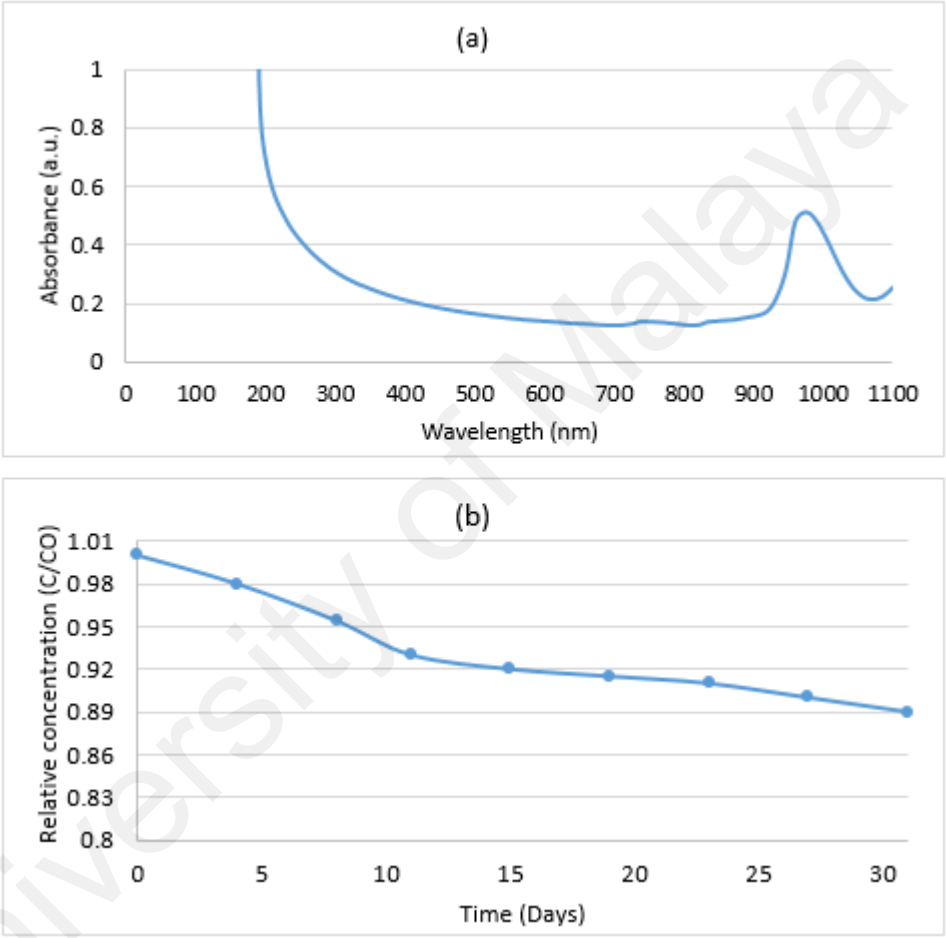

Figure 4.13. (a) Plot of absorbance versus wavelength for SiO_2 based water nanofluid at 0.1 wt% and (b) plot of colloidal stability of SiO_2 in water.

Table 4.4 demonstrates the particle size distributions and zeta potential for Al_2O_3 and SiO_2 nanofluids. First, Al_2O_3 shows no big aggregation and coagulation at highest concentrations of 0.1 wt%. It can be seen that the particle size distribution for Al_2O_3

nanofluids show a gradual increase in the overall hydrodynamic size, which substantiates the formation of small aggregation, which is in agreement with UV-vis results. On the other hand, SiO_2 shows good dispersion and coagulation at highest concentrations of 0.1 wt%. According to the stabilization theory, the electrostatic repulsions between the particles increase if zeta potential has a high absolute value which then leads to a good stability of the suspensions. Particles with a high surface charge tend not to agglomerate, since contact is opposed.

Zeta potential is one of the common procedures for characterization of dispersion stability of the colloids and provides a measure of the magnitude and sign of the effective surface charge associated with the double layer around the colloid particle. The measurement of the zeta potential has carried out the electrophoretic behavior and additional details to understand the dispersion behaviour of metal oxides in water. Table 4.4 is also shown the zeta-potential and the polydispersity index (PDI) for Al_2O_3 and SiO_2 at their natural pH. The zeta-potential and polydispersity index (PDI) are commonly utilized as an index of the magnitude of electrostatic interaction between colloidal particles and thus can be considered as a measure of the colloidal stability of the solution. According to Table 4.4, zeta potential must be as large as possible (positively or negatively) to make a common repulsive force between the particles. It can be seen that after 1hour sonication, Al_2O_3 shows a more positively charged and is around +50 mV over a period of 7 days. The zeta potential results of SiO_2 suggest an appropriate stability over a period of 7 days at 25°C. Indeed, the zeta-potential gradually shows some fluctuations over a period of 7 days, in spite of remaining mostly stable with time. Nanofluids with zeta-potential above +30 mV or below -30 mV are having good stability (Vandsburger, 2010). It implies that the force of electrostatic repulsion between metal oxides is sufficient to get over the attraction force between particles.

Table 4.4. Zeta potential, average particle size distribution, mobility and polydispersity Index (PDI) of Al_2O_3 and SiO_2 in distilled water.

No.	Sample	Time (Day)	Average particle size distributions (nm)	Polydispersity index (PDI)	Zeta Potential (mV)	Mobility (μmcm/Vs)
1	Al_2O_3	7	138.2	0.192	50.1	3.93
2	SiO_2	7	207.9	0.274	-35.4	-2.776

4.6 Thermo-physical properties

4.6.1 Viscosity

Viscosity of nanofluids is one of the most critical parameter, which determines the quality of the heat transfer fluid. Similar to the base fluids, temperature is the main effective parameter on viscosity of nanofluids. A good understanding of the rheological properties and flow behavior of nanofluids is necessary before nanofluids can be commercialized in the heat transfer applications. These factors influencing the viscosity include concentration, size of nanoparticles, temperature of nanofluids, shear rate, etc. Thus, more investigations should be carried out on the viscosity of nanofluids. As expected, distilled water exhibits a Newtonian behavior within the shear rate range investigated. The viscosity value of distilled water was 1.034, which closely matches with its theoretical values at 20℃. The relative deviation is less than 2.5%. This is of the same order of magnitude as the experimental uncertainty. In general, the viscosity plots show close resemblance to the distilled water (DW) measurement with negligibly small increase in magnitude at increasing nanoparticle concentration. Figure 4.14 reports the viscosity of PGGNP-water viscosity versus shear rate at various concentrations and temperatures as a function of all tested temperatures. While nanofluids and base fluids

are strongly dependent on temperature, it is also observed in Figure 4.14 that the viscosity was decreased at higher temperatures. This is expected due to the weakening of the inter-particle and inter-molecular adhesion forces and similar trends have also been observed in almost all other varieties of nanofluids. It can be seen clearly that viscosity was increased for higher concentration of PGGNP-water. This can be realized in such a way that, once the concentration increases, the nanoparticles make agglomeration within the suspension. This consequently, results in the increase of internal shear stress in nanofluid because of the greater force needed for dissipating the solid element of the dispersion and hence an increase in viscosity.

In order to determine the rheological behaviors of PGGNP-water and TMP-treated GNP nanofluids, the viscosity of the aqueous GNPs versus shear rate was measured at the temperature range of 20 to 50℃ and the results are shown in Figure 4.14 and Figure 4.15. It is also interesting that nanofluids of low concentrations showing almost same viscosity values of the higher concentration. It shows that loading of the GNPs nanoparticles increase the friction and flowing resistance of fluids which ultimately causes increase of viscosity. While by rising the temperature, the nanoparticles are motivated more and create a higher space for them. This is expected due to the weakening of the inter-particle and inter-molecular adhesion forces and similar trends are also been observed for almost all other varieties of nanofluids. Following the trend of water, the samples of GNPs nanofluid also exhibit the shear thinning property. The cause of this non-Newtonian shear thinning can be explained generally as follows. At low shear rates, as the spindle rotates in the fluid, the structure of the fluid molecule changes temporarily and gradually align themselves in the direction of increasing shear and produce less resistance and hence a reduction in viscosity. When the shear rate is high enough the maximum amount of shear ordering possible is attained, the aggregates are broken down to smaller size decreasing the friction and hence the viscosity (Nabeel

Rashin & Hemalatha, 2013). If the shear rate is further increased it will not make any alteration to the viscosity. Due to small size and large surface area of nanoparticle there is possibility for structuring at low shear rates and a deformation and restructuring at high shear rates. Hence, nanofluid also follows the same trend. It is observed that at all the temperatures the shear thinning property is more pronounced at higher concentrations. This points out that at low concentrations the nature of base fluid plays a major role in shear thinning, but at higher concentrations there is significant contribution from the interaction between nanoparticle and fluid.

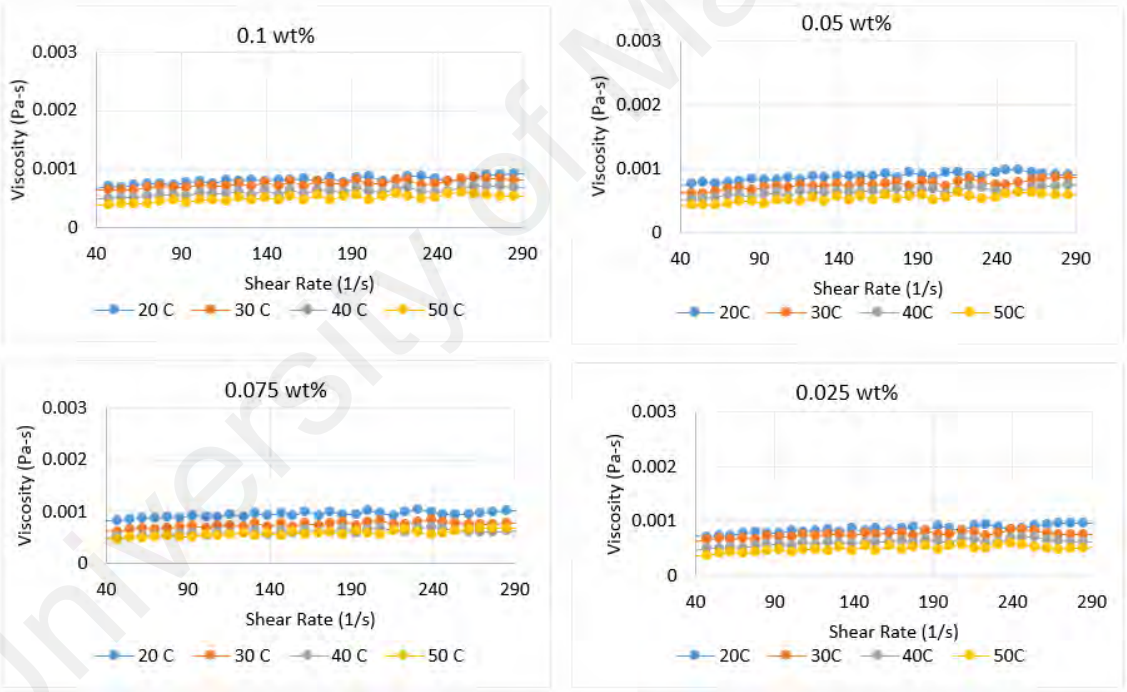

Figure 4.14. Plots of viscosity versus shear rate at various concentrations and temperatures for PGGNP-water.

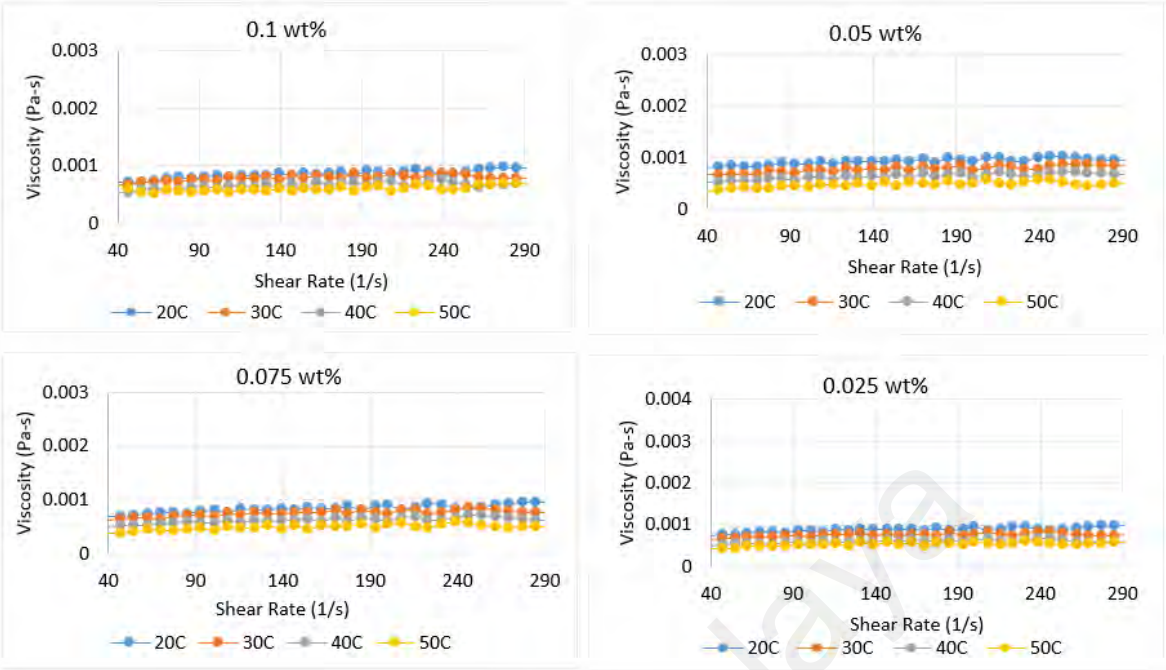

Figure 4.15. Plots of viscosity versus shear rate at various concentrations and temperatures for TMP-treated GNP.

In order to determine the rheological behaviors of metal oxide nanofluids (Al_2O_3 and SiO_2), the viscosity of the aqueous metal oxides versus shear rate was measured at the temperature range of 20 to 50°C and the results are shown in Figure 4.16 and Figure 4.17. In Figure 4.16 and 4.17, viscosities of Al_2O_3 and SiO_2 nanofluids without any surfactants are plotted as a function of concentrations and temperature. The results showed that shear thinning occurred at the 0.025wt% to 0.1wt%. The degree of shear thinning increases as the solid content in colloid increases. It was also noticed that the viscosities of nanofluids were getting close to the solvent viscosity at high shear rates. The results indicates that prepared nanofluids are suitable to use at elevated temperatures. Since, by increasing the temperature, thermal movement of molecules and Brownian motion intensifies, and intra-molecular interactions become weakened. In addition, rheological test on nanofluids revealed that the higher concentration will

increase the viscosity; however, other investigated parameters such as temperature and size areas have an important influence on viscosity behavior of nanofluids. In addition, a rheometer consists of outer (chamber) cylinder, and inner (spindle) cylinder and the nanofluid is located between them. As the spindle rotates in the nanofluid, the structure of the nano-particles molecule changes temporarily and slowly align themselves in the direction of increasing shear. A Newtonian fluid has the same viscosity when stronger or weaker forces (shear rate) are applied.

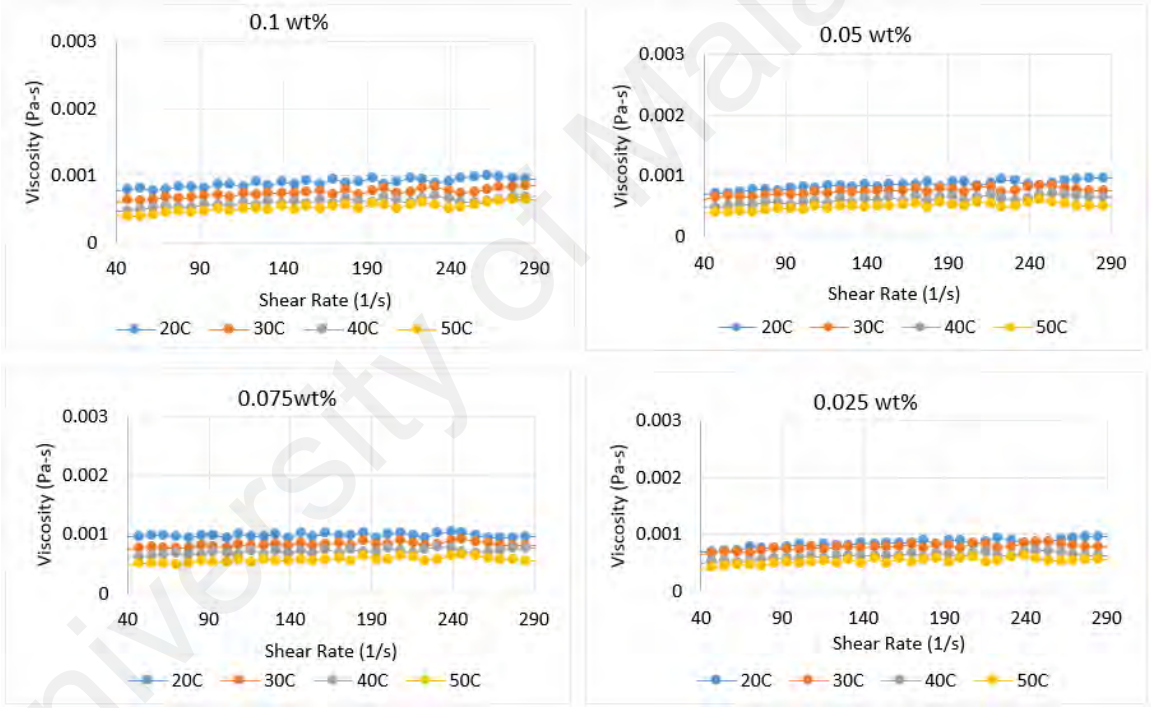

Figure 4.16. Plots of viscosity versus shear rate at various concentrations and temperatures for Al_2O_3.

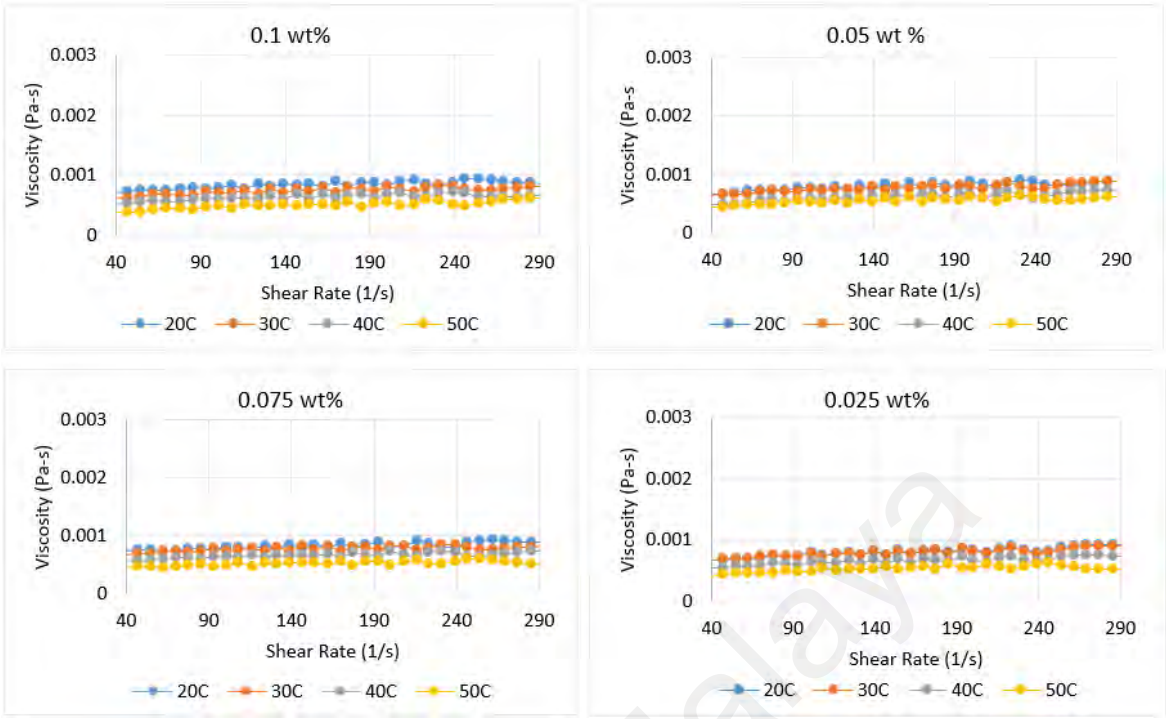

Figure 4.17. Plots of viscosity versus shear rate at various concentrations and temperatures for SiO_2.

It is observed experimentally that the prepared nanofluids are suitable to use at elevated temperatures; however, other investigated parameters such as temperature and concentration have important influence on viscosity behavior.

4.6.2 Thermal conductivity

Thermal conductivity of all the sample nanofluids at all concentrations were measured at temperature range from 25°C to 50°C by using KD2 pro thermal conductivity meter (Decagon Devices, Inc., Pullman, WA, USA) which is based on transient hot wire method. Four different weight concentrations (0.025%, 0.05%, 0.075% and 0.1%) were considered and the variation of thermal conductivity with concentration and temperature were studied. Therefore to prevent from sharp increase in effective viscosity, in this study both functionalized nanofluids were considered at low concentrations. Figure 4.18 (a and b) shows the thermal conductivity plot of PGGNP-water and TMP-treated GNP as a function of temperature and concentration. The

increase in thermal conductivity with temperature is more sensible in PGGNP-water and TMP-treated GNP. Thus, it confirms that the temperature play a key role in increasing the thermal conductivity of both coolants. The main mechanism for thermal conductivity enhancement with increase of temperature is attributed to the Brownian motion of the nanoparticles suspended in the base-fluid (Amiri, Sadri, Shanbedi, Ahmadi, Chew, et al., 2015; Aravind et al., 2011). The dynamic viscosities of both coolants were measured at the temperature 30°C. The dynamic viscosity of the nanofluids is the function of temperature and weight concentration. Similar to other coolants, the rheological behavior of both nanofluids showed an enhancement of viscosity with increasing concentration of nanofluids.

There is also a rising trend between the density of nanofluids and weight concentration, thus as the weight concentration increases the density increases. The GNP nanoparticle density is an important parameter for the increased friction factor and pressure drop of the coolants. Since the density of GNP is more than the basefluid, the density of nanofluid increases with concentration. The specific heat capacity of the PGGNP-water and TMP-treated GNP were measured at bulk temperature of 30°C (See Table 4.1 and Table 4.2)

In the present study, two types of nanoparticles were selected to prepare the water-based nanofluids due to their chemical stability. Preparation of nanofluids is the key step in the use of nanoparticles for stable nanofluids. Two step method has been employed in producing Al_2O_3 and SiO_2 nanofluids. Thermal conductivity of Al_2O_3 and SiO_2 nanofluids at all concentrations were measured at temperature range from 25°C to 50°C by using KD2 pro thermal conductivity meter (Decagon Devices, Inc., Pullman, WA, USA). Four different weight concentrations (0.025%, 0.05%, 0.075% and 0.1%) were considered and the variation of thermal conductivity with concentration and

temperature are studied. Therefore to prevent from sharp increase in effective viscosity, in this study both metal oxide nanofluids were considered at low concentrations. Figure 4.18 (c and d) shows the thermal conductivity plot of Al_2O_3 and SiO_2 as a function of temperature and concentration. As seen from Figure 4.18 (a and b), the thermal conductivity enhancement increases non-linearly with nanoparticles concentration for both types of nanofluids. The maximum enhancement for Al_2O_3 and SiO_2 were found up to 7.4% and 9%, respectively compared to the base fluids.

In comparison to Al_2O_3, the SiO_2 nanofluids have displayed superiority in performance. The increase in thermal conductivity with temperature is more sensible in SiO_2. In both nanofluids a trend shows that thermal conductivity increased with the increase in volume fraction. Thus, it confirms that the temperature play a key role in increasing the thermal conductivity of both coolants.

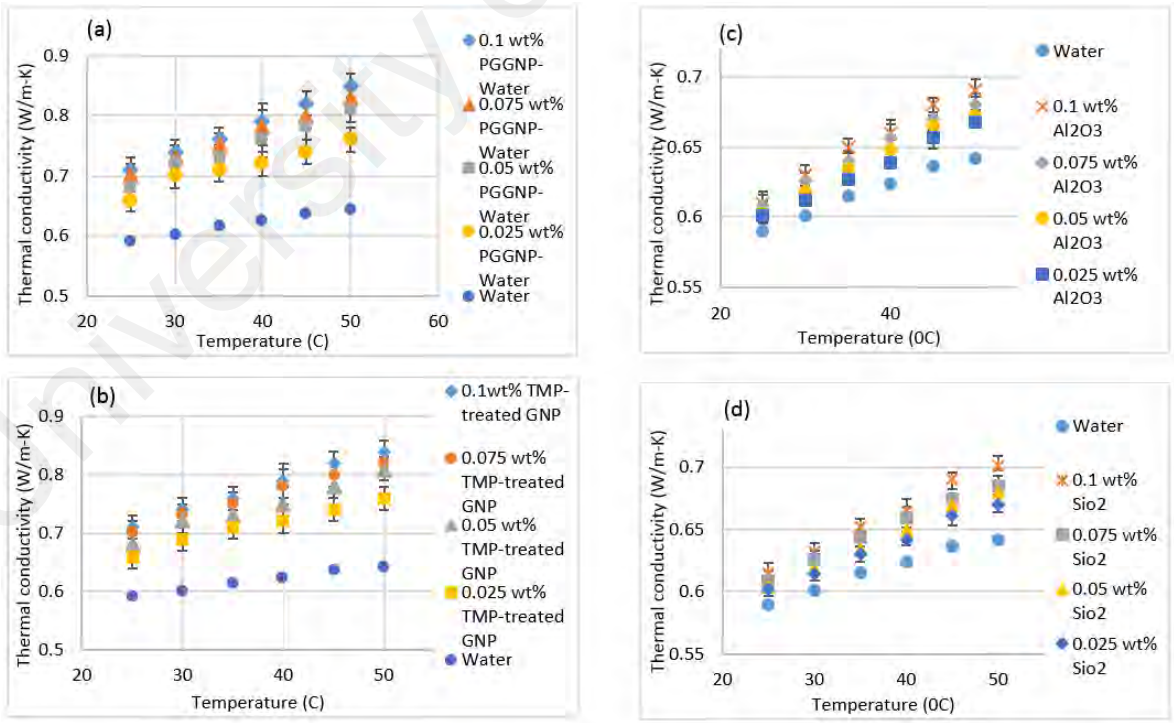

Figure 4.18. Thermal conductivity of (a) PGGNP-water, (b) TMP-treated GNP, (c) Al_2O_3 and (d) SiO_2 as a function of concentration and temperature

Figure 4.19 shows the thermal conductivity ratio for PGGNP-water, TMP-treated GNP, Al_2O_3 and SiO_2 nanofluids measured at different temperatures ranges from 25^0C to 50^0C. The linear dependence of thermal conductivity enhancement on temperature was obtained Figure 4.19a. From Figure 4.19, a similar trend of thermal conductivity enhancement is observed by increasing concentration and temperature. The enhancement of thermal conductivity for PGGNP-water is seen to be 20-32% at weight concentration of 0.1wt% and temperature range from 25°C to 50°C. Where in TMP-treated GNP the enhancement was found up to 31% higher than base fluid which is little lower than PGGNP-water as shown in Figure 4.19b. The enhancement of thermal conductivity for Al_2O_3 is seen to be 3-7.4% in weight concentration of 0.1wt% at temperature range from 25°C to 50°C as shown in Figure 4.19c. Similarly, in SiO_2 the enhancement was found up to 9% higher than base fluid as shown in Figure 4.19d. It was also observed that for the same weight percentage and temperature, functionalized GNPs presents higher thermal conductivity values than those of the other metal oxide nanofluids at the same concentrations.

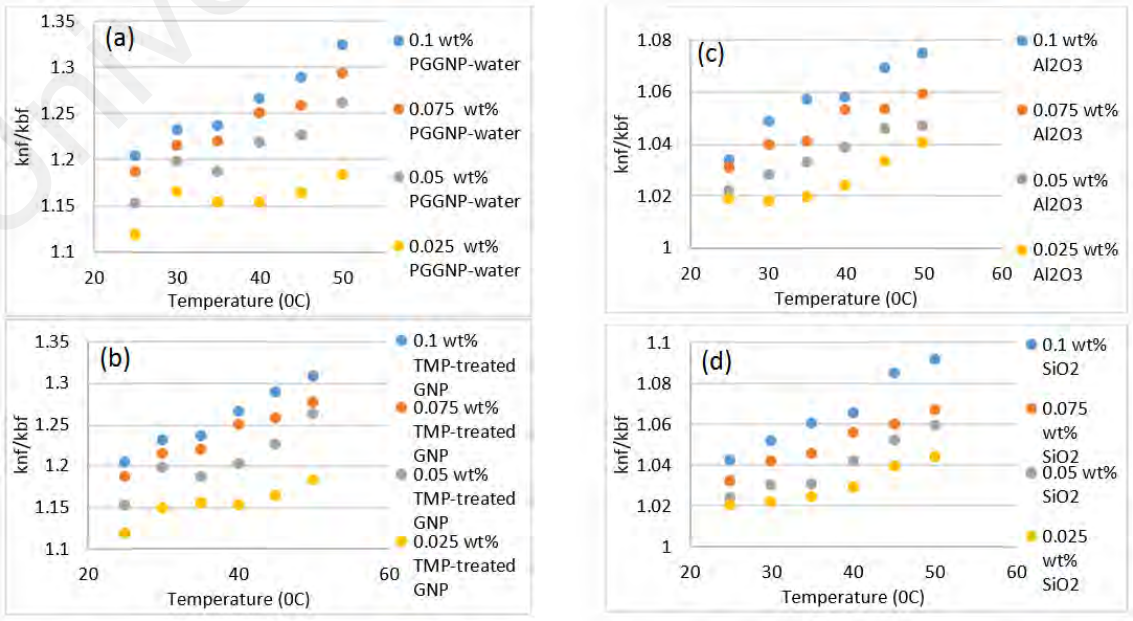

Figure 4.19. Thermal conductivity ratios of (a) PGGNP-water, (b) TMP-treated GNP, (c) Al_2O_3 and (d) SiO_2 with different concentrations and temperatures.

Table 4.5 to 4.8 shows the results of Specific heat, Density and Viscosity of PGGNP-water, TMP-treatred GNP, Al_2O_3 and SiO_2 nanofluids with different concentrations. Results shows the behavior of density of nanofluids. The data show that the temperature has also impact on density of nanofluids. Density of all nanofluids is higher than the base fluid (water) and with increase of temperature, density of nanofluid goes on decreasing. Further if nanoparticle weight concentration increases from 0.025 wt% to 0.1wt% density is increased. A heat flux type differential calorimeter was (TA DSC Q20) used to measure the specific heat capacity of nanofluids. DSC, is a thermal analysis technique that looks at material's heat capacity (Cp) change with temperature. A sample of known mass is heated or cooled and the changes in its heat capacity are tracked as changes in the heat flow. The term differential scanning calorimeter refers to both the techniques of measuring calorimetric data while scanning as well, which is a specific instrument design. The technique can be carried out with other types of instruments. Range of DSC is (-50 to 350°C).

Table 4.5. Specific heat, Dynamic viscosity and density of the PGGNP-Water at the bulk temperature of 30^0C

PGGNP-water Concentration	Density (kg/ m^3)	Specific heat (J/kg-K)	Viscosity (Pa-s)
0.1	1055.863	2807.352	0.003129
0.075	1040.232	3058.304	0.002347
0.05	1025.058	3358.526	0.001705
0.025	1010.32	3724.108	0.001192

Table 4.6. Specific heat, Dynamic viscosity and density of the TMP-treated GNP at the bulk temperature of 30^0C.

TMP-treated GNP Concentration	Density (kg/ m^3)	Specific heat (J/kg-K)	Viscosity (Pa-s))
0.1	1055.863	2807.352	0.003130

0.075	1040.232	3058.304	0.00235
0.05	1025.058	3358.526	0.001706
0.025	1010.32	3724.108	0.001193

Table 4.7. Specific heat, Dynamic viscosity and density of the Al_2O_3 at the bulk temperature of 30^0C.

Al_2O_3 Concentrations	Density (kg/m3)	Specific heat (J/kg-K)	Viscosity (Pa-s)
0.1	1072.747	3039.524	0.002155
0.075	1052.473	3261.876	0.001719
0.05	1032.95	3519.326	0.001351
0.025	1014.139	3820.899	0.001046

Table 4.8. Specific heat, Dynamic viscosity and density of the SiO_2 at the bulk temperature of 30^0C.

SiO_2 Concentrations	Density (kg/m3)	Specific heat (J/kg-K)	Viscosity (Pa-s)
0.1	1057.886	2796.342	0.003001
0.075	1041.705	3048.497	0.002265
0.05	1026.011	3350.635	0.00166
0.025	1010.783	3719.252	0.001174

CHAPTER 5: DATA REDUCTION, CALIBRATION, EXPERIMENTAL OBSERVATION AND ANALYSIS

5.1 Introduction

In this chapter the methodology of determining the heat transfer coefficient and friction factor are described. The experimental procedure and data reductions are discussed with the experimental results being validated for distilled water against the standard equations, such as the Gnielinski, Petukhov, and Dittus–Boelter for turbulent flow. Furthermore, for the pressure drop the results were compared and correlated with Power law, Blasius and Petukhov in turbulent flow conditions. The purpose of this validation was to ensure that the experimental setup can take accurate measurements with water before any test is conducted on the nanofluids.

5.2 Data reduction

5.2.1 Heat transfer coefficient

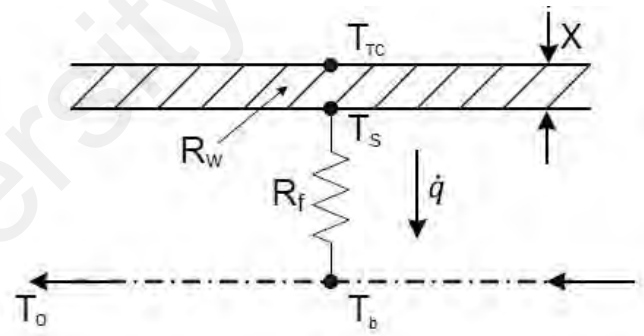

Figure 5.1. Schematic of the (a) resistances inside the test section and (b) control volume around the mean fluid temperature

Figure 5.1 shows the schematic of the test section showing the thermal resistances from which the local heat transfer coefficient is calculated by Equation (5.1). All measurements were taken at constant heat flux of 23870 W/m^2 and 18565 W/m^2 and

data were taken by steady state conditions at the chosen velocity, surface temperature and bulk temperature. The inlet temperature was fixed at 30℃ with the help of refrigerated bath circulators. The velocity was systematically increased, the heat flux was fixed, ΔT and the local surface temperatures were recorded using the data acquisition system for heat transfer study. The local heat transfer coefficient, $h_c(x)$ was calculated from Equation (5.1).

$$h_c = \frac{\dot{q}}{T_w - T_b} \tag{5.1}$$

The terms in this equation were determined as explained below. The energy input to the heater, (the heat flux, $\dot{q}$) was the amount of total heat supplied through the phase angle power controller to the heaters divided by the heated surface area A. the wall temperature T_w was calculated from the temperature measured in the test section by the thermocouples, T_{TC} with a correction to account for the distance of the thermocouple below the heating surface to the inner wall of the pipe in fluid contact. Equation (A1) represents the T_w and the wall resistance for each of the thermocouples (λ/x) was determined by calibration of the test rig with water as presented in Appendix A.

The wall temperature, T_b was a position-weighted value of the inlet and outlet temperatures (T_i and T_b respectively). Equation (5.2) represents bulk temperature as a function of inlet and outlet temperatures. This was based on the assumption that the fluid temperature was increased linearly over the heated section and remained constant in the unheated section of the rig. Length

$$T_b = T_i + \frac{Thermocouples\ possition}{heating\ \text{Length}}(T_o - T_i) \tag{5.2}$$

The heat flux, $\dot{q}$, was determined from the electrical energy input, $Q = V.I$, and the inner surface area, $A_s = \pi.D.L$. The electrical energy input remained constant at 700 and 900W throughout the measurements thus resulting in a constant heat flux (18565 W/m^2 and 23870 W/m^2, respectively). The equation of the heat flux is given by equation (5.3):

$$\dot{q} = \frac{P}{A} = \frac{V \times I}{\pi DL} \tag{5.3}$$

The temperature profile between the thermocouple and the fluid inside the circular pipe and the bulk temperature are calculated using the Wilson plot method (Fernández-Seara, Uhía, Sieres, & Campo, 2007; Kazi et al., 2014). The exact and real wall, the fluid temperatures, and the heat flux are measured to calculate the convective heat transfer coefficient (Sadeghinezhad, Emad et al., 2014a).

An estimation of the heat flux, heat transfer coefficient, Nusselt number, friction factor, and Reynolds number are presented in Equations (5.4-5.7).

(a) The Nusselt number is defined by Equation (5.4).

$$Nu = \frac{hD}{k} \tag{5.4}$$

(b) The friction factor is defined by Equation (5.5).

$$f = \frac{\Delta P}{\left(\frac{L}{D}\right)\left(\frac{\rho v^2}{2}\right)} \tag{5.5}$$

(c) The Reynolds number is defined by Equation (5.6).

$$Re = \frac{\rho VD}{\mu} \quad (5.6)$$

(d) The Prandtl number is defined by Equation (5.7).

$$Pr = \frac{\mu C_p}{k} \quad (5.7)$$

The temperature dependent thermal conductivity of stainless steel is found from a linear curve fit of data found in the ASM Handbook. The resulting linear fit for the temperature dependent is the following function:

$$k_w(T) = 0.0127\,.\,T + 13.23188 \quad (5.8)$$

5.3 Experimental procedure

An investigation of the heat transfer behavior of the nanofluids was performed by evaluating the Nusselt number and the heat transfer coefficient. The measurements were performed in the bulk velocity range of 1 to 3 m/s for the distilled water and the nanofluids, which caused the Re number to vary from 3,900–11,700. The heat transfer coefficients were calculated based on the measured values for the inlet, outlet, and inner wall temperatures and the flow rates. The pressure drops over the tube was measured, and from these results, the friction factors were calculated. From the insulation surface temperatures, convective and radioactive heat loss to the surroundings were evaluated and found negligible. The heat loss can be calculated by the Equation (5.9) and Table Figure 5.2 shows the Average 3.96% heat loss from the test sections.

$$Q = VI = \dot{m} C_p (T_{in} - T_{out}) \quad (5.9)$$

Table 5.1. Heat loss calculations

Velocity (m/s)	Reynolds number	Input 700 Watt	Output (Watt)	Heat loss Percentage error (%)
1	3905	700	659.3058	5.813459
1.5	5858	700	692.3377	1.094618
2	7811	700	692.8704	1.018508
2.5	9764	700	657.9739	6.003735
3	11717	700	658.6398	5.908597

While, the influence of external surface heat radiation is considered, the surface temperature of the bare duct shown in Figure 5.3, and the complete heat transfer rate is calculated by the Equation (5.10-5.11).

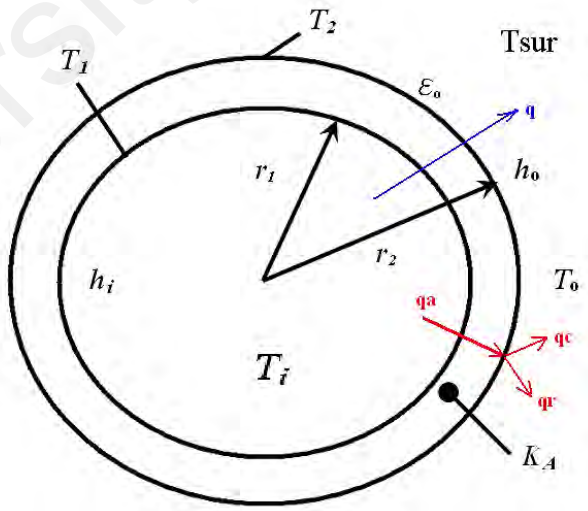

Figure 5.2. A non-insulated tube and its thermal resistance diagram

Since the test section surface area is very small compared with that of surroundings, thus the effect of emissivity of surroundings can be neglected.

$$q_a = q_c + q_r \tag{5.10}$$

$$q_c = \frac{T_2 - T_1}{\frac{1}{h_0 2\pi r_2 L}} \tag{5.11}$$

$$q_r = \sigma\varepsilon(T_2^4 - T_{sur}^4) \tag{5.12}$$

According to Wong, K.-L., Salazar, Prasad, and Chen (2011), the convective heat coefficient ratio percentage between radiation and convection is defined as Equation (5.13). If the value of $HR < 10\%$, the influence of heat radiation can be neglected. Figure 5.4 shows the insulation temperature (T_2) and ambient temperature versus fluid velocity at different heat flux for the water run.

$$HR = \frac{q_r}{q_c} \times 100 \tag{5.13}$$

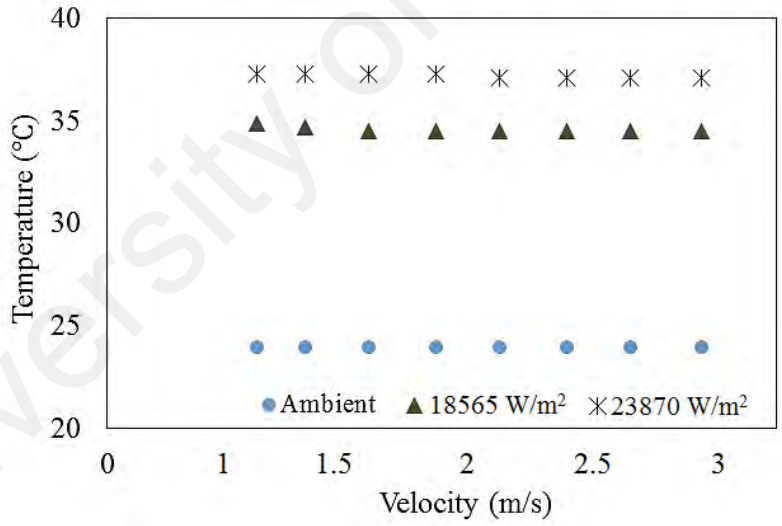

Figure 5.3. Outer insulation and surrounding temperature at different velocity for the water run.

In order to demonstrate the main differences between the heat transfer characteristics of situations while considering heat radiation, the detail data of the insulated material is enlisted in Table 5.1.

Table 5.2. Insulation details

Insolation thickness (t)	Insulation thermal conductivity (k_s)	Heat transfer coefficient for the outside of insulation (h_{sur})	Emissivity of the insulation (ε)
25mm	0.038W/m.K	10W/m^2.K	0.8

From the practical numerical results of this study, it is found that the heat radiation could be neglected due to the HR=5.8%.

Comparisons of the Nusselt numbers or the heat transfer coefficients at an equal Reynolds number is unreliable and is uninteresting from a practical perspective (Yu, W, France, Timofeeva, Singh, & Routbort, 2010). The comparison of nanofluids at the same Reynolds number is common in the literature for nanofluid fields (Bitaraf Haghighi et al., 2012; Davarnejad, Barati, & Kooshki, 2013; Rea et al., 2009; Sadeghinezhad, Emad et al., 2014a). Based on many literatures, comparing the heat transfer at the same flow rates (pumping power) is considered a more appropriate method in nanofluids study (Bitaraf Haghighi et al., 2012; Haghighi, Ehsan B et al., 2014; Kazi et al., 2014). Additionally, comparing the heat transfer coefficients for two different fluids at the same Reynolds number requires a higher flow rate (pumping power) for the fluid and a higher viscosity. Hence, the higher heat transfer at same Re number is not only because of the nanofluids performance, but might be due to the higher flow rate of nanofluids like viscosity effect (for measuring at same Re number) (Bitaraf Haghighi et al., 2012). Due to these reasons, it might be better to choose constant velocity instead of constant Re number (Sadeghinezhad, Emad et al., 2014a).

5.4 Validation test for distilled water

Prior to carrying out the set of detailed experiments on the selected nanofluids, a set of initial experiments were performed for water as the base fluid, in order to assess the

accuracy and reliability of the experimental setup. The experimental results for DW at constant heat flux conditions were compared with the results from the standard equations. The empirical correlations of Gnielinsky, Petukhov and DittuseBoelter (Dittus & Boelter, 1985; Heris, Shokrgozar, Poorpharhang, Shanbedi, & Noie, 2013) were selected for comparison with the obtained results especially for test of accuracy of the setup in the turbulent region (Kayhani, Soltanzadeh, Heyhat, Nazari, & Kowsary, 2012).

The Gnielinski equation for turbulent flow is given in Equation (5.14)

$$Nu = \frac{\left(\frac{f}{8}\right)(Re - 1000)Pr}{1 + 12.7\left(\frac{f}{8}\right)^{0.5}(Pr^{2/3} - 1)} \qquad (5.14)$$

Which is applied in the range of $0.5<Pr<2000$ and $3000<Re<5\times10^6$.

The friction factor for a fully developed turbulent flow depends on the Re number and is calculated by the equation (5.15).

$$f = \frac{\Delta P}{\left(\frac{L}{D}\right)\left(\frac{\rho v^2}{2}\right)} \qquad (5.15)$$

The Dittus–Boelter equation for turbulent flow is given in Equation (5.16)

$$Nu = 0.023Re^{0.8}Pr^{0.4} \qquad (5.16)$$

Which is applicable in the range of $Re>10^4$, $0.6<Pr<200$.

The Petukhov equation for turbulent flow is presented by Equation (5.17)

$$Nu = \frac{\left(\frac{f}{8}\right)RePr}{1.07 + 12.7\left(\frac{f}{8}\right)^{0.5}(Pr^{2/3} - 1)} \qquad (5.17)$$

Which is applied in the range of $0.5<Pr<2000$ and $3000<Re<5\times10^6$.

Figure 5.5 (a and b) shows a comparison between the experimentally average Nusselt number and the data from the above-mentioned equations (Equations (5.14-5.17)). The experimental data and classical correlations agree well. Data from the Gnielinski equation and the experimental Nusselt number for distilled water are better than the data from the other equations and validate the accuracy of the experimental setup with an error rate of less than 10%. Based on the literature (Yunus, 2003), at lower Re number the Gnielinski equation is more accurate and at higher Re number Petukhov equation is more accurate as observed in the reliability test of the experimental setup.

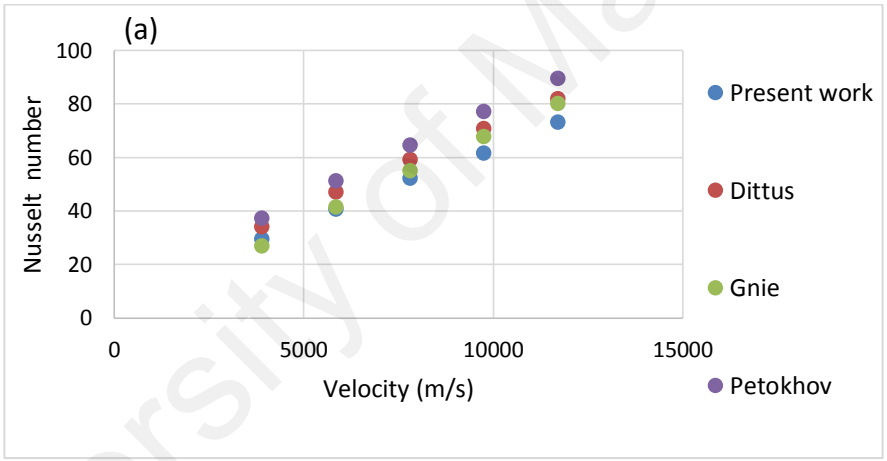

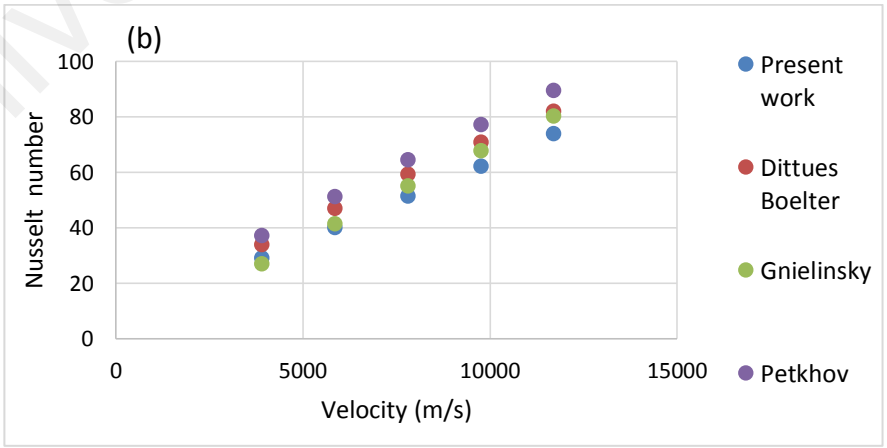

Figure 5.4 Measured average Nusselt number and the prediction correlations for distilled water versus the velocity at different heat fluxes; (a) 18565 W/m^2 (b) 23870 W/m^2

The data of experimental friction factor are derived from the measurements of the pressure drop along the length of the test section. To verify the friction factor data, the experimental results for DW are validated by the Blasius equation (Chandra Sekhara Reddy & Vasudeva Rao, 2014) , the Power law and Petukhov correlations (Kazi et al., 2014). Among all equations Power law showed the more accuracy with DW data.

The Power law Equation (5.18) is the most simple equation for solving the Darcy friction factor. Because the Power law Equation (has no term for pipe roughness, it is valid only to smooth pipes. However, the Blasius equation is sometimes used in rough pipes because of its simplicity. The Power law Equation is valid up to the Reynolds number 10^5.

$$f = 0.184\, Re^{0.2} \qquad (5.18)$$

Figure 5.6 shows the validation of the friction loss data from the experimental investigation, and the above-mentioned equations have an error rate of less than 10%.

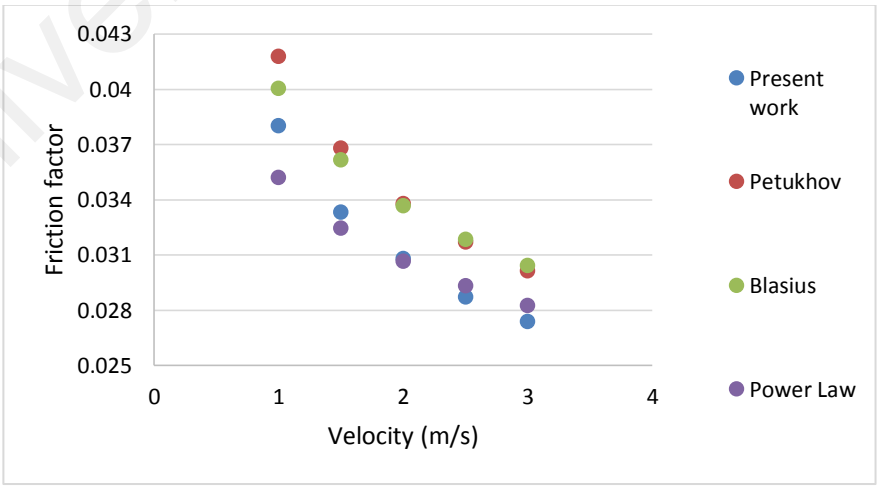

Figure 5.5. Friction factor as a function of velocity for distilled water

5.5 Uncertainty analysis of the test results

The uncertainty analysis of the measured data along with the relevant parameters obtained from the data reduction process is presented in Table 5.2 and is estimated based on the error propagation method (Kumaresan, Mohaideen Abdul Khader, Karthikeyan, & Velraj, 2013; Taylor, J. R., 1997).

Table 5.3. Uncertainty ranges.

Variable name	Uncertainty range
Nu, avg	±10%
Nu, Local	±8%
h, avg	±6%
h, local	±9%
f	±10%

The full uncertainty analysis could be found in Appendix A.

5.6 Data reproducibility

In the pipe flow studies for DW as the base fluids for data reproducibility. Figure 5.7 (a and b) represents heat transfer coefficient as a function of velocity for two runs of DW at the bulk temperature of 30℃. It is observed that the data reproduced well, test rig was highly accurate and remains within $<$ 1% error.

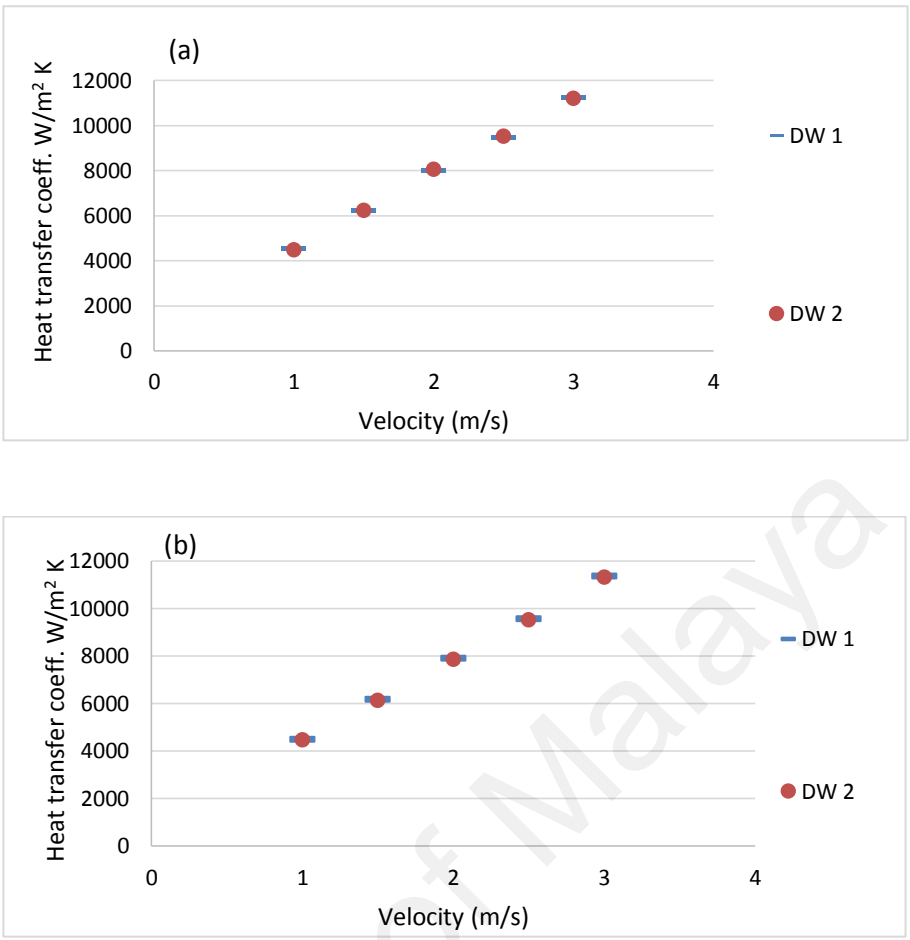

Figure 5.6. Heat transfer coefficient as a function of velocity for two different water runs at two different heat fluxes of (a) 18565 W/m^2 and (b) 23870 W/m^2.

.

Similarly, the frictional pressure drop (ΔP/L) data for two runs of DW at bulk temperature 30℃ is presented in Figure 5.8. The reproducibility is good and remains within < 1% error.

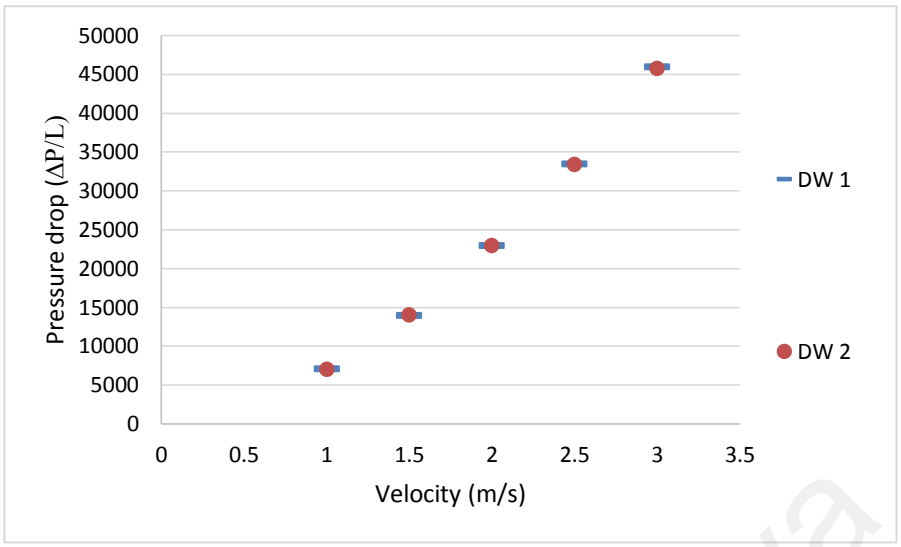

Figure 5.7. Frictional head loss as a function of velocity for two different DW runs

CHAPTER 6: STUDY OF HEAT TRANSFER AND FRICTION FACTOR OF NANOFLUIDS IN CLOSED CONDUIT

6.1 Convective heat transfer to functionalized GNPs and Metal oxide nanofluids

Present study focuses on investigation of the role of using functionalized GNPs and metal oxides towards improving the convective heat transfer performance in closed conduit. To the author‘s knowledge, this is the first report that focused on the development and use of a novel functionalization approach for preparing highly dispersed propylene glycol-treated Graphene Nanoplatelets-based water nanofluid (PGGNP-Water) and Trimethylolpropane tris [poly(propylene glycol), amine terminated] ether -treated Graphene Nanoplatelets (TMP-treated GNP) in convective heat transfer study. Series of experiments on the selected GNP’s nanofluids were conducted considering a novel approach to improve the heat transfer performance.

Previous works on using carbon based material in convective heat transfer experiment adopted ionic surfactant, polymer or acid treatment approach to improve the solubility of the colloid (Amiri et al., 2012; Lee, K.J. et al., 2007; Wensel, J. et al., 2008). As mentioned in the previous segment, surfactant suffers from low temperature degradation and requires higher amount in proportion to particle loading which raise concern on increasing the thermal resistance of the colloid (Wensel, J. et al., 2008). The use of ionic and nonionic polymers although capable of segregating the particle would adversely impact on the hydrodynamic performance of the colloidal system due to high molecular weight of the compound (Razi et al., 2011). In this study all selected materials were prepared without any surfactant. The present research highlighted on the investigation of the use of functionalized GNPs and metal oxides nanofluids in an effort to improve the convective heat transfer performance in closed conduit configuration. Forced convective heat transfer is preferred and used in heat transfer applications

because of its controllability and applicability. To perform the tests on the heat transfer to nanofluids, a series of experiment were conducted with GNPs and metal oxide nanofluids at different concentrations and heat fluxes.

6.2 PGGNP-Water, TMP-treated GNP, Al_2O_3 and SiO_2 nanofluids

6.2.1 Effect of heat flux on heat transfer coefficient and Nusselt number

The convective heat transfer coefficient of PGGNP-Water and TMP-treated GNP for different weight concentrations at two different heat fluxes was investigated in 4mm diameter copper test section. The convective heat transfer coefficients of both the functionalized nanofluids are presented in Figure 6.1 (a and b) and Figure 6.2 (a and b). Both figures show the heat transfer coefficient as a function of nanofluid concentrations at flow velocities of 1 m/s to 3 m/s. The experimental results clearly shows that PGGNP-water nanofluids enhance the convective heat transfer coefficient and this enhancement increases with increasing nanoparticle concentration. It is seen that the augmentations of the convective heat transfer coefficient of PGGNP-Water significantly exceed those of the thermal conductivity enhancements for different weight concentrations. In all concentrations, the convective heat transfer coefficient increases by increasing the velocity, which shows an improvement in the heat transfer potential of the both nanofluids compared to distilled water. The increment of heat transfer coefficient is attributable to Brownian motion of the nanoparticles, thermal diffusion and thermophoresis (Liang, Jizu, Minli, & Detian, 2015). The heat transfer enhancement is attributed to the thin thermal boundary layer in which higher velocities are present, the improved thermal conductivity and the reduced thermal resistance between the flowing nanofluid and the inner wall surface temperature of the tube. The maximum enhancement in heat transfer coefficient of PGGNP-Water at heat fluxes 23870 W/m^2 and 18565 W/m^2 were, 119% and 85% respectively, in comparison to

water at concentration of 0.1wt%. This substantial enhancement is obtained by adding a very small amount of PGGNP nanoparticles to the distilled water. There was slightly decrement in heat transfer coefficient by decreasing the weight concentration of the PGGNP. At weight percentage of 0.025 the increment in heat transfer coefficient was found 76% and 71% corresponding to the heat fluxes of 23870 W/m^2 and 18565 W/m^2 respectively. Therefore at lower weight percentage of PGGNP the heat transfer coefficient increment was 5% higher at constant heat flux of 23870 W/m^2 compared to 18565 W/m^2.

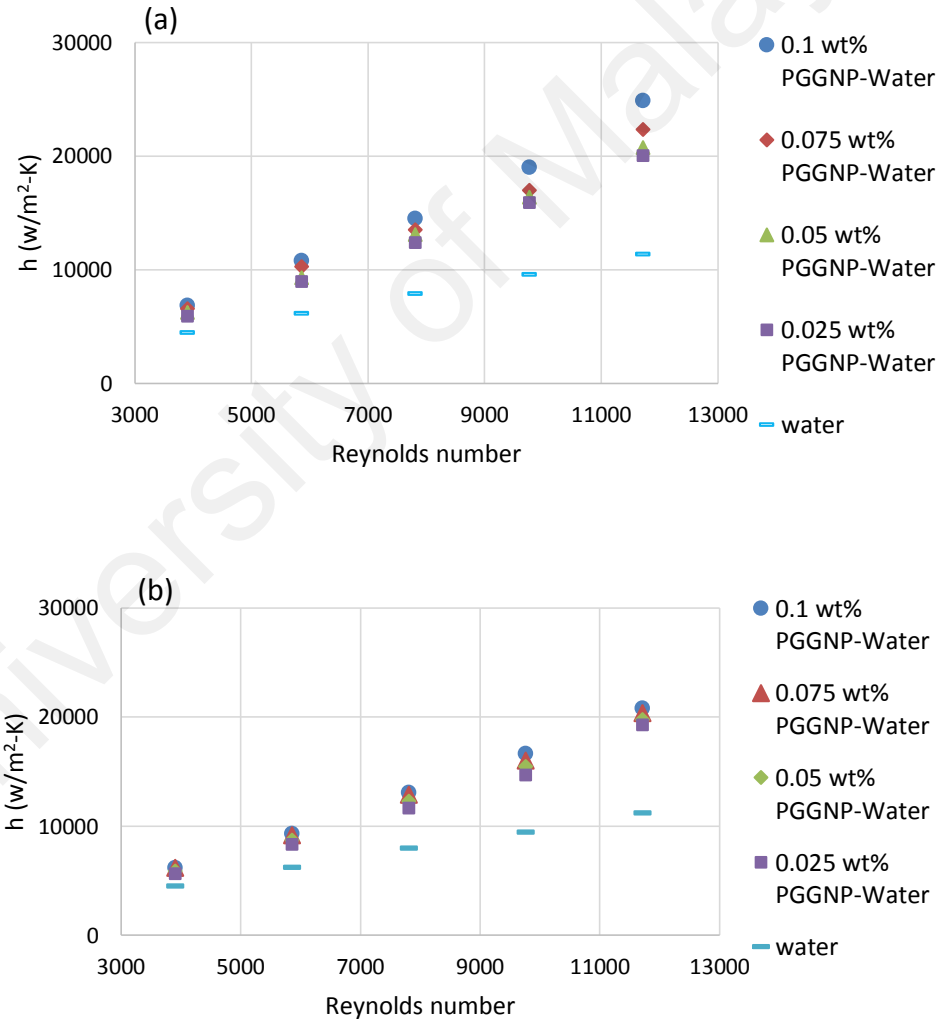

Figure 6.1. The effects of Reynolds number and concentration of PGGNP-Water on the convective heat transfer coefficient at inlet temperature of 30°C and input heat of (a) 23870 W/m^2 and (b) 18565 W/m^2.

It is seen that the augmentations of the convective heat transfer coefficient of TMP-treated GNP significantly exceed those of the thermal conductivity enhancements for different weight concentrations. The maximum heat transfer coefficient enhancements for TMP-treated GNP at heat fluxes of 23870 W/m^2 and 18565 W/m^2 were, 107% and 72% respectively, in comparison to water at the weight concentration of 0.1 wt% and constant velocity of 3m/sec. This substantial enhancement was obtained by adding a very small amount of TMP-treated GNP nanoparticles to the distilled water. There was slightly decrement in heat transfer coefficient by decreasing the weight concentration of the TMP-treated GNP. At weight percentage of 0.025 the increment was found at heat flux of 23870 W/m^2 and 18565 W/m^2 75% and 66% respectively. Therefore, at lower weight percentage of GNP the heat transfer coefficient increment was 9% higher at constant heat flux of 23870 W/m^2 compared to 18565 W/m^2.

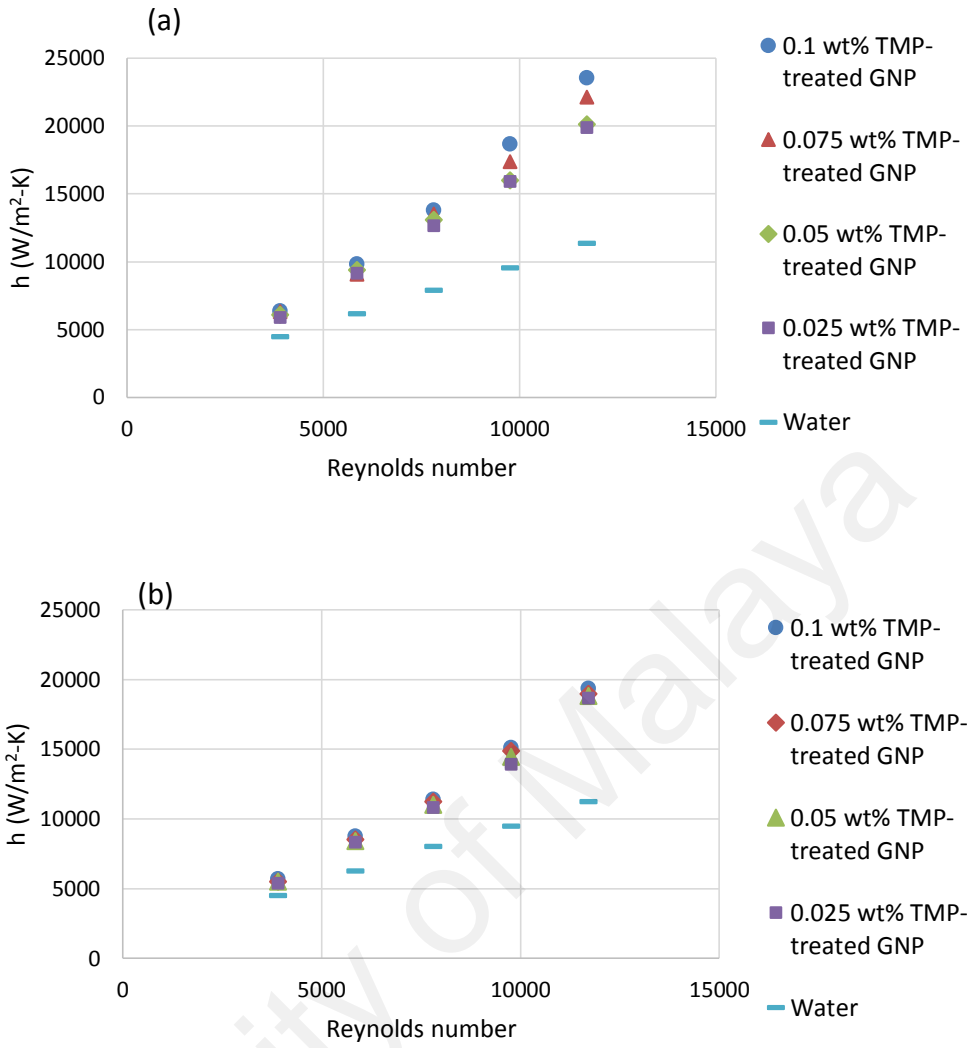

Figure 6.2. The effects of Reynolds number and concentration of TMP-treated GNP on the convective heat transfer coefficient at inlet temperature of 30^0C at input power of (a) 23870 W/m^2 and (b) 18565 W/m^2.

Previous studies claimed that the reasons for the heat transfer enhancement of the nanofluids included the mixing effects of the particles near the wall, particle migration, particle shape and rearrangement, the Brownian motion of the particles, the thermal conductivity enhancement, a reduction of the boundary layer thickness, and a delay in the boundary layer development. In addition, the thermal entry length for a fully developed flow in the turbulent region should be expressed as x ≥10Dr. According to

the experimental findings, there are two reasons for the convective heat transfer enhancement of the nanofluids: delay and disturbance of the thermal boundary layers and the excellent thermal conductivity enhancement of the PGGNP-water and TMP-treated GNP-water nanofluid. The chaotic movements created from the Brownian motion and the migration of GNP nanoparticles could affect the development of the thermal boundary layer in the entrance region (Haghighi, E. B. et al., 2014; Kim, D. et al., 2009). The reason for larger enhancement of the convective heat transfer compared to that of thermal conductivity was introduced by Arvand et al (Aravind et al., 2011; Aravind & Ramaprabhu, 2013) using a simple analogy that the connective heat transfer is proportional to $k/\delta t$, where δt is the thickness of thermal boundary layer. Thus, to increase the convective heat transfer coefficient, k can be increased and/or δt can be decreased. According to Ding and Arvind (Aravind et al., 2011; Ding et al., 2006), carbon nanomaterials such as CNTs and graphene have a tendency to decrease the thermal boundary layer thickness. Higher thermal conductivity or lower difference between temperatures of bulk fluid and tube wall can be introduced as the main reason for aforementioned enhancement in the convective heat transfer coefficient. More studies, typically flow visualization studies, should be conducted to get a clearer picture of the heat transfer enhancement mechanism.

In order to evaluate the ratio of convective to conductive heat transfer of both functionalized nanofluids, the average Nusselt number of the nanofluids as a function of the Reynolds number at different heat fluxes is presented in Figures 6.3 (a) and (b) and Figures 6.4 (a) and (b) . Experimentally, for all cases the average Nusselt number of the PGGNP-Water and TMP-treated GNP showed good increment. The effect of weight concentrations of the PGGNP-Water nanofluids on Nusselt number has been noted. The highest average Nusselt number was calculated at 0.1 wt%, Re = 11770, heat flux of

23870 W/m^2 and 0.1 wt%, Re = 11770, heat flux of 18565 W/m^2. The higher Nusselt number for the PGGNP-Water nanofluids is attributed to the decrease in circulation temperature by increasing thermal conductivity of working fluid, which decreases the temperature difference between the tube wall and bulk fluid in close conduit. The maximum increment in Nusselt number for PGGNP-water was found up to 84% and 54% in comparison to water at the heat fluxes of 23870 W/m^2 and 18565, respectively.

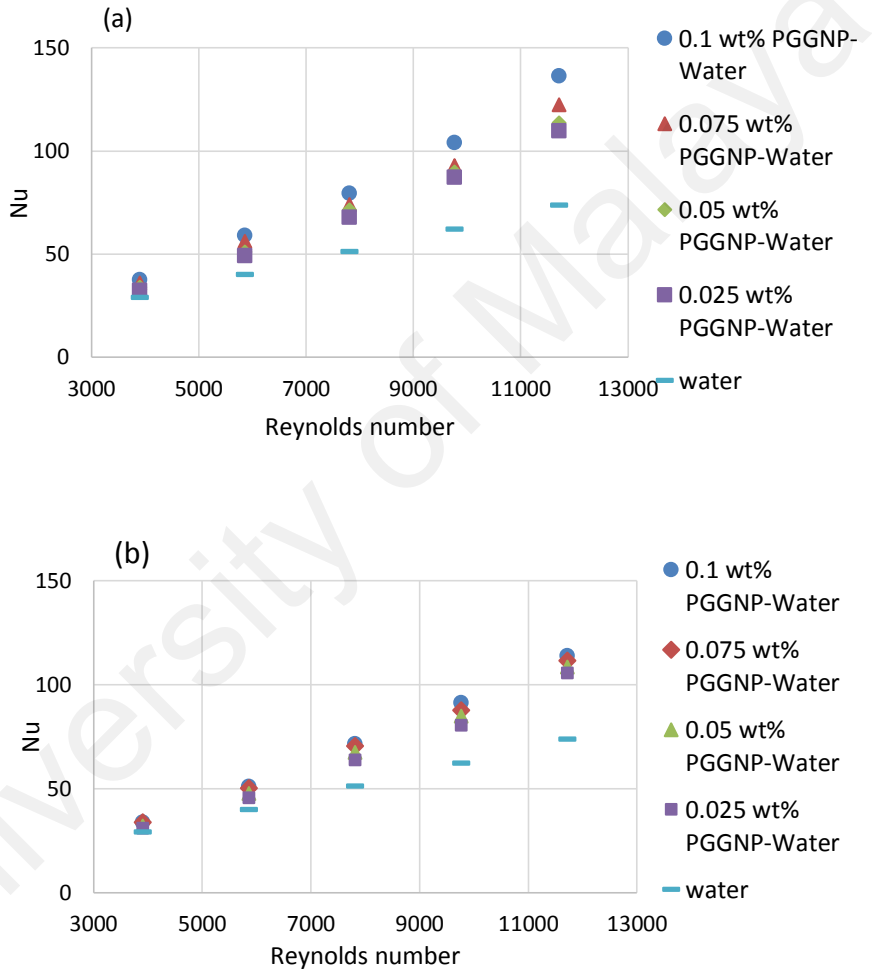

Figure 6.3. The average Nusselt number of PGGNP-Water at different concentrations and Reynolds number at input of (a) 23870 W/m^2 and (b) 18565 W/m^2.

For the case of TMP-treated GNP the highest nusselt number was calculated 127 at *Re* = 11770, with heat fluxes of 23870 W/m^2 and 18565 W/m^2 (at maximum velocity of

3 m/sec and 0.1 wt%) due to the improved thermal conductivity and the reduced thermal resistance between the flowing nanofluid and the inner wall surface of the tube. The higher Nusselt number for the TMP-treated GNP nanofluids is attributed to the decrease in circulation temperature by increasing thermal conductivity of working fluid, which decreases the temperature difference between the tube wall and bulk fluid in close conduit. The Nusselt number for TMP-treated GNP showed increment up to 72% and 43%, at the heat fluxes of 23870 W/m^2 and 18565 W/m^2, respectively.

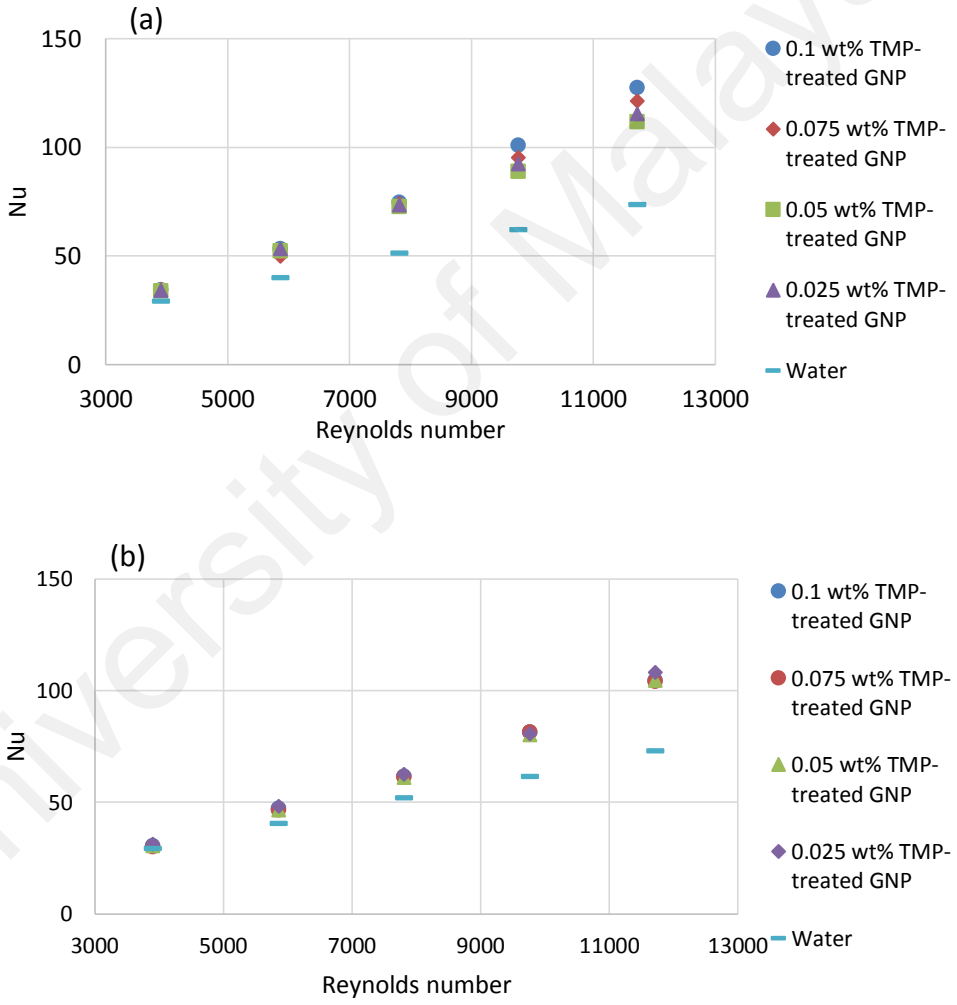

Figure 6.4. The average Nusselt number of TMP-treated GNP at different concentrations and Reynolds number at input power of (a) 23870 W/m^2 and (b) 18565 W/m^2.

The convective heat transfer coefficient of Al_2O_3 and SiO_2 nanofluids for different weight concentrations at two different heat fluxes was investigated in 4mm diameter copper test section. It is seen that the augmentations of the convective heat transfer coefficient of Al_2O_3 significantly exceed those of the thermal conductivity enhancements for different weight concentrations. The convective heat transfer coefficient of Al_2O_3 is shown in Figure 6.5. The maximum heat transfer coefficient enhancements for Al_2O_3 at heat fluxes of 23870 W/m^2 and 18565 W/m^2 were, 29% and 24% respectively, for the weight concentration of 0.1 wt% at constant velocity. This substantial enhancement was obtained by adding a very small amount of Al_2O_3 nanoparticles to the distilled water. There was slightly decrement in heat transfer coefficient by decreasing the weight concentration of the Al_2O_3. At weight percentage of 0.025 the increment was found 24% and 19% at heat fluxes of 23870 W/m^2 and 18565 W/m^2 respectively. Therefore, at lower weight percentage of Al_2O_3 the heat transfer coefficient increment was 5% higher at constant heat flux of 23870 W/m^2 compared to 18565 W/m^2.

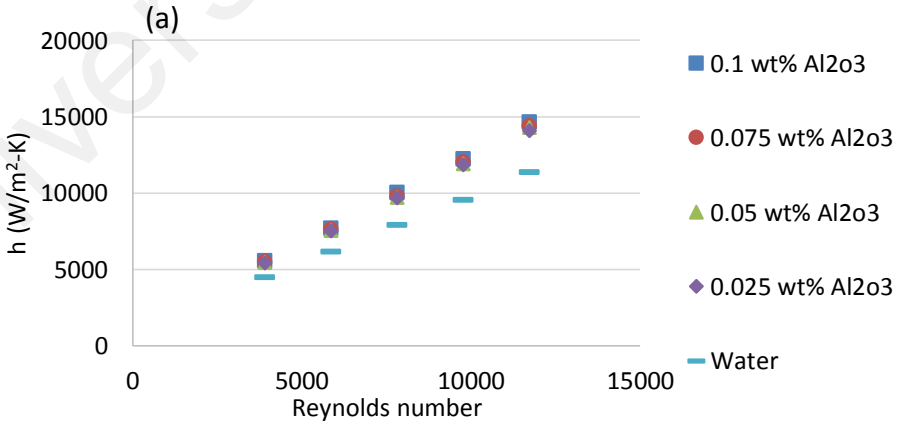

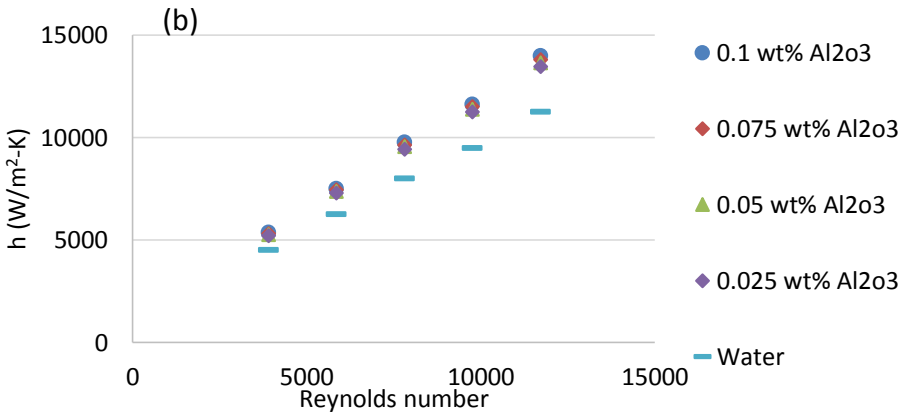

Figure 6.5. The effects of Reynolds number and concentration of Al_2O_3 on the convective heat transfer coefficient at inlet temperature of 30^0C and input power of (a) 23870 W/m^2 and (b) 18565 W/m^2

The convective heat transfer coefficient of SiO_2 nanofluids for different weight concentrations at two different heat fluxes was investigated in 4mm diameter copper test section as presented in Figure 6.6 (a and b). Both figures shows the heat transfer coefficient as a function of nanofluid concentrations at flow velocities of 1 m/s to 3 m/s. The experimental results clearly shows that SiO_2 nanofluids enhance the convective heat transfer coefficient and this enhancement increases with increasing nanoparticle concentration. It is seen that the augmentations of the convective heat transfer coefficient of SiO_2 significantly exceed those of the thermal conductivity enhancements for different weight concentrations. In all concentrations, the convective heat transfer coefficient increases by increasing the velocity, which shows an improvement in the heat transfer potential of the both nanofluids compared to distilled water. The increment of heat transfer coefficient is attributable to Brownian motion of the nanoparticles, thermal diffusion and thermophoresis (Liang et al., 2015). The maximum enhancement in heat transfer coefficient of SiO_2 at heat fluxes of 23870 W/m^2 and 18565 W/m^2 were, 31% and 24% respectively, at concentration of 0.1wt%. This substantial enhancement is obtained by adding a very small amount of SiO_2 nanoparticles to the distilled water. There was slightly decrement in heat transfer coefficient by decreasing the weight

concentration of the SiO_2. At weight percentage of 0.025 the increment in heat transfer coefficient was found 26.4% and 21% at heat fluxes of 23870 W/m^2 and 18565 W/m^2 respectively. Therefore at lowest weight percentage of SiO_2 the heat transfer coefficient increment was 5% higher at constant heat flux of 23870 W/m^2 compared to 18565 W/m^2.

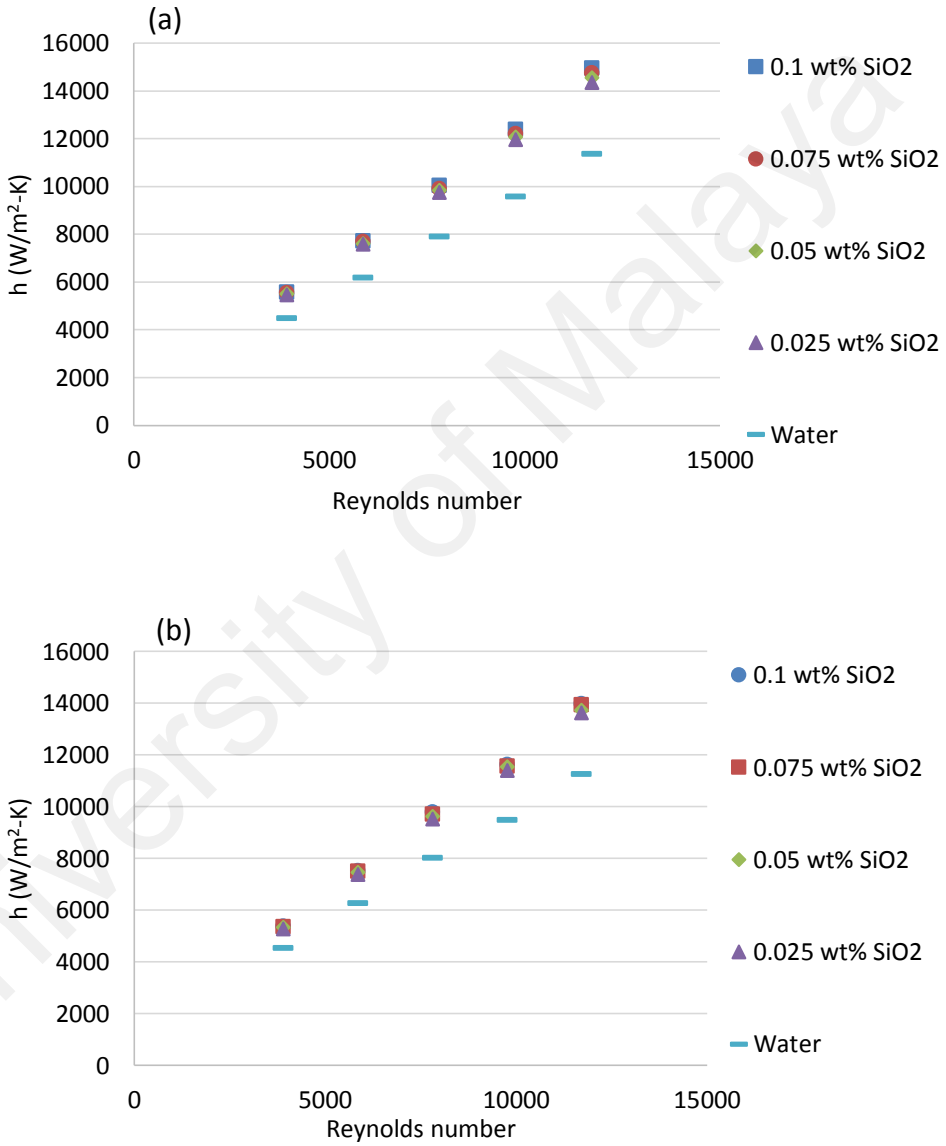

Figure 6.6. The effects of Reynolds number and concentration of SiO_2 on the convective heat transfer coefficient at inlet temperature of 30^{0}C and input power of (a) 23870 W/m^2 and (b) 18565 W/m^2

In order to evaluate the ratio of convective to conductive heat transfer of both metal oxide, the average Nusselt number of the nanofluids as a function of the Reynolds number at different heat fluxes is presented in Figure 6.7 (a) and (b) and Figure 6.8 (a) and (b). Experimentally, for all cases the average Nusselt number of the Al_2O_3 and SiO_2 showed good increment. The effect of weight concentrations of the Al_2O_3 nanofluids on Nusselt number has been noted. The highest average Nusselt number was calculated at 0.1 wt%, Re = 11770, heat flux of 23870 W/m^2 and 0.1 wt%, Re = 11770, heat flux of 18565 W/m^2. The higher Nusselt number for the Al_2O_3 nanofluids is attributed to the decrease in circulation temperature by increasing thermal conductivity of working fluid, which decreases the temperature difference between the tube wall and bulk fluid in close conduit. The maximum increment in Nusselt number was found up to 26% and 20% at the heat fluxes of 23870 W/m^2 and 18565, respectively.

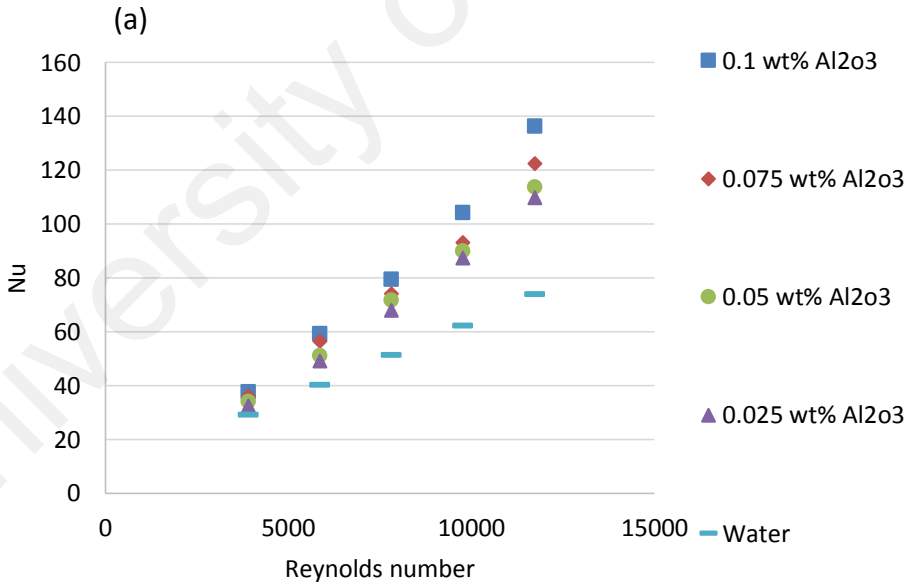

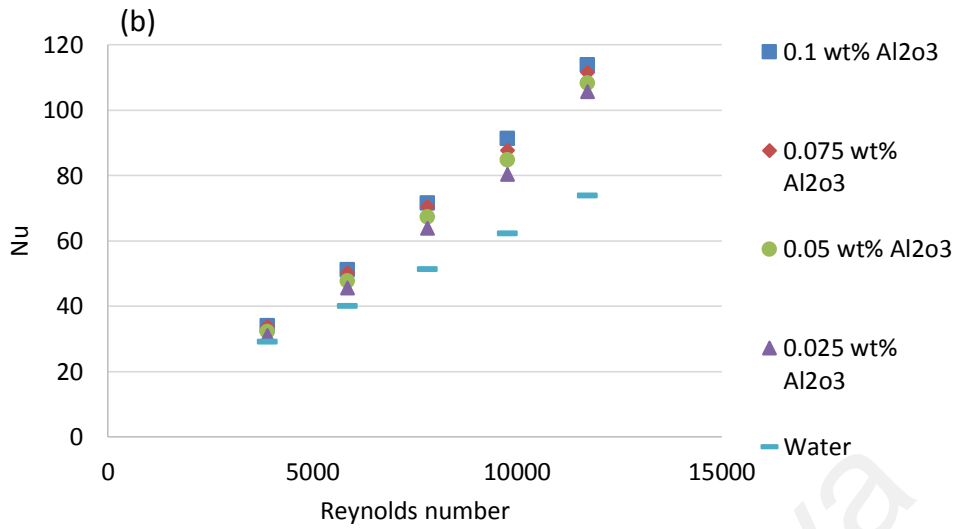

Figure 6.7. The average Nusselt number of Al_2O_3 at different concentrations and Reynolds number at input power of (a) 23870 W/m^2 and (b) 18565 W/m^2

For the case of SiO_2, the highest nusselt number was calculated at *Re* = 11770, with heat fluxes of 23870 W/m^2 and 18565 W/m^2 (at maximum velocity of 3 m/sec and 0.1 wt%) due to the improved thermal conductivity and the reduced thermal resistance between the flowing nanofluid and the inner wall surface of the tube. The higher Nusselt number for the SiO_2 is attributed to the decrease in circulation temperature by increasing thermal conductivity of working fluid, which decreases the temperature difference between the tube wall and bulk fluid in close conduit. The Nusselt number for SiO_2 showed increment up to 28%, and 20% at the heat fluxes of 23870 W/m^2 and 18565 W/m^2 respectively.

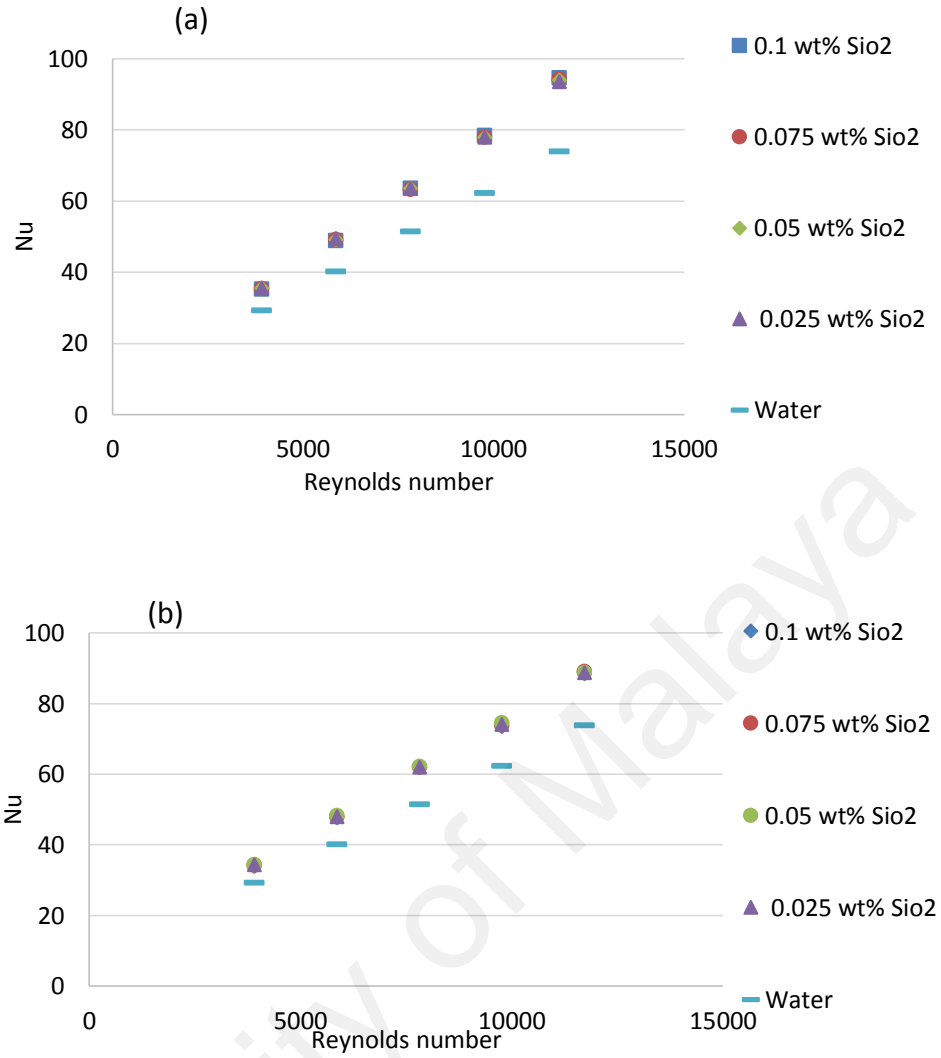

Figure 6.8. The average Nusselt number of SiO_2 at different concentrations and Reynolds number at input power of (a) 23870 W/m^2 and (b) 18565 W/m^2.

6.2.2 Effect of size (diameter)

To investigate the effect of size of the test section on heat transfer performance of the nanofluids, three different diameters were selected for this study which are 2mm, 4mm and 15mm, with stainless steel material.

The convective heat transfer coefficient of PGGNP-Water, TMP-treated GNP, Al_2O_3 and SiO_2 nanofluids at weight concentration of 0.1 wt%, heat flux of 23870 W/m^2 were investigated in test section of 2mm diameter. The convective heat transfer coefficient of all the selected nanofluids are presented in Figure 6.9. It shows the heat transfer

coefficient as a function of nanofluid concentrations at flow velocities of 1 m/s to 3 m/s. The experimental results clearly show the good degree of enhancement of convective heat transfer coefficient and this enhancement increases with increasing of the velocity. It is seen that the augmentations of the convective heat transfer coefficient of nanofluids significantly exceed those of the thermal conductivity enhancements for different weight concentrations. In all nanofluids, the convective heat transfer coefficient increases by increasing the velocity, which shows an improvement in the heat transfer potential of the both nanofluids compared to distilled water. In the test section of 2mm diameter, the maximum enhancement in heat transfer coefficient of PGGNP-Water, TMP-treated GNP, Al_2O_3 and SiO_2 nanofluids at heat flux of 23870 W/m^2 was 116%, 109%, 32% and 34% respectively. This substantial enhancement is obtained by adding a very small amount of nanoparticles to the distilled water.

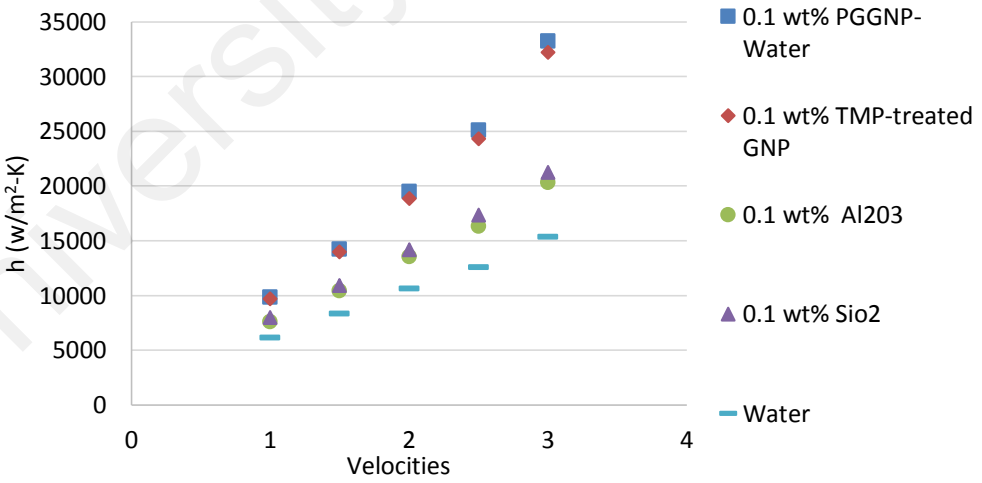

Figure 6.9. The effects of diameter and velocity of nanofluids on the convective heat transfer coefficient at inlet temperature of 30^{0}C at input power of 23870 W/m^2.

In order to evaluate the ratio of convective to conductive heat transfer of PGGNP-Water, TMP-treated GNP, Al_2O_3 and SiO_2 nanofluids, the average Nusselt number of the nanofluids as a function of the Reynolds number at heat flux of 23870 W/m^2 is presented in Figure 6.10. Experimentally, for all cases the average Nusselt number of the PGGNP-Water, TMP-treated GNP, Al_2O_3 and SiO_2 showed good increment. The effect of weight concentrations of the PGGNP-Water, TMP-treated GNP, Al_2O_3 and SiO_2 nanofluids on Nusselt number has been noted. The highest average Nusselt number was calculated at 0.1 wt%, Re = 11770, heat flux of 23870 W/m^2.

The higher Nusselt number for the nanofluid is attributed to the decrease in circulation temperature by increasing thermal conductivity of working fluid, which decreases the temperature difference between the tube wall and bulk fluid in close conduit. The maximum increment in Nusselt number of PGGNP-Water, TMP-treated GNP, Al_2O_3 and SiO_2 was found up to 79%, 74%, 26.4% and 26.7% at the heat flux of 23870 W/m^2, respectively.

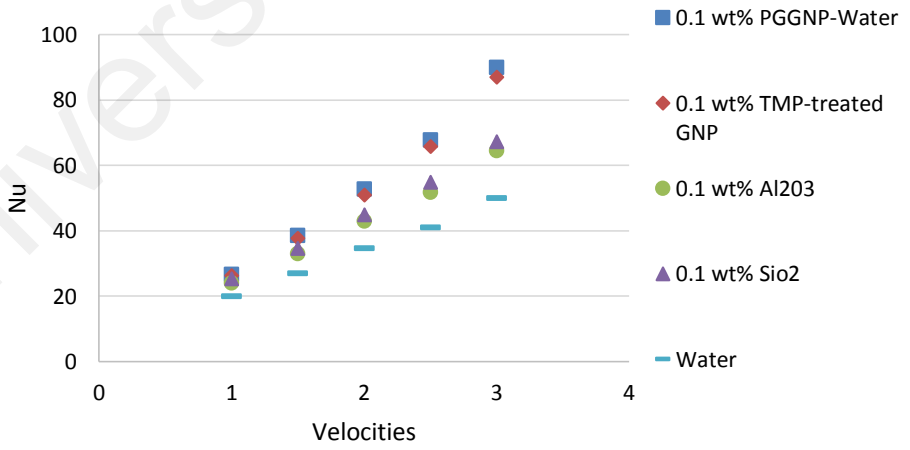

Figure 6.10. The average Nusselt number of nanofluids at different velocities with input power of 23870 W/m^2

The convective heat transfer coefficient of PGGNP-Water, TMP-treated GNP, Al_2O_3 and SiO_2 nanofluids at weight concentration of 0.1 wt%, heat flux of 23870 W/m^2 were investigated in test section of 4mm diameter. The convective heat transfer coefficient of all selected nanofluids are presented in Figure 6.11. Figure 6.11 shows the heat transfer coefficient as a function of nanofluid concentrations at flow velocities of 1 m/s to 3 m/s. The experimental results clearly show the good degree of enhancement of convective heat transfer coefficient and this enhancement increases with increasing the velocity. It is seen that the augmentations of the convective heat transfer coefficient of nanofluids significantly exceed those of the thermal conductivity enhancements for different weight concentrations. In all nanofluids, the convective heat transfer coefficient increases by increasing the velocity, which shows an improvement in the heat transfer potential of the both nanofluids compared to distilled water. In the test section of 4mm diameter, the maximum enhancement in heat transfer coefficient of PGGNP-Water, TMP-treated GNP, Al_2O_3 and SiO_2 nanofluids at heat flux of 23870 W/m^2 was 100.6%, 93%, 26.4% and 31% respectively. This substantial enhancement is obtained by adding a very small amount of nanoparticles to the distilled water. By comparing the data of 4mm and 2mm test sections, in 4mm test section the heat transfer coefficient results are slightly lower than 2mm section, as shown in Table 6.2

In order to evaluate the ratio of convective to conductive heat transfer of PGGNP-Water, TMP-treated GNP, Al_2O_3 and SiO_2 nanofluids, the average Nusselt number of the nanofluids as a function of the Reynolds number at heat flux of 23870 W/m^2 is presented in Figure 6.12. Experimentally, for all cases the average Nusselt number of the PGGNP-Water, TMP-treated GNP, Al_2O_3 and SiO_2 show good increment. The effect of weight concentrations of the PGGNP-Water, TMP-treated GNP, Al_2O_3 and SiO_2 nanofluids on Nusselt number has been noted. The highest average Nusselt

number was calculated at 0.1 wt%, Re = 11770, heat flux of 23870 W/m^2. The higher Nusselt number for the nanofluid is attributed to the decrease in circulation temperature by increasing thermal conductivity of working fluid, which decreases the temperature difference between the tube wall and bulk fluid in close conduit. The maximum increment in Nusselt number of PGGNP-Water, TMP-treated GNP, Al_2O_3 and SiO_2 was found up to 66.7%, 60.6%, 23.4% and 25% at flux of 23870 W/m^2, respectively. The summary of the results is shown in table 6.2.

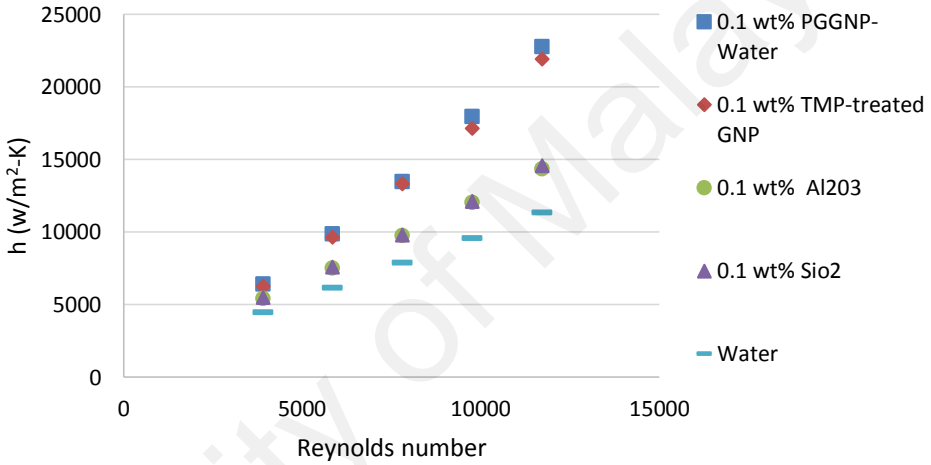

Figure 6.11. The effects of diameter and velocity of nanofluids on the convective heat transfer coefficient at inlet temperature of 30^{0}C and input power of 23870 W/m^2.

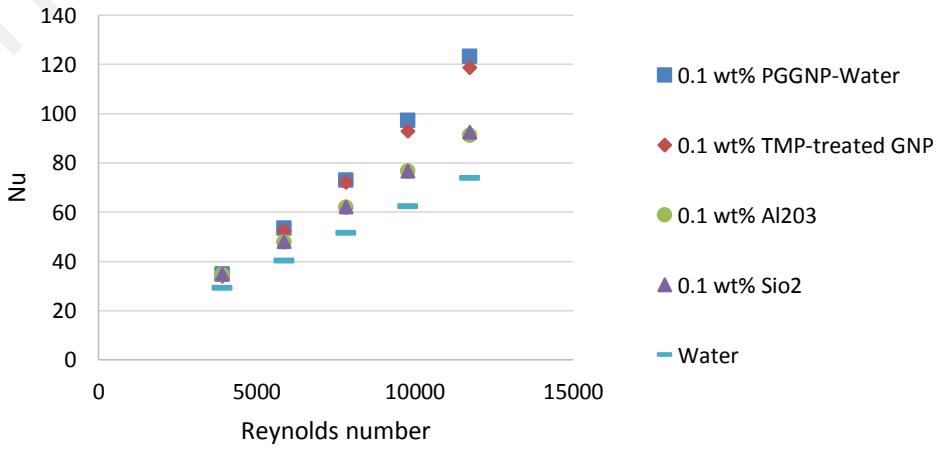

Figure 6.12. The average Nusselt number of nanofluids at different velocities with input power of 23870 W/m^2

The convective heat transfer coefficient of PGGNP-Water, TMP-treated GNP, Al_2O_3 and SiO_2 nanofluids at weight concentration of 0.1 wt%, heat flux of 23870 W/m^2 were investigated in test section of 15mm diameter. The convective heat transfer coefficient of all selected nanofluids are presented in Figure 6.13. Figure 6.13 shows the heat transfer coefficient as a function of nanofluid concentrations at flow velocities of 1-3 m/s. The experimental results clearly show the good degree of enhancement of convective heat transfer coefficient and this enhancement increases with increasing of the velocity. It is seen that the augmentations of the convective heat transfer coefficient of nanofluids significantly exceed those of the thermal conductivity enhancements for different weight concentrations. In all nanofluids, the convective heat transfer coefficient increases by increasing the velocity, which shows an improvement in the heat transfer potential of the both nanofluids compared to distilled water. In the test section of 15mm diameter, the maximum enhancement in heat transfer coefficient of PGGNP-Water, TMP-treated GNP, Al_2O_3 and SiO_2 nanofluids at heat flux of 23870 W/m^2 was 91.7%, 85.78%, 24.25% and 26.37% respectively. This substantial enhancement is obtained by adding a very small amount of nanoparticles to the distilled water. By comparing the data of 15mm and 4mm test sections, in 15mm test section the heat transfer coefficient results are slightly lower than that of 4mm section, as shown in Table 6.2.

In order to evaluate the ratio of convective to conductive heat transfer of PGGNP-Water, TMP-treated GNP, Al_2O_3 and SiO_2 nanofluids, the average Nusselt number of the nanofluids as a function of the Reynolds number at heat flux of 23870 W/m^2 is

presented in Figure 6.14. For all cases the average Nusselt number of the PGGNP-Water, TMP-treated GNP, Al_2O_3 and SiO_2 showed good increment. The effect of weight concentrations of the PGGNP-Water, TMP-treated GNP, Al_2O_3 and SiO_2 nanofluids on Nusselt number has been noted and found the highest average Nusselt number at 0.1 wt%, Re = 11770, heat flux of 23870 W/m^2. The higher Nusselt number for the nanofluid is attributed to the decrease in circulation temperature by increasing thermal conductivity of working fluid, which decreases the temperature difference between the tube wall and bulk fluid in close conduit. The maximum increment in Nusselt number of PGGNP-Water, TMP-treated GNP, Al_2O_3 and SiO_2 was found up to 59.34%, 54.47%, 21.30% and 22.97% at flux of 23870 W/m^2, respectively. The summary of the results is shown in table 6.2.

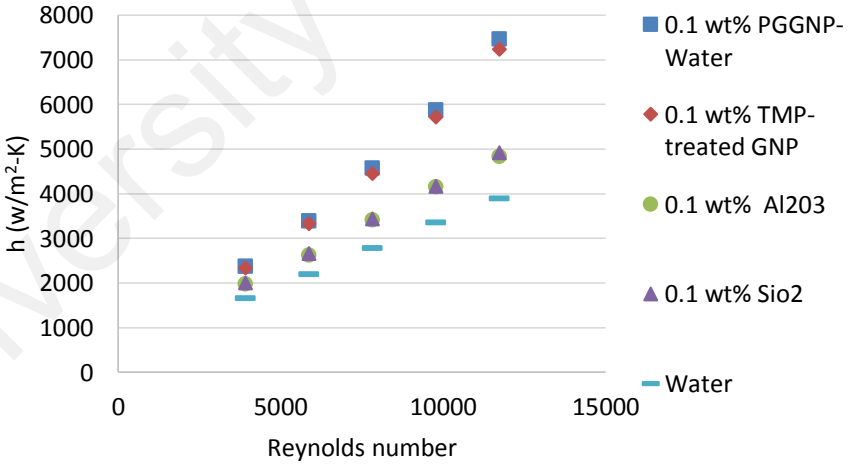

Figure 6.13. The effects of diameter and velocity of nanofluids on the convective heat transfer coefficient at inlet temperature of 30^{0}C and input power of 23870 W/m^2.

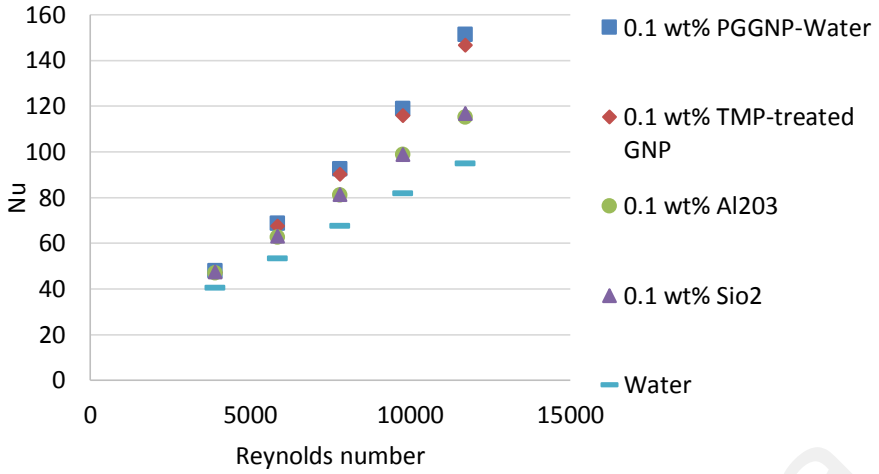

Figure 6.14. The average Nusselt number of nanofluids at different velocities with input power of 23870 W/m^2

Table 6.1. Summary of the effect of the size on the heat transfer performance and friction factor of nanofluids

Nanofluids	Daimater 2mm			Daimater 4mm			Daimater 15mm		
	Heat trans. Coeff. (%)	Nu increment (%)	Friction factor increase (%)	Heat trans. Coeff. (%)	Nu increment (%)	Friction factor increase (%)	Heat trans. Coeff. (%)	Nu increment (%)	Friction factor increase (%)
PGGNP-water	116.4	79	5.53	100.68	66.7	7	91.7	59.3	7.61
TMP-treated GNP	109.7	74	5.53	93.25	60.6	6.9	85.87	54.4	7.60
Al_2O_3	32.2	26.4	3.87	26.45	23.4	4.74	24.25	21.3	5.91
SiO_2	34.6	26.7	5.33	31.15	25	6.15	26.37	22.9	6.70

6.2.3 Effect of Materials

To investigate the material effect on heat transfer performance of the nanofluids, three different materials were used for this study which are copper, aluminium and stainless steel with same diameter of 4mm, respectively.

The convective heat transfer coefficient of PGGNP-Water, TMP-treated GNP, Al_2O_3 and SiO_2 nanofluids at weight concentration of 0.1 wt%, heat flux of 23870 W/m^2 were investigated in copper test section with diameter of 4mm. The convective heat transfer coefficient of all selected nanofluids are presented in Figure 6.15. Figure 6.15 shows the heat transfer coefficient as a function of nanofluid concentrations at flow velocities of 1 m/s to 3 m/s. The experimental results clearly shows the good degree of enhancement of convective heat transfer coefficient and this enhancement increases with increasing the velocity. It is seen that the augmentations of the convective heat transfer coefficient of nanofluids significantly exceed those of the thermal conductivity enhancements for different weight concentrations. In all nanofluids, the convective heat transfer coefficient increases by increasing the velocity, which shows an improvement in the heat transfer potential of the both nanofluids compared to distilled water. In the copper test section, the maximum enhancement in heat transfer coefficient of PGGNP-Water, TMP-treated GNP, Al_2O_3 and SiO_2 nanofluids at heat flux of 23870 W/m^2 was 119.1%, 107.59%, 29.1% and 31.6% respectively. This substantial enhancement is obtained by adding a very small amount of nanoparticles to the distilled water.

In order to evaluate the ratio of convective to conductive heat transfer of PGGNP-Water, TMP-treated GNP, Al_2O_3 and SiO_2 nanofluids, the average Nusselt number of the nanofluids as a function of the Reynolds number at heat flux of 23870 W/m^2 is presented in Figure 6.16. Experimentally, for all cases the average Nusselt number of

the PGGNP-Water, TMP-treated GNP, Al_2O_3 and SiO_2 showed good increment. The effect of material and velocity of the PGGNP-Water, TMP-treated GNP, Al_2O_3 and SiO_2 nanofluids on Nusselt number have been noted. The highest average Nusselt number was calculated at 0.1 wt%, Re = 11770 and heat flux of 23870 W/m^2. The higher Nusselt number for the nanofluid is attributed to the decrease in circulation temperature by increasing thermal conductivity of working fluid, which decreases the temperature difference between the tube wall and bulk fluid in close conduit. The maximum increment in Nusselt number of PGGNP-Water, TMP-treated GNP, Al_2O_3 and SiO_2 was found up to 82%, 72.5%, 26% and 28% at the heat flux of 23870 W/m^2, respectively.

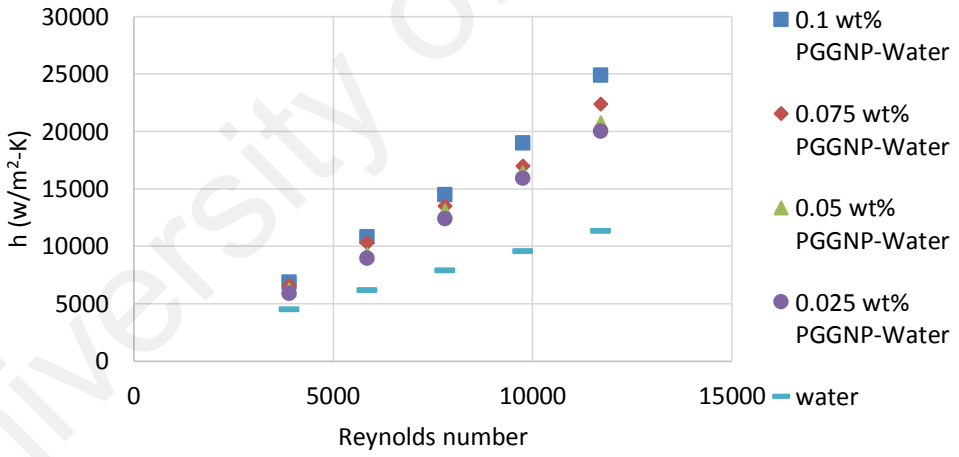

Figure 6.15. The effects of material and velocity of nanofluids on the convective heat transfer coefficient at inlet temperature of 30^{0}C at input power of 23870 W/m^2.

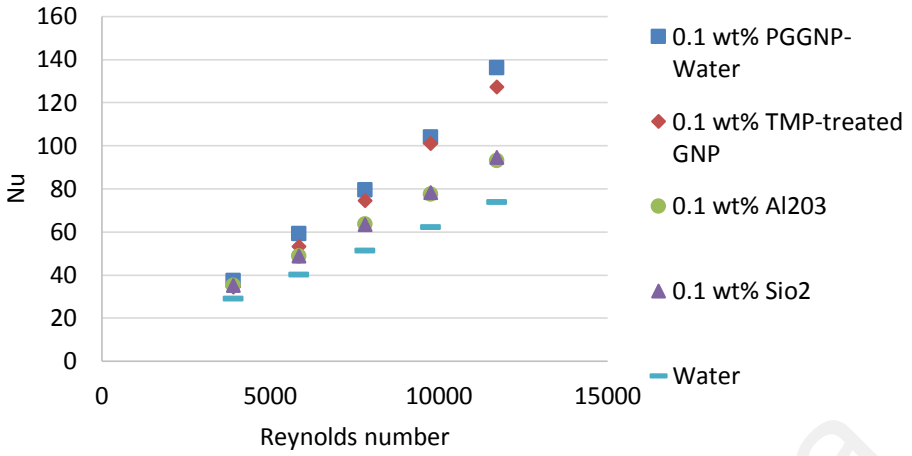

Figure 6.16. The average Nusselt number of nanofluids at different velocities with input power of 23870 W/m^2

The convective heat transfer coefficient of PGGNP-Water, TMP-treated GNP, Al_2O_3 and SiO_2 nanofluids at weight concentration of 0.1 wt%, heat flux of 23870 W/m^2 were investigated in aluminium test section of diameter 4mm. The convective heat transfer coefficient of all selected nanofluids are presented in Figure 6.17. It shows the heat transfer coefficient as a function of nanofluid concentrations at flow velocities of 1 m/s to 3 m/s. The experimental results clearly show a good degree of enhancement of convective heat transfer coefficient and this enhancement increases with increasing the velocity. It is seen that the augmentations of the convective heat transfer coefficient of nanofluids significantly exceed those of the thermal conductivity enhancements for different weight concentrations. In all nanofluids, the convective heat transfer coefficient increases by increasing the velocity, which shows an improvement in the heat transfer potential of the both nanofluids compared to distilled water. In aluminium test section, the maximum enhancement in heat transfer coefficient of PGGNP-Water, TMP-treated GNP, Al_2O_3 and SiO_2 nanofluids at heat flux of 23870 W/m^2 were 110.2%, 96.1%, 27.73% and 29.28% respectively. This substantial enhancement is obtained by adding a very small amount of nanoparticles to the distilled water. By

comparing the current results with copper test section the heat transfer coefficient results are slightly lower in aluminium test section.

In order to evaluate the ratio of convective to conductive heat transfer of PGGNP-Water, TMP-treated GNP, Al_2O_3 and SiO_2 nanofluids, the average Nusselt number of the nanofluids as a function of the Reynolds number at heat flux of 23870 W/m^2 is presented in Figure 6.18. For all cases the average Nusselt number of the PGGNP-Water, TMP-treated GNP, Al_2O_3 and SiO_2 showed good increment. The effect of material and velocity on the PGGNP-Water, TMP-treated GNP, Al_2O_3 and SiO_2 nanofluids on Nusselt number have been noted. The highest average Nusselt number was calculated at 0.1 wt%, Re = 11770 and heat flux of 23870 W/m^2. The higher Nusselt number for the nanofluid is attributed to the decrease in circulation temperature by increasing thermal conductivity of working fluid, which decreases the temperature difference between the tube wall and bulk fluid in close conduit. The maximum increment in Nusselt number of PGGNP-Water, TMP-treated GNP, Al_2O_3 and SiO_2 were found up to 74.75%, 63%, 24.69% and 25.8% respectively at the heat flux of 23870 W/m^2.

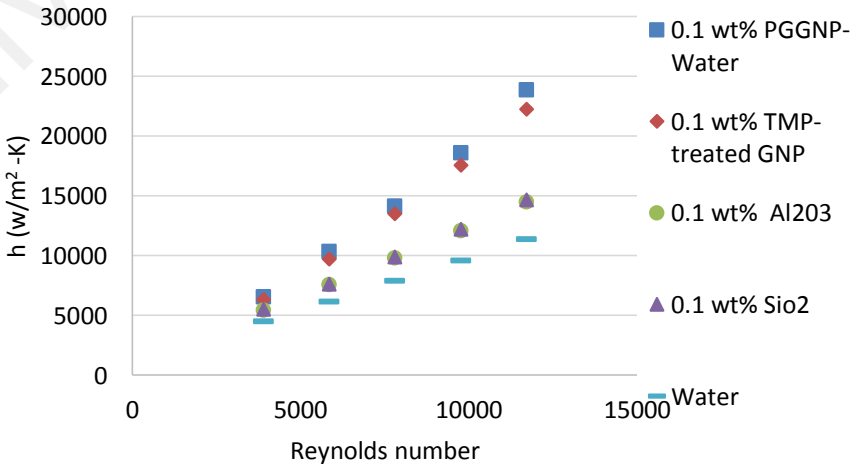

Figure 6.17. The effects of material and velocity of nanofluids on the convective heat transfer coefficient at inlet temperature of 30^0C and input power of 23870 W/m^2.

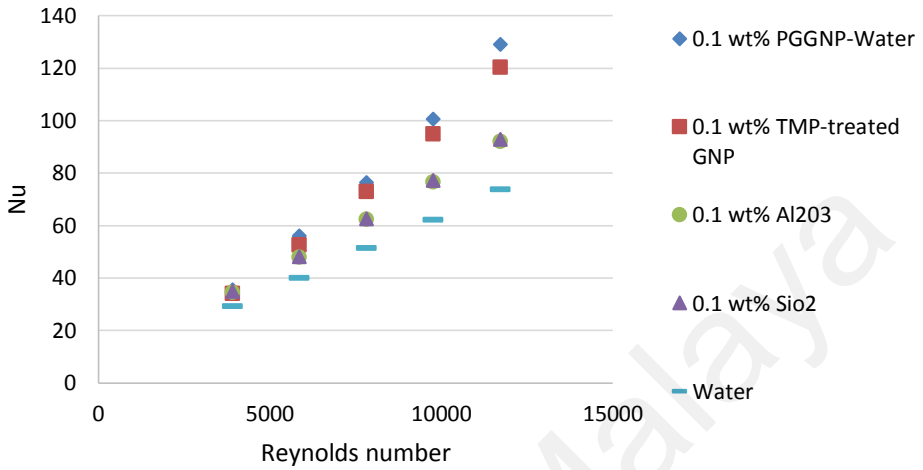

Figure 6.18. The average Nusselt number of nanofluids at different velocities with input power of 23870 W/m^2

The convective heat transfer coefficient of PGGNP-Water, TMP-treated GNP, Al_2O_3 and SiO_2 nanofluids at weight concentration of 0.1 wt%, heat flux of 23870 W/m^2 were investigated in stainless test section of diameter 4mm. The convective heat transfer coefficient of all selected nanofluids are presented in Figure 6.19. It shows the heat transfer coefficient as a function of nanofluid concentrations at flow velocities of 1 m/s to 3 m/s. The experimental results clearly show the good degree of enhancement of convective heat transfer coefficient and this enhancement increases with increasing the velocity. It is seen that the augmentations of the convective heat transfer coefficient of nanofluids significantly exceed those of the thermal conductivity enhancements for different weight concentrations. In all nanofluids, the convective heat transfer coefficient increases by increasing the velocity, which shows an improvement in the

heat transfer potential of the both nanofluids compared to distilled water. In the Stainless steel test section, the maximum enhancement in heat transfer coefficients of PGGNP-Water, TMP-treated GNP, Al_2O_3 and SiO_2 nanofluids at heat flux of 23870 W/m^2 were 100.68%, 93.25%, 26.45% and 28.45% respectively. This substantial enhancement is obtained by adding a very small amount of nanoparticles to the distilled water. By comparing the current data with the data from aluminium and copper test sections the heat transfer coefficient results are slightly lower in stainless steel test section.

In order to evaluate the ratio of convective to conductive heat transfer of PGGNP-Water, TMP-treated GNP, Al_2O_3 and SiO_2 nanofluids, the average Nusselt number of the nanofluids as function of the Reynolds number at heat flux of 23870 W/m^2 are presented in Figure 6.20. Experimentally, for all cases the average Nusselt number of the PGGNP-Water, TMP-treated GNP, Al_2O_3 and SiO_2 showed good increment. The effect of material and velocity of the PGGNP-Water, TMP-treated GNP, Al_2O_3 and SiO_2 nanofluids on Nusselt number have been noted. The highest average Nusselt number was calculated at 0.1 wt%, Re = 11770 and heat flux of 23870 W/m^2. The higher Nusselt number for the nanofluid is attributed to the decrease in circulation temperature by increasing thermal conductivity of working fluid, which decreases the temperature difference between the tube wall and bulk fluid in close conduit. The maximum increment in Nusselt number of PGGNP-Water, TMP-treated GNP, Al_2O_3 and SiO_2 were found up to 66.7%, 60.6%, 23.44% and 25% respectively at the heat flux of 23870 W/m^2.

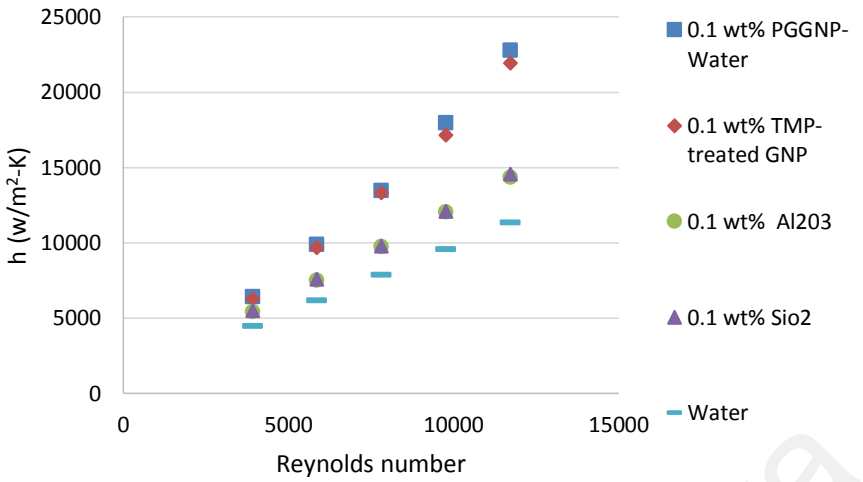

Figure 6.19. The effects of material and velocity of nanofluids on the convective heat transfer coefficient at inlet temperature of 30^0C and input power of 23870 W/m^2.

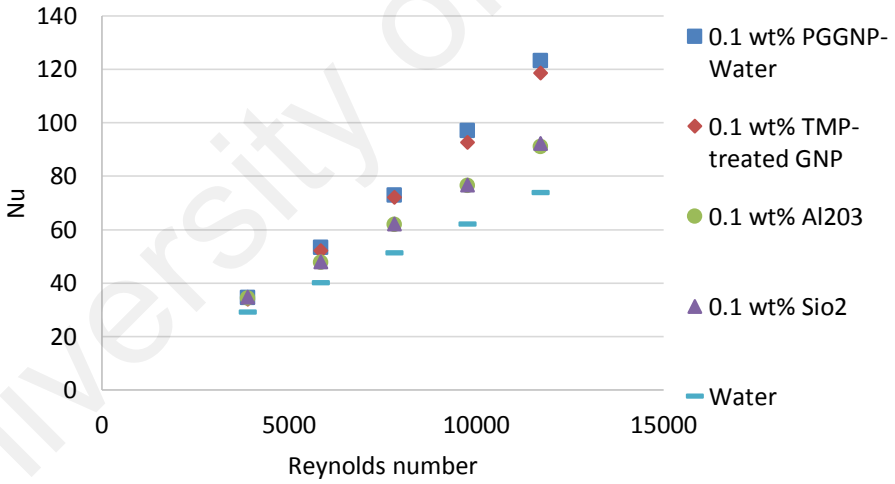

Figure 6.20. The average Nusselt number of nanofluids at different velocities with input power of 23870 W/m^2

Table 6.2. Summary of the effect of material on the heat transfer performance and friction factor of nanofluids

Nanofluids	Copper material			Aluminium material			Stainless steel material		
	Heat trans. Coeff. (%)	Nu (%) increment	Friction factor increase (%)	Heat trans. Coeff. (%)	Nu (%) increment	Friction factor increase (%)	Heat trans. Coeff. (%)	Nu (%) increment	Friction factor increase (%)
PGGNP-water	119.1	84	10.2	110.2	74.74	7.88	100.68	66.78	7.08
TMP-treated GNP	107.59	72	10	96.1	63	7.21	93.25	60.6	6.95
Al_2O_3	29.1	26	5.92	27.73	24.69	4.87	26.45	23.4	4.74
SiO_2	31.6	28	7.14	29.2	25.8	6.28	28.46	25	6.1

6.2.4 Pressure drop

The friction factor of PGGNP-Water and TMP-treated GNP nanofluids flowing through the test section was measured under various conditions including different concentrations and velocities. Figure 6.21 (a and b) and Figure 6.22 (a and b) show the measured friction factor for the PGGNP-Water nanofluid for all concentrations, as function of the flow velocity. It was observed that, the friction factor increases as the concentration of nanofluids increases, although there are some fluctuations in measured friction factor for different velocities. At 0.1wt% of PGGNP-Water the highest increment in friction factor was calculated from 4% to 10.2% at velocities from 1 to

3m/s. It can be seen that as the velocity increases, the dependence of friction factor on the concentration of PGGNP-water decreases.

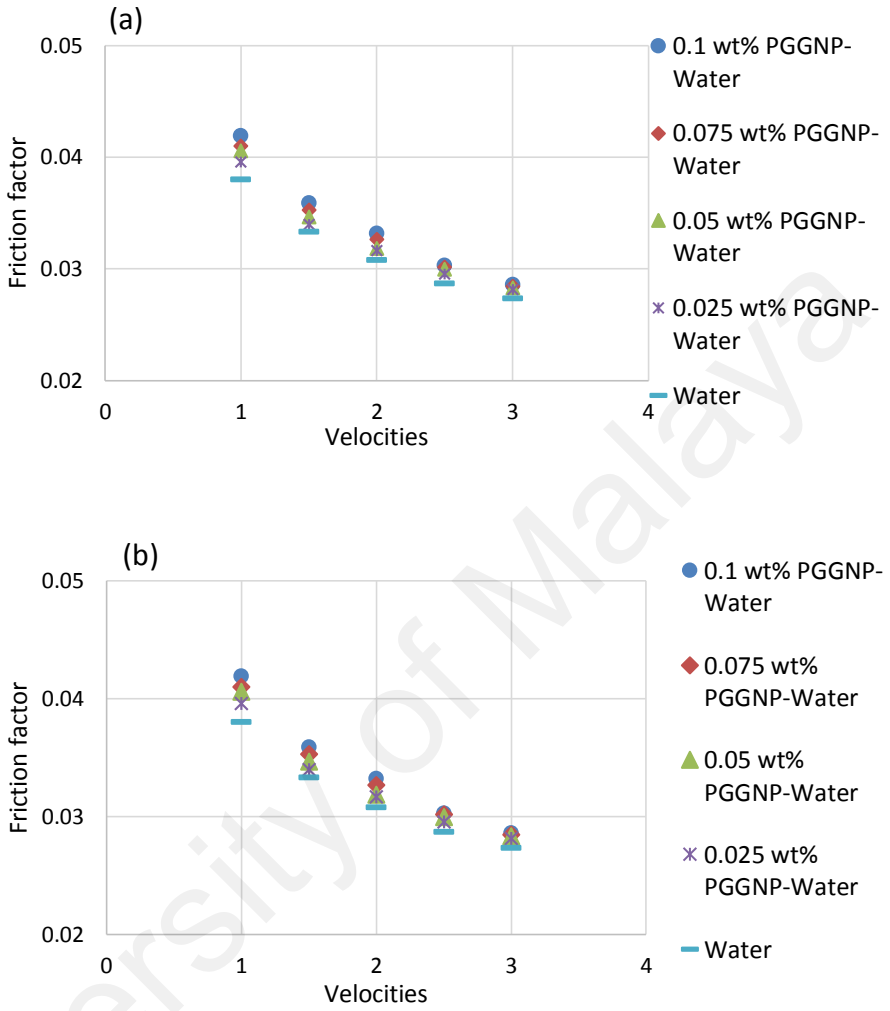

Figure 6.21. Friction factor of PGGNP-Water at different velocities at inlet temperature of 30°C and input power of (a) 23870 W/m^2 and (b) 18565 W/m^2

The TMP-treated GNP showed the highest increment in friction factor from 4% to 10.2% at concentration of 0.1wt% and velocities from 1 to 3m/s. Consequently, it was observed that as the velocity increases, the dependence of friction factor on the concentration of TMP-treated GNP decreases.

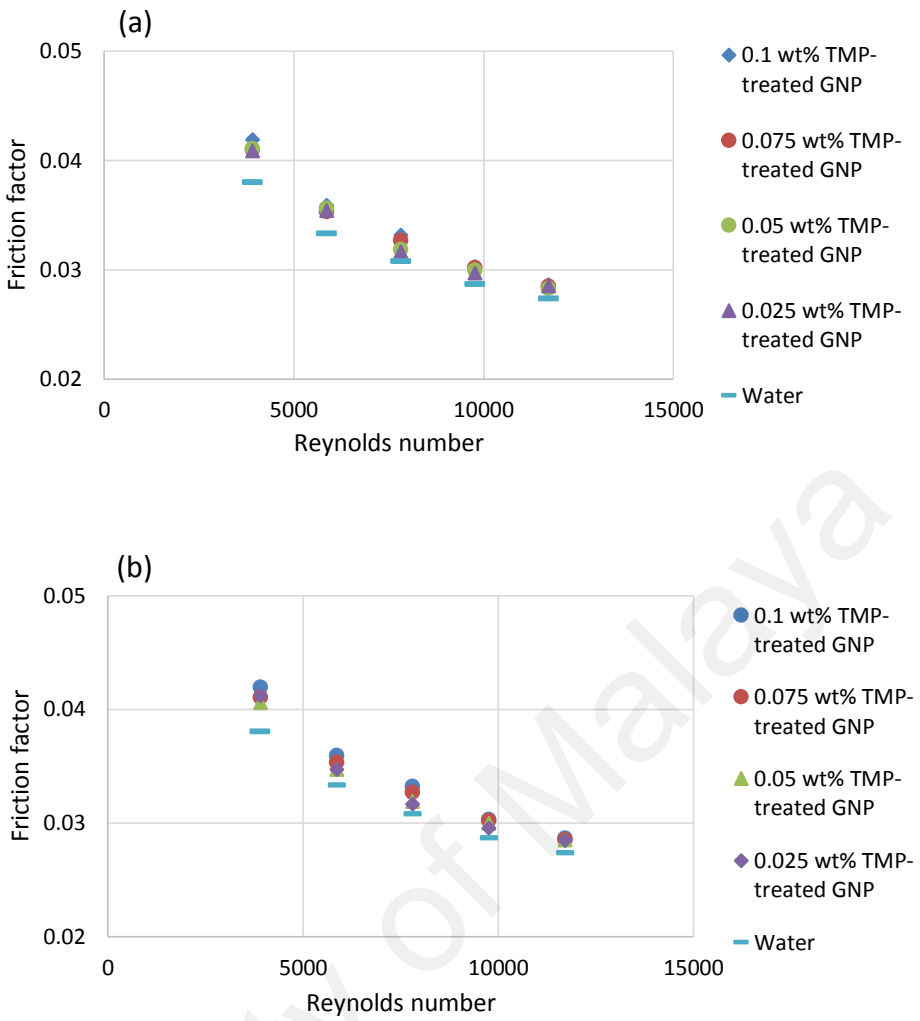

Figure 6.22. Effect of Reynolds number and concentration of TMP-treated GNP on the friction factor at inlet temperature of 30°C with input power of (a) 23870 W/m^2 and (b) 18565 W/m^2.

The friction factor of Al_2O_3 and SiO_2 nanofluids flowing through the test section was measured under various conditions including different concentrations and velocities. Figure 6.23 (a and b) and Figure 6.24 (a and b) shows the measured friction factor for the Al_2O_3 and SiO_2 nanofluids for all concentrations, as function of the flow velocity. It was observed that, the friction factor increases as the concentration of nanofluids increases, although there are some fluctuations in measured friction factor for different velocities. At 0.1wt% of Al_2O_3 the highest increment in friction factor were calculated

from 2.9% to 5.92% at velocities from 1 to 3m/s. It can be seen that as the velocity increases, the dependence of friction factor on the concentration of Al_2O_3 decreases.

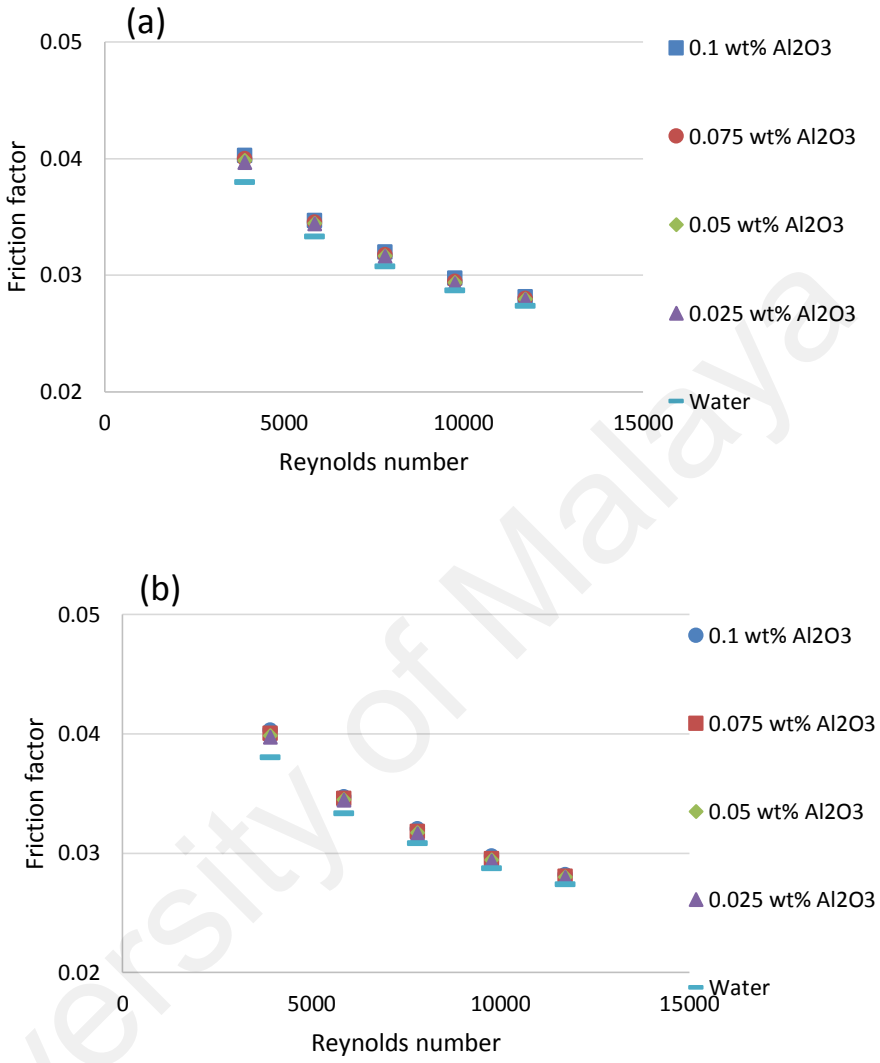

Figure 6.23. Effect of Reynolds number and concentration of Al_2O_3 on the friction factor at inlet temperature of 30°C with input power of (a) 23870 W/m^2 and (b) 18565 W/m^2.

The SiO_2 nanfluid showed the highest increment in friction factor from 3% to 7% at concentration of 0.1wt% and velocities from 1 to 3m/s. Consequently, it was observed that as the velocity increases, the dependence of friction factor on the concentration of SiO_2 decreases.

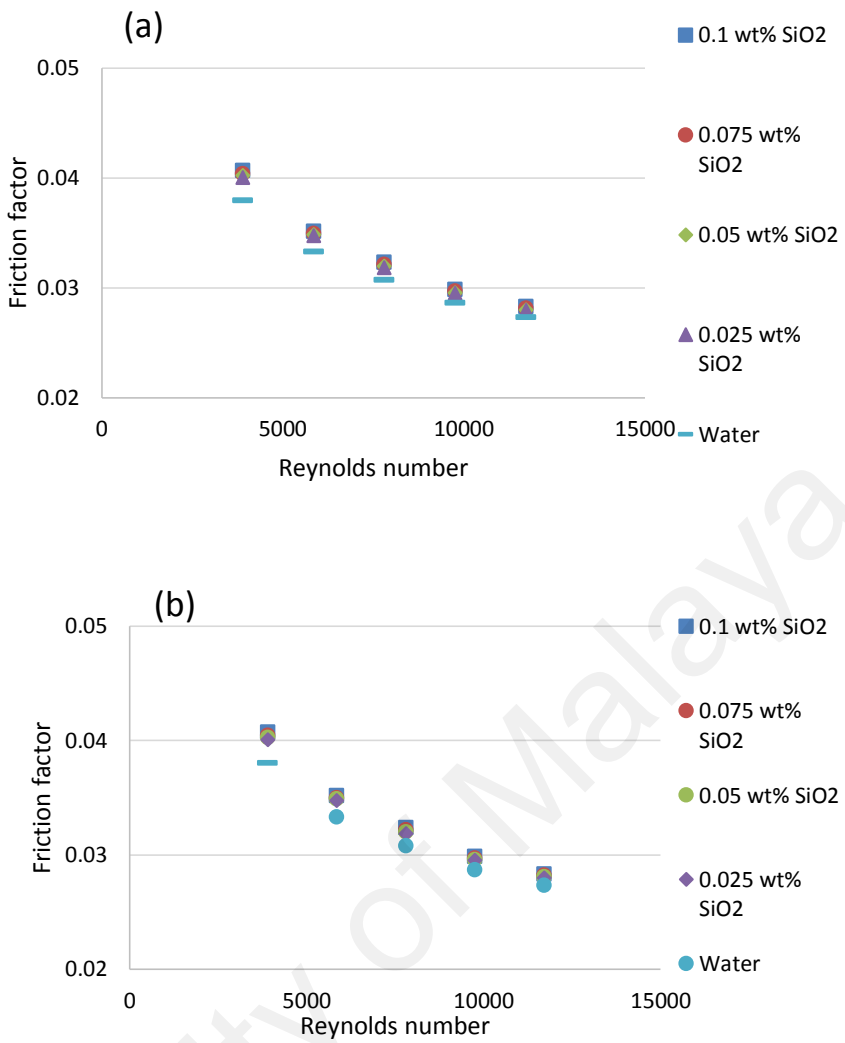

Figure 6.24. Effect of Reynolds number and concentration of SiO_2 on the friction factor at inlet temperature of 30°C with input power of (a) 23870 W/m^2 and (b) 18565 W/m^2.

At low extent of the Reynolds numbers, Brownian motion can be the main important parameter that influenced on the momentum transfer between the nanoparticles and base-fluid molecules. Thus, as the Brownian motion increase, in the presence of both type of nanofluids the friction factor increases with higher slope as compared with basefluid (Shanbedi, Amiri, Rashidi, Heris, & Baniadam, 2015; Shanbedi, Heris, Baniadam, Amiri, & Maghrebi, 2012). However, this mechanism is not dominant when high extent of *Re*. In summary, the velocity of working fluid can be considered as the

most important parameter in increasing the friction factor at the high extent of *Re*. Overall, the low difference between friction factors of the basefluid, metal oxides and functionalized nanofluids suspensions at different volume flow rates is attributed to the insignificant gap between viscosities of basefluids and nanofluids. The friction factor change is based on the viscous drag effects of the nanofluids. Therefore, the nanoparticle density is an important parameter for increasing the friction factor of nanofluids. In the flow regime, the pressure drop is directly proportional to viscosity of fluid. This increment in viscosity leads to an undesired increase in pumping power. Therefore, the design of a heat exchanger for efficient heat transfer and minimum pumping power is important in terms of energy savings and could cause considerable errors when assessing the performance of nanofluids (pumping power and heat transfer) in various thermal applications.

6.2.5 Performance index of the tested nanofluids

The economic performance of PGGNP-Water, TMP-treated GNP, Al_2O_3 and SiO_2 nanofluids are typically evaluated by using the performance index (ε), which expressed as the ratio of the heat transfer rate to the pressure drop. Earlier studies (e.g. samira et al (Samira, Saeed, Motahare, & Mostafa, 2014)) showed that by the addition of nanoparticles in base fluids, it increases the heat transfer rate and also increases the pressure drop, which is undesirable. Performance index is then introduced to investigate the combined effect of both parameters. The variations of the performance index of the PGGNP-Water and TMP-treated GNP, Al_2O_3 and SiO_2 nanofluids are shown at different Reynold number and various concentrations in Figure 6.25 to Figure 6.28. It is seen that the performance index of all the samples are greater than 1, which indicates the effectiveness of the prepared nanofluids for convective heat transfer.

It can be seen that performance index of PGGNP-Water increases along with the increase in Reynolds number. The Figure 25 shows that the performance index curves of the PGGNP-water for different concentrations reach their peaks at Reynolds 11700. The highest thermal performance of PGGNP-Water increased up to 1.97 and 1.66 at *Re* 11700, 0.1 wt% concentration and at constant heat fluxes of 23870 W/m^2 and 18565 W/ m^2.

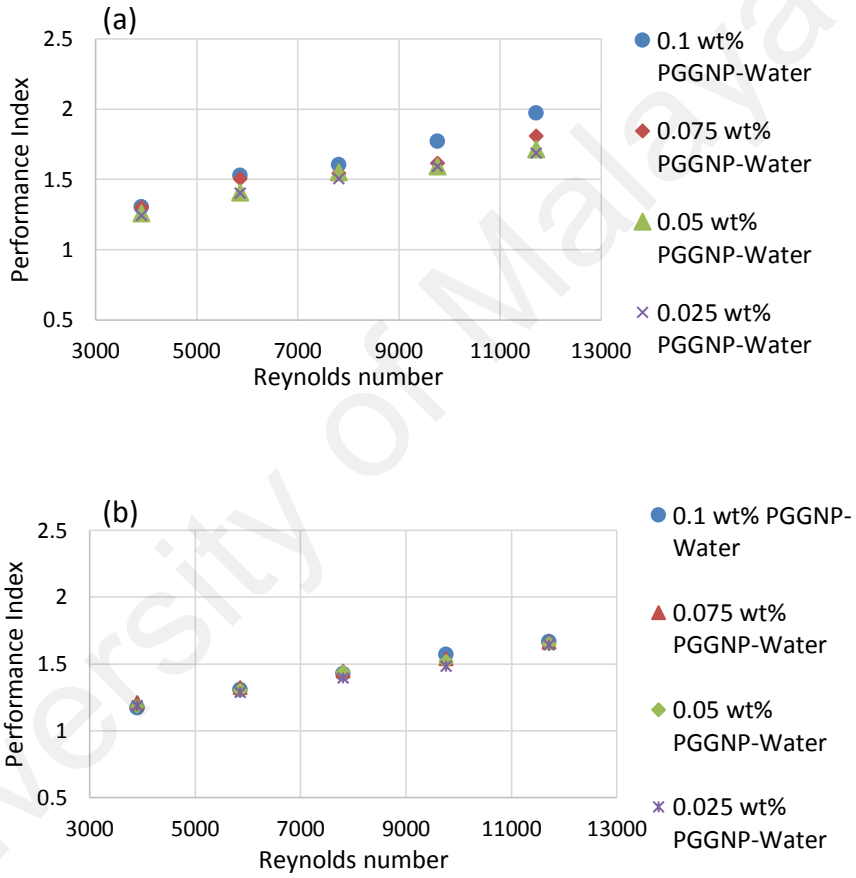

Figure 6.25. Performance index of PGGNP-Water at different concentrations versus Reynolds number at input of (a) 23870 W/m^2 and (b) 18565 W/m^2

The performance index of TMP-treated GNP was obtained with an increase in the weight fraction of TMP-treated GNP. It can be seen that performance index of both TMP-treated GNP increases along with the increase in Reynolds number (see Figure

6.26). The highest thermal performance of TMP-treated GNP increased up to 1.87 and 1.55 at constant heat flux of 23870 W/m^2 and 18565 W/ m^2 at 0.1wt% and 11700 *Re*.

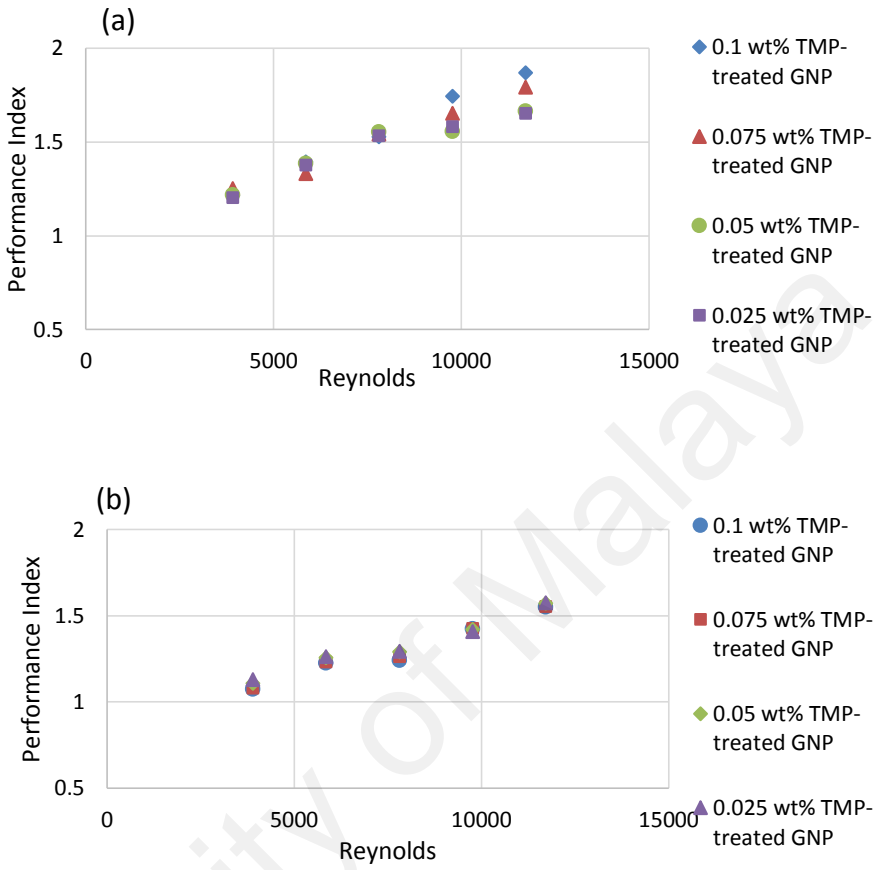

Figure 6.26. Performance index of TMP-treated GNP at different concentrations versus Reynolds number at input power of (a) 23870 W/m^2 and (b) 18565 W/m^2.

The performance index of Al_2O_3 and SiO_2 were also obtained with an increase in the weight fraction from (0.025wt% to 0.1wt%). It can be seen that performance index of both nanofluids increases along with the increase in Reynolds number as shown in Figures 6.27 and 6.28. The highest thermal performance of Al_2O_3 increased up to 1.16 and 1.12 at constant heat flux of 23870 W/m^2 and 18565 W/ m^2 at 0.1wt% and 11700 *Re*. While the highest thermal performance of SiO_2 increased up to 1.19 and 1.13 at

constant heat flux of 23870 W/m^2 and 18565 W/ m^2 at 0.1wt% and 11700 *Re*. The performance index of SiO_2 was observed slightly higher than Al_2O_3.

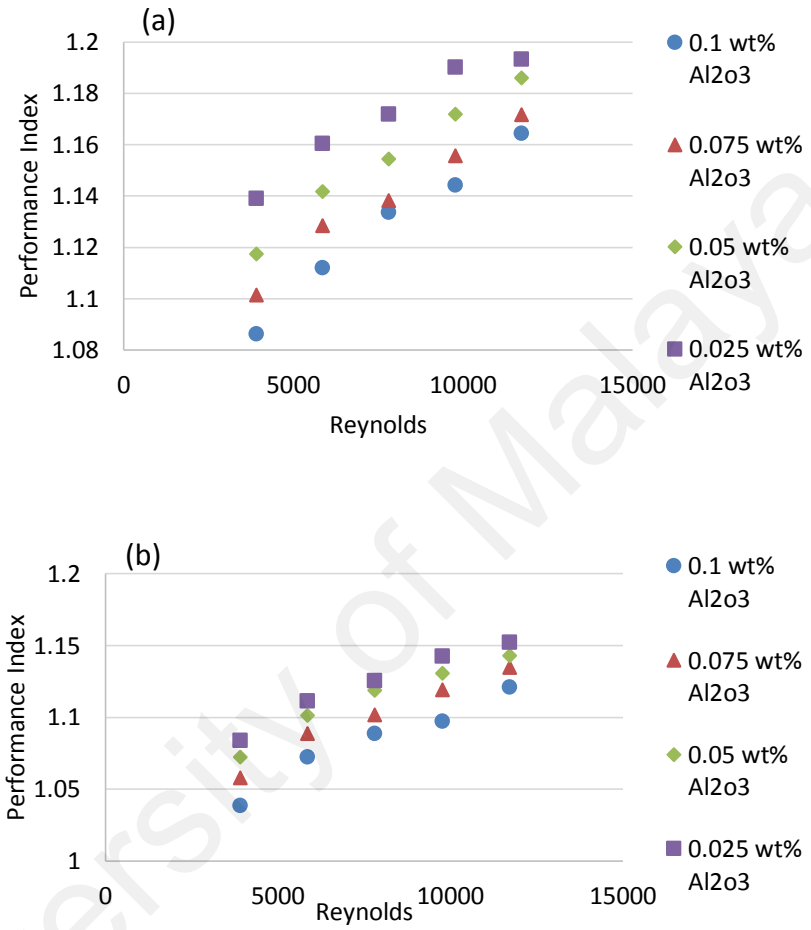

Figure 6.27. Performance index of Al_2O_3 at different concentrations versus Reynolds number at input power of (a) 23870 W/m^2 and (b) 18565 W/m^2.

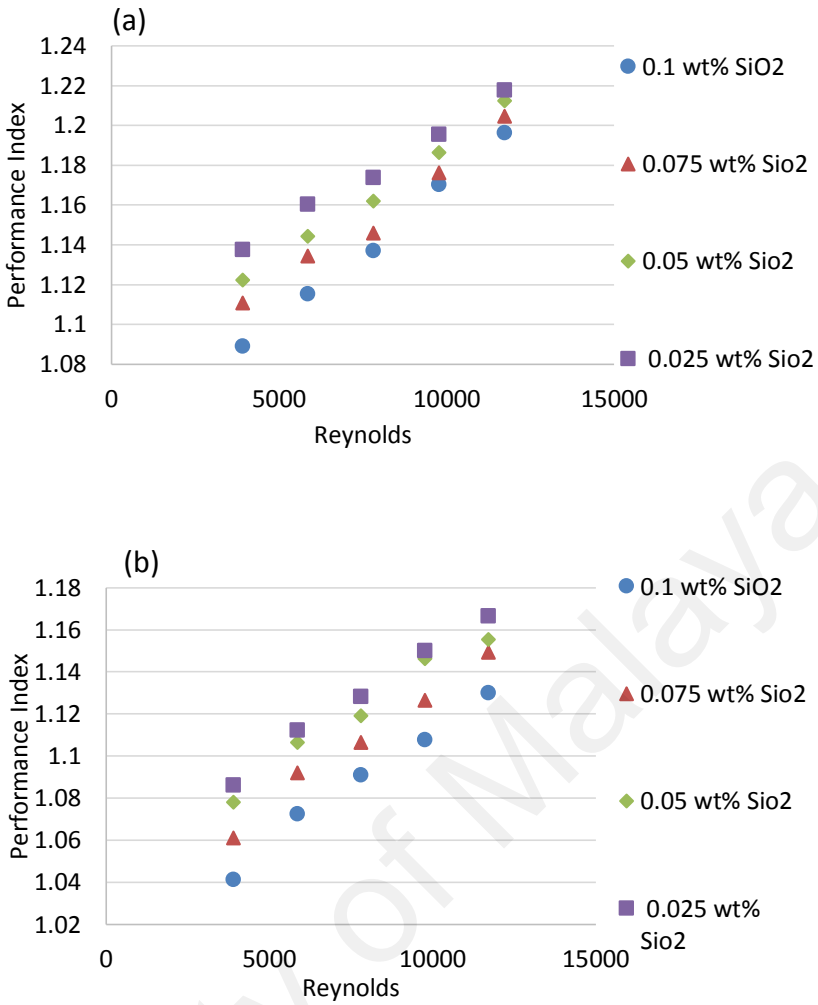

Figure 6.28. Performance index of SiO_2 at different concentrations versus Reynolds number at input power of (a) 23870 W/m^2 and (b) 18565 W/m^2.

Furthermore, above all nanofluids show that the thermal performance factor increases as nanofluids concentration rises. This phenomena is attributable to the increases of viscosity and thermal conductivity of nanofluids. Increasing the viscosity of a nanofluid reduces the thickness of boundary layer, which results in a heat transfer augmentation, while increasing the thermal conductivity raises the thermal performance factor. These results also confirm that the positive effects of heat transfer exceeds the negative effects of pressure drop for PGGNP-Water, TMP-treated GNP, Al_2O_3 and SiO_2 coolants for a wide range of inlet temperatures, concentrations, and velocities; thus

indicating excellent capability of the synthesized PGGNP-Water, TMP-treated GNP and metal oxide nanofluids for convective heat transfer.

6.2.6 Pumping power

Power consumption and pumping characteristics in a loop is a critical parameter in terms of economy as well as energy saving. Pumping power can be considered as an economic performance indicators in a loop system for evaluating the operability of fluid and performance of power plant. In addition the design of a heat exchanger for efficient heat transfer and minimum pumping power is important in terms of energy savings and could cause considerable errors when assessing the performance of nanofluids (pumping power and heat transfer) in various thermal applications. The pumping power or work required to circulate a coolant can be calculated by Equation (6.1).

$$\mathbf{P}_{Pump} = \Delta P \frac{\dot{m}}{\rho} \qquad (6.1)$$

Where ΔP is the pressure drop, $\dot{m}$ is the mass flow rate and ρ is the fluid density. In the actual case of a fully developed condition and a turbulent region in a circular tube with uniform heat flux at the wall, the expression for the pumping power could be introduced by Equation (6.2) (Mansour, Galanis, & Nguyen, 2007).

$$\frac{W_{nf}}{W_{bf}} = \left(\frac{\mu_{nf}}{\mu_{bf}}\right)^{0.25} \left(\frac{\rho_{bf}}{\rho_{nf}}\right)^{2} \qquad (6.2)$$

Where Wnf and Wbf are the pumping power in the presence of nanofluid and basefluid, respectively.

Figure 6.29 to Figure 6.32 compares the pumping power of PGGNP-Water, TMP-treated GNP, Al_2O_3 and SiO_2 nanofluids at two different heat fluxes and at various concentrations. The figures show that there is a slight increase in the pumping power

with the nanofluids loading, and the effect of temperature variation is negligible (Yu, Wenhua, France, Timofeeva, Singh, & Routbort, 2012). While increasing or decreasing the constant heat flux there was negligible difference in the pumping power.

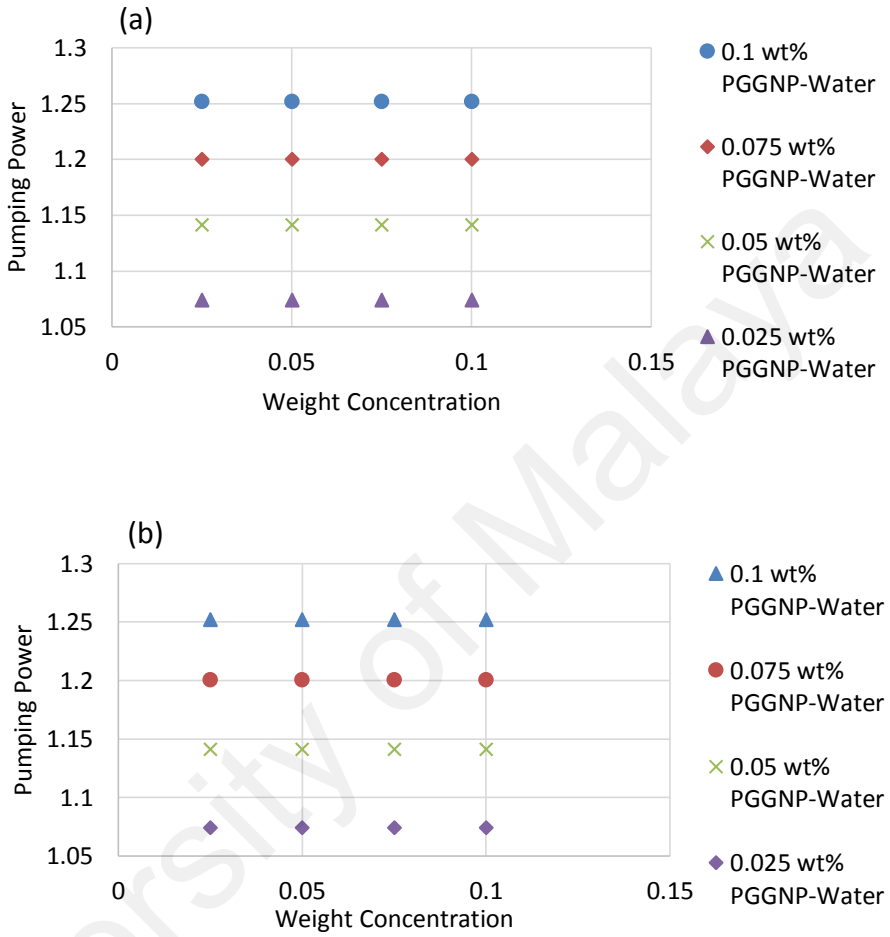

Figure 6.29. Pumping power of PGGNP-water at different concentrations for input power of (a) 23870 W/m^2 and (b) 18565 W/m^2.

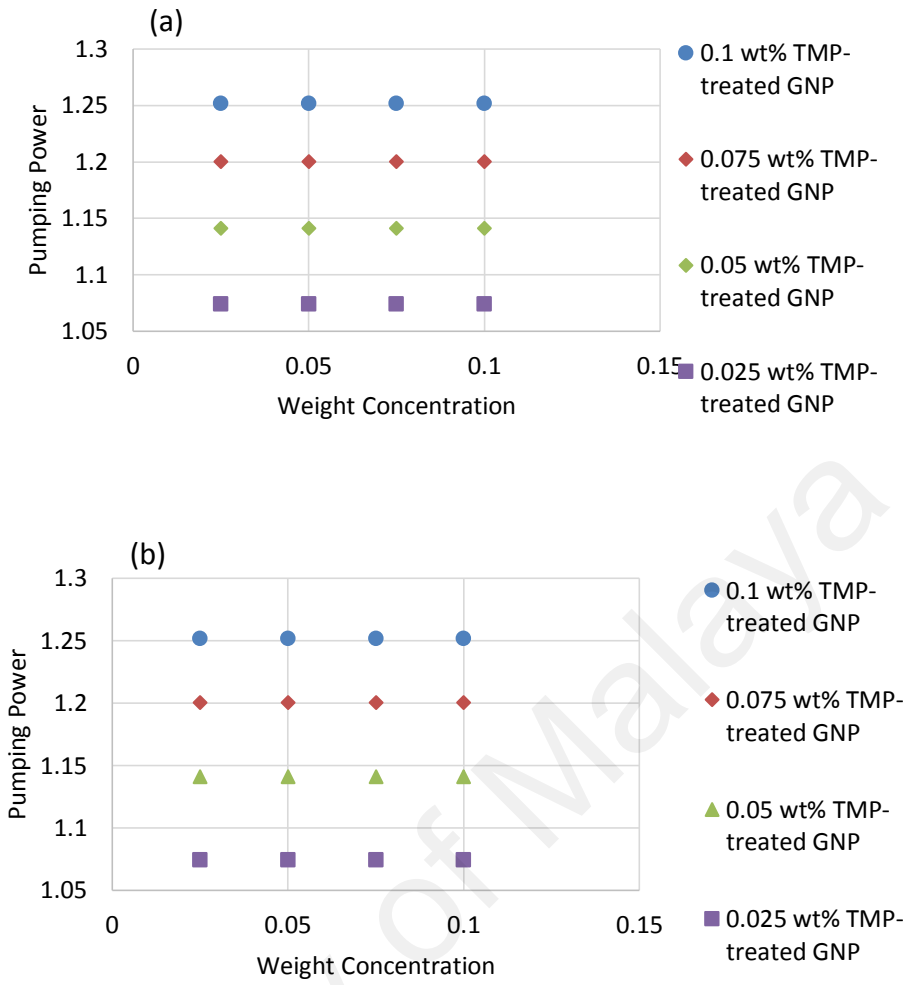

Figure 6.30. Pumping power of TMP-treated GNP at different concentrations and temperatures at input power of (a) 23870 W/m^2 and (b) 18565 W/m^2.

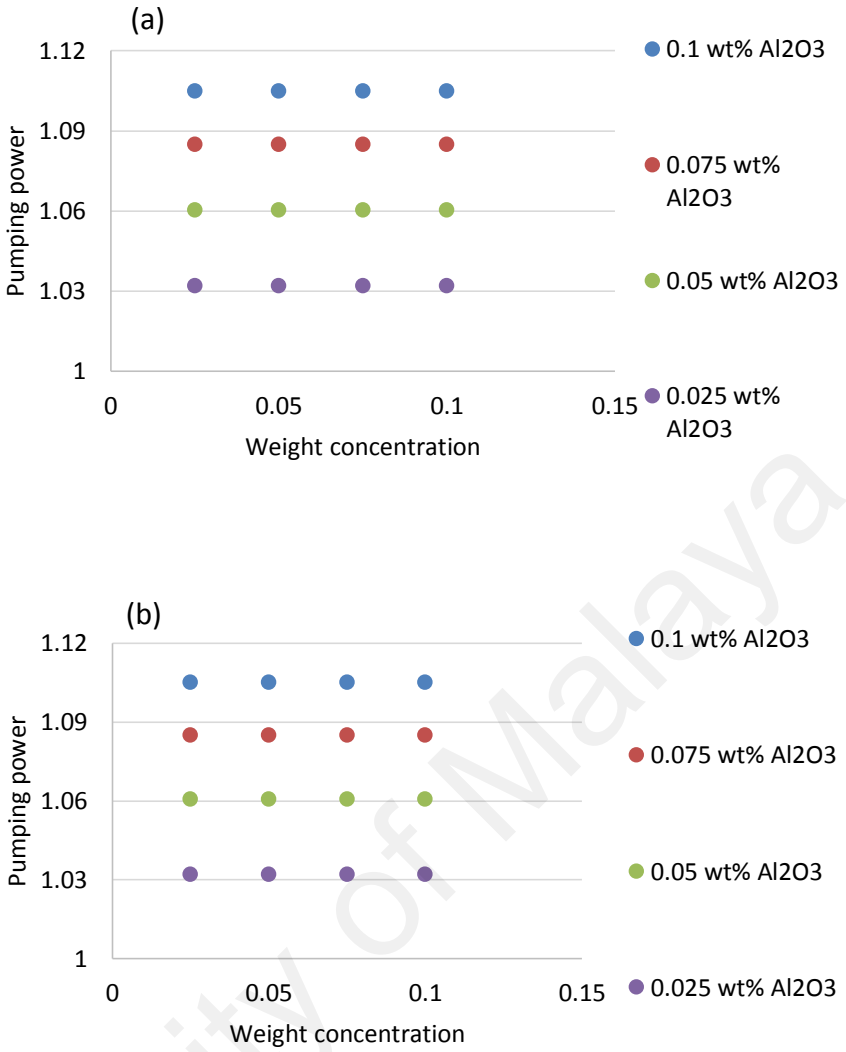

Figure 6.31. Pumping power Al_2O_3 at different concentrations and temperatures at input power of (a) 23870 W/m^2 and (b) 18565 W/m^2.

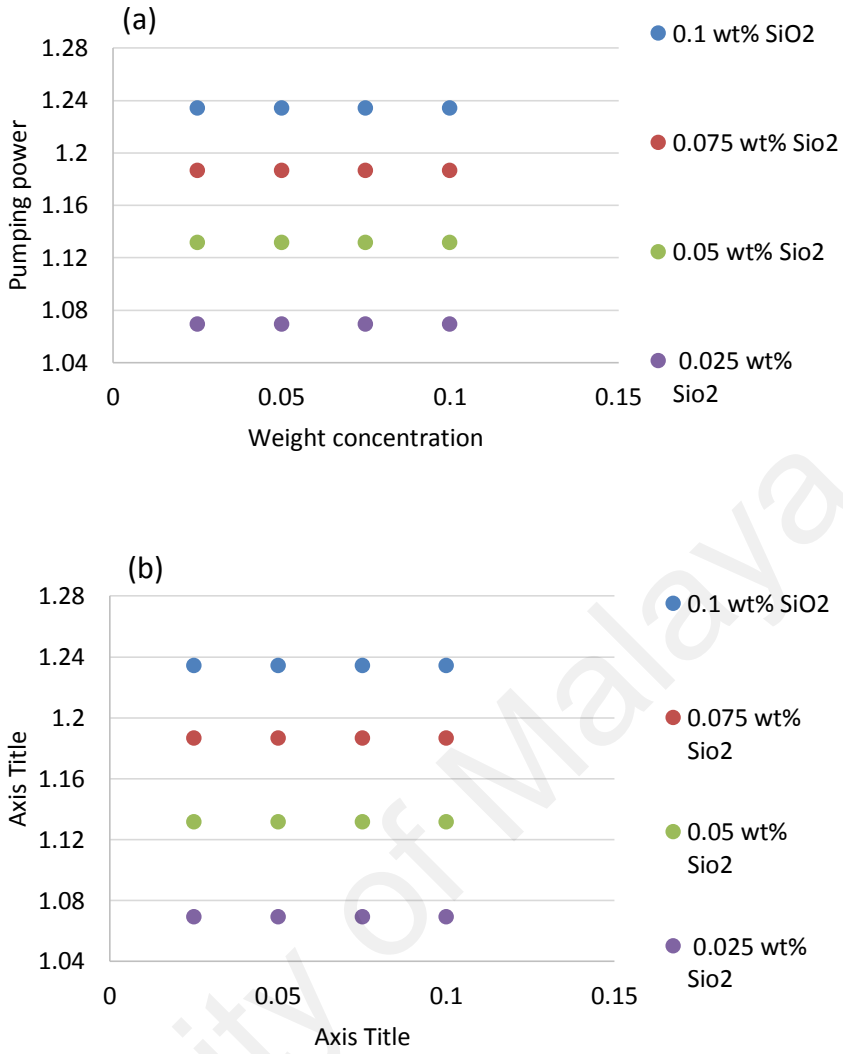

Figure 6.32. Pumping power SiO_2 at different concentrations and temperatures at input power of (a) 23870 W/m^2 and (b) 18565 W/m^2.

In conclusion, for the heat transfer performance of the both functionalized and metal oxide nanofluids compared with the base fluid at a constant Reynolds number or at a constant flow rate, the data from a constant flow rate comparison show good results under certain conditions, such as the consumption of the similar pumping power for the nanofluid and the base fluid.

6.2.7 Efficiency of loop

Performance index presented the convective heat transfer efficiency in terms of pressure drop and rate of heat transfer. The increase in required pumping power is of course undesirable, while the heat transfer coefficient enhancement is highly desirable. To include these conflicting parameters, Yu et al. (Yu, Wenhua et al., 2012) suggested another type of efficiency (efficiency of loop), which is a combination of the heat transfer coefficient (h) and the pumping power (W). The efficiency was measured by the ratio of the heat transfer coefficient enhancement to the pumping power increase.

$$\eta = \frac{h_{nf}/h_{bf}}{W_{nf}/W_{bf}} \qquad (6.3)$$

As discussed above, the efficiency of loop should be higher than 1 for being a cost-effective system. It can be seen in Figures 6.33 to 6.36 that the efficiency of loop is higher than 1 at all concentrations and Reynolds number indicating the promising potential of PGGNP-Water, TMP-treated GNP, Al_2O_3 and SiO_2 for being an alternative nanofluid in the convective heat transfer. The effect of the selected noparticles on viscosity is small, and all the nanofluids behave similarly to pure fluid. In addition the benefit of functionalized GNP and metal oxide nanofluids on enhancement of heat transfer is larger than the increase in pumping power and all the nanofluids have the potential for commercial viability.

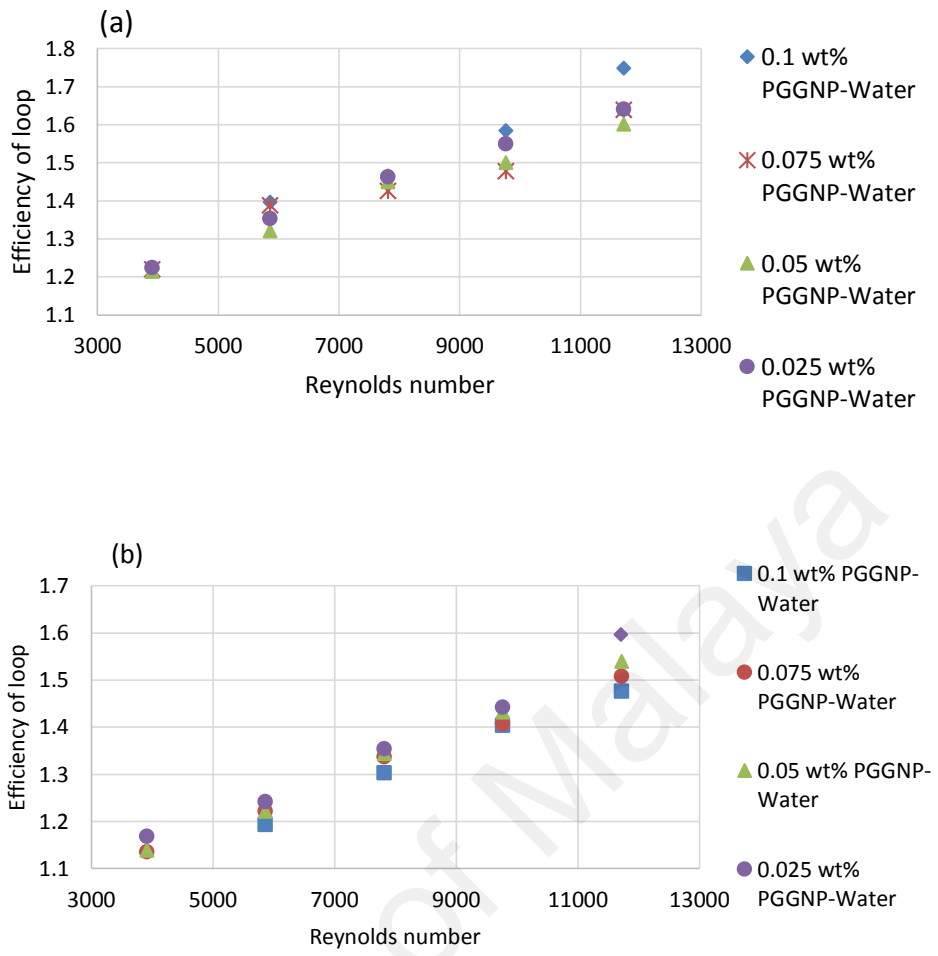

Figure 6.33. Efficiency of loop for the PGGNP-Water at different concentrations and Reynolds number at input power of (a) 23870 W/m^2 and (b) 18565 W/m^2.

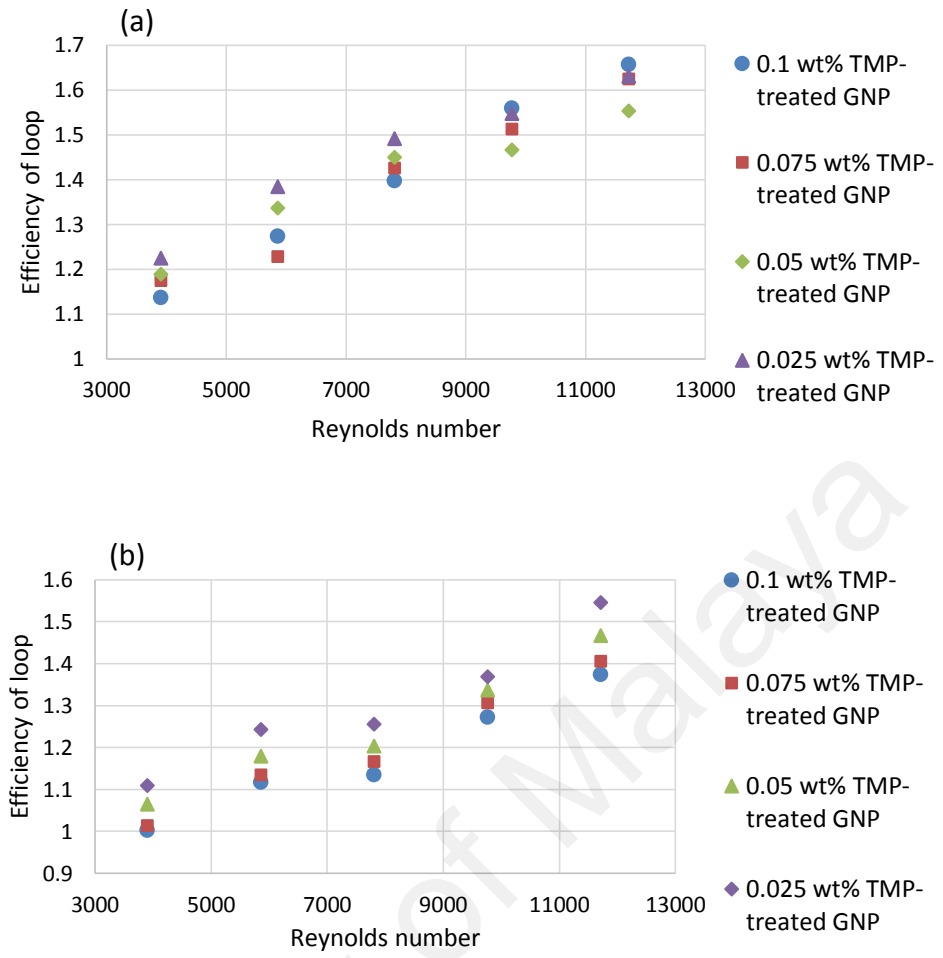

Figure 6.34. Efficiency of loop for the TMP-treated GNP at different concentrations and Reynolds number at input power of (a) 23870 W/m^2 and (b) 18565 W/m^2.

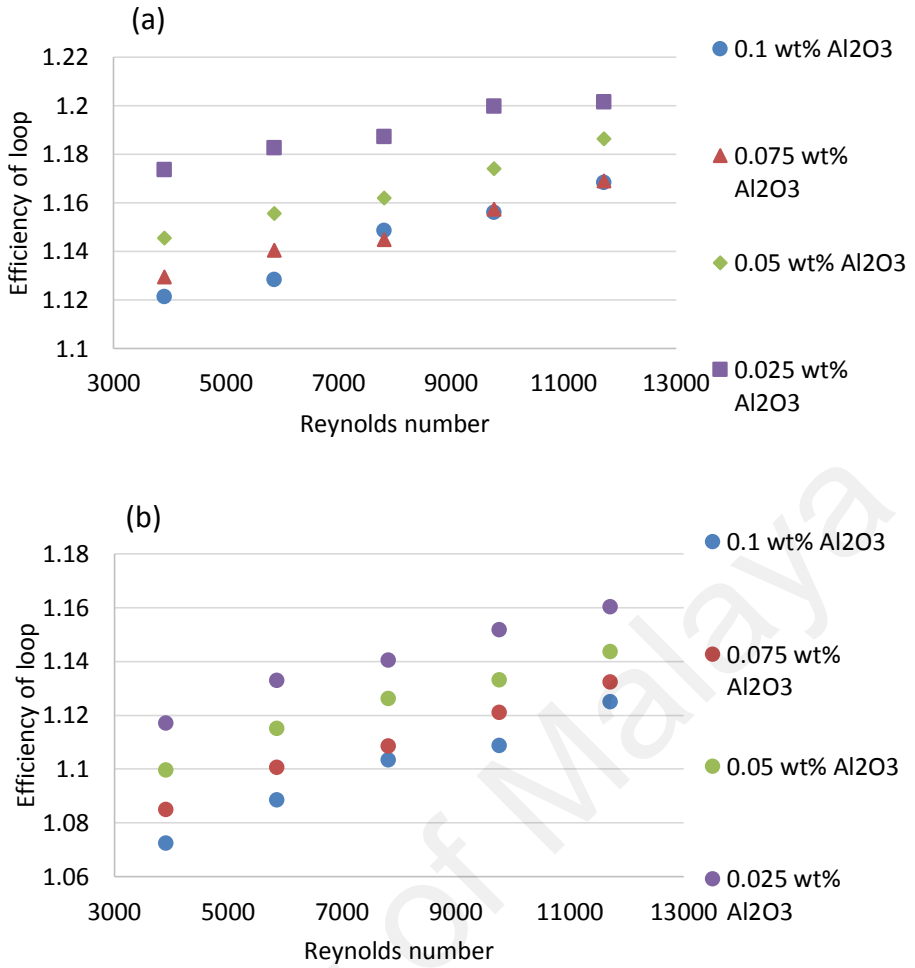

Figure 6.35. Efficiency of loop for the Al_2O_3 at different concentrations and Reynolds number at input power of (a) 23870 W/m^2 and (b) 18565 W/m^2.

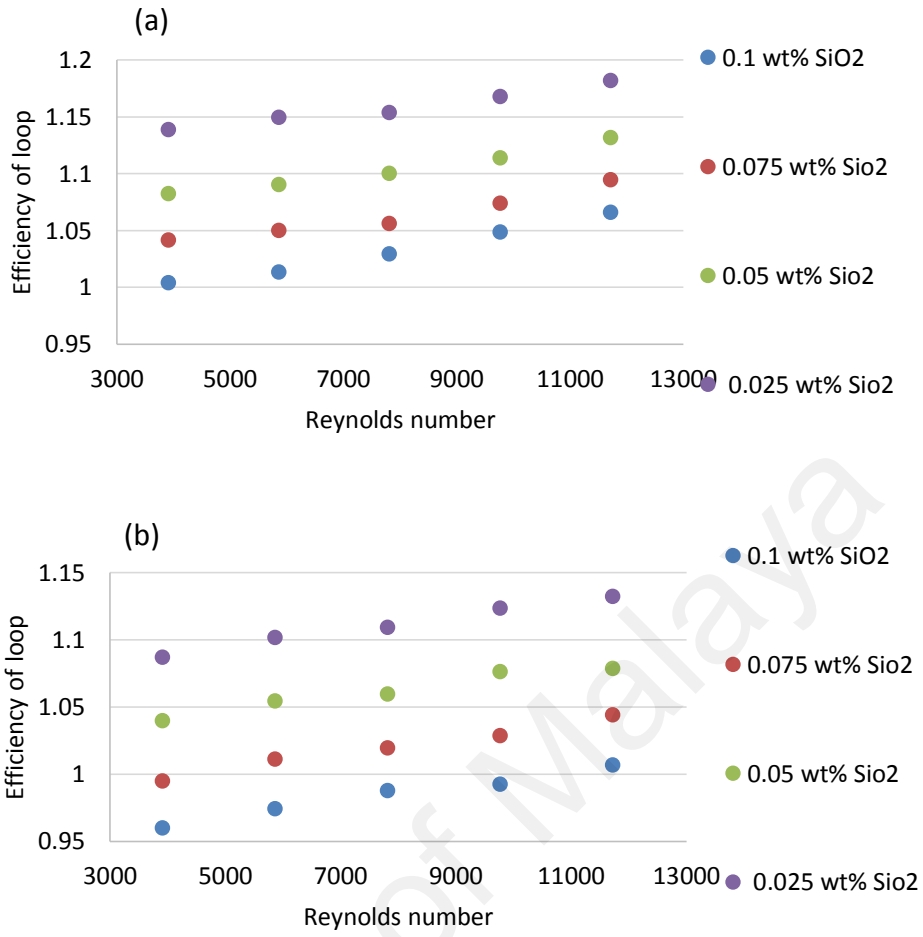

Figure 6.36. Efficiency of loop for the SiO_2 at different concentrations and Reynolds number at input power of (a) 23870 W/m^2 and (b) 18565 W/m^2

6.3 Numerical investigation of heat transfer to PGGNP-water nanofluids

The prediction of convective heat transfer has a vital importance because it directly affects design and operational conditions. It means that the better the prediction, the higher the accuracy of heat transfer performance evaluation. Although conventional heat transfer applications are accurately predicted by heat transfer correlations or solutions to differential equations, there are still debates on estimation of relatively new subjects such as convective heat transfer of nanofluids.

According to literature, and as mentioned in the previous section, there are two ways of modeling convective heat transfer of nanofluids; these are single phase modeling and

two phase modeling. Single phase modeling assumes base fluid and nanoparticles mix homogeneously, there is no additional mechanism to contribute to heat transfer other than existing mechanisms for pure fluids. Two phase modeling states that there are other mechanisms caused by the relative motion between the base fluid and the nanoparticles; such as thermophoresis and thermal dispersion.

In the current study, Two-phase modeling of the convective heat transfer of nanofluid is performed. However, there are still several differences from conventional theories or correlations used to estimate convective heat transfer, which may affect heat transfer performance of nanofluids. In addition, the Two-phase modeling is relatively simpler approach and there is not too much difference between the two approaches especially for higher nanoparticle volumetric fractions as used in the current study.

6.3.1 Methodology

6.3.1.1 Boundary conditions

An investigation of the heat transfer behavior of the PGGNP-water nanofluids was performed by evaluating the velocity and the surface temperature. Two uniform heat fluxes of 18565 W/m^2 and 23870 W/m^2 are applied at the tube wall. The effects of PGGNP-water nanoparticle weight concentration (φ) ranging from 0.025% to 0.1% in the basefluid and the effect Reynolds number (Re) ranging from 3900 to 11700 are investigated. Thus, the uniform axial velocity of flow at the inlet and the constant and uniform heat flux on the wall are defined as the boundary conditions of the problem. At the tube inlet section, a uniform axial velocity based on the Reynolds number and the profile temperature of T_{in} =30°C, are assumed. The no-sleep boundary condition is also considered on the wall for the base fluid and the nanoparticles. For the two-phase flow, the velocity of particles is assumed the same as that of the base fluid at the pipe inlet. A Two-phase model adopted here to describe the turbulent heat transfer to the PGGNP-

water nanofluids in a horizontal copper tube subjected to a uniform heat flux at its outer surface, as shown in Figure 6.37.

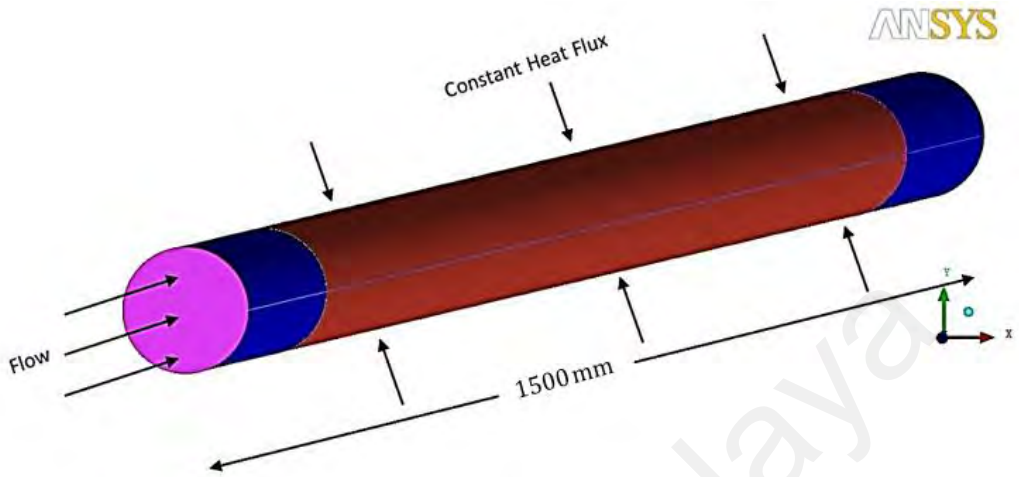

Figure 6.37. 3D schematic view of the test sections.

6.3.1.2 Numerical method

The numerical methods available in the commercial CFD package of ANSYS Fluent, V15 have been applied for the current study. Fluent uses a finite volume approach to convert the governing partial differential equations into a system of discrete algebraic equations. As discretization methods, a second-order upwind scheme are selected for the momentum, turbulent kinetic energy and turbulent dissipation rate equations whereas the first order upwind for energy equation is selected. For two-phase calculations, the phase momentum equations with the shared pressure are solved in a coupled and segregated fashion. The phase coupled SIMPLE (PC-SIMPLE) algorithm is employed for the pressure-velocity coupling. PC-SIMPLE is an extension of the SIMPLE algorithm to multiphase flows. The velocities are solved which are coupled by phases, but in a segregated fashion. The scaled residuals for the velocity components and energy are set equal to 10^{-8} and 10^{-9}, respectively.

The mixture model, based on a single fluid two phase approach, is used in the simulation by assuming that the coupling between phases is strong, and particles closely follow the flow. Each phase has its own velocity vector field, and within any control volume there is a volume fraction of primary phase and also a volume fraction of the secondary phase. Instead of utilizing the governing equations of each separately, the continuity, momentum and energy equations for the mixture are employed. A nanofluid composed of water and PGGNP-water nanoparticles flowing in a long tube with uniform heating at the wall boundary is considered. Therefore, the dimensional equations for steady state mean conditions are 6.4 to 6.6 (Shih, 1984):

a). Continuity equation

$$\nabla.\left(\rho_{eff}\overline{V}\right)=0 \tag{6.4}$$

b). Momentum equations

$$\nabla.(\rho_{eff}\overline{V}\overline{V})=-\nabla\overline{P}+\mu_{eff}\nabla^2\overline{V}-\rho_{eff}\nabla.(\overline{v'v'}) \tag{6.5}$$

c). Conservation of energy

$$\nabla.(\rho_{eff}C_{p,eff}\overline{V}\overline{T})=\nabla.((\mathrm{k}_{eff}+\mathrm{k}_t)\nabla\overline{T}) \tag{6.6}$$

In the above equations, the symbols $\bar{V}$, $\bar{P}$ and $\bar{T}$ represent the time averaged flow variables, while the symbol v' represents the fluctuations in velocity. The term in the momentum equations $\rho_{eff}\nabla.(\overline{v'v'})$ represents the turbulent shear stress. The terms of k_{eff} and k_t represent the effective molecular conductivity and the turbulent thermal conductivity, respectively.

To model flow in the turbulent regime, the standard *k*-ε model can be employed, based on the Launder and Spalding study (Launder & Spalding, 1974), which has considered the equations 6.7 to 6.10 as follows:

$$\nabla.(\rho_{eff}kV) = \nabla.[(\frac{\mu_t}{\sigma_k})\nabla(k)] + G_k - \rho_{eff}\varepsilon \tag{6.7}$$

$$\nabla.(\rho_{eff}\varepsilon V) = \nabla.[\frac{\mu_t}{\sigma_\varepsilon}\nabla\varepsilon] + \frac{\varepsilon}{k}(C_{1\varepsilon}G_k - C_{2\varepsilon}\rho_{eff}\varepsilon) \tag{6.8}$$

$$G_k = \mu_t(\nabla V + (\nabla V)^T),\ \mu_t = \rho_{eff}C_\mu\frac{k^2}{\varepsilon} \tag{6.9}$$

$$C_\mu = 0.09, \sigma_k = 1.00, \sigma_\varepsilon = 1.30, C_{1\varepsilon} = 1.44, C_{2\varepsilon} = 1.92 \tag{6.10}$$

Where μ_{eff} and μ_t are the effective viscosity of nanofluid and coefficient of viscosity in turbulent regime, respectively.

6.3.1.3 Mesh dependency

The meshing tool available in ANSYS is used to construct the computational mesh. A structured mesh based on a rectangular grid is used throughout the domain. While the

radial lengths of the domain are divided into 40 mesh elements with a bias towards the top of the domain, the axial lengths are divided to 500 elements without any bias. The model typically has about 20,000 elements. A non-uniform grid was used in the meshing step, close to the wall grids as smaller to get better results. Several grid distributions have been tested to ensure that the calculated results are grid independent. Figure 6.38 draws the comparison of Nusselt numbers versus Reynolds numbers based on water for three different grid distributions. It is shown that all these results are independent of the number of grid points. For decrease in computational time and effort, the selected grid consists of 500 and 40 nodes in the axial and radial directions, respectively.

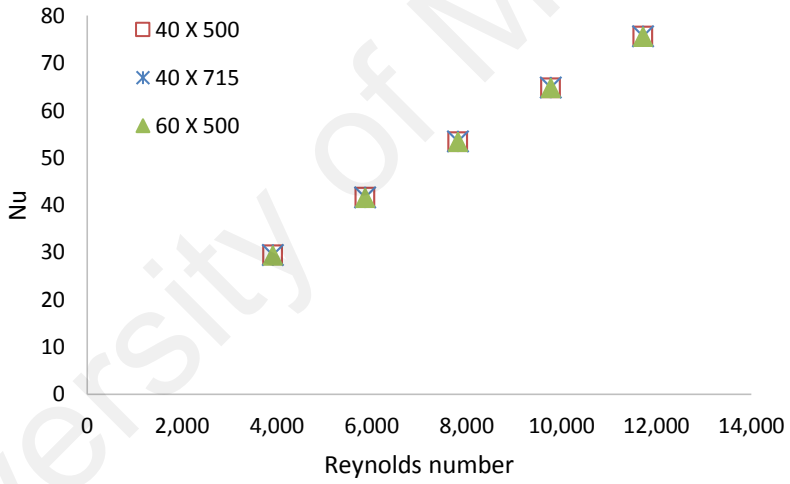

Figure 6.38. Comparison of Nusselt numbers versus Reynolds numbers for water at three different grid distributions.

6.3.1.4 Simulation cases

The turbulent forced convection of PGGNP-water nanofluid at different Re numbers and weight fractions in a heated tube were investigated using two-phase mixture models. Considering 2 different heat fluxes on the tube wall, 5 different Re numbers in

the range of 3900 to 11700 and mass fractions of 0.025wt% to 0.1wt%, there are 50 simulation cases in this study.

6.3.2 Results and discussion

6.3.2.1 Validation of the numerical method for the case of distilled water

The numerical results for DW at constant heat flux conditions were compared with the experimental results of DW and correlation of Dittus-Boelter and Gnielinski. Figure 6.39 shows that the comparison between the experimental tube surface temperature and the data from the numerical simulation for Reynolds number range of 3900 to 11700 at two constant heat fluxes of 18565 W/m^2 and 23870 W/m^2. It can be seen that linear increases in surface temperature along the pipe and those increment occurred with increase of Reynolds number and heat fluxes for both experimental and numerical results (see Figure 6.39 a and b). There is a good agreements between numerical and experimental data with a maximum error of less than 4% for DW.

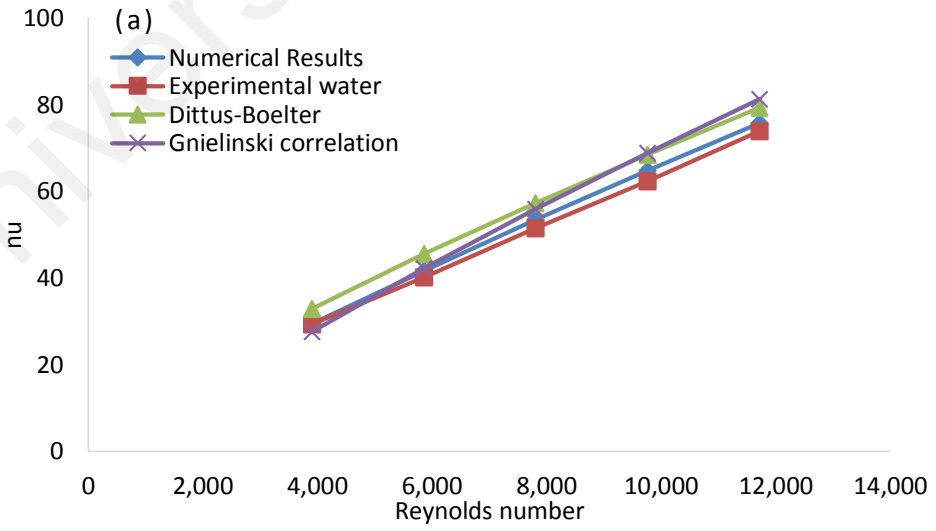

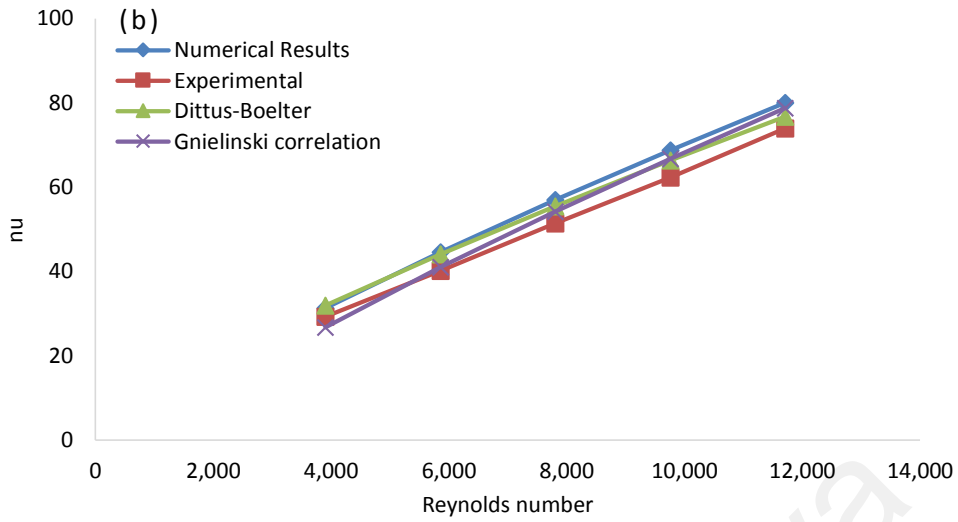

Figure 6.39. Comparison Nusselt numbers various Reynolds numbers obtained by two-phase mixture method and Gnielinski and Dittus-boelter equations at (a) q= 18565 W/m^2 (b) q=23870 W/m^2.

6.3.2.2 Thermal analysis of PGGNP-water

The numerical study on the turbulent forced convection turbulent flow of PGGNP-water in a tube has been performed at various Reynolds numbers and weight concentrations. There are 450 cases of simulations where weight concentration of 0.025%, 0.05%, and 0.1% and the Reynolds numbers of 3900, 5859, 7812, 9765 and 11700 have been selected. Figure 6.40 (a and b) are respectively presented the convective heat transfer coefficients of pure water and PGGNP-water nanofluids as a function of the Reynolds number. It can be seen that some lines with different slopes, which has increased with the increase in Reynolds number as well as concentration of PGGNP-water. This phenomenon can be attributed to the higher thermal conductivity of basefluid in the presence of PGGNP-water. For example, about 119% increase in the convective heat transfer coefficient is obtained at Reynolds number of 11,700 in the presence of 0.1 wt.% of PGGNP-water. This effect was much more realized at higher concentrations of nanofluids by which, the heat transfer rate was suppressed, and that

could be signified by the constricted movement of the thermally conductive particulates within the nanofluid, leading to an eventual reduction in the molecular momentary diffusion. This, in turn, indicates a tradeoff between the effective heat transport and rheological behaviour of the nanofluids. The heat transfer by convection was largely influenced by the particle size, lower molecular momentum diffusivity, flow restriction, and an increase in both the dynamic viscosity and thermal boundary layer thickness. In addition, all concentrations of PGGNP-water were compared with numerical results which shows good agreement at both the constant heat fluxes as shown in Figure 6.40 (a and b).

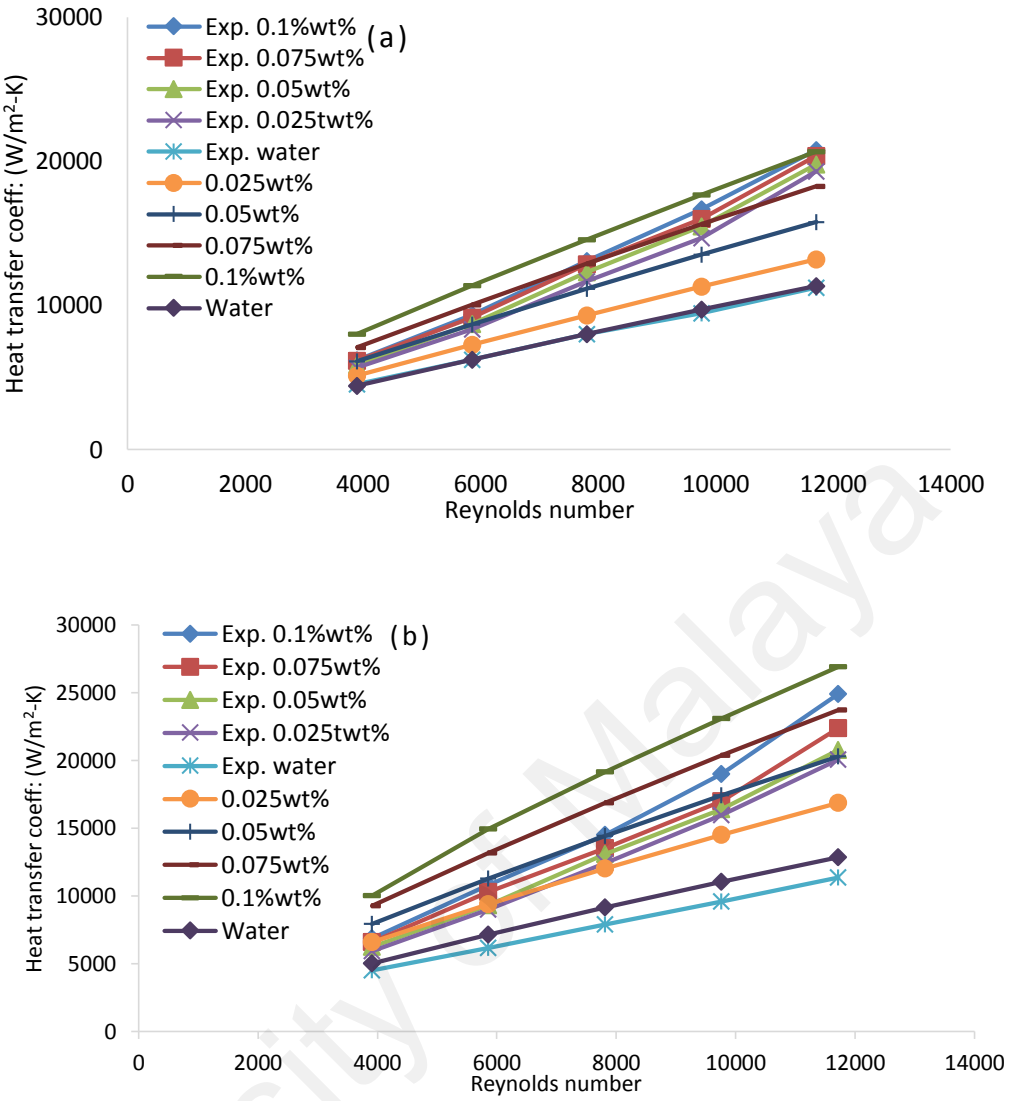

Figure 6.40. Comparison of the convective heat transfer coefficients at various Reynolds numbers and weight concentrations at (a) q= 18565 W/m^2 (b) q=23870 W/m^2.

Average Nusselt numbers of the PGGNP-water nanofluids as a function of the velocity at different heat fluxes are presented in Figure 6.41. Generally, for all cases the average Nusselt numbers of the PGGNP-water nanofluids experienced good increment with increase of velocity in both numerical and experimental results. Effect of weight concentrations of the PGGNP-water nanofluids on average Nusselt numbers has been noted where the highest average Nusselt number showed at 0.1wt%, Re 11700 and heat flux of 23870 W/m^2 due to the improved thermal conductivity and the reduced thermal

resistance between the flowing nanofluid and the inner wall surface of the tube. The Nusselt number (Nu) was increased up to 84% and 54%, for the heat fluxes of 23870 W/m^2 and 18565 W/m^2 at 0.1wt%, respectively.

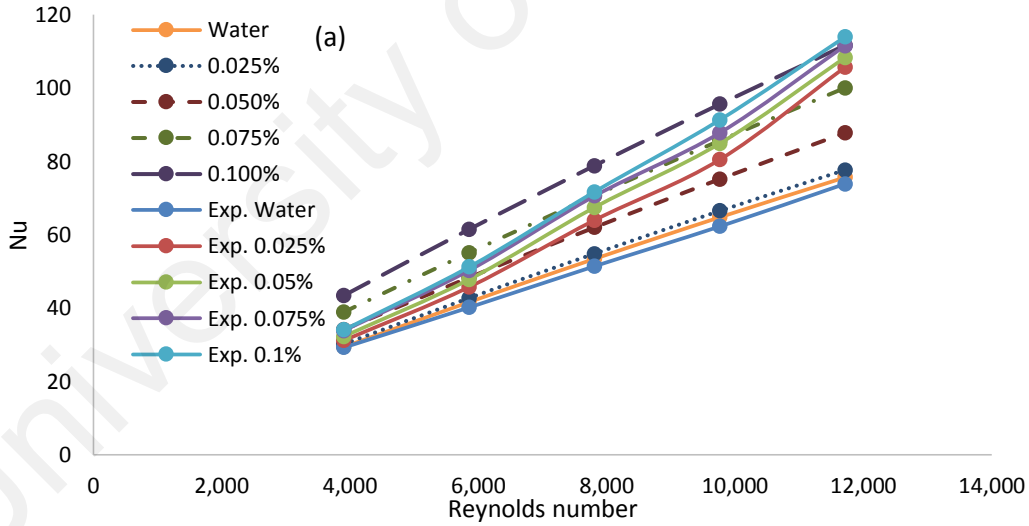

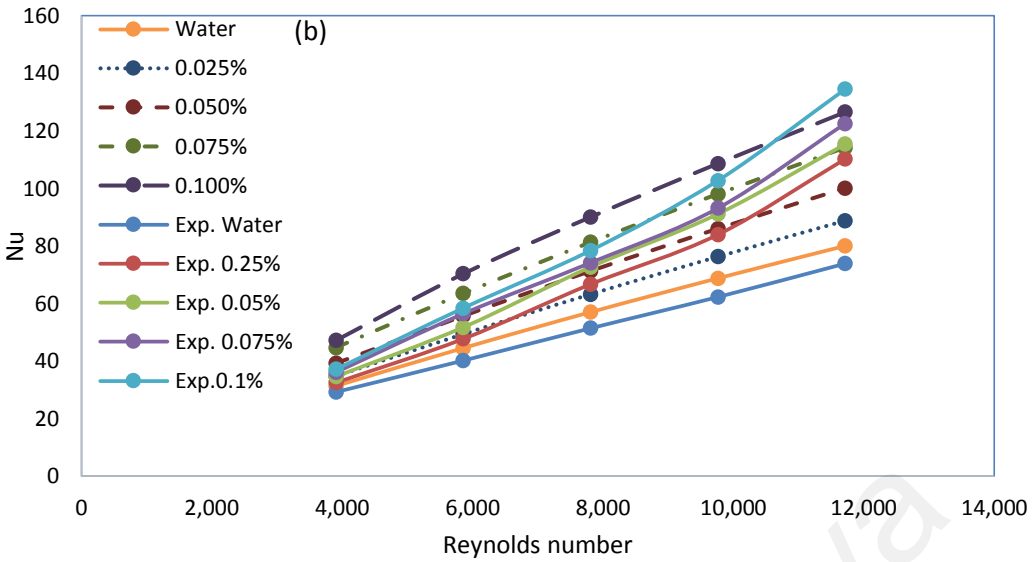

Figure 6.41. Average Nusselt numbers various Reynolds numbers and weight concentrations at (a) q= 18565 W/m^2 (b) q=23870 W/m^2.

6.3.2.3 Pressure drop

Figure 6.42 shows the effect of Reynolds number and concentration of PGGNP-water based nanofluids on the pressure drop. As shown in Figure 6.42, as the inlet velocity and concentration of nanofluids increases, the pressure drop increases. The pressure drops for PGGNP-water nanofluids at various concentrations are not quit close to that for water pressure drop. This observation confirms that the effect of PGGNP-water concentration on the viscosity of nanofluids and consequently on the pressure drop is significant. The increased pressure drop could be related to the viscous drag effects and density gradient of nanoparticles dispersed in the base fluid. It is noteworthy that, during the flow of nanofluids, the formation of the temporal flocculation (or nanoclusters) of nanoparticles in the fluid medium, which had not been fragmented and re-structured to primary particles, would have resembled the higher viscosity of nanofluids. This aspect could be verified further from Equation (5.5), wherein the friction factor as a function of the pressure drop was largely dependent on the density

gradient of the nanofluids experienced with increased concentrations of nanoparticles. Moreover, the nanofluid layer in close vicinity to the inner tube wall surface was prone to higher shear stress with relatively low velocity, which manifested in low viscosity with the addition of nanoparticles. However, the rotation of nanoclusters, which has to be in line with the direction of fluid flow, was expected to be constricted by the momentary shear disturbances encountered around the nanoparticles (Madhesh, Parameshwaran, & Kalaiselvam, 2014). It is thus found that, the density of the nanoparticles also plays a vital role, thus, the resistance offered to the flow with increased concentration, has led to the increased friction and pressure drop of nanofluids, compared to the base fluid.

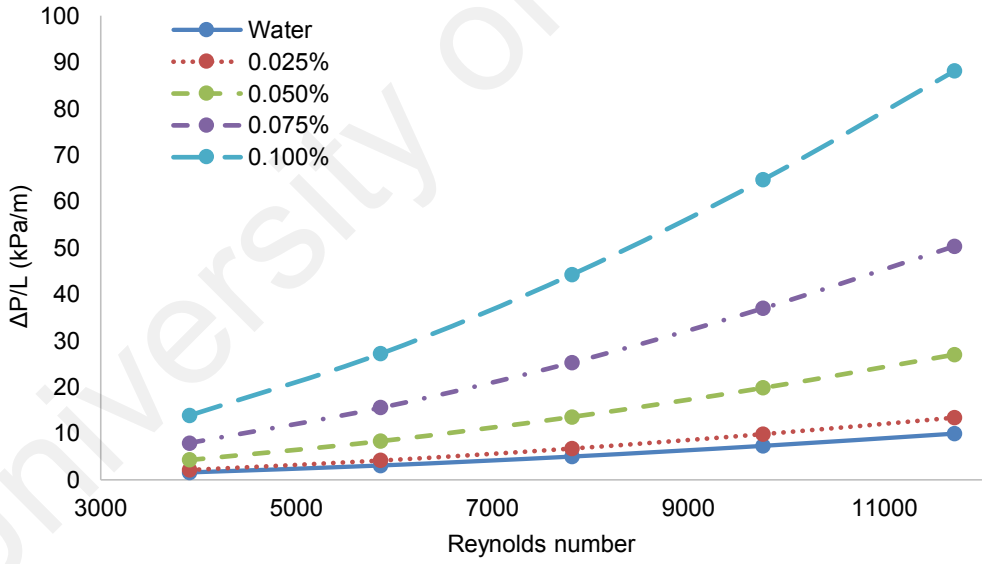

Figure 6.42. Effect of Reynolds number and concentration of PGGNP-water based water nanofluids on the pressure drop.

6.4 CONCLUSION

In this Chapter, forced convective heat transfer to nanofluids is investigated considering the heat transfer coefficient and the Nusselt number enhancement at

constant flow rate. It is concluded that the heat transfer coefficient of a nanofluid is enhanced with respect to the base fluid at a constant velocity. This enhancement comes from the thermal conductivity enhancements. On the other hand, the usage of nanofluids depends also on the pumping power performance of nanofluids. In this Chapter, the estimation of the nanofluid heat transfer is achieved. The constant velocity analyses help to understand the nanofluid heat transfer value deviation from the conventional theories. Hence, the higher heat transfer at the same Re number is not only because of the nanofluids performance, but might be due to the higher flow rate of nanofluids (for measuring at same Re number, where the higher viscosity reduces Re number). Due to these reasons, it might be better to choose constant velocity instead of constant Re number. Therefore, it is required to investigate pumping power behavior of the nanofluids and a comparison between the base fluids and nanofluids is also needed to understand the performance enhancement.

The performance comparison between the nanofluids and the base fluids is actually more important than the heat transfer estimation because this issue determines whether the nanofluid should be used instead of the base fluid. The heat transfer estimation is crucial parameter that affects the heat transfer/pumping power considerations.

The convective heat transfer performance and the flow characteristics of a functionalized GNP's and metal oxide nanofluids flowing in horizontal tubes with two heat fluxes in a fully developed turbulent region were experimentally investigated. Functionalized GNP's (PGGNP-water, TMP-treated GNP) and metal oxide (Al_2O_3 and SiO_2) nanofluids with various concentrations ranging from 0.025 to 0.1 wt% were prepared using a two-step method without any surfactant. The convective heat transfer characteristics and the pressure drop were measured for the flow through a circular tube. The following conclusions were obtained.

1. PGGNP-water, TMP-treated GNP, Al_2O_3 and SiO_2 showed good improvement in thermal performance. The maximum enhancement in thermal conductivity was found in PGGNP-water up to 32% compared to basefluid.
2. The use of the Functionalized GNP's nanofluids provided significantly higher heat transfer coefficients up to 119%.
3. The convective heat transfer coefficient increases with the increase of flow rate and heat flux.
4. A significant enhancement of the convective heat transfer coefficient and the Nusselt number up to 0.1 wt% of the functionalized GNPs were provided improved thermal conductivity and the reduced thermal resistance at the inner wall surface of the tube.
5. The pressure drop and the friction factor of the nanofluid increased by 3% to 10.2% compared to the base fluid. Therefore, the nanofluid results in only a minor penalty in terms of the pumping power, which indicates that it is suitable for some specific practical applications.
6. An increase of the thermal performance could be obtained as 1.97, 1.87, 1.16 and 1.19 for the PGGNP-water, TMP-treated GNP, Al_2O_3 and SiO_2 nanofluids respectively at a heat flux of 23870 W/m^2 and 0.1 wt% concentration. All the selected nanofluids at concentrations provide a good option for the replacement of the conventional working fluids in heat transfer applications.
7. Thermophysical properties of PGGNP-water nanofluids along with two-phase modelling via ANSYS open a new gateway for investigation of convective heat transfer coefficient and pressure drop. Heat transfer enhancement of functionalized PGGNP-water in a turbulent heat exchanger has been considered

in the presence of CFD two-phase mixture model. The validation results confirmed the applicability of Fluent to simulate heat transfer phenomena in the presence of GNP nanofluids.

Additional work is required to investigate the effects of the different nanoparticle concentrations and the different parameters of the convective heat transfer coefficients and flow features of the nanofluids.

CHAPTER 7: GENERAL CONCLUSIONS

This research work focused on heat transfer and friction loss characteristics of propylene glycol-Treated Graphene Nanoplatelets (PGGNP-water), trimethylolpropane tris [poly(propylene glycol), amine terminated] ether-Treated Graphene Nanoplatelets (TMP-treated GNP-water), Al_2O_3 and SiO_2 water based nanofluids. In this investigation the convective heat transfer in circular tubes of different diameters and materials were considered at constant wall heat fluxes of 23870 W/m^2 and 18565 W/m^2 respectively. The experiments were conducted at Reynolds number range, 3,900 to11,700. A novel functionalization approach for preparing highly dispersed propylene glycol-Treated Graphene Nanoplatelets-based water nanofluid (PGGNP-water) and Trimethylolpropane tris [poly(propylene glycol), amine terminated] ether -Treated Graphene Nanoplatelets (TMP-treated GNP-water) were developed. Characterization instruments showed a good degree of GNP functionalization with PG and TMP functionality. Stability study showed more than 88% of both PGGNP- water and TMP-treated GNP-water dispersed even after 1 month. In the materials effect study the copper material showed highest heat transfer performance while in size effect study the lowest diameter showed the maximum increment in heat transfer performance. In this research all the prepared nanofluids have provided significant enhancement in heat transfer characteristics. The measured thermal conductivity, viscosity, specific heat capacity and density of all samples showed reasonable performance required for a good heat exchanging liquid. The following conclusions could be drawn from the observations.

1. Thermal performance enhancement of 20-32% and 20-31% for the PGGNP-water and TMP-treated GNP-water respectively could be achieved.
2. In metal oxides the maximum enhancement for Al_2O_3 and SiO_2 could be achieved up to 7.4% and 9%, respectively compared to the basefluid.

3. A significant enhancement in the heat transfer coefficient up to 119% and 107% could be observed for PGGNP-water and TMP-treated GNP-water respectively at heat flux of 23870 W/m^2. Similiarly for metal oxides the heat transfer coefficient up to 29% and 31% could be achived for Al_2O_3 and SiO_2 respectively at heat flux of 23870 W/m^2.
4. The significient increment, up to 84%, 72%, 26% and 28% in Nusselt number could be achieved for the PGGNP-water, TMP-treated GNP-water, Al_2O_3 and SiO_2 respectively at the specific heat flux of 23870 W/m^2 and at concentration of 0.1 wt%.
5. The Friction factor of both the PGGNP-water and TMP-treated GNP-water nanofluid could be increased by 4% to 10.2% compared to the base fluid. Whereas Al_2O_3 and SiO_2 could achieve increment up to 5.9% and 7.1%, respectively. So, good heat transfer enhancement could be obtained at a cost of little more frictional pressure drop.
6. The highest thermal performance of PGGNP-water and TMP-treated GNP-water nanofluid increased up to 1.97 and 1.87 at constant heat flux of 23870 W/m^2, 0.1wt% and 11700 *Re*. All concentrations of PGGNP-water and TMP-treated GNP-water nanofluids provide a good option as an alternative for the conventional working fluids in heat transfer applications.
7. Thermophysical properties of PGGNP-water nanofluids along with two-phase modelling via ANSYS open a new gateway for investigation of convective heat transfer coefficient and pressure drop. Heat transfer enhancement of functionalized PGGNP-water in a turbulent flow heat exchanger has been considered in a CFD two-phase mixture model. The validation results confirmed the applicability of Fluent to simulate heat transfer phenomena in the presence of GNP nanofluids.

When it comes to the convective heat transfer to nanofluids, in the theoretical analysis part, and classical correlations for DW shows that the experimental data provides accurate results.

8. Examination of convective heat transfer coefficient, h_c for the flow of nanofluids shows that h_c is higher for the case of nanofluids due to flattening in the radial temperature profile as a consequence of thermal dispersion. It is seen that the effect of thermal conductivity enhancement on heat transfer coefficient enhancement is more pronounced than the effect of Nusselt number enhancement, due to quotient form of expression for Nu number.
9. Investigation of the effect of nanofluid particle size on heat transfer results in complicated trends due to the opposing effects of thermal conductivity and thermal dispersion on heat transfer in terms of particle size dependence. Evaluation of heat transfer performance is also analyzed by considering constant pumping power case and observing the heat transfer performance criterion, which depends on the boundary condition, for the nanofluids and the base fluids. However, the recommendation of nanofluid as advantageous alternative to conventional and heat transfer liquid is limited to specific applications. It could be inferred that the heat transfer performance depends on different important parameters for the fully developed region. Actually, the theoretical analysis gives similar results for the boundary conditions but may have slightly different performance ratios. The important parameters depend on nanofluid thermo-physical properties and nanofluid convective heat transfer behavior.

RECOMMENDATIONS FOR FUTURE WORK

The present works have highlighted several new insights towards pursuing an enhancement in convective heat transfer and thermophysical properties. The knowledge acquired on the studied particles in-terms of their chemical and morphological structures would become a platform for devising better strategy to achieve much higher colloidal stability. At present, there is significant discrepancy in thermal conductivity data of nanofluids. For the practical application of nanofluids in heat transfer devices, these discrepancies should be eliminated by systematically investigating the effects of some parameters on thermal conductivity of nanofluids. In the literature, the research about the effects of clustering, pH value, and ultrasonic vibration on thermal conductivity is very limited and further research is required regarding the effects of these parameters.

A very broad spectrum of work was covered surrounding nanofluids, hence not every aspect could be covered in detail and thus some questions are still unanswered. Therefore, future recommended work should include the followings:

1. The preparation of nanofluids is a critical part, if not the most important part, when wanting the optimal heat transfer performance. In a poorly prepared nanofluid the nanoparticles settle out of suspension, which leads to a large increase in viscosity due to the agglomeration of the nanoparticles. Most preparation methods found in the literature are for metallic nanoparticles and very few exist for non-metallic. Hence, intensive studies should be conducted for the discovery of proper preparation technique for carbon based nanofluids.
2. The unique chemical structure of Graphene nanoplatelets (GnP) which consist of pristine aromatic basal plane structure with hydrophilic groups at the peripheral site allow further covalent functionalization at the edge via salinization process

to improve its solubility. Further, similar to PGGNP-water and TMP-treated GNP-water, the resultant product would serve as substrate for π interaction with other carbon based materials aiming to further alteration of the morphological structure which can be beneficial in shear flow system.

3. Experimental on convective heat transfer performance can be extended by incorporating the above materials. Investigation on heat transfer augmentation can be further conducted at much higher Re as well as at different test section configurations (i.e. different cross section profile, diameter, sudden contraction and expansion etc.)
4. After a properly prepared nanofluid an investigation on the thermal conductivity and viscosity should be done. There exists numerous correlations for the thermal conductivity and viscosity but they are all study specific, and they can only be used for that specific nanofluid. Hence a study on the thermal conductivity and viscosity for nanofluids of different nanoparticle should be performed in order to get unified correlations.
5. In this study only four types of nanofluids were investigated, hence other different types of nanofluids functionalized as well as metal oxides should be investigated.
6. The present numerical approach can be extended by increasing the dimensionalities within the computational domain. This may include reformulating the fully developed inlet boundary condition to suit the higher dimensional requirements. It is also interesting to adopt single simulation strategy to compare with the existing two phase approach since it was observed experimentally that the increase in heat transfer is much higher in comparison to the thermophysical property enhancement. The challenge remains to physically

model the particle-particle and particle-fluid interactions within the computational domain to replicate the actual pehnomena.

REFERENCES

Abareshi, M., Goharshadi, E. K., Mojtaba Zebarjad, S., Khandan Fadafan, H., & Youssefi, A. (2010). Fabrication, characterization and measurement of thermal conductivity of Fe3O4 nanofluids. *Journal of Magnetism and Magnetic Materials, 322*(24), 3895-3901. doi: http://dx.doi.org/10.1016/j.jmmm.2010.08.016

Abbasian Arani, A. A., & J. Amani. (2012). Experimental study on the effect of TiO2–water nanofluid on heat transfer and pressure drop. *Exp. Thermal Fluid Sci, 42*, 107–115.

Abdulagatov, I. M., & Azizov, N. D. (2006). Experimental study of the effect of temperature, pressure and concentration on the viscosity of aqueous NaBr solutions. *J. Solution Chem, 35*, 705–738

Ahmadreza.Abbasi. Baharanchi. (2013). Application of Nanofluid for Heat Transfer Enhancement (Spring 2013) (PID: 2739168) *Introduction to Nanotechnology*.

Al-Nimr, M. d. A., & Al-Dafaie, A. M. A. (2014). Using nanofluids in enhancing the performance of a novel two-layer solar pond. *Energy, 68*(0), 318-326. doi: http://dx.doi.org/10.1016/j.energy.2014.03.023

Albadr, J., Tayal, S., & Alasadi, M. (2013). Heat transfer through heat exchanger using Al2O3 nanofluid at different concentrations. *Case Studies in Thermal Engineering, 1*(1), 38-44. doi: http://dx.doi.org/10.1016/j.csite.2013.08.004

Alexander, A., A. Balandin, Suchismita. Ghosh, Wenzhong. Bao, Irene. Calizo, Desalegne. Teweldebrhan, . . . Lau, C. N. (2008). Superior thermal conductivity of single-layer graphene. *Nano Letters,, 8*(3), 902–907.

Amiri, A., Sadri, R., Shanbedi, M., Ahmadi, G., Chew, B., Kazi, S., & Dahari, M. (2015). Performance dependence of thermosyphon on the functionalization approaches: an experimental study on thermo-physical properties of graphene nanoplatelet-based water nanofluids. *Energy Conversion and Management, 92*, 322-330.

Amiri, A., Sadri, R., Shanbedi, M., Ahmadi, G., Kazi, S., Chew, B., & Zubir, M. N. M. (2015). Synthesis of ethylene glycol-treated Graphene Nanoplatelets with one-pot, microwave-assisted functionalization for use as a high performance engine coolant. *Energy Conversion and Management, 101*, 767-777.

Amiri , A., Shanbedi. M, Eshghi. H, Heris. S.Z, & M., B. (2012). Highly dispersed multiwalled carbon nanotubes decorated with Ag nanoparticles in water and experimental investigation of the thermophysical properties. *J Phys Chem C, 116*(56), 3369–3375.

Anoop, K. B., Sundararajan, T., & Sarit Das., K. (2009). "Effect of Particle Size on the Convective Heat Transfer in Nanofluid in the Developing Region. *International Journal of Heat and Mass Transfer 52*.

Aravind, S. S. J., Baskar, P., Baby, T. T., Sabareesh, R. K., Das, S., & Ramaprabhu, S. (2011). Investigation of Structural Stability, Dispersion, Viscosity, and Conductive Heat Transfer Properties of Functionalized Carbon Nanotube Based Nanofluids. *The J. of Phy. Chemistry C, 115*(34), 16737-16744. doi: 10.1021/jp201672p

Aravind, S. S. J., & Ramaprabhu, S. (2013). Graphene-multiwalled carbon nanotube-based nanofluids for improved heat dissipation. *RSC Advances, 3*(13), 4199-4206. doi: 10.1039/C3RA22653K

Arzani, H. K., Amiri, A., Kazi, S. N., Chew, B. T., & Badarudin, A. (2015). Experimental and numerical investigation of thermophysical properties, heat transfer and pressure drop of covalent and noncovalent functionalized graphene nanoplatelet-based water nanofluids in an annular heat exchanger. *International Communications in Heat and Mass Transfer, 68*. doi: http://dx.doi.org/10.1016/j.icheatmasstransfer.2015.09.007

Assael, M. J., C.F. Chen, I. Metaxa, & Wakeham, W. A. (2004). Thermal conductivity of suspensions of carbon nanotubes in water. *Int. J. Thermophys, 25*, 971–985.

Barber, J., Brutin, D., & Tadrist, L. (2011). A review on boiling heat transfer enhancement with nanofluids. *Nanoscale Res Lett, 6*(1).

Batchelor, G. K. (1977). The effect of Brownian motion on the bulk stress in a suspension of spherical particles,. *Journal of Fluid Mechanics, 83*(1), 97–117.

Bhattacharya, P., Saha, S. K., Yadav, A., Phelan, P. E., & Prasher, R. S. (2004). Brownian dynamics simulation to determine the effective thermal conductivity of nanofluids. *Journal of Applied Physics, 95*(11), 6492-6494.

Bianco, V., Manca, O., & Nardini, S. (2014). Performance analysis of turbulent convection heat transfer of Al2O3 water-nanofluid in circular tubes at constant wall temperature. *Energy, 77*(0), 403-413. doi: http://dx.doi.org/10.1016/j.energy.2014.09.025

Bitaraf Haghighi, E., Anwar, Z., Lumbreras, I., Mirmohammadi, S. A., Behi, M., Khodabandeh, R., & Palm, B. (2012). *Screening Single Phase Laminar Convective Heat Transfer of Nanofluids in a Micro-tube.* Paper presented at the Journal of Physics: Conference Series.

Branch, C. A. (1991). *Heat transfer and heat transfer fouling in evaporators with Kraft pulp black liquor.* University of Auckland.

Buongiorno, J., Venerus, D. C., Prabhat, N., McKrell, T., Townsend, J., Christianson, R., . . . Alvarado, J. L. (2009). A benchmark study on the thermal conductivity of nanofluids. *Journal of Applied Physics, 106*(9), 094312-094312-094314.

Buorgiorno, J. (2009). A benchmark study on thermal conductivity on nanofluids. *Journal of Applied Physics, 1006*.

Carine.T. Wamkam, Michael. K. Opoku, Haiping. Hong, & Pauline, S. (2011). Effects of p H on heat transfer nanofluids containing ZrO 2 and TiO 2 nanoparticles. *Journal of Applied Physics, 109*.

Chandra Sekhara Reddy, M., & Vasudeva Rao, V. (2014). Experimental investigation of heat transfer coefficient and friction factor of ethylene glycol water based TiO_2 nanofluid in double pipe heat exchanger with and without helical coil inserts. *International Communications in Heat and Mass Transfer, 50*(0), 68-76. doi: http://dx.doi.org/10.1016/j.icheatmasstransfer.2013.11.002

Chandrasekar, M., Suresh, S., & Senthilkumar, T. (2012). Mechanisms proposed through experimental investigations on thermophysical properties and forced convective heat transfer characteristics of various nanofluids – A review. *Renewable and Sustainable Energy Reviews, 16*(6), 3917-3938. doi: http://dx.doi.org/10.1016/j.rser.2012.03.013

Chang, H., Chen, X. Q., Jwo, C. S., & Chen, S. L. (2009). Electrostatic and Sterical Stabilization of CuO Nanofluid Prepared by Vacuum Arc Spray Nanofluid Synthesis System(ASNSS). *Materials transactions, 50*(8), 2098-2103.

Chen, G., W. Yu, D. Singh, D. Cookson, & Roubort, J. (2008). Application of SAXS to the study of particle-size-dependent thermal conductivity in silica nanofluids. *J. Nanopart. Res., 10*, 1109–1114.

Chen, H., Ding, Y., & Tan, C. (2007). Rheological behaviour of nanofluids. *New journal of physics, 9*(10), 367.

Chen, H., Witharana, S., Jin, Y., Kim, C., & Ding, Y. (2009). Predicting thermal conductivity of liquid suspensions of nanoparticles (nanofluids) based on rheology. *Particuology, 7*(2), 151-157. doi: http://dx.doi.org/10.1016/j.partic.2009.01.005

Chen, H., & Yang, W. (2008). Heat transfer and flow behaviour of aqueous suspensions of titanate nanotubes (nanofluids). *Powder Technology*.

Chiesa, M., & A.J. Simonsen. (2007). *The importance of suspension stability for the hot-wire measurements of thermal conductivity of colloidal suspensions.* Paper presented at the 16th Australasian Fluid Mechanics Conference

Cho, B. C. P. a. Y. I. (1998). Hydrodynamic and heat transfer study of dispersed fluids with submicron metallic oxide particles *Experimental Heat Transfer, 11*, 151-170.

Choi. (1995). Enhancing Thermal Conductivity of fluids with nanoparticles. *Developments and Application of Non-Newtonian Flow, ASME*, 99-105.

Choi, C., H.S Yoo, & J.M Oh. (2008). Preparation and heat transfer properties of nanoparticle-in-transformer oil dispersions as advanced energy efficient coolants. *Curr Appl Phys, 8*, 710–712.

Choi, S. U. S. (209). Nanofluids: From Vision to Reality Through Research. *J. Heat Transfer, 131*(3).

Choi, S. U. S., & Eastman, J. A. (1995). Enhancing thermal conductivity of fluids with nanoparticles. *Developments and Applications of Non-Newtonian Flows, ASME, 231*(66), 99–105.

Choi, S. U. S., Z.G. Zang, W. Yu, F.E. Lookwood, & Grulke, E. A. (2001). Anomalous thermal conductivity enhancement in nanutube suspension. *Appl. Phys. Lett., 79*, 2252–2254.

Choi, S. U. S., Zhang, Z. G., Yu, W., Lockwood, F. E., & Grulke, E. A. (2001). Anomalous thermal conductivity enhancement in nanotube suspensions. *Applied Physics Letters, 79*(14), 2252-2254.

Choi, U. S. S. (1995). Enhancing Thermal Conductivity of fluids with nanoparticles. *Developments and Application of Non-Newtonian Flow, ASME*, 99-105.

Chon, C. H., & Kihm, K. D. (2005). Thermal conductivity enhancement of nanofluids by Brownian motion. *American society of mechanical engineers journal of heat transfer, 127*(8), 810.

Chung, K. L., C.L. Hung, & H.T. Su. (2004). A Study of Magnetic Field Effect on Nanofluid Stability of CuO. *Materials transactions, 545*(4), 1375 to 1378.

Chung, S. J., J.P. Leonard, I. Nettleship, J.K. Lee, Y. Soong, D.V. Martello, & Chyu, M. K. (2009). Characterization of ZnO nanoparticle suspension in water: effectiveness of ultrasonic dispersion. *Powder Technology, 194*, 75–80.

Cowan, R. (1963). Pulse Method of Measuring Thermal Conductivity at High Temperature. *Journal of Applied Physics, 34*, 926-927.

Das, S. K., Choi, S. U. S., & Yu, W. (2008). Nanofluids Science and Technology *Wiley-Interscience*

Das, S. K., Choi, S. U. S., Yu, W., & Pradeep, T. (2007). Nanofluids: Science and Technology New Jersey: John Wiley & Sons, Inc.

Das, S. K., Putra, N., Thiesen, P., & Roetzel, W. (2003). Temperature dependence of thermal conductivity enhancement for nanofluids *Journal of Heat Transfer, 125*, 567-574.

Daungthongsuk, W., & Wongwises, S. (2007). A critical review of convective heat transfer of nanofluids. *Renewable and Sustainable Energy Reviews, 11*(5), 797-817. doi: http://dx.doi.org/10.1016/j.rser.2005.06.005

Davarnejad, R., Barati, S., & Kooshki, M. (2013). CFD simulation of the effect of particle size on the nanofluids convective heat transfer in the developed region in a circular tube. *SpringerPlus, 2*(1), 1-6.

David Martinez, C. M. (2009). *Heat Transfer Enhancement of Spray Cooling with Nanofluids.* (Master of Science in Mechanical Engineering), University of South Florida.

De Robertis, E., Cosme, E. H. H., Neves, R. S., Kuznetsov, A. Y., Campos, A. P. C., Landi, S. M., & Achete, C. A. (2012). Application of the modulated temperature

differential scanning calorimetry technique for the determination of the specific heat of copper nanofluids. *Applied Thermal Engineering, 41*(0), 10-17. doi: http://dx.doi.org/10.1016/j.applthermaleng.2012.01.003

Dehkordi, B. L. (2011). *Study of Thermophysical Properties of Alumina Nanofluids.* (Master Thesis), University of Malaya, Kuala Lumpur, Malaysia.

Deryaguin, B. V., & L. Landac. (1941). Theory of the stability of strongly charged lyophobic sols and the adhesion of strongly charged particles in solutions of electrolytes. *Acta Physicochimica URSS, 14*, 633–662.

Diebold, U. (2003). The surface science of titanium dioxide. *Surf. Sci. Rep, 48*, 53–229.

Ding, Y., Alias, H., Wen, D., & Williams, R. A. (2006). Heat transfer of aqueous suspensions of carbon nanotubes (CNT nanofluids). *Int. J. of Heat and Mass Transfer, 49*(1–2), 240-250. doi: http://dx.doi.org/10.1016/j.ijheatmasstransfer.2005.07.009

Dittus, F. W., & Boelter, L. M. K. (1985). Heat transfer in automobile radiators of the tubular type. *International Communications in Heat and Mass Transfer, 12*(1), 3-22. doi: http://dx.doi.org/10.1016/0735-1933(85)90003-X

Duangthongsuk, W., & S. Wongwises. (2008). Heat Transfer Enhancement and Pressure Drop Characteristics of TiO2-Water Nanofluid in a Double-Tube Counter Flow Heat Exchanger. *International Journal of Heat and Mass Transfer, 52*(7-8).

Duangthongsuk, W., & S. Wongwises. (2010). An Experimental Study on the Heat Transfer and Pressure Drop of TiO2- Water Nanofluids Flowing under a Turbulent Regime. *International Journal of Heat and Mass Transfer, 53*(1-3).

Duangthongsuk, W., & Wongwises, S. Comparison of the effects of measured and computed thermophysical properties of nanofluids on heat transfer performance. *Experimental Thermal and Fluid Science 34 (2010) 616–624*.

Eastman, J. A., Choi, S. U. S., Li, S., Yu, W., & Thompson, L. J. (2001). Anomalously increased effective thermal conductivities of ethylene glycol-based nanofluids containing copper nanoparticles. *Applied Physics Letters, 78*(6), 718-720.

Eastman, J. A., Choi, U. S., Li, S., Thompson, L. J., & Lee, S. (1997). *Enhanced thermal conductivity through the development of nanofluids.* Paper presented at the Materials Research Society Symposium Proceedings.

Eastman, J. A., Phillpot, S. R., Choi, S. U. S., & Keblinski, P. (2004). Thermal transport in nanofluids 1. *Annu. Rev. Mater. Res., 34*, 219-246.

El-Brolossy, T. A., & Saber, O. (2013). Non-intrusive method for thermal properties measurement of nanofluids. *Experimental Thermal and Fluid Science, 44*(0), 498-503. doi: http://dx.doi.org/10.1016/j.expthermflusci.2012.08.011

Epstein, N. (1988). Monitoring Fouling. *Proceedings of Fouling in Heat Exchangers Course, University of Auckland, New Zealand*, 5.1-5.35.

Evans, W., Fish, J., & Keblinski, P. (2006). Role of Brownian motion hydrodynamics on nanofluid thermal conductivity. *Applied Physics Letters, 88*(9), 093116-093116-093113.

Evans, W., Prasher, R., Fish, J., Meakin, P., Phelan, P., & Keblinski, P. (2008). Effect of aggregation and interfacial thermal resistance on thermal conductivity of nanocomposites and colloidal nanofluids. *International Journal of Heat and Mass Transfer, 51*(5–6), 1431-1438. doi: http://dx.doi.org/10.1016/j.ijheatmasstransfer.2007.10.017

Fang, X., Fan, L., Ding, Q., Wang, X., Yao, X., Hou, J., . . . Cen, K. (2013). Increased thermal conductivity of eicosane-based composite phase change materials in the presence of graphene nanoplatelets. *Energy Fuels, 27*(7), 4041-4047.

Fedele, L., L. Colla, S. Bobbo, S. Barison, & Agresti, F. (2011). Experimental stability analysis of different water based nanofluids. *Nano Res. Lett, 6*, 300.

Fendler, J. H. (2001). Colloid chemical approach to nanotechnology. *Korean Journal of Chemical Engineering, 18*, 1–6.

Fernández-Seara, J., Uhía, F. J., Sieres, J., & Campo, A. (2007). A general review of the Wilson plot method and its modifications to determine convection coefficients in heat exchange devices. *Applied Thermal Engineering, 27*(17), 2745-2757.

Firme III, C. P., & Bandaru, P. R. (2010). Toxicity issues in the application of carbon nanotubes to biological systems. *Nanomedicine: Nanotechnology, Biology and Medicine, 6*(2), 245-256.

Fotukain, S. M., & M. N. Esfahany. (2010). Experimental Study of Turbulent Convective Heat Transfer and Pressure Drop of Dilute CuO/Water Nanofluid inside a Circular Tube. *International Communications in Heat and Mass Transfer, 37*(2), 214-219.

Garg, J., Poude, B., Chiesa, M., Gordon, J. B., Ma, J. J., Wang, J. B., . . . Chen, G. (2008). Enhanced thermal conductivity and viscosity of copper nanoparticles in ethylene glycol nanofluid. *Journal of Applied Physics, 1003*.

Ghadimi, A., Saidur, R., & Metselaar, H. S. C. (2011). A review of nanofluid stability properties and characterization in stationary conditions. *International Journal of Heat and Mass Transfer, 54*(17–18), 4051-4068. doi: http://dx.doi.org/10.1016/j.ijheatmasstransfer.2011.04.014

Gharagozloo, P. E., Eaton, J. K., & Goodson, K. E. (2008). Diffusion, aggregation, and the thermal conductivity of nanofluids. *Applied Physics Letters, 93*(10), 103110-103110-103113.

Ghozatloo, A., Rashidi, A., & Shariaty-Niassar, M. (2014). Convective heat transfer enhancement of graphene nanofluids in shell and tube heat exchanger. *Experimental Thermal and Fluid Science, 53*(0), 136-141. doi: http://dx.doi.org/10.1016/j.expthermflusci.2013.11.018

Ghozatloo, A., Shariaty-Niasar, M., & Rashidi, A. M. (2013). Preparation of nanofluids from functionalized Graphene by new alkaline method and study on the thermal conductivity and stability. *International Communications in Heat and Mass Transfer, 42*(0), 89-94. doi: http://dx.doi.org/10.1016/j.icheatmasstransfer.2012.12.007

Goodarzi, M., Safaei, M. R., Vafai, K., Ahmadi, G., Dahari, M., Kazi, S. N., & Jomhari, N. (2014). Investigation of nanofluid mixed convection in a shallow cavity using a two-phase mixture model. *International Journal of Thermal Sciences, 75*(0), 204-220. doi: http://dx.doi.org/10.1016/j.ijthermalsci.2013.08.003

Goodwin, J. W., & Hughes, R. W. (2000). Rheology for Chemists—An Introduction (London: The Royal Society of Chemistry.

Goudarzi, K., Nejati, F., Shojaeizadeh, E., & Asadi Yousef-abad, S. K. (2015). Experimental study on the effect of pH variation of nanofluids on the thermal efficiency of a solar collector with helical tube. *Experimental Thermal and Fluid Science, 60*(0), 20-27. doi: http://dx.doi.org/10.1016/j.expthermflusci.2014.07.015

Gu, B., Hou, B., Lu, Z., Wang, Z., & Chen, S. (2013). Thermal conductivity of nanofluids containing high aspect ratio fillers. *International Journal of Heat and Mass Transfer, 64*(0), 108-114. doi: http://dx.doi.org/10.1016/j.ijheatmasstransfer.2013.03.080

Gupta, H. K., G.D Agrawal, & J. Mathur. (2012). An overview of Nanofluids: A new media towards green environment *International journal of environmental sciences, 3*(3).

Gupta, S. S., Siva, V. M., Krishnan, S., Sreeprasad, T., Singh, P. K., Pradeep, T., & Das, S. K. (2011). Thermal conductivity enhancement of nanofluids containing graphene nanosheets. *Journal of Applied Physics, 110*(8), 084302.

Habibzadeh, S., Kazemi-Beydokhti, A., Khodadadi, A. A., Mortazavi, Y., Omanovic, S., & Shariat-Niassar, M. (2010). Stability and thermal conductivity of nanofluids of tin dioxide synthesized via microwave-induced combustion route. *Chemical Engineering Journal, 156*(2), 471-478. doi: http://dx.doi.org/10.1016/j.cej.2009.11.007

Haddad, Z., Abid, C., Oztop, H. F., & Mataoui, A. (2014). A review on how the researchers prepare their nanofluids. *International Journal of Thermal Sciences, 76*(0), 168-189. doi: http://dx.doi.org/10.1016/j.ijthermalsci.2013.08.010

Hagen, K. D. (1999). *Heat transfer with applications*: Prentice Hall Englewood Cliffs, New Jersey, USA.

Haghighi, E. B., N. Nikkam, M , S., M. Behi, S.A. Mirmohammadi, H. Poth, . . . B. Palm. (2013). Shelf stability of nanofluids and its effect on thermal conductivity and viscosity. *Measurement Science And Technology, 24*.

Haghighi, E. B., Saleemi, M., Nikkam, N., Khodabandeh, R., Toprak, M. S., Muhammed, M., & Palm, B. (2014). Accurate basis of comparison for

convective heat transfer in nanofluids. *International Communications in Heat and Mass Transfer, 52*, 1–7. doi: http://dx.doi.org/10.1016/j.icheatmasstransfer.2014.01.002

Haghighi, E. B., Saleemi, M., Nikkam, N., Khodabandeh, R., Toprak, M. S., Muhammed, M., & Palm, B. (2014). Accurate basis of comparison for convective heat transfer in nanofluids. *Int. Commun Heat Mass Transfer, 52*, 1-7.

Haitao. Zhu, Dongxiao. Han, Zhaoguo. Meng, Daxiong. Wu, & Zhang, C. (2011). Preparation and thermal conductivity of CuO nanofluid via a wet chemical method. *Nanoscale Research Letters, 6*(181).

Halelfadl, S., Maré, T., & Estellé, P. (2014). Efficiency of carbon nanotubes water based nanofluids as coolants. *Experimental Thermal and Fluid Science, 53*(0), 104-110. doi: http://dx.doi.org/10.1016/j.expthermflusci.2013.11.010

Halelfadla, S., Estelléb, P., & Maréa, T. (2014). Heat transfer properties of aqueous carbon nanotubes nanofluids in coaxial heat exchanger under laminar regime. *Experimental Thermal and Fluid Science, 55*, 174–180.

Hamilton, R. L., & Crosser, O. K. ((1962)). Thermal conductivity of heterogeneous twocomponent systems. *Industrial & Engineering Chemistry Fundamentals 1 . (3)* 187–191.

Han, D., Meng, Z., Wu, D., Zhang, C., & Zhu, H. (2011). Thermal properties of carbon black aqueous nanofluids for solar absorption. *Nanoscale Research Letters, 6*(1), 1-7.

Han, Z., & Fina, A. (2011). Thermal conductivity of carbon nanotubes and their polymer nanocomposites: A review. *Progress in Polymer Science, 36*(7), 914-944. doi: http://dx.doi.org/10.1016/j.progpolymsci.2010.11.004

Han, Z. H., F. Y. Cao, & B. Yang. (2008). Synthesis and thermal characterization of phase-changeable indium/polyalphaolefin nanofluids. *Applied Physics Letters, 92*(24).

Harikrishnan, S., Magesh, S., & Kalaiselvam, S. (2013). Preparation and thermal energy storage behaviour of stearic acid–TiO2 nanofluids as a phase change material for solar heating systems. *Thermochimica Acta, 565*(0), 137-145. doi: http://dx.doi.org/10.1016/j.tca.2013.05.001

Hashin, Z., & Shtrikman, S. (1962a). A variational approach to the theory of the effective magnetic permeability of multiphase materials *J. Appl. Phys., 33*, 3125–3131.

Hashin, Z., & Shtrikman, S. (1963). A variational approach to the theory of elastic behavior of multiphase materials. *J. Mech. Phys. Solids, 11*, 127–140.

Hassan, M., Sadri, R., Ahmadi, G., Dahari, M. B., Kazi, S. N., Safaei, M. R., & Sadeghinezhad, E. (2013). Numerical Study of Entropy Generation in a Flowing Nanofluid Used in Micro-and Minichannels. *Entropy, 15*(1), 144-155.

Hasselman, D. P. H., & Johnson, L. F. (1987). Effective thermal conductivity of composites with interfacial thermal barrier resistance. *J. Compos. Mater, 21*, 508–515.

He, Y., Jin, Y., Chen, H., Ding, Y., Cang, D., & Lu, H. (2007). Heat transfer and flow behaviour of aqueous suspensions of TiO2 nanoparticles (nanofluids) flowing upward through a vertical pipe. *International Journal of Heat and Mass Transfer, 50*(11–12), 2272-2281. doi: http://dx.doi.org/10.1016/j.ijheatmasstransfer.2006.10.024

Heris, S. Z., Shokrgozar, M., Poorpharhang, S., Shanbedi, M., & Noie, S. H. (2013). Experimental Study of Heat Transfer of a Car Radiator with CuO/Ethylene Glycol-Water as a Coolant. *Journal of Dispersion Science and Technology, 35*(5), 677-684. doi: 10.1080/01932691.2013.805301

Heyhat, M. M., Kowsary, F., Rashidi, A. M., Momenpour, M. H., & Amrollahi, A. (2013). Experimental investigation of laminar convective heat transfer and pressure drop of water-based Al2O3 nanofluids in fully developed flow regime. *Experimental Thermal and Fluid Science, 44*(0), 483-489. doi: http://dx.doi.org/10.1016/j.expthermflusci.2012.08.009

Hindawi. (2014). Hindawi publishing corporation: Heat transfer and nanofluids, Retrived on March 2014. Available at: http://www.hindawi.com/search/all/nanofluids/.

Hong, Yang, H. S., & Choi, C. J. (2005). Study of the enhanced thermal conductivity of Fe nanofluids. *Journal of Applied Physics, 97*(6), 064311-064311-064314.

Hong, K. S., Hong, T. K., & Yang, H. S. (2006). Thermal conductivity of Fe nanofluids depending on the cluster size of nanoparticles. *Applied Physics Letters, 88*(3), 031901-031901-031903.

Huminic, G., & Huminic, A. (2012). Application of nanofluids in heat exchangers: A review. *Renewable and Sustainable Energy Reviews, 16*(8), 5625-5638. doi: http://dx.doi.org/10.1016/j.rser.2012.05.023

Hwang, K., Jang, S. P., & Choi, S. (2009). Flow and convective heat transfer characteristics of water based Al2O3 nanofluid in fully developed laminar flow regime. *International Journal of Heat and Mass Transfer, 52*, 193-199.

Hwang, Y., Lee, J.-K., Lee, J.-K., Jeong, Y.-M., Cheong, S.-i., Ahn, Y.-C., & Kim, S. H. (2008). Production and dispersion stability of nanoparticles in nanofluids. *Powder Technology, 186*(2), 145-153. doi: http://dx.doi.org/10.1016/j.powtec.2007.11.020

Hwang, Y., Lee, J. K., Lee, C. H., Jung, Y. M., Cheong, S. I., Lee, C. G., . . . Jang, S. P. (2007). Stability and thermal conductivity characteristics of nanofluids. *Thermochimica Acta, 455*(1–2), 70-74. doi: http://dx.doi.org/10.1016/j.tca.2006.11.036

Incropera, F., Lavine, A. S., & DeWitt, D. (2011). Fundamentals of Heat and Mass Transfer. In Wiley (Ed.).

Iranidokht, V., Hamian, S., Mohammadi, N., & Shafii, M. B. (2013). Thermal conductivity of mixed nanofluids under controlled pH conditions. *International Journal of Thermal Sciences, 74*(0), 63-71. doi: http://dx.doi.org/10.1016/j.ijthermalsci.2013.07.008

Ismay, M. J. L., Doroodchi, E., & Moghtaderi, B. (2013). Effects of colloidal properties on sensible heat transfer in water-based titania nanofluids. *Chemical Engineering Research and Design, 91*(3), 426-436. doi: http://dx.doi.org/10.1016/j.cherd.2012.10.005

J. Routbort. (2009). Argonne National Lab, Michellin North America, St. Gobain Corp. , http://www1.eere.energy.gov/industry/nanomanufacturing/pdfs/nanofluids_industrial_cooling.pdf.

Jamal-Abad, M. T., Zamzamian, A., & Dehghan, M. (2013). Experimental studies on the heat transfer and pressure drop characteristics of Cu–water and Al–water nanofluids in a spiral coil. *Experimental Thermal and Fluid Science, 47*(0), 206-212. doi: http://dx.doi.org/10.1016/j.expthermflusci.2013.02.001

Jang, S. P., & Choi, S. U. S. (2004). Role of Brownian motion in the enhanced thermal conductivity of nanofluids. *Applied Physics Letters, 84*(21), 4316-4318.

Jha, N., & Ramaprabhu, S. (2008). Synthesis and Thermal Conductivity of Copper Nanoparticle Decorated Multiwalled Carbon Nanotubes Based Nanofluids. *The Journal of Physical Chemistry C, 112*(25), 9315-9319. doi: 10.1021/jp8017309

Jia-Fei, Z., Zhong-Yang, L. U. O., Ming-Jiang, N. I., & Ke-Fa, C. E. N. (2009). Dependence of nanofluid viscosity on particle size and pH value. *Chinese Physics Letters, 26*(6), 066202.

Kabelec, S., & Anoop, K. B. (2008). *Experimental convective heat transfer with nanofluids.* Paper presented at the ASME 2008 6th International Conference on Nanochannels, Microchannels, and Minichannels.

Kabelec, S., & Kuhnke, J. F. (2006). Heat Transfer Mechanisms in Nanofluids – Experiments and Theory. *International Heat Transfer Conference, DOI: 10.1615/IHTC13.p30.110*.

Kakaç, S., & Pramuanjaroenkij, A. (2009). Review of convective heat transfer enhancement with nanofluids. *International Journal of Heat and Mass Transfer, 52*(13–14), 3187-3196. doi: http://dx.doi.org/10.1016/j.ijheatmasstransfer.2009.02.006

Kallay, N., & Å½alac, S. (2002). Stability of nanodispersions: A model for kinetics of aggregation of nanoparticles. *Journal of Colloid and Interface Science, 253*(1), 70-76.

Kamiński, M., & Ossowski, R. L. (2014). Prediction of the effective parameters of the nanofluids using the generalized stochastic perturbation method. *Physica A: Statistical Mechanics and its Applications, 393*(0), 10-22. doi: http://dx.doi.org/10.1016/j.physa.2013.09.015

Karimipour, A., Hemmat Esfe, M., Safaei, M. R., Toghraie Semiromi, D., Jafari, S., & Kazi, S. N. (2014). Mixed convection of copper–water nanofluid in a shallow inclined lid driven cavity using the lattice Boltzmann method. *Physica A: Statistical Mechanics and its Applications, 402*(0), 150-168. doi: http://dx.doi.org/10.1016/j.physa.2014.01.057

Kaufui, V. W., & D.L Omar. (2010). Applications of Nanofluids: Current and Future. *Advances in Mechanical Engineering*.

Kayhani, M., Soltanzadeh, H., Heyhat, M., Nazari, M., & Kowsary, F. (2012). Experimental study of convective heat transfer and pressure drop of TiO_2 water nanofluid. *International Communications in Heat and Mass Transfer, 39*(3), 456-462.

Kazi, S. N. (2001). *Heat transfer to fibre suspensions : studies in fibre characterisation and fouling mitigation.* (PhD), University of Auckland. (THESIS 2001-K23)

Kazi, S. N., Duffy, G. G., & Chen, X. D. (2014). Validation of heat transfer and friction loss data for fibre suspensions in a circular and a coaxial pipe heat exchanger. *International Journal of Thermal Sciences, 79*(0), 146-160. doi: http://dx.doi.org/10.1016/j.ijthermalsci.2014.01.001

Keblinski, P., Phillpot, S. R., Choi, S. U. S., & Eastman, J. A. (2002). Mechanisms of heat flow in suspensions of nano-sized particles (nanofluids). *International Journal of Heat and Mass Transfer, 45*(4), 855-863.

Keblinski, P., Prasher, R., & Eapen, J. (2008). Thermal conductance of nanofluids: is the controversy over? *Journal of Nanoparticle Research, 10*(7), 1089-1097.

Keblinski, P., S.R. Phillpot, S.U.S. Choi, & Eastman, J. A. (2002). Mechanism of heat flow in suspensions of nano-sized particles (nanofluids) *Int. J. Heat Mass Transfer, 46*, 2665–2672.

Keblinski, P., & Thomin, J. (2006). Hydrodynamic field around a Brownian particle. *Physical Review E, 73*(1), 010502.

Khairul, M. A., Alim, M. A., Mahbubul, I. M., Saidur, R., Hepbasli, A., & Hossain, A. (2014). Heat transfer performance and exergy analyses of a corrugated plate heat exchanger using metal oxide nanofluids. *International Communications in Heat and Mass Transfer, 50*(0), 8-14. doi: http://dx.doi.org/10.1016/j.icheatmasstransfer.2013.11.006

Kim, D., Kwon, Y., Cho, Y., Li, C., Cheong, S., Hwang, Y., . . . Moon, S. (2009). Convective heat transfer characteristics of nanofluids under laminar and turbulent flow conditions. *Curr. Appl. Phys, 9*(2), e119−e123.

Kim, Y. J., Ma, H., & Yu, Q. (2010). Plasma nanocoated carbon nanotubes for heat transfer nanofluids. *Nanotechnology, 21*.

Koo, J., & Kleinstreuer, C. (2004). A new thermal conductivity model for nanofluids. *Journal of Nanoparticle Research, 6*(6), 577-588.

Krieger, I. M., & Dougherty, T. J. (1959). A mechanism for non-newtonian flow in suspensions of rigid spheres. *Trans.Soc. Rheology, 3*, 137–152

Krishnamurthy, S., Bhattacharya, P., Phelan, P. E., & Prasher, R. S. (2006). Enhanced mass transport in nanofluids. *Nano letters, 6*(3), 419-423.

Kumar, D. H., Patel, H. E., Kumar, V. R. R., Sundararajan, T., Pradeep, T., & Das, S. K. (2004). Model for heat conduction in nanofluids. *Physical review letters, 93*(14), 144301.

Kumaresan, V., Mohaideen Abdul Khader, S., Karthikeyan, S., & Velraj, R. (2013). Convective heat transfer characteristics of CNT nanofluids in a tubular heat exchanger of various lengths for energy efficient cooling/heating system. *International Journal of Heat and Mass Transfer, 60*, 413-421.

Kwak, K., & Kim, C. (2005). Viscosity and thermal conductivity of copper oxide nanofluid dispersed in ethylene glycol Koraa. *Australia Rheology J., 17*.

L.Q. Wang, & Wei, X. H. (2009). Nanofluids: Synthesis, heat conduction, and extension. *Journal of Heat Transfer, 131*.

Lamas, B., Abreu, B., Fonseca, A., Martins, N., & Oliveira, M. (2012). Assessing colloidal stability of long term MWCNT based nanofluids. *Journal of Colloid and Interface Science, 381*(1), 17-23. doi: http://dx.doi.org/10.1016/j.jcis.2012.05.014

Lamas, B., Abreu, B., Fonseca, A., Martins, N., & Oliveira, M. (2014). Critical analysis of the thermal conductivity models for CNT based nanofluids. *International Journal of Thermal Sciences, 78*(0), 65-76. doi: http://dx.doi.org/10.1016/j.ijthermalsci.2013.11.017

Larson, R. G. (2005). The rheology of dilute solutions of flexible polymers: progress and problems. *J. Rheology, 49*, 1–70.

Launder, B. E., & Spalding, D. (1974). The numerical computation of turbulent flows. *Computer methods in applied mechanics and engineering, 3*(2), 269-289.

Laura. Fedele, Laura. Colla, & Bobbo, S. (2012). Viscosity and thermal conductivity measurements of water-based nanofluids containing titanium oxide nanoparticles. *Int. J. Refrig, 35* 1359–1366.

Lee, Choi, S. U. S., Li, S., & Eastman, J. A. (1999). Measuring thermal conductivity of fluids containing oxide nanoparticles. *Journal Name: Journal of Heat Transfer; Journal Volume: 121; Journal Issue: 2; Other Information: PBD: May 1999*, Medium: X; Size: pp. 280-289.

Lee, D., Kim, J. W., & Kim, B. G. (2006). A new parameter to control heat transport in nanofluids: surface charge state of the particle in suspension. *The Journal of Physical Chemistry B, 110*(9), 4323-4328.

Lee, J.-H., Hwang, K. S., Jang, S. P., Lee, B. H., Kim, J. H., Choi, S. U. S., & Choi, C. J. (2008). Effective viscosities and thermal conductivities of aqueous nanofluids

containing low volume concentrations of Al2O3 nanoparticles. *International Journal of Heat and Mass Transfer, 51*(11–12), 2651-2656. doi: http://dx.doi.org/10.1016/j.ijheatmasstransfer.2007.10.026

Lee, J., Han, K., & Koo, J. (2014). A novel method to evaluate dispersion stability of nanofluids. *International Journal of Heat and Mass Transfer, 70*(0), 421-429. doi: http://dx.doi.org/10.1016/j.ijheatmasstransfer.2013.11.029

Lee, J. H., Lee, T., & Jeong, Y. H. (2013). The effect of pressure on the critical heat flux in water-based nanofluids containing Al2O3 and Fe3O4 nanoparticles. *International Journal of Heat and Mass Transfer, 61*(0), 432-438. doi: http://dx.doi.org/10.1016/j.ijheatmasstransfer.2013.02.018

Lee, K. J., S.-H. Yoon, & Jang, J. (2007). Carbon nanofibers: a novel nanofilter for nanofluid applications. *Small, 3*, 1209–1213.

Lee, K. J., Yoon, S. H., & Jang, J. (2007). Carbon nanofibers: a novel nanofiller for nanofluid applications. *Small, 3*(7), 1209-1213.

Lee, S. W., Kim, K. M., & Bang, I. C. (2013). Study on flow boiling critical heat flux enhancement of graphene oxide/water nanofluid. *International Journal of Heat and Mass Transfer, 65*, 348-356.

Lee, S. W., Park, S. D., Kang, S., Bang, I. C., & Kim, J. H. (2011). Investigation of viscosity and thermal conductivity of SiC nanofluids for heat transfer applications. *International Journal of Heat and Mass Transfer, 54*(1–3), 433-438. doi: http://dx.doi.org/10.1016/j.ijheatmasstransfer.2010.09.026

Leong, K. Y., Saidur, R., Kazi, S. N., & Mamun, A. H. (2010). Performance investigation of an automotive car radiator operated with nanofluid-based coolants (nanofluid as a coolant in a radiator). *Applied Thermal Engineering, 30*(17–18), 2685-2692. doi: http://dx.doi.org/10.1016/j.applthermaleng.2010.07.019

Lerche, D. (2002). Dispersion Stability and Particle Characterization by Sedimentation Kinetics in a Centrifugal Field. *Journal of Dispersion Science and Technology, 23*(5).

Li, C., & Peterson, G. (2006). Experimental investigation of temperature and volume fraction variations on the effective thermal conductivities of nanoparticle suspensions (nanofluids). *Journal of Applied Physics, 99*.

Li, D., & W. Fang. (2012). Preparation and stability of silver/kerosene nanofluids. *Nanoscale Research Letters, 7*(362).

Li, F.-C., Yang, J.-C., Zhou, W.-W., He, Y.-R., Huang, Y.-M., & Jiang, B.-C. (2013). Experimental study on the characteristics of thermal conductivity and shear viscosity of viscoelastic-fluid-based nanofluids containing multiwalled carbon nanotubes. *Thermochimica Acta, 556*(0), 47-53. doi: http://dx.doi.org/10.1016/j.tca.2013.01.023

Li, Q., & Xuan, Y. (2002). Convective heat transfer and flow characteristics of Cu–water nanofluid. *Science China, Series E: Technology Science,, 45*(4), 408–416.

Li, X. F., Zhu, D. S., Wang, X. J., Wang, N., Gao, J. W., & Li, H. (2008). Thermal conductivity enhancement dependent pH and chemical surfactant for Cu-H< sub> 2</sub> O nanofluids. *Thermochimica Acta, 469*(1), 98-103.

Li, Y. H., W. Qu, & Feng, J. C. (2008). Temperature dependence of thermal conductivity of nanofluids. *Chin. Phys. Lett., 25*, 3319–3322.

Liang, Z., Jizu, L., Minli, B., & Detian, G. (2015). Effect of Vibration on Forced Convection Heat Transfer for SiO2–Water Nanofluids. *Heat Transfer Engineering, 36*(5), 452-461.

Liu, J., Wang, F., Zhang, L., Fang, X., & Zhang, Z. (2014). Thermodynamic properties and thermal stability of ionic liquid-based nanofluids containing graphene as advanced heat transfer fluids for medium-to-high-temperature applications. *Renewable Energy, 63*(0), 519-523. doi: http://dx.doi.org/10.1016/j.renene.2013.10.002

Liu, Y., Loh, W. Q., Ananthanarayanan, A., Yang, C., Chen, P., & Xu, C. (2014). Correction: Fluorescence quenching between unbonded graphene quantum dots and gold nanoparticles upon simple mixing. *RSC Advances, 4*(83), 44151-44151. doi: 10.1039/C4RA90012J

Lo, C. H., T.T Tsung, & L.C Chen. (2005). Shape-controlled synthesis of Cu-based nanofluid using submerged arc nanoparticle synthesis system (SANSS). *J Cryst Growth, 277*, 636-642.

Lomascolo, M., Colangelo, G., Milanese, M., & de Risi, A. (2015). Review of heat transfer in nanofluids: Conductive, convective and radiative experimental results. *Renewable and Sustainable Energy Reviews, 43*(0), 1182-1198. doi: http://dx.doi.org/10.1016/j.rser.2014.11.086

M. Mehrali, E. Sadeghinezhad, S. Tahan Latibari, S.N Kazi, M. Mehrali, M. Nashrul Bin Mohd Zubir, & Metselaar, H. S. C. (2014). Investigation of thermal conductivity and rheological properties of nanofluids containing graphene nanoplatelets. *Nanoscale Research Letters, 9*(12).

M. Memari, A. Golmakani, & A.M. Dehkordi. (2011). Mixed-convection flow of nanofluids and regular fluids in vertical porous media with viscous heating. *Ind. Eng. Chem. Res. Chem. Res., 50*(15), 9403–9414.

M.P. Beck, Y.H. Yuan, P. Warrier, & Teja, A. S. (2010). The thermal conductivity of aqueous nanofluids containing ceria nanoparticles. *J. Appl. Phys, 107*.

M.S Youssef, A.A Aly, & E.B Zeidan. (2012). Computing the Pressure Drop of Nanofluid Turbulent Flows in a Pipe Using an Artificial Neural Network Model *Open Journal of Fluid Dynamics, 2*, 130-136.

Madhesh, D., Parameshwaran, R., & Kalaiselvam, S. (2014). Experimental investigation on convective heat transfer and rheological characteristics of Cu–TiO_2 hybrid nanofluids. *Experimental Thermal and Fluid Science, 52*, 104-115.

Mahboobeh, H., S.S. Sara, A. Hossein, & K.G Elaheh. (2013). Nanofluids for Heat Transfer Enhancement – A Review. *Physical Chemistry Research, 1*(1).

Mahian, O., Kianifar, A., Kalogirou, S. A., Pop, I., & Wongwises, S. (2013). A review of the applications of nanofluids in solar energy. *International Journal of Heat and Mass Transfer, 57*(2), 582-594. doi: http://dx.doi.org/10.1016/j.ijheatmasstransfer.2012.10.037

Mahian, O., Mahmud, S., & Heris, S. Z. (2012). Analysis of entropy generation between co-rotating cylinders using nanofluids. *Energy, 44*(1), 438-446. doi: http://dx.doi.org/10.1016/j.energy.2012.06.009

Mangrulkar C.K., & Kriplani V.M. (2013). Nanofluid Heat Transfer-A Review *International Journal of Engineering and Technology, 3*(2).

Manimaran, R., K. Palaniradja, N. Alagumurthi, S. Sendhilnathan, & J. Hussain. (2014). Preparation and characterization of copper oxide nanofluid for heat transfer applications. *Appl Nanosci, 4*, 163–167.

Mansour, R. B., Galanis, N., & Nguyen, C. T. (2007). Effect of uncertainties in physical properties on forced convection heat transfer with nanofluids. *Applied Thermal Engineering, 27*(1), 240-249.

Maxwell, J. C. (1873a). Treatise on Electricity and Magnetism. Clarendon Press, Oxford, 1873.

Maxwell, J. C. (1873b). Treatise on Electricity and Magnetism. In O. Clarendon Press (Ed.).

Maxwell, J. C. (1881). A treatise on Electricity and Magnetism. *Oxford University Press, Cambridge*.

Mehrali, M., Sadeghinezhad, E., Latibari, S. T., Kazi, S. N., Mehrali, M., Zubir, M. N. B. M., & Metselaar, H. S. C. (2014). Investigation of thermal conductivity and rheological properties of nanofluids containing graphene nanoplatelets. *Nanoscale Research Letters, 9*(1), 1-12.

Mehrali, M., Sadeghinezhad, E., Latibari, S. T., Kazi, S. N., Mehrali, M. Z., Mohd, N. M., & Metselaar, H. S. (2014). Investigation of thermal conductivity and rheological properties of nanofluids containing graphene nanoplatelets. *Nanoscale Research Letters, 9*(1), 1-12.

Mehrali, M., Sadeghinezhad, E., Tahan Latibari, S., Mehrali, M., Togun, H., & Zubir, M. N. M. (2014). Preparation, characterization, viscosity, and thermal conductivity of nitrogen-doped graphene aqueous nanofluids. doi: http://dx.doi.org/10.1007/s10853-014-8424-8. *Journal of Materials Science*, 1-16.

Mehrali, M., Sadeghinezhad, E., Tahan Latibari, S., Mehrali, M., Togun, H., Zubir, M. N. M., . . . Metselaar, H. (2014). Preparation, characterization, viscosity, and thermal conductivity of nitrogen-doped graphene aqueous nanofluids. *Journal of Materials Science, 49*(20), 7156-7171. doi: http://dx.doi.org/10.1007/s10853-014-8424-8

Meng, Z., Wu, D., Wang, L., Zhu, H., & Li, Q. (2012). Carbon nanotube glycol nanofluids: Photo-thermal properties, thermal conductivities and rheological behavior. *Particuology, 10*(5), 614-618. doi: http://dx.doi.org/10.1016/j.partic.2012.04.001

Meriläinen, A., Seppälä, A., Saari, K., Seitsonen, J., Ruokolainen, J., Puisto, S., . . . Ala-Nissila, T. (2013). Influence of particle size and shape on turbulent heat transfer characteristics and pressure losses in water-based nanofluids. *International Journal of Heat and Mass Transfer, 61*(0), 439-448. doi: http://dx.doi.org/10.1016/j.ijheatmasstransfer.2013.02.032

Moffat, R. J. (1988). Describing the uncertainties in experimental results. *Experimental Thermal and Fluid Science, 1*(1), 3-17. doi: http://dx.doi.org/10.1016/0894-1777(88)90043-X

Mondragón, R. (2012). Characterization of physical properties of nanofluids for heat transfer application. *J. Phys.: Conf. Ser. , 2012395 012017*.

Mondragon, R., Julia, J. E., Barba, A., & Jarque, J. C. (2012). Characterization of silica–water nanofluids dispersed with an ultrasound probe: A study of their physical properties and stability. *Powder Technology, 224*(0), 138-146. doi: http://dx.doi.org/10.1016/j.powtec.2012.02.043

Mukherjee, S., & Paria, S. (2013). Preparation and Stability of Nanofluids-A Review. *Journal of Mechanical and Civil Engineering, 9*(2).

Munkhbayar, B., Bat-Erdene, M., Sarangerel, D., & Ochirkhuyag, B. (2013). Effect of the collision medium size on thermal performance of silver nanoparticles based aqueous nanofluids. *Composites Part B: Engineering, 54*(0), 383-390. doi: http://dx.doi.org/10.1016/j.compositesb.2013.05.021

Munkhbayar, B., Tanshen, M. R., Jeoun, J., Chung, H., & Jeong, H. (2013). Surfactant-free dispersion of silver nanoparticles into MWCNT-aqueous nanofluids prepared by one-step technique and their thermal characteristics. *Ceramics International, 39*(6), 6415-6425. doi: http://dx.doi.org/10.1016/j.ceramint.2013.01.069

Murakami, H., & Nakashima, N. (2006). Soluble carbon nanotubes and their applications. *Journal of Nanoscience and Nanotechnology, 6*(1), 16-27.

Murshed, S. M. S., Leong, K. C., & Yang, C. Enhanced thermal conductivity of TiO2–water based nanofluids. *International Journal of Thermal Sciences 44 (2005)*

367–373.

Murshed, S. M. S., Leong, K. C., & Yang, C. (2005). Enhanced thermal conductivity of TiO2–water based nanofluids. *International Journal of Thermal Sciences, 44*, 367–373.

Murshed, S. M. S., & Nieto de Castro, C. A. (2014). Superior thermal features of carbon nanotubes-based nanofluids – A review. *Renewable and Sustainable Energy Reviews, 37*(0), 155-167. doi: http://dx.doi.org/10.1016/j.rser.2014.05.017

Murshed, S. M. S., Nieto de Castro, C. A., Lourenço, M. J. V., Lopes, M. L. M., & Santos, F. J. V. (2011). A review of boiling and convective heat transfer with nanofluids. *Renewable and Sustainable Energy Reviews, 15*(5), 2342-2354. doi: http://dx.doi.org/10.1016/j.rser.2011.02.016

Nabeel Rashin, M., & Hemalatha, J. (2013). Synthesis and viscosity studies of novel ecofriendly ZnO–coconut oil nanofluid. *Experimental Thermal and Fluid Science, 51*(0), 312-318. doi: http://dx.doi.org/10.1016/j.expthermflusci.2013.08.014

Nakashima, N., Tomonari, Y., & Murakami, H. (2002). Water-Soluble Single-Walled Carbon Nanotubes via Noncovalent Sidewall-Functionalization with a Pyrene-Carrying Ammonium Ion. *Chemistry Letters, 31*(6), 638-639.

Nasiri, A., Shariaty-Niasar, M., Rashidi, A., & Khodafarin, R. (2012). Effect of CNT structures on thermal conductivity and stability of nanofluid. *International Journal of Heat and Mass Transfer, 55*(5), 1529-1535.

Nguyen, C. T., Desgranges, F., Roy, G., Galanis, N., Mare, T., Boucher, S., & Angue Mintsa, H. (2007). Temperature and particle-size dependent viscosity data for water-based nanofluidsâ€“Hysteresis phenomenon. *International Journal of Heat and Fluid Flow, 28*(6), 1492-1506.

Nikkam, N., Ghanbarpour, M., Saleemi, M., Haghighi, E. B., Khodabandeh, R., Muhammed, M., . . . Toprak, M. S. (2014). Experimental investigation on thermo-physical properties of copper/diethylene glycol nanofluids fabricated via microwave-assisted route. *Applied Thermal Engineering, 65*(1–2), 158-165. doi: http://dx.doi.org/10.1016/j.applthermaleng.2014.01.003

Nikkhah, Z., Karimipour, A., Safaei, M. R., Forghani-Tehrani, P., Goodarzi, M., Dahari, M., & Wongwises, S. (2015). Forced convective heat transfer of water/functionalized multi-walled carbon nanotube nanofluids in a microchannel with oscillating heat flux and slip boundary condition. *International Communications in Heat and Mass Transfer, 68*, 69-77. doi: http://dx.doi.org/10.1016/j.icheatmasstransfer.2015.08.008

Nkurikiyimfura, I., Wang, Y., & Pan, Z. (2013). Heat transfer enhancement by magnetic nanofluids—A review. *Renewable and Sustainable Energy Reviews, 21*(0), 548-561. doi: http://dx.doi.org/10.1016/j.rser.2012.12.039

Olhero, S. M., & Ferreira, J. M. F. (2004). Influence of particle size distribution on rheology and particle packing of silica based suspensions. *Powder Technology, 139*, 69-75.

Overbeek, J. T. G. (1952). Diffuse double layer after Gouy and Chapman. *H.R. Kruyt (Ed.), Colloid Science I, Irreversible Systems, Elsevier, Amsterdam*, 128–132.

Pang, C., & Y.T. Kang. (2012). *Stability and Thermal Conductivity Characteristics of Nanofluids (H2O/CH3OH + NaCl + Al2O3 Nanoparticles) for CO2 Absorption Application.* Paper presented at the International Refrigeration and Air Conditioning Conference, July 16-19, 2012, Purdue.

Pantzali, M. N., A.A. Mouza, & S.V. Paras. (2009). Investigating the efficacy of nanofluids as coolants in plate heat exchangers (PHE). *Chem Eng Sci, 64*, 3290–3300.

Patel, H. E., Das, S. K., Sundararajan, T., Sreekumaran Nair, A., George, B., & Pradeep, T. (2003). Thermal conductivities of naked and monolayer protected metal nanoparticle based nanofluids: Manifestation of anomalous enhancement and chemical effects. *Applied Physics Letters, 83*(14), 2931-2933.

Paul, G., Sarkar, S., Pal, T., Das, P. K., & Manna, I. (2012). Concentration and size dependence of nano-silver dispersed water based nanofluids. *Journal of Colloid and Interface Science, 371*(1), 20-27. doi: http://dx.doi.org/10.1016/j.jcis.2011.11.057

Peyghambarzadeh, S. M., Hashemabadi, S. H., Chabi, A. R., & Salimi, M. (2014). Performance of water based CuO and Al2O3 nanofluids in a Cu–Be alloy heat sink with rectangular microchannels. *Energy Conversion and Management, 86*(0), 28-38. doi: http://dx.doi.org/10.1016/j.enconman.2014.05.013

Phelan, P. E., & Lai, W. Y. (2009). Cooling electronics with nanofluids: laminar convective heat transfer. *Electronics cooling, 15*.

Philip, J., & Shima, P. D. (2012). Thermal properties of nanofluids. *Advances in Colloid and Interface Science, 183–184*(0), 30-45. doi: http://dx.doi.org/10.1016/j.cis.2012.08.001

Phuoc, T. X., Massoudi, M., & Chen, R.-H. (2011). Viscosity and thermal conductivity of nanofluids containing multi-walled carbon nanotubes stabilized by chitosan. *International Journal of Thermal Sciences, 50*(1), 12-18. doi: http://dx.doi.org/10.1016/j.ijthermalsci.2010.09.008

Ponmani, S., William, J. K. M., Samuel, R., Nagarajan, R., & Sangwai, J. S. (2014). Formation and characterization of thermal and electrical properties of CuO and ZnO nanofluids in xanthan gum. *Colloids and Surfaces A: Physicochemical and Engineering Aspects, 443*(0), 37-43. doi: http://dx.doi.org/10.1016/j.colsurfa.2013.10.048

Ponmozhi, J., F.A.M.M. Gonçalves, A.G.M. Ferreira, I.M.A. Fonseca, S. Kanagaraj, N. Martins, & Oliveira, M. S. A. (2009). Thermodynamic and transport properties of CNT–water based nanofluids. *J. Nano Res., 11*, 101–106.

Popiel, C. O., & Wojtkowiak, J. (1998). Simple Formulas for Thermophysical Properties of Liquid Water for Heat Transfer Calculations (from 0°C to 150°C). *Heat transfer engineering, 19*(3), 87-101. doi: 10.1080/01457639808939929

Prasher, R., Bhattacharya, P., & Phelan, P. E. (2005). Thermal conductivity of nanoscale colloidal solutions (nanofluids). *Physical review letters, 94*(2), 25901.

Prasher, R., Bhattacharya, P., & Phelan, P. E. (2006). Brownian-motion-based convective-conductive model for the effective thermal conductivity of nanofluids. *Journal of Heat Transfer, 128*(6), 588-595.

Prasher, R., Phelan, P. E., & Bhattacharya, P. (2006). Effect of aggregation kinetics on the thermal conductivity of nanoscale colloidal solutions (nanofluid). *Nano letters, 6*(7), 1529-1534.

Prasher, R., Song, D., Wang, J., & Phelan, P. (2006). Measurements of nanofluid viscosity and its implications for thermal applications. *Applied Physics Letters, 89*(13), 133108-133108-133103.

R. Sadri, G. Ahmadi, H. Togun, M. Dahari, S.N Kazi, E. Sadeghinezhad, & Zubir, N. (2014). An experimental study on thermal conductivity and viscosity of nanofluids containing carbon nanotubes. *Nanoscale Research Letters, 9*(1).

Rahul, A. B., & B.S. Kothawale. (2013). A Review on applications and challenges of Nano-fluids as coolant in Automobile Radiator *International Journal of Scientific and Research Publications, 3*(8).

Ramires, M. L., de Castro, C. A. N., Nagasaka, Y., Nagashima, A., Assael, M. J., & Wakeham, W. A. (1995). Standard reference data for the thermal conductivity of water. *Journal of Physical and Chemical Reference Data, 24*, 1377. doi: http://dx.doi.org/10.1063/1.555963

Rao, C. N. R., & Sood, A. K. (2013). *Graphene: Synthesis, Properties, and Phenomena*: Wiley.

Rao, Y. (2010a). Nanofluids: Stability, phase diagram, rheology and applications. *Particuology, 8* 549–555.

Rao, Y. (2010b). Nanofluids: Stability, phase diagram, rheology and applications. *Particuology, 8*(6), 549-555. doi: http://dx.doi.org/10.1016/j.partic.2010.08.004

Razi, P., Akhavan-Behabadi, M. A., & Saeedinia, M. (2011). Pressure drop and thermal characteristics of CuO–base oil nanofluid laminar flow in flattened tubes under constant heat flux. *International Communications in Heat and Mass Transfer, 38*(7), 964-971. doi: http://dx.doi.org/10.1016/j.icheatmasstransfer.2011.04.010

Rea, U., McKrell, T., Hu, L.-w., & Buongiorno, J. (2009). Laminar convective heat transfer and viscous pressure loss of alumina–water and zirconia–water nanofluids. *International Journal of Heat and Mass Transfer, 52*(7–8), 2042-2048. doi: http://dx.doi.org/10.1016/j.ijheatmasstransfer.2008.10.025

Rohsenow, W. M., Hartnett, J. P., & Ganic, E. N. (1985). Handbook of heat transfer applications. *New York, McGraw-Hill Book Co., 1985, 973 p. No individual items are abstracted in this volume., 1*.

S, S., K, V., P, S., & M, C. (2012). Effect of Al2O3–Cu/water hybrid nanofluid in heat transfer. *Exp Thermal Fluid Sci, 38*, 54–60.

S. Mukherjee, & S. Paria. (2013). Preparation and Stability of Nanofluids-A Review. *Journal of Mechanical and Civil Engineering, 9*(2).

S.A. Angayarkanni, & J. Philip. (2015). Review on thermal properties of nanofluids: Recent developments. *Advances in Colloid and Interface Science, 225*, http://dx.doi.org/10.1016/j.cis.2015.1008.1014. doi: http://dx.doi.org/10.1016/j.cis.2015.08.014

Sadeghinezhad, E., Kazi, S. N., Sadeghinejad, F., Badarudin, A., Mehrali, M., Sadri, R., & Reza Safaei, M. (2014). A comprehensive literature review of bio-fuel performance in internal combustion engine and relevant costs involvement. *Renewable and Sustainable Energy Reviews, 30*(0), 29-44. doi: http://dx.doi.org/10.1016/j.rser.2013.09.022

Sadeghinezhad, E., Mehrali, M., Tahan Latibari, S., Mehrali, M., Kazi, S. N., Oon, S., & Metselaar, H. S. C. (2014a). Experimental Investigation of Convective Heat Transfer Using Graphene Nanoplatelet Based Nanofluids under Turbulent Flow Conditions. *Industrial & Engineering Chemistry Research, 53*(31), 12455–12465. doi: http://dx.doi.org/10.1021/ie501947u

Sadeghinezhad, e., mehrali, m., Tahan Latibari, S., Mehrali, M., Kazi, S. N., Oon, S., & Metselaar, H. S. C. (2014b). An experimental investigation of convective heat transfer using graphene nanoplatelet based nanofluids under turbulent flow conditions. doi: 10.1021/ie501947u. *Industrial & Engineering Chemistry Research*.

Sadri, R., Ahmadi, G., Togun, H., Dahari, M., Kazi, S. N., Sadeghinezhad, E., & Zubir, N. (2014a). An experimental study on thermal conductivity and viscosity of nanofluids containing carbon nanotubes. *Nano. sc. research letters, 9*(1), 151.

Sadri, R., Ahmadi, G., Togun, H., Dahari, M., Kazi, S. N., Sadeghinezhad, E., & Zubir, N. (2014b). An experimental study on thermal conductivity and viscosity of nanofluids containing carbon nanotubes. *Nanoscale Research Letters, 9*(1).

Saidur, R., Kazi, S. N., Hossain, M. S., Rahman, M. M., & Mohammed, H. A. (2011). A review on the performance of nanoparticles suspended with refrigerants and lubricating oils in refrigeration systems. *Renewable and Sustainable Energy Reviews, 15*(1), 310-323. doi: http://dx.doi.org/10.1016/j.rser.2010.08.018

Saidur, R., Leong, K. Y., & Mohammad, H. A. (2011). A review on applications and challenges of nanofluids. *Renewable and Sustainable Energy Reviews, 15*(3), 1646-1668. doi: http://dx.doi.org/10.1016/j.rser.2010.11.035

Sajadi, A. R., & M.H. Kazemi. (2011). Investigation of Turbulent Convective Heat Transfer and Pressure Drop of TiO2/Water Nanofluid in Circular Tube. *International Communications in Heat and Mass Transfer, 38*(10), 1474-1478.

Salman, B. H., Mohammed, H. A., Munisamy, K. M., & Kherbeet, A. S. (2013). Characteristics of heat transfer and fluid flow in microtube and microchannel

using conventional fluids and nanofluids: A review. *Renewable and Sustainable Energy Reviews, 28*(0), 848-880. doi: http://dx.doi.org/10.1016/j.rser.2013.08.012

Samira, P., Saeed, Z., Motahare, S., & Mostafa, K. (2014). Pressure drop and thermal performance of CuO/ethylene glycol (60%)-water (40%) nanofluid in car radiator. *Korean Journal of Chemical Engineering*, 1-8. doi: 10.1007/s11814-014-0244-7

Sarkar, J. (2011). A critical review on convective heat transfer correlations of nanofluids. *Renewable and Sustainable Energy Reviews, 15*(6), 3271-3277. doi: http://dx.doi.org/10.1016/j.rser.2011.04.025

Sarkar, S., Ganguly, S., & Biswas, G. (2012). Mixed convective heat transfer of nanofluids past a circular cylinder in cross flow in unsteady regime. *International Journal of Heat and Mass Transfer, 55*(17–18), 4783-4799. doi: http://dx.doi.org/10.1016/j.ijheatmasstransfer.2012.04.046

Sarkar, S., Ganguly, S., Dalal, A., Saha, P., & Chakraborty, S. (2013). Mixed convective flow stability of nanofluids past a square cylinder by dynamic mode decomposition. *International Journal of Heat and Fluid Flow, 44*(0), 624-634. doi: http://dx.doi.org/10.1016/j.ijheatfluidflow.2013.09.004

Schroeder, S. P., & Morris, G. K. (2010). Nanofluids in a Forced-Convection Liquid Cooling System– Benefits and Design Challenges *Thermal and Thermomechanical Phenomena in Electronic Systems (ITherm), 2010 12th IEEE Intersociety Conference on*.

Seon, H. A., & Kim, M. H. (2011). A Review on Critical Heat Flux Enhancement With Nanofluids and Surface Modification. *J. Heat Transfer, 134*(2).

Shanbedi, M., Amiri, A., Rashidi, S., Heris, S. Z., & Baniadam, M. (2015). Thermal Performance Prediction of Two-Phase Closed Thermosyphon Using Adaptive Neuro-Fuzzy Inference System. *Heat Transfer Engineering, 36*(3), 315-324.

Shanbedi, M., Heris, S. Z., Amiri, A., Hosseinipour, E., Eshghi, H., & Kazi, S. (2015). Synthesis of aspartic acid-treated multi-walled carbon nanotubes based water coolant and experimental investigation of thermal and hydrodynamic properties in circular tube. *Energy Conversion and Management, 105*, 1366-1376.

Shanbedi, M., Heris, S. Z., Baniadam, M., Amiri, A., & Maghrebi, M. (2012). Investigation of heat-transfer characterization of EDA-MWCNT/DI-water nanofluid in a two-phase closed thermosyphon. *Ind. & Engg. Chem. Research, 51*(3), 1423-1428.

Shanthi, R., Shanmuga, S. A., & Velraj, R. (2012). Heat transfer enhancement using nanofluids: A review. *Thermal science, 16*(2), 423-444.

Sharma, A. K., Tiwari, A. K., & Dixit, A. R. (2016). Rheological behaviour of nanofluids: A review. *Renewable and Sustainable Energy Reviews, 53*, 779-791. doi: http://dx.doi.org/10.1016/j.rser.2015.09.033

Shih, T. M. (1984). *Numerical heat transfer*: CRC Press.

Singh, A. K., & V. S. Raykar. (2008). Microwave synthesis of silver nanofluids with polyvinylpyrrolidone (PVP) and their transport properties. *Colloid and Polymer Science, 286*(14-15), 1667–1673.

Singh, D. K., D.K. Pandey, R.R. Yadav, & Singh, D. A. (2012). Study of nanosized zinc oxide and its nanofluid. *J. Phys. Ind. Acad. Sci., 78*(5), 759–766.

Solangi, K. H., Kazi, S. N., Luhur, M. R., Badarudin, A., Amiri, A., Sadri, R., . . . Teng, K. H. (2015). A comprehensive review of thermo-physical properties and convective heat transfer to nanofluids. *Energy, 89*, 1065-1086. doi: http://dx.doi.org/10.1016/j.energy.2015.06.105

Sommers, A. D., & Yerkes, K. L. (2010). Experimental investigation into the convective heat transfer and system-level effects of Al2O3-propanol nanofluid. *Journal Nanopart Research, 12*, 1003-1014.

Sonawane, S. S., Khedkar, R. S., & Wasewar, K. L. (2013). Study on concentric tube heat exchanger heat transfer performance using Al2O3 – water based nanofluids. *International Communications in Heat and Mass Transfer, 49*(0), 60-68. doi: http://dx.doi.org/10.1016/j.icheatmasstransfer.2013.10.001

Sundar, L. S., Farooky, M. H., Sarada, S. N., & Singh, M. K. (2013). Experimental thermal conductivity of ethylene glycol and water mixture based low volume concentration of Al2O3 and CuO nanofluids. *International Communications in Heat and Mass Transfer, 41*(0), 41-46. doi: http://dx.doi.org/10.1016/j.icheatmasstransfer.2012.11.004

Sundar, L. S., K.V Sharma, & S. Parveen. (2009). Heat transfer and friction factor analysis in a circular tube with Al2O3 nanofluid by using computational fluid dynamics. *International Journal of Nanoparticles, 2*, 191–199.

Sundar, L. S., M.T. Naik, K.V. Sharma, M.K. Singh, T. Ch, & S. Reddy. (2012). Experimental investigation of forced convection heat transfer and friction factor in a tube with Fe3O4 magnetic nanofluid. *Exp. Thermal Fluid Sci, 37*, 65–71.

Sundar, L. S., Singh, M. K., & Sousa, A. C. M. (2014). Enhanced heat transfer and friction factor of MWCNT–Fe3O4/water hybrid nanofluids. *International Communications in Heat and Mass Transfer, 52*(0), 73-83. doi: http://dx.doi.org/10.1016/j.icheatmasstransfer.2014.01.012

Suresh, S., K.P. Venkitaraj, P. Selvakumar, & Chandrasekar, M. (2012). Effect of Al2O3–Cu /water hybrid nanofluid in heat transfer. *Experimental Thermal and Fluid Science, 38*, 54–60.

Suresh, S., Venkitaraj, K. P., Selvakumar, P., & Chandrasekar, M. (2011). Synthesis of Al2O3–Cu/water hybrid nanofluids using two step method and its thermo physical properties. *Colloids and Surfaces A: Physicochemical and Engineering Aspects, 388*(1–3), 41-48. doi: http://dx.doi.org/10.1016/j.colsurfa.2011.08.005

T.T, B., & R. Sundara. (2011). Synthesis and transport properties of metal oxide decorated graphene dispersed nanofluids. *J Phys Chem C, 115*(17), 8527–8533.

Tabandeh-Khorshid, M., Omrani, E., Menezes, P. L., & Rohatgi, P. K. Tribological performance of self-lubricating aluminum matrix nanocomposites: Role of graphene nanoplatelets. *Engineering Science and Technology, an International Journal*. doi: http://dx.doi.org/10.1016/j.jestch.2015.09.005

Tantra, R., Schulze, P., & Quincey, P. (2010). Effect of nanoparticle concentration on zeta-potential measurement results and reproducibility. *Particuology, 8*(3), 279-285. doi: http://dx.doi.org/10.1016/j.partic.2010.01.003

Taylor, J. R. (1997). *An introduction to error analysis: the study of uncertainties in physical measurements*: University science books.

Taylor, R., S. Coulombe, T. Otanicar, P. Phelan, A. Gunawan, W. Lv, . . . H.Tyagi. (2013). Small particles, big impacts: A review of the diverse applications of nanofluids. *J. Appl. Phys., 113*.

Taylor, R. A., & Phelan, P. E. (2009). Pool boiling of nanofluids: Comprehensive review of existing data and limited new data. *International Journal of Heat and Mass Transfer, 52*(23–24), 5339-5347. doi: http://dx.doi.org/10.1016/j.ijheatmasstransfer.2009.06.040

Teng, T. P., Y.H. Hung, C.S. Jwo, Chen, C. C., & L.Y. Jeng. (2011). Pressure Drop of TiO2 Nanofluid in Circular Pipes. *Particuology, 9*(5), 486-491.

Tessy Theres Baby, S. R. (2010). Investigation of thermal and electrical conductivity of graphene based nanofluids. *Applied Physics Letters, 108*.

Tie, P., Li, Q., & Xuan, Y. (2014). Heat transfer performance of Cu–water nanofluids in the jet arrays impingement cooling system. *International Journal of Thermal Sciences, 77*(0), 199-205. doi: http://dx.doi.org/10.1016/j.ijthermalsci.2013.11.007

Timofeeva, E. V., Gavrilov, A. N., McCloskey, J. M., & Tolmachev, Y. V. Thermal conductivity and particle agglomeration in alumina nanofluids:experiment and theory. *Physical Review 76 (2007) 061203*.

Timofeeva, E. V., Gavrilov, A. N., McCloskey, J. M., & Tolmachev, Y. V. (2007). Thermal conductivity and particle agglomeration in alumna nanofluids: experiment and theory. *Physical Review 76 (2007) 061203, 76*.

Timofeeva, E. V., Routbort, J. L., & Singh, D. (2009). Particle shape effects on thermophysical properties of alumina nanofluids. *Journal of Applied Physics*.

Tiwari, A. K., Ghosh, P., & Sarkar, J. (2013). Heat transfer and pressure drop characteristics of CeO2/water nanofluid in plate heat exchanger. *Applied Thermal Engineering, 57*(1–2), 24-32. doi: http://dx.doi.org/10.1016/j.applthermaleng.2013.03.047

Togun, H., Safaei, M. R., Sadri, R., Kazi, S. N., Badarudin, A., Hooman, K., & Sadeghinezhad, E. (2014). Numerical simulation of laminar to turbulent nanofluid flow and heat transfer over a backward-facing step.doi: http://dx.doi.org/10.1016/j.amc.2014.04.051. *Applied Mathematics and Computation, 239*, 153-170.

Tu, J. P., Dinh, N., & Theofanous, T. (2004). *An experimental study of nanofluid boiling heat transfer.* Paper presented at the Proceedings of 6th international symposium on heat transfer, Beijing, China.

Tuqa. Abdulrazzaq, Hussein. Togun, M.K.A Ariffin, S.N. Kazi, A. Badarudin, N.M. Adam, . . . E. Sadeghinezhad. (2013). Enhancements Of Heat Transfer Nanofluid Flow In Circular Pipe With Twisted TapeInserts: Review. *Australian Journal of Basic and Applied Sciences, 7*(9), 97-102.

Udbhav.Ojha, Sumitesh. Das, & Subhrakanti. Chakraborty. (2010). Stability, pH and Viscosity Relationships in Zinc Oxide Based Nanofluids Subject to Heating and Cooling Cycles. *Journal of Materials Science and Engineering, 4*(7).

Ulzie Rea, Tom McKrell, Lin-wen Hu, & Buongiorno, J. (2008). Laminar convective heat transfer and viscous pressure loss of alumina–water and zirconia–water nanofluids. *International Journal of Heat and Mass Transfer*, 2042-2048.

Vajjha, R. S., D. K. Das, & D. P. Kulkarni. (2010). Development of New Correlations for Convective Heat Transfer and Friction Factor in Turbulent Regime for Nanofluids. *International Journal of Heat and Mass Transfer, 53*(21-22), 4607-4618.

Vajjha, R. S., & Das, D. K. (2012). A review and analysis on influence of temperature and concentration of nanofluids on thermophysical properties, heat transfer and pumping power. *International Journal of Heat and Mass Transfer, 55*(15–16), 4063-4078. doi: http://dx.doi.org/10.1016/j.ijheatmasstransfer.2012.03.048

Vandsburger, L. (2010). *Synthesis and Covalent Surface Modification of Carbon Nanotubes for Preparation of Stabilized Nanofluid Suspensions*.

Verwey, E. J. W., & Overbeek, J. T. G. (1948). Theory of the stability of lyophobic colloids. *Elsevier, Amsterdam*.

Vladkov, M., & Barrat, J. L. (2006). Modeling transient absorption and thermal conductivity in a simple nanofluid. *Nano letters, 6*(6), 1224-1228.

W. Azmi, K. Sharma, P. Sarma, R. Mamat, & S. Anuar. (2014). Comparison of convective heat transfer coefficient and friction factor of TiO2 nanofluid flow in a tube with twisted tape inserts. *Int. J. Therm. Sci. , 81*, 84–93.

W. Nan, R. Birringer, D. R. Clarke, & H. Gleiter. (1997). Effective thermal conductivity of particulate composites with interfacial thermal resistance. *Journal of Applied Physics, 81*(10).

Wamkam, C. T., M.K. Opoku, H. Hong, & Smith, P. (2011). Effects of pH on heat transfer nanofluids containing ZrO2 and TiO2 nanoparticles. *J. Appl. Phys., 109*.

Wang, Zhou, L. P., & Peng, X. F. (2003). A fractal model for predicting the effective thermal conductivity of liquid with suspension of nanoparticles. *International Journal of Heat and Mass Transfer, 46*(14), 2665-2672.

Wang, B.-X., Zhou, L.-P., & Peng, X.-F. (2003). A fractal model for predicting the effective thermal conductivity of liquid with suspension of nanoparticles. *International Journal of Heat and Mass Transfer, 46*(14), 2665-2672. doi: http://dx.doi.org/10.1016/S0017-9310(03)00016-4

Wang, B., Wang, X., Lou, W., & Hao, J. (2012). Thermal conductivity and rheological properties of graphite/oil nanofluids. *Colloids and Surfaces A: Physicochemical and Engineering Aspects, 414*(0), 125-131. doi: http://dx.doi.org/10.1016/j.colsurfa.2012.08.008

Wang, L. Q., & Quintard, M. (2009). Nanofluids of the future, L.Q. Wang (Ed.), Advances in transport phenomena, Springer-Verlag, Heidelberg. 179–243.

Wang, X. J., Li, X. F., Xu, Y. H., & Zhu, D. S. (2014). Thermal energy storage characteristics of Cu–H2O nanofluids. *Energy, 78*(0), 212-217. doi: http://dx.doi.org/10.1016/j.energy.2014.10.005

Wang, X. J., X. Li, & Yang, S. (2009). Influence of pH and SDBS on the stability and thermal conductivity of nanofluids. *Energy Fuels, 23*, 2684–2689.

Wang, X. Q., & A.S. Mujumdar. (2008). A review on nanofluids - part ii: experiments and applications *Brazilian Journal of Chemical Engineering, 25*(4), 631 - 648.

Wasan, D., Nikolov, A., & Moudgil, B. (2005). Colloidal dispersions: Structure, stability and geometric confinement. *Powder Technology, 153*(3), 135-141. doi: http://dx.doi.org/10.1016/j.powtec.2004.12.005

Wasp, F. J. Solid–Liquid Slurry Pipeline Transportation. *Trans Tech, Berlin, 1977*.

Wei, X., & Wang, L. (2010). Synthesis and thermal conductivity of microfluidic copper nanofluids. *Particuology, 8*(3), 262-271. doi: http://dx.doi.org/10.1016/j.partic.2010.03.001

Wei, X. H., H.T. Zhu, T.T. Kong, & Wang, L. Q. (2009). Synthesis and thermal conductivity of Cu2O nanofluids. *International Journal of Heat and Mass Transfer,, 52*, 4371–4374.

Wei, Y., & Huaqing, X. (2012). A review on nanofluids: preparation, stability mechanisms, and applications. *J. Nanomaterials, 2012*, 1-17. doi: 10.1155/2012/435873

Wei, Y., & Xie, H. (2012). A Review on Nanofluids: Preparation, Stability Mechanisms, and Applications, Article ID 435873, doi:10.1155/2012/435873. *Journal of Nanomaterials*.

Wen, D., & Ding, Y. (2004). Experimental investigation into convective heat transfer of nanofluids at the entrance region under laminar flow conditions. *International Journal of Heat and Mass Transfer, 47*(24), 5181-5188.

Wen, D., & Ding, Y. (2005). Experimental investigation into the pool boiling heat transfer of aqueous based Î³-alumina nanofluids. *Journal of Nanoparticle Research, 7*(2), 265-274.

Wen, D., & Ding, Y. (2006). "Natural convective heat transfer of suspension of titanium dioxide nanoparticles (nanofluids). *IEEE Transactions of Nanotechnology 5*(3).

Wen, D., Ding, Y., Cui, Z., & Wang, B. X. (2004). Effective thermal conductivity of aqueous suspensions of carbon nanotubes (carbon nanotube nanofluids). *Journal of Thermophysics and Heat Transfer, 18*(4), 481-485.

Wensel, J., B. Wright, D. Thomas, W. Douglas, B. Mannhalter, W. Cross, . . . Roy, W. (2008). Enhanced thermal conductivity by aggregation in heat transfer nanofluids containing metal oxide nanoparticles and carbon nanotubes. *Appl. Phys. Lett., 92*.

Wensel, J., Wright, B., Thomas, D., Douglas, W., Mannhalter, B., Cross, W., . . . Roy, W. (2008). Enhanced thermal conductivity by aggregation in heat transfer nanofluids containing metal oxide nanoparticles and carbon nanotubes. *Applied Physics Letters, 92*(2), 023110-023110-023113.

Williams, W. C., Bang, I. C., Forrest, E., Hu, L. W., & Buongiorno, J. (2007). *Preparation and characterization of various nanofluids.* Paper presented at the Proceedings of the NSTI Nanotechnology Conference and Trade Show (Nanotech'06).

Williams, W. C., Buongiorno, J., & Hu, L. (2008). Experimental Investigation of Turbulent Convective Heat Transfer and Pressure Loss of Alumina/Water and Zirconia/Water Nanoparticle Colloids (Nanofluid) in Horizontal Tubes. *Journal of Heat Transfer, 130*.

Wilson, E. E. (1915). A basis for rational design of heat transfer apparatus. *Trans. ASME, 37*(47), 47-82.

Witharana, S. (2011). *Thermal Transport in Nanofluids: Boiling heat transfer.* (Doctor of Philosophy), The University of Leeds.

Witharana, S., C. Hodges, D. Xu, X. Lai, & Y. Ding. (2012). Aggregation and settling in aqueous polydisperse alumina nanoparticle suspensions. *Journal of Nanoparticle Research, 14*.

Witharana, S., H. Chen, & Y. Ding. (2011). Stability of nanofluids in quiescent and shear flow fields. *Nanoscale Research Letters, 6*(231).

Witharana, S., Palabiyik, I., Musina, Z., & Ding, Y. (2013). Stability of glycol nanofluids — The theory and experiment. *Powder Technology, 239*(0), 72-77. doi: http://dx.doi.org/10.1016/j.powtec.2013.01.039

Wong, K.-L., Salazar, J. L. L., Prasad, L., & Chen, W.-L. (2011). The inaccuracy of heat transfer characteristics for non-insulated and insulated spherical containers neglecting the influence of heat radiation. *Energy Conversion and Management, 52*(3), 1612-1621.

Wong, K. F. V., & Kurma, T. (2008). Transport properties of alumina nanofluids. *Nanotechnology, 19*(34), 345702.

Wu, J. M., & Zhao, J. (2013). A review of nanofluid heat transfer and critical heat flux enhancement—Research gap to engineering application. *Progress in Nuclear Energy, 66*(0), 13-24. doi: http://dx.doi.org/10.1016/j.pnucene.2013.03.009

Xian-Ju, W., & Xin-Fang, L. (2009). Influence of pH on Nanofluids' Viscosity and Thermal Conductivity. *Chinese Physics Letters, 26*(5), 056601.

Xie, Wang, Xi, & Liu. (2002). Thermal conductivity of suspensions containing nanosized SiC particles. *International Journal of Thermophysics, 23*(2), 571-580.

Xie, H. (2002). Thermal conductivity enhancement of suspensions containing nanosized alumina particles. *Journal of Applied Physics, 91*.

Xie, H., Lee, H., & Youn, W. (2003). Nanofluids containing multi-walled carbon nanotubes and their enhanced thermal conductivities. *Journal of Applied Physics, 94*.

Xie, H., Wang, J., Xi, T., Liu, Y., Ai, F., & Wu, Q. (2002). Thermal conductivity enhancement of suspensions containing nanosized alumina particles. *Journal of Applied Physics, 91*(7), 4568-4572.

Xing, M., Yu, J., & Wang, R. (2015). Experimental study on the thermal conductivity enhancement of water based nanofluids using different types of carbon nanotubes. *International Journal of Heat and Mass Transfer, 88*(0), 609-616. doi: http://dx.doi.org/10.1016/j.ijheatmasstransfer.2015.05.005

Xuan, Li, Q., & Hu, W. (2003). Aggregation structure and thermal conductivity of nanofluids. *AIChE Journal, 49*(4), 1038-1043.

Xuan, Y., & Li, Q. (2000). Heat transfer enhancement of nanofluids. *International Journal of Heat and Fluid Flow, 21*(1), 58-64.

Xuan, Y. M., Li, Q., & Wang, J. (2003). Investigation on convective heat transfer and flow features of nanofluids. *Journal of Heat Transfer, 1125*.

Xue, Q., & Xu, W. M. (2005). A model of thermal conductivity of nanofluids with interfacial shells. *Materials Chemistry and Physics, 90*(2), 298-301.

Yang, J.-C., Li, F.-C., Zhou, W.-W., He, Y.-R., & Jiang, B.-C. (2012). Experimental investigation on the thermal conductivity and shear viscosity of viscoelastic-fluid-based nanofluids. *International Journal of Heat and Mass Transfer, 55*(11–12), 3160-3166. doi: http://dx.doi.org/10.1016/j.ijheatmasstransfer.2012.02.052

Yang, L., Du, K., Niu, X., Li, Y., & Zhang, Y. (2011). An experimental and theoretical study of the influence of surfactant on the preparation and stability of ammonia-water nanofluids. *International Journal of Refrigeration, 34*(8), 1741-1748. doi: http://dx.doi.org/10.1016/j.ijrefrig.2011.06.007

Yang, Y. (2011). *Characterizations and Convective Heat Transfer Performance of Nanofluids.* (Doctor of Philosophy), Lehigh University.

Yang, Y., Zhang, Z. G., Grulke, E. A., Anderson, W. B., & Wu, G. (2005). Heat transfer properties of nanoparticle-in-fluid dispersions (nanofluids) in laminar flow. *International Journal of Heat and Mass Transfer, 48*(6), 1107-1116.

Yanga, J. C., F.C. Lia, H.P. Xua, Y.R. Hea, Y.M. Huanga, & Jianga, B. C. (2013). Heat Transfer Performance of Viscoelastic-Fluid-based Nanofluid Pipe Flow at Entrance Region. *Experimental Heat Transfer: A Journal of Thermal Energy Generation, Transport, Storage, and Conversion*.

Yarmand, H., Gharehkhani, S., Ahmadi, G., Shirazi, S. F. S., Baradaran, S., Montazer, E., . . . Dahari, M. (2015). Graphene nanoplatelets–silver hybrid nanofluids for enhanced heat transfer. *Energy Conversion and Management, 100*, 419-428. doi: http://dx.doi.org/10.1016/j.enconman.2015.05.023

You, S. M., Kim, J. H., & Kim, K. H. (2003). Effect of nanoparticles on critical heat flux of water in pool boiling heat transfer. *Applied Physics Letters, 83*(16), 3374-3376.

Yu, W., & Choi, S. U. S. The role of interfacial layers in the enhanced thermal conductivity of nanofluids: a renovated Maxwell model *Journal of Nanoparticle Research 5 (2003) 167–171.*

Yu, W., & Choi, S. U. S. (2004). The role of interfacial layers in the enhanced thermal conductivity of nanofluids: a renovated Hamiltonâ€“Crosser model. *Journal of Nanoparticle Research, 6*(4), 355-361.

Yu, W., France, D., Timofeeva, E., Singh, D., & Routbort, J. (2010). Thermophysical property-related comparison criteria for nanofluid heat transfer enhancement in turbulent flow. *Applied Physics Letters, 96*(21), 213109.

Yu, W., France, D. M., Singh, D., Timofeeva, E. V., Smith, D. S., & Routbort, J. L. (2010). Mechanisms and models of effective thermal conductivities of nanofluids. *Journal of Nanoscience and Nanotechnology, 10*(8), 4824-4849.

Yu, W., France, D. M., Timofeeva, E. V., Singh, D., & Routbort, J. L. (2012). Comparative review of turbulent heat transfer of nanofluids. *International Journal of Heat and Mass Transfer, 55*(21–22), 5380-5396. doi: http://dx.doi.org/10.1016/j.ijheatmasstransfer.2012.06.034

Yu.W. France, D, R., & J.S. Choi. (2008). Review and comparison of nanofluid thermal conductivity and heat transfer enhancements. *Heat Transfer Engineering, 29*(5), 432-460.

Yulong Ding, H. A., Dongsheng Wen, Richard A. Williams. (2006). Heat transfer of aqueous suspensions of carbon nanotubes (CNT nanofluids). *International Journal of Heat and Mass Transfer, 49*, 240–250

Yunus, A. C. (2003). Heat transfer: a practical approach. *MacGraw-Hill*.

Zeinali Heris, S., Etemad, S. G., & Nasr Esfahany, M. (2006). Experimental investigation of oxide nanofluids laminar flow convective heat transfer. *International Communications in Heat and Mass Transfer 33*, 529–535

Zhang, H., Shao, S., Xu, H., & Tian, C. (2013). Heat transfer and flow features of Al2O3–water nanofluids flowing through a circular microchannel – Experimental results and correlations. *Applied Thermal Engineering, 61*(2), 86-92. doi: http://dx.doi.org/10.1016/j.applthermaleng.2013.07.026

Zhao, N., Yang, J., Li, H., Zhang, Z., & Li, S. (2016). Numerical investigations of laminar heat transfer and flow performance of Al2O3–water nanofluids in a flat tube. *International Journal of Heat and Mass Transfer, 92*, 268-282. doi: http://dx.doi.org/10.1016/j.ijheatmasstransfer.2015.08.098

Zheng, R., Gao, J., Wang, J., Feng, S.-P., Ohtani, H., Wang, J., & Chen, G. (2011). Thermal percolation in stable graphite suspensions. *Nano Lett., 12*(1), 188-192.

Zhou, M., Bi, H., Lin, T., Lü, X., Wan, D., Huang, F., & Lin, J. (2014). Heat transport enhancement of thermal energy storage material using graphene/ceramic composites. *Carbon, 75*(0), 314-321. doi: http://dx.doi.org/10.1016/j.carbon.2014.04.009

Zhu, D., Li, X., Wang, N., Wang, X., Gao, J., & Li, H. (2009). Dispersion behavior and thermal conductivity characteristics of Al2O3–H2O nanofluids. *Current Applied Physics, 9*(1), 131-139. doi: http://dx.doi.org/10.1016/j.cap.2007.12.008

Zhu, D. S. (2009). Dispersion Behavior and Thermal Conductivity Characteristics of Al2O3–H2O Nanofluids. *Current Applied Physics, 9*.

Zhu, H.-t., Lin, Y.-s., & Yin, Y.-s. (2004). A novel one-step chemical method for preparation of copper nanofluids. *Journal of Colloid and Interface Science, 277*(1), 100-103. doi: http://dx.doi.org/10.1016/j.jcis.2004.04.026

Zubir, M. N. M., Badarudin, A., Kazi, S., Misran, M., Amiri, A., Sadri, R., & Khalid, S. (2015). Experimental investigation on the use of highly charged nanoparticles to improve the stability of weakly charged colloidal system. *Journal of Colloid and Interface Science*.

LIST OF PUBLICATIONS

JOURNAL ARTICLES:

Related to thesis:

1. **KH Solangi,** SN Kazi, MR Luhur, A Badarudin, A Amiri, Rad Sadri, MNM Zubir, Samira Gharehkhani, KH Teng. A comprehensive review of thermo-physical properties and convective heat transfer to nanofluids. Energy. Vol 89, pages, 1065-1086.
2. **K.H Solangi,** Ahmad Amiri, Mohd Nashrul Mohd Zubir, S. N. Kazi, A. Badarudin. Experimental investigation of heat transfer performance and frictional loss of functionalized GNP based water coolant in a closed conduit flow. RSC Advances. 2016, Vol. 6, 4552
3. Mohd Nashrul Mohd Zubir, **Solangi K.H,** A Badarudin, SN Kazi, Misni Misran, Ahmad Amiri, Rad Sadri. Journal of Colloid and Interface Science. Experimental investigation on the use of highly charged nanoparticles to improve the stability of weakly charged colloidal system. Volume 454, 15 September 2015, Pages 245–255.
4. **K.H Solangi,** Ahmad Amiri, Mohd Nashrul Mohd Zubir, S. N. Kazi, A. Badarudin. Experimental investigation of the prypylene glycol treated graphene nanoplatelets of closed conduit turbulent convective heat transfer. International communications in heat and mass transfer. **Accepted**

Unrelated to the thesis:

1 **Solangi, K.H.,** Islam, M.R., Saidur, R., Rahim, N.A., and Fayaz, H., A review on global solar energy policy. Renewable and Sustainable Energy Reviews, 2011. 15(4): 2149-2163.

2 **KH Solangi,** R Saidur, MR Luhur, MM Aman, A Badarudin, SN Kazi, TNW Lwin, NA Rahim, MR Islam. Social acceptance of solar energy in Malaysia: users' perspective. Clean Technologies and Environmental Policy. October 2015, Volume 17, Issue 7, pp 1975-1986.

3 A review of Safety, Health and Environmental (SHE) issues of solar energy system. MM Aman, **KH Solangi,** MS Hossain, A Badarudin, GB Jasmon, H Mokhlis. Renewable and Sustainable Energy Reviews 41, 1190-1204

4 Rahim, N. A., Saidur, R., **Solangi, K. H.,** Othman, M., & Amin, N. (2011). Survey of grid-connected photovoltaic inverters and related systems. Clean Technologies and Environmental Policy, 1-13. Retrieved from www.scopus.com

5 Saidur, R., Islam, M. R., Rahim, N. A., & **Solangi, K. H.** (2010). A review on global wind energy policy. Renewable and Sustainable Energy Reviews, 14(7), 1744-1762.

6 Saidur, R., Rahim, N.A., Islam, M.R., and **Solangi, K.H.,** Environmental impact of wind energy. Renewable and Sustainable Energy Reviews, 2011. 15(5): 2423-2430.

7 M. R. Islam, R. Saidur, N. A. Rahim and **K. H. Solangi** (2010). Renewable Energy Research in Malaysia. Engineering e-Transaction (ISSN 1823-6379) Vol. 4, No. 2, December 2009, pp 69-72 Online at http://ejum.fsktm.um.edu.my

8 M. R. Islam, R. Saidur, N. A. Rahim and **K. H. Solangi (2010).** Usage of Solar Energy and Its Status in Malaysia, Engineering e-Transaction (ISSN 1823-6379) Vol. 5, No. 1, June 2010, pp 6-10, Online at http://ejum.fsktm.um.edu.my Received 5 May 2010; accepted 28 May 2010.

9 Energy policy to promote photovoltaic generation. SM Moosavian, NA Rahim, J Selvaraj, **KH Solangi.** Renewable and Sustainable Energy Reviews 25, 44-58

10 M R Islam, N A Rahim, **K H Solangi,** R Saidur. Assessing wind energy potentiality for selected sites in Malaysia. Energy Education Science and Technology Part A-Energy Science and Research.

11 NA Madlool, R Saidur, HH Mohammed, **KH Solangi,** NA Rahim. Energy savings measures for clinker production in cement industry. Advanced Materials Research 347, 3120-3125.

12 M.R Luhur, A.L Manganhar, S.H Siyal, **K.H Solangi.** Analysis of force dynamics for airfoil in the wake of different grids. Engineering, science & technology, 2015. 17, 1.

13 MM Aman, GB Jasmon, KH Solangi, AHA Bakar, H Mokhlis. Optimum simultaneous DG and capacitor placement on the basis of minimization of power losses. International Journal of Computer and Electrical Engineering. 2013, Vol. 5, issue 5. 516-522.

Conference proceedings:

1 Present solar energy potential and strategies in China. **KH Solangi,** R Saidur, NA Rahim, MR Islam, H Fayaz. Second International Conference on Environmental Science and Technology (ICEST 2011) Singapore.

2 Public acceptance of solar energy: The case of Peninsular Malaysia. **KH Solangi**, A Badarudin, SN Kazi, TNW Lwin, MM Aman. TENCON Spring Conference, 2013 IEEE, 540-543.

3 **Solangi, K.H.,** Badarudin, A., Kazi, S.N., Aman, M.M. A comparative study of Electricity Situation in Bangladesh, India, Malaysia and Pakistan. 2nd International Conference on Mechanical, Automotive and Aerospace Engineering (ICMAAE 2013). 2013/7/2

4 **K.H Solangi,** R, Saidur, N.A. Rahim, M.R. Islam and H. Fayaz. Current solar energy policy and potential in Malaysia. 3rd International Conference on Science and Technology Application in industry and education, ICSTIE 2010 UiTM Pulau Pinang Malaysia, 16-17 December, 2010, Paper No. 31.

5 **K.H Solangi,** T.N.W. Lwin, N.A. Rahim, M.S. Hossain, R. Saidur, H. Fayaz. Development of Solar Energy and Present Policies in Malaysia. 2011 IEEE First Conference on Clean Energy and Technology CET. 978-1-4577-1354-5/11/$26.00 2011 © IEEE

6 M.R. Islam, R, Saidur, N.A. Rahim, **K.H Solangi**. Assessment and Analysis of Wind Energy Potential at Mersing, Malaysia. 3rd International Conference on Science and Technology Application in industry and education, ICSTIE 2010 UiTM Pulau Pinang Malaysia, 16-17 December, 2010, Paper No. 13.

7 Global solar energy use and social viability in Malaysia. MS Hossain, NA Rahim, **KH Solangi,** R Saidur, H Fayaz, NA Madlool. Clean Energy and Technology (CET), 2011 IEEE First Conference on, 187-192. 27-29 June 2011. Kuala Lumpur

8 Fayaz, H.; Rahim, N.A.; Saidur, R.; Solangi, K.H.; Niaz, H.; Hossain, M.S. Solar energy policy: Malaysia vs developed countries. Clean Energy and

Technology (CET), 2011 IEEE First Conference on Year: 2011. Pages: 374 378, DOI: 10.1109/CET.2011.6041512